NASA

LMSC-A984158
22 FEB 1971

HANDBOOK OF EXTERNAL REFRIGERATION SYSTEMS FOR LONG TERM CRYOGENIC STORAGE

PREPARED FOR

MANNED SPACECRAFT CENTER
UNDER CONTRACT NAS 9-10412

LMSC
SPACE SYSTEMS DIVISION

REFRIGERATION HANDBOOK

LOCKHEED MISSILES & SPACE COMPANY
A GROUP DIVISION OF LOCKHEED AIRCRAFT CORPORATION
SPACE SYSTEMS DIVISION • SUNNYVALE, CALIFORNIA

CR-115190
LMSC-A984158
22 February 1971

HANDBOOK OF EXTERNAL REFRIGERATION SYSTEMS FOR LONG-TERM CRYOGENIC STORAGE

PREPARED FOR

THOMAS L. DAVIES
MANNED SPACECRAFT CENTER
NATIONAL AERONAUTICS AND SPACE ADMINISTRATION

Prepared by

H. L. Jensen, T. C. Nast, A. P. M. Glassford,
R. M. Vernon, W. F. Ekern

Lockheed Missiles & Space Company
Sunnyvale, California

FOREWORD

A 14-month study was conducted by Lockheed Missiles & Space Company for the Propulsion and Power Division of the Manned Spacecraft Center of the National Aeronautics and Space Administration under Contract NAS9-10412. The study, entitled Investigation of External Refrigeration Systems for Long-Term Cryogenic Storage, was initiated to present sufficient information and procedures for evaluating the usefulness of a small closed-cycle cryogenic refrigeration system for space applications.

The material developed in the study is presented in four documents, as follows:

- An Investigation of External Refrigeration Systems for Long-Term Cryogenic Storage - Systems Review Report, LMSC A903162 28 May 1970
- An Investigation of External Refrigeration Systems for Long-Term Cryogenic Storage - Final Report LMSC-A981632, 22 February 1971
- Handbook of External Refrigeration Systems for Long-Term Cryogenic Storage LMSC-A984158 22 Feb 1971
- An Investigation of External Refrigeration Systems for Long-Term Cryogenic Storage - Summary Report LMSC-A984159 22 February 1971

The material contained herein is the Handbook (the third of the above mentioned documents). It contains data that have been extracted from the Final Report (the second document) and provides procedures and summary data for conducting systems trade-off analyses. For more complete data and study background, the Final Report should be consulted.

CONTENTS

ILLUSTRATIONS

Figure | Page

TABLES

Section 1
INTRODUCTION

This handbook of External Refrigeration Systems for long Term Cryogeric Storage has been prepared to aid the engineer/planner working in the aerospace sciences. The primary purpose of the handbook is to present data and procedures for conducting selection and optimization studies of cryogenic space borne refrigeration systems. Data have been included on the major elements of the refrigeration system including the refrigerator itself, the cryogenic tankage, the heat absorption system, the heat rejection system, and the power supply. An example case for conducting the trade-off studies has been described in the following section.

The data in this handbook covers the following parameter ranges:

- o Cooling load: 1 to 100 watts (3.4 to 341 BTU/Hr)
- o Cryogenic tankage: 20 to 280 cu. ft.
- o Cooling load temperatures: 7.5 to 200^{o}R (4.2 to 110^{o}K)
- o Mission duration: 6 to 24 months

The information presented on each element is limited to that which is needed to make first estimate approximations for obtaining overall system size, weight, and performance. It is not intended that this handbook be used for detail design analyses of a particular element or machine.

It is expected that with the data and procedures presented herein one can define the system requirements and the type of program required to achieve his objectives. The data will help in identifying system characteristics in the following areas:

- o Magnitudes and temperature levels of cooling loads
- o Interface requirements between load and refrigerator such as; whether the refrigerator can be integrated with the cooling load or whether the heat must be transferred by heat pipe, convective loop or other

thermal link from a remote location; duty cycle; heat flux and temperature level control requirements, etc.

- Nature of spacecraft power supply, particularly as defined in terms of system penalties for both primary thermal power and generated electrical power, since both electrically and thermally powered refrigerators exist.
- Interface requirements between power source and refrigerator. For electrically powered systems this requirement would be quite simple. For thermally powered systems it must be decided whether the source can be integrated with the load or should be located remotely and thermally linked.
- Interface requirements between refrigerator and spacecraft heat rejection systems. Heat must be rejected from the refrigerator at temperatures in the general range of earth ambient temperatures. It must be transported from the refrigerator to the radiator by a heat transport mechanism.
- Maintenance possibilities. Depending upon the particular mission, this will range from zero maintenance to a maximum value considerably less than that permissible for ground and airborne units.
- Required operational lifetime.

Section 2

PROCEDURES AND SAMPLE CALCULATIONS

2.1 INTRODUCTION

The material presented in this handbook can be effectively used to conduct refrigeration systems trade-off studies. A separate section has been devoted to each major element of the refrigeration system as follows.

Section	System Element
3	Refrigerators
4	Refrigerator Failure Characteristics
5	Thermal Environment
6	Cryogenic Tankage & Heat Leak
7	Heat Rejection
8	Heat Absorption
9	Power Supplies

In addition to data found in these sections a set of cryogen property data and conversion units are given in Section 10 and 11 respectively.

Each section can be used to assemble data on the refrigeration system to whatever degree of iteration or depth that the engineer/planner may care to go. To illustrate the use of the material an example has been prepared.

2.2 EXAMPLE CALCULATIONS

As an aid in utilizing the information presented in this handbook, an example case was worked through for a hypothetical system. The hypothetical system consisted of refrigeration of an LH_2 storage tank so that no venting took place for a period of six months in earth orbit. The orbit selected was a 200 NM earth orbit assuming a 100% sunlit condition. The tank was assumed spherical in shape with an 8 ft. diameter and a capacity of 1100 lbs. of LH_2. It was further assumed that the tank pressure was allowed to vary from 5 to 30 psia and that all of the propellant was utilized at the end of the mission. (No intermittent burns).

In order to define the preliminary characteristics of the system it was initially assumed that the cooling from the refrigeration system was continuous rather than intermittent.

Additional characteristics and assumptions are shown on the flow sheet of Table 2-1.

The flow sheet was set up to show how the problem was formulated and to show the interaction between the system parameters. This flow diagram is quite general in nature, and it will provide a guide for a wide variety of conditions and systems which may be analyzed. However, it is not intended to be a rigid guide in analyzing all refrigeration design problems, and some types of systems will require a different analysis scheme.

The step by step procedure by which the system parameters are arrived at is shown in the Table. In the example case, the data from which the parameters were derived are identified on the flow sheet by the appropriate figure and table number. The derivation of the various parameters is shown and explained in the Table.

In analyzing a system, the initial selection of the cycle can be dictated by a variety of major system restraints. For example, if the power available is a primary restriction on the system, the Stirling cycle, which requires the minimum power may be chosen. If the available space in the immediate region to be cooled is extremely limited it may be necessary to choose one of the the systems which utilize a separable, remote compressor such as the Gifford-McMahan unit. If a large supply of waste heat is available from an auxiliary system component, say an isotope unit it may be desirable to consider the heat driven Vuilleumier cycle refrigerator. If an extremely long mission duration is required, the air-bearing Brayton cycle units may be the only ones with potential for the desired lifetime.

The various refrigerator systems have been adequately described in the handbook to give the engineer/planner sufficient insight to recognize the advantages and disadvantages of the various cycles. Some of the primary characteristics of the various cycles are succinctly summarized in Table 2-2.

FOLDOUT FRAME /

PROPELLANT TANK AND INSULATION PARAMETERS

Tank:

Spherical
8 ft. diameter
V = 275 ft^3 (Fig. 6-1)
A_s = 202 ft^2 (Fig. 6-2)
M_{LH_2} = 1100 lbs (Fig. 10-1)
(10% ullage assumed)
Allowable Pressure Variation:
5 psia to 30 psia (17°K to 23°K)

Heat Leak:

Insulation: assume goldized mylar/silk net 1 inch thick
Q = 0.05 w/ft^2 (Fig. 6-6)
$Q_{ins.}$ = 10.1 w
Supports: 3.5 x 10^{-4} w/lb (Fig. 6-7)
Q_s = 0.385 w
Lines and Instrumentation:
Q = 3 x 10^{-4} w/lb (Fig. 6-8)
Q_L = 0.330 w
Total:
$Q_{ins.}$ = 10.10 w
Q_s = .39
Q_L = .33
Q_T = 10.82 w

MISSION PARAMETERS

Orbital Parameters:

200 nm earth orbit
Polar orbit
No roll
100% sunlit orbit

Vehicle Surface Characteristics:

Assume optical solar reflector
Solar absorptance (α_s) = 0.050 (Table 5-1)
Infrared Emittance (ϵ_I) = 0.80
α_s/ϵ_I = .0625
T_s = 200°K (Figs. 5-7 to 5-10)

Mission Duration: 6 months (4320 hrs.)

State of the Art: near future

Propellant Usage Schedule: 100% propellant burned at end of mission; 6 months.

DEFINITION OF REFRIGERATION REQUIREMENTS

Nominal Cooling Required: 10.8 w
Design Cooling: 13 w (+20%)
Nominal Cooling Temperature: 20°K
Cooling Range: 17 to 23°K

PRELIMINARY CHARACTERISTICS OF SELECTED REFRIGERATION CYCLE

Primary Assumptions:

(a) Near present SOTA Stirling cycle unit
(b) Waste heat rejection at 300°K
(c) Continuous cooling of propellant
(d) 13 w cooling at 20°K (allows 20% degradation over lifetime)

Parameters:

Coefficient of Performance (COP) = 0.0065 (Fig. 3-14)
Power input = 2000 w
Specific weight = 12 lbs/w (Fig. 3-19)
Weight = 156 lbs
Specific volume = 95 in^3/w (Fig. 3-24)
Volume = 1,240 in^3 = 0.72 ft^3
Cool-down time = 15 mins + 35 mins/lb mass (Table 3-3, I.D. No. 6 and Fig. 3-30)

Similar Existing Units:

Phillips X-20 Prototype (Table 3-3, I.D. No. 6)

Reliability:

REFRIGERATOR TO PROPELLANT TANK HEAT EXCHANGER

Assumptions:

(a) Allow 1°K gradient between tank wall and refrigerator
(b) Transfer 13 w at 20°K nominal temperature
(c) Assume forced convection helium loop with tank wall heat exchanger

Parameters:

Tank wall heat exchanger area = 0.1 ft^2 (Fig. 8-4)
Heat exchanger weight = 0.15 lbs (Fig. 8-5)
Flow rate = 0.005 lbs/sec
Fan and motor weight 5 lbs (Fig. 8-6)

In this example a heat pipe exchanger and/or solid link conductor should also be considered.

Tank wall heat exchanger area = 0.1 ft^2
(Fig. 8-4)
Heat exchanger weight = 0.15 lbs (Fig. 8-5)
Flow rate = 0.005 lbs/sec
Fan and motor weight 5 lbs (Fig. 8-6)

In this example a heat pipe exchanger and/or solid link conductor should also be considered.

Specific volume = 95 in^3/w (Fig. 3-24)
Volume = 1,240 in^3 = 0.72 ft^3
Cool-down time = 15 mins + 35 mins/lb mass (Table 3-3, I.D. No. 6 and Fig. 3-30)

Similar Existing Units:

Phillips X-20 Prototype (Table 3-3, I.D. No. 6)

Reliability:

Assume Mean Time to Failure (MTTF) in the range of 2000 to 4000 hrs. (Table 4-1)
Assume Failure Rate Characteristics expressed by Weibull No. of 3.44 (Fig. 4-1)
Value of MTTF/Mission Duration (Life Ratio) in the range of $\frac{2000}{4320} = 0.463$ to $\frac{4000}{4320} = 0.926$
Resulting Reliability Ranges from Negligible to 0.40
(@ Life Ratio = 0.463)
(@ Life Ratio = 0.926) (Fig. 4-1)

PRELIMINARY POWER INPUT REQUIREMENTS

Minimum Power Input = 2000 w

POWER SUPPLY CHARACTERISTICS

Minimum Power Required: 2000 w

Design Power Level: 2200 w (allow 10% degradation)

Type: Solar Photovoltaic, large area erectable panel type

Parameters:

Specific power: 20 w/lb (Table 9-6)
Weight: 110 lbs
Weight includes deployment and orientation devices, excludes battery weight
Specific area: 0.1 ft^2/w (Table 9-8)
Area: 220 ft^2

WASTE HEAT REJECTION CHARACTERISTICS

Heat Rejection:

$\dot{Q}_{reject.}$ = cooling load + power input to refrigerator
$\dot{Q}_{reject.}$ = 13 w + 2200 w = 2213 w

Assumptions:

Assume T_{rej} = 300°K
Radiator using forced circulation loop
Assume negligible solar or earth heat inputs
Coolant fluid temperature rise = 20°K
Triangular aluminum fin
Optical solar reflectors utilized as emitting surface

Parameters:

Radiator area = 75 ft^2 (Fig. 7-8)
Radiator weight = 80 lbs (Fig. 7-9)
Coolant flow rate = 0.06 lbs/sec (p.7-5)
Circulation motor and pump wt = 4 lbs (Fig. 7-11)
Circulation motor and pump power = 10 w (Fig. 7-12)

PRELIMINARY SYSTEM DEFINITION

Item	Weights	Sizes	Power Requirement
Cooling rate:			13 w
Refrigerator:	156 lbs	0.72 ft^3	2000 w
Waste heat rad:	84 lbs	75 ft^2	10 w (pump)
Refrigerator-tank exch.:	5 lbs	0.1 ft^2	50 (fan & motor)
Power supply:	110 lbs	220 ft^2	2273 (initial; allows 10% degradation)
Sub-total	355 lbs		
10% for misc. hdw.	35 lbs		
Total preliminary wt.	390 lbs		

Reliability:

Optimistic = 0.40

COMPARISON WITH VENTED SYSTEM (NON-REFRIGERATED)

Assumptions:

Initial pressure = 15 psia
Vent at 30 psia

Parameters:

Pressure rises from P_i (15 psia) to P_{vent} (30 psia) in 14 days (Fig. 2)
Vent losses = 713 lbs

Table 2-2

REFRIGERATOR SUMMARY

Cycle	General Comments
Stirling	Most efficient and lightest cycle Long development history
Gifford-McMahon Taconis Solvay	Somewhat longer lifetime than Stirling cycle, relatively heavy and inefficient. Separable compressor allows small cooling head to be placed in extremely small envelope near cooled item.
Vuilleumier	Efficiency and weight nearly equal to Stirling cycle, can be driven by heat power. Lifetime similar to Stirling, recently developed.
Brayton/Claude	Relatively heavy and inefficient, use of air bearings to eliminate wear leads to potential for very long lifetime. Recently developed for small systems. Complex machinery requires relatively long development period. Weight becomes more competitive at high cooling rates.

In the example case the Stirling cycle was chosen in order to minimize system weight and determine what the maximum weight savings compared to a vented (non-refrigerated) system would be. The power supply selected was the solar photovoltaic large area erectable panel type. This system represents near state-of-the-art (SOTA), and appears to be the best choice for these conditions. An efficiency degradation of 10% over the 6 month lifetime was assumed for the solar cells.

The waste heat rejection was assumed to take place at 300°K and a triangular aluminum fin geometry was assumed for the radiator. A forced circulation loop utilizing water and allowing a temperature rise of 20°K in the radiator was assumed. An optional choice would be to assume the use of heat pipes to transfer the heat from the refrigerator to the radiator.

The required refrigeration load was based on primary assumptions of one inch of multi-layer insulation. The selection of one inch of insulation was arbitrary, and a trade-off of system weight vs insulation thickness is required to further optimize the system weight. A 20% degradation of the refrigerator cooling capability during its six-month operating period - to allow for wearing of parts and resulting loss in efficiency - was assumed.

The degradation of thermal efficiency with time can only be determined from actual data on the particular units. Such data is not presently available, however a 20% reduction was assumed to indicate that consideration of this effect should be made.

The reliability of such a system was estimated from the mean time to failure (MTTF) estimates given in the handbook (2000 hrs. conservative, 4000 hrs. optimistic) and a selection of the failure rate characteristics given by a Weibull number of 3.44. The reliability resulting from those assumptions ranged from negligibly small to 0.4 corresponding to the conservative and optimistic values of MTTF.

It is important to recognize that definitive reliability data on the various cycles is not available and can only be obtained by extensive testing. Both conservative and optimistic values of MTTF are presented in order to allow rough estimates of lifetime and to emphasize the fact that extensive failure rate data is not available.

The resulting major parameters of the system follow:

System weight	= 390 lbs.
Power input requirement	= 2273 W
Solar cell power unit area	= 220 ft^2
Waste heat radiator area	= 75 ft^2
Refrigerator volume	= 0.72 ft^3
Reliability	= $\approx$ 0 (conservative) to 0.4 (optimistic)

A comparison of the vent losses corresponding to a non-refrigerated system assuming a maximum allowable tank pressure of 30 psia shows a total of 713 lbs. of H_2 vented. The potential weight savings for a refrigerated system is therefore 713 lbs. minus 390 lbs. or 323 lbs.

This example of a preliminary systems analysis therefore indicates the potential of a substantial weight savings over a vented system, but an unsatisfactory reliability for a near future SOTA Stirling refrigerator.

This example forms the starting point of a parametric variation of the various assumptions. Among the variation of system parameters that must be investigated to better assess the trade-offs and find an optimum system are the following:

a) Techniques of improving reliability:
- Consider use of redundant refrigeration units
- Consider intermittent operation of refrigerators
- Consider cycles with longer potential lifetimes

All of the above improvements in reliability are accompanied by a system weight increase.

b) Effect of Heat Rejection Temperature

- Optimum heat rejection temperature may be found to minimize weight
- Heat rejection temperatures much removed from 300°K may require some development efforts to produce a refrigerator to reject heat at a different temperature.

c) Effect of insulation thickness

- Effect of insulation thickness on refrigerator heat load and resulting system changes requires investigation.

d) Effect of cycle selection

- Various cycles may be analyzed for comparison with the example which utilizes the Stirling cycle.
- Consideration of VM cycle with solar collector or radioisotope heat source.
- Consideration of GM for intermediate improvement in reliability and more flexibility of space envelope.
- Consideration of air bearing Brayton cycle for maximum potential mission lifetime.

The effects of these variations can be assessed with the data presented in this handbook.

SECTION 3
REFRIGERATORS

3.1 GENERAL THEORY

A refrigerator is a device which absorbs heat at one temperature and rejects it at a higher temperature. In order to perform this operation, an expenditure of mechanical work is required, as shown in Fig. 3-1. According to the second law of thermodynamics, this operation must result in a zero or positive change of entropy. In terms of the quantities shown in Fig. 3-1

$$\frac{q_a}{T_a} \geq \frac{q_c}{T_c} \tag{3-1}$$

According to the First Law of Thermodynamics

$$q_a = q_c + W \tag{3-2}$$

Thus,

$$W \geq q_c \left[\frac{T_a - T_c}{T_c}\right] \tag{3-3}$$

Equations 3-1, 3-2, and 3-3 relate to a system of heat source, heat sink, mechanical, refrigerator and mechanical work source. It is sometimes desirable to include the work source in the definition of the refrigerator, in which case the situation shown in Fig. 3-2 applies. In this case the work input required by the refrigerator is generated by an engine, which takes heat from a high temperature source, rejects heat to a lower temperature sink, and produces work. For the whole system the operation must produce a zero or positive production of entropy. If both engine and refrigerator share a common sink, then

$$\frac{q_a}{T_a} \geq \frac{q_h}{T_h} + \frac{q_c}{T_c} \tag{3-4}$$

According to the First Law of Thermodynamics

$$q_a = q_h + q_c \tag{3-5}$$

thus,

$$q_h \geq q_c \cdot \left[\frac{T_h}{T_c} \cdot \frac{T_a - T_c}{T_h - T_a}\right] \tag{3-6}$$

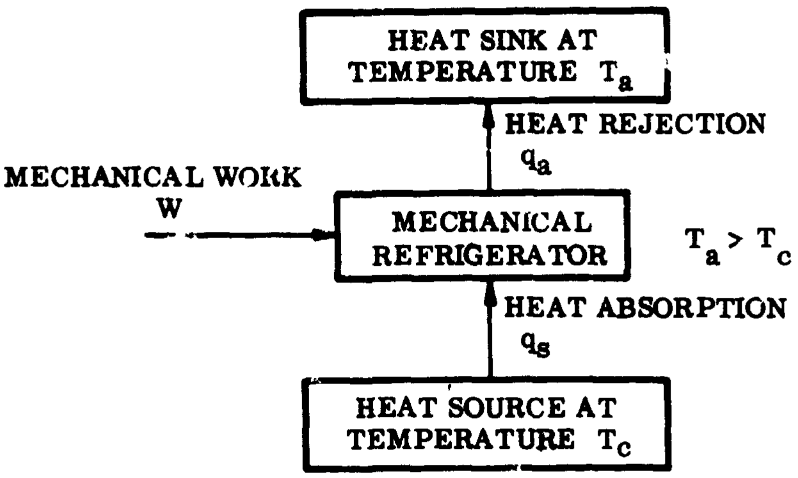

Figure 3-1 Mechanically-Powered Refrigerator Operation

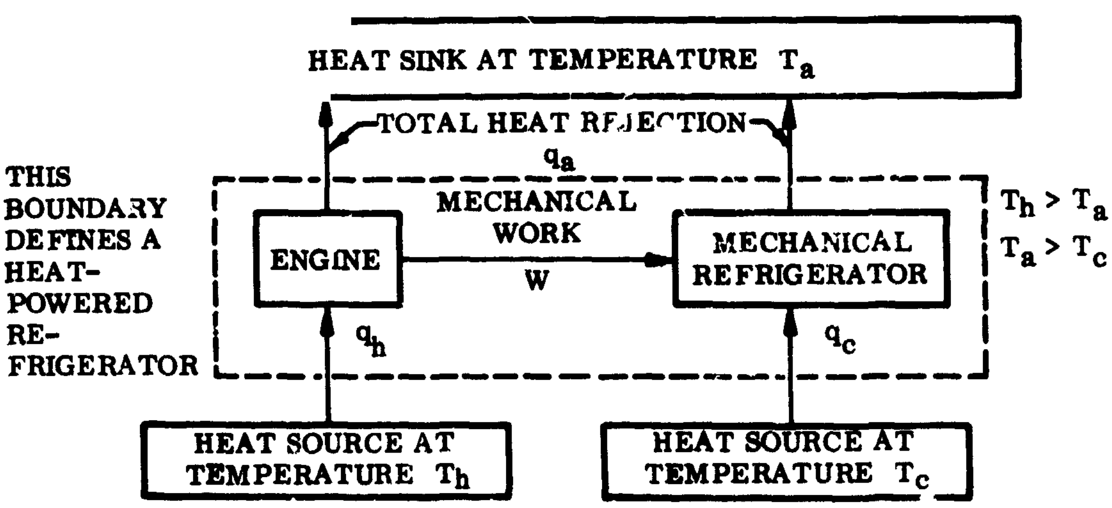

Figure 3-2 Heat-Powered Refrigerator Operation

There is no input of mechanical work to the system. Energy is supplied as heat and the whole system may be called a "heat-powered refrigerator". The performance of a refrigerator is customarily expressed by its "coefficient of performance" - "c.o.p.".

$$\text{c.o.p} = \frac{\text{refrigerator effect}}{\text{power supplied}}$$

This function is a satisfactory basis for comparison if all systems are of the type of Fig. 3-1. For most mechanical refrigerators, the source of power will be electrical energy converted to mechanical power via an electric motor. The electrical energy will originally have been produced by some process whose operation is completely independent of the refrigerator, and its influence may be neglected for comparison purposes. In the case of heat-powered refrigerators, the coefficient of performance is of less value as a standard; however, it may be used to form a common comparison criterion of both types of systems.

Some heat-powered refrigerators operate by electrical resistance heating, while others operate on heat input from a primary source, such as radioisotope or solar collector. If the heat input, q_h, in Eq. 3-6 were to be provided by an electrical heater, then based upon electrical power consumption, q_h would clearly be greater than W in Eq. 3-3, and the refrigerator of Fig. 3-1 would be always superior in efficiency. If, however, the means of obtaining heat and electric power are included in the assessment of power required, then a different conclusion may possibly be reached. It was not intended that generalized expressions for the behavior of power sources be included in this report; however, one should consider the power source to obtain the proper perspective on refrigerator systems.

The heat and work interactions implied by the devices shown in Fig. 3-1 and 3-2 are produced by circulating a fluid through the system and causing it to undergo appropriate processes at the heat source and sink. The First Law of Thermodynamics can be written for working fluid in a given process as follows:

$$\left\{\begin{matrix}\text{heat addition}\\ \text{to the fluid}\end{matrix}\right\} = \left\{\begin{matrix}\text{increase in internal energy}\\ \text{of the fluid}\end{matrix}\right\} + \left\{\begin{matrix}\text{work performed}\\ \text{by the fluid}\end{matrix}\right\}$$

Heat may be transferred from the load to the fluid by causing the latter to perform expansion work and replacing this energy with heat from the load either during or after expansion. Heat may be transferred from the fluid to the sink by performing work on the fluid by compressing it and rejecting this energy to the heat sink during or after compression. In either case, the system requires a compressor and sink heat exchanger, and an expander and load heat exchanger. The device of Fig. 3-1 will require a source of mechanical work which may be provided by some type of separate motor. The device of Fig. 3-2 produces the necessary mechanical work by incorporating a heat engine within the system. A heat engine is a reversed refrigerator, so this system will require an expander and source heat exchanger and a compressor and heat sink exchanger in addition to the refrigerator components. These components are essential to all refrigerators.

3.2 IDEAL THERMODYNAMIC CYCLES

It is desirable to keep the values of W and q_h in Eq. 3-3 and 3-6, respectively, as small as possible with respect to q_c. Their values will be a minimum when all cycle processes are reversible, i.e., they produce no overall increase in entropy. Cycles based upon reversible processes can be conceived but are impossible to execute in practice. In fact, practical refrigeration cycles are notable for their very high degree of irreversibility, and successful practical cycles are usually based on expeditious juggling of the many sources of performance loss. This characteristic highly irreversible behavior is traceable to the basic expression for entropy change, dq/T. It is apparent that the entropy changes associated with a given quantity of transferred heat is very much greater at low temperatures than at high temperatures. Much more emphasis must, therefore, be placed upon cold end performance than ambient or hot end performance, and the resulting practical cycles frequently bear little resemblance to textbook ideal cycles. Nevertheless, it is useful to review the basic ideal cycles in order to obtain a better understanding of their faults and to indicate why the variations shown in the practical cycles of the next section are necessary.

<u>The Carnot Cycle</u> is the best known reversible cycle, shown on the temperature entropy diagram of Fig. 3-3. The compression/cooling and expansion/heating process are accomplished isothermally. The heat transfer processes during these phases are effected over negligibly small temperature differences, resulting in no increase in entropy. The fluid is cooled and heated between these temperatures by isentropic expansion and compression, respectively.

In practice, the isothermal processes require an infinitely long duration if finite quantities of heat are to be transferred across infinitesmal temperature difference. It is necessary to run practical machines at relatively high speeds and compression is generally accomplished so fast that the process is adiabatic and the working fluid temperature rises. The heat of compression would thus be rejected to the sink after compression and across a finite temperature difference. The same comment applies to the expander and the heat from the cooling load. Another serious limitation of the Carnot cycle is that the ratio of the minimum sink temperature to the load temperature is governed by the pressure ratio used in the compression and expansion processes.

$$\frac{T_a}{T_c} = \left[\frac{P_2}{P_1}\right]^{\frac{\alpha-1}{\alpha}} \qquad (3\text{-}7)$$

This places a severe restriction upon the practical temperature range.

A second reversible cycle is **the <u>Erricson Cycle</u>, shown in Fig. 3-4 on a** temperature-entropy diagram. Compression and expansion are performed isothermally, as in the Carnot cycle, and the same comments apply. However, heating and cooling is accomplished at constant pressure in a heat exchanger. If the exchanger is 100 percent efficient, which is to say that the temperature difference between the working fluid and exchanger is zero at all points, the cycle is reversible. **The Erricson cycle has the desirable quality of** being able to span large temperature differences. It would undoubtedly be the most popular refrigeration cycle were it possible to perform reversible heat transfer in all the components. In practical machines the compression and expansion processes are performed so rapidly that they are closer to being adiabatic than isothermal.

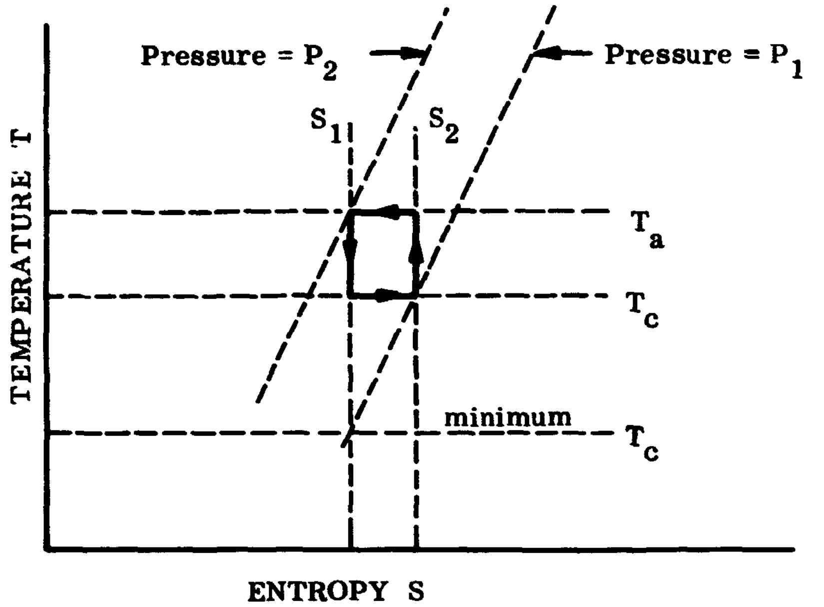

Fig. 3-3 The Carnot RefrigerationCycle

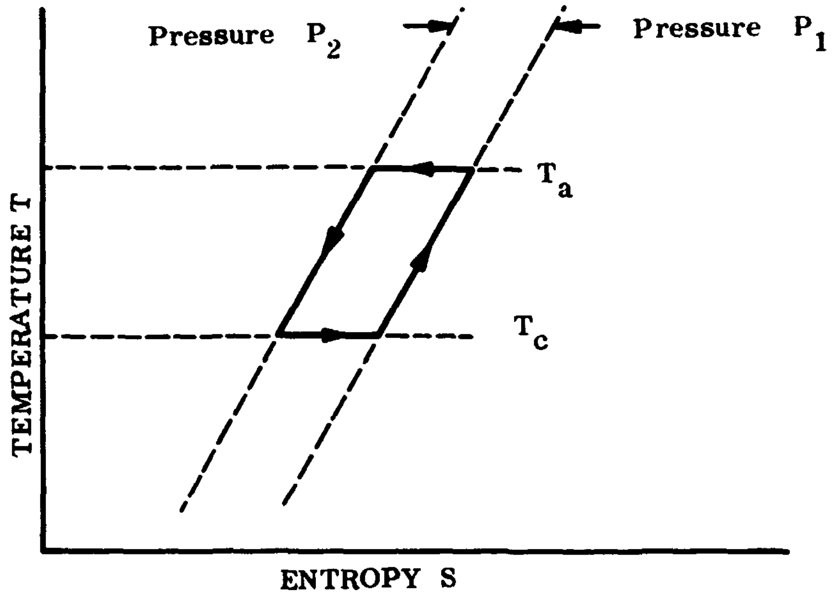

Fig. 3-4 The Erricson Refrigeration Cycle

3.3 PRACTICAL REFRIGERATION SYSTEMS

The cycles selected for inclusion were limited to those which it was felt had potential for satisfying the requirements of this study, i.e., long-term operation, low weight and volume, and high thermal efficiency.

The various systems can be divided into two broad groups: one employing counterflow heat exchangers, and another employing regenerative heat exchangers (See Fig. 3-5). If counterflow exchangers are used, then the working fluid flows at constant rate and direction through all the system components. These components can hence be designed for continuous steady-state operation at prescribable conditions. This category includes Claude, Joule-Thomson, and orthodox Brayton-cycle systems. On the other hand, those systems which employ regenerative heat exchangers must make some provision for intermittently reversing the direction of flow and alternately compressing and decompressing the working fluid in the regenerator. This can be performed in a refrigerator in which the cycle processes are executed successively in different regions of the same component. The working fluid is compressed while it occupies the warm end and the regenerator spaces, and is expanded while it occupies the cold end and regenerator spaces.

The second category includes the Stirling, Vuillenmier, and the "separable component systems", the Gifford-McMahon, modified Taconis, and modified Solvay.

In the Stirling refrigerator, compression and expansion is effected mechanically by movement of a single piston. The Vuilleumier refrigerator is essentially a heat-powered version of the Stirling refrigerator in which the compression and expansion of the working fluid is effected thermally by movement of a part of the fluid between hot and ambient spaces.

The separable component systems achieve compression and expansion of the working fluid by successively operating inlet and exhaust valves to admit and release the high-pressure working fluid. The presence of valves permits the use of a separate remote compressor.

A brief description of the individual cycles will now be given.

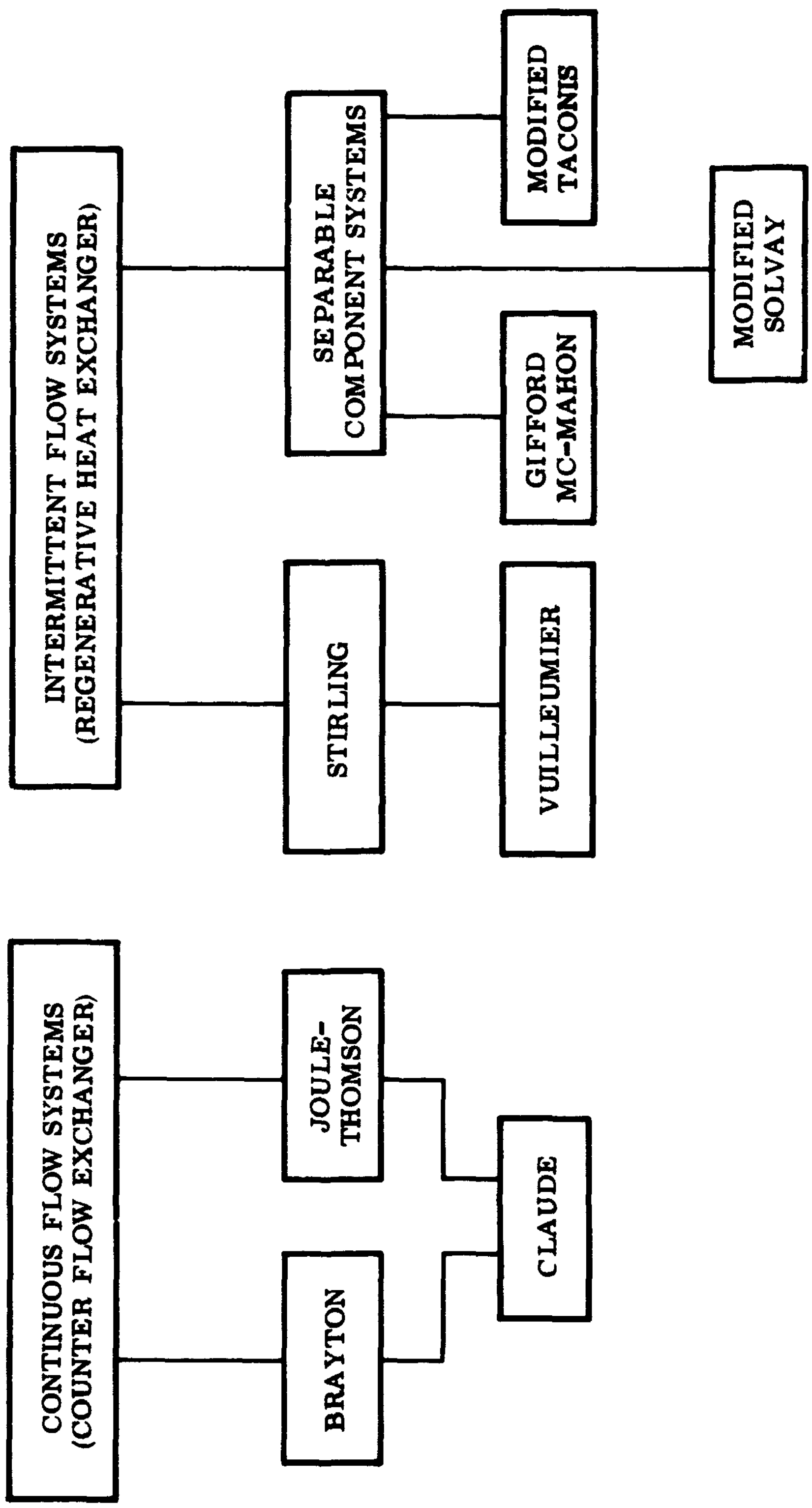

Fig. 3-5 Cycles Included for Analysis

3.3.1 Stirling Cycle

These refrigerators, which are commonly called Stirling refrigerators, do not in practice operate on the ideal Stirling cycle. Due to the speed of operation, heat cannot be transferred to and from the working spaces fast enough to permit isothermal compression and expansion. As a result, these processes are carried out under conditions closer to adiabatic, and the necessary heat transfer is effected in separate heat exchangers. This operation is more characteristic of the Brayton cycle. The truly characteristic feature of the practical so-called Stirling refrigerator and its derivatives is the use of regenerative heat exchangers.

In the refrigeration application heat exchangers are used to exchange heat between high- and low-pressure gas streams -- meaning that the single flow passage in the regenerator must be alternately pressurized and depressurized. This could be achieved by using a continuously operating compressor and expander, ballast tanks, or dual regenerators, and reversing valves between compressor and regenerator and expander and compressor. Such a system would incur substantial losses due to irreversible sudden compression and expansion when the valves were switched and due to the pressure drop through the valves. The practical Stirling refrigerator avoids these losses because the regenerator is in communication with the expander and compressor at all times, resulting in smooth - and therefore less irreversible - pressure cycling in the regenerator, and elimination of flow losses through the valves.

The operation of a Stirling refrigerator is shown in Figure 3-6.

In position 1, the working fluid occupies the ambient space, after-cooler, and regenerator. From 1 to 2, the fluid is compressed by inward motion of the compression piston. From 2 to 3, the compressed fluid is transferred from the ambient end to the cold end at constant overall volume by equal increment of both pistons. During this transfer, heat of compression is rejected to the after cooler and the temperature is reduced to the cold end temperature in the regenerator. With the fluid now occupying the cold space, load heat exchangers, and regenerator, the fluid is expanded by outward movement of the expander piston, 3 to 4. The fluid is returned from the cold

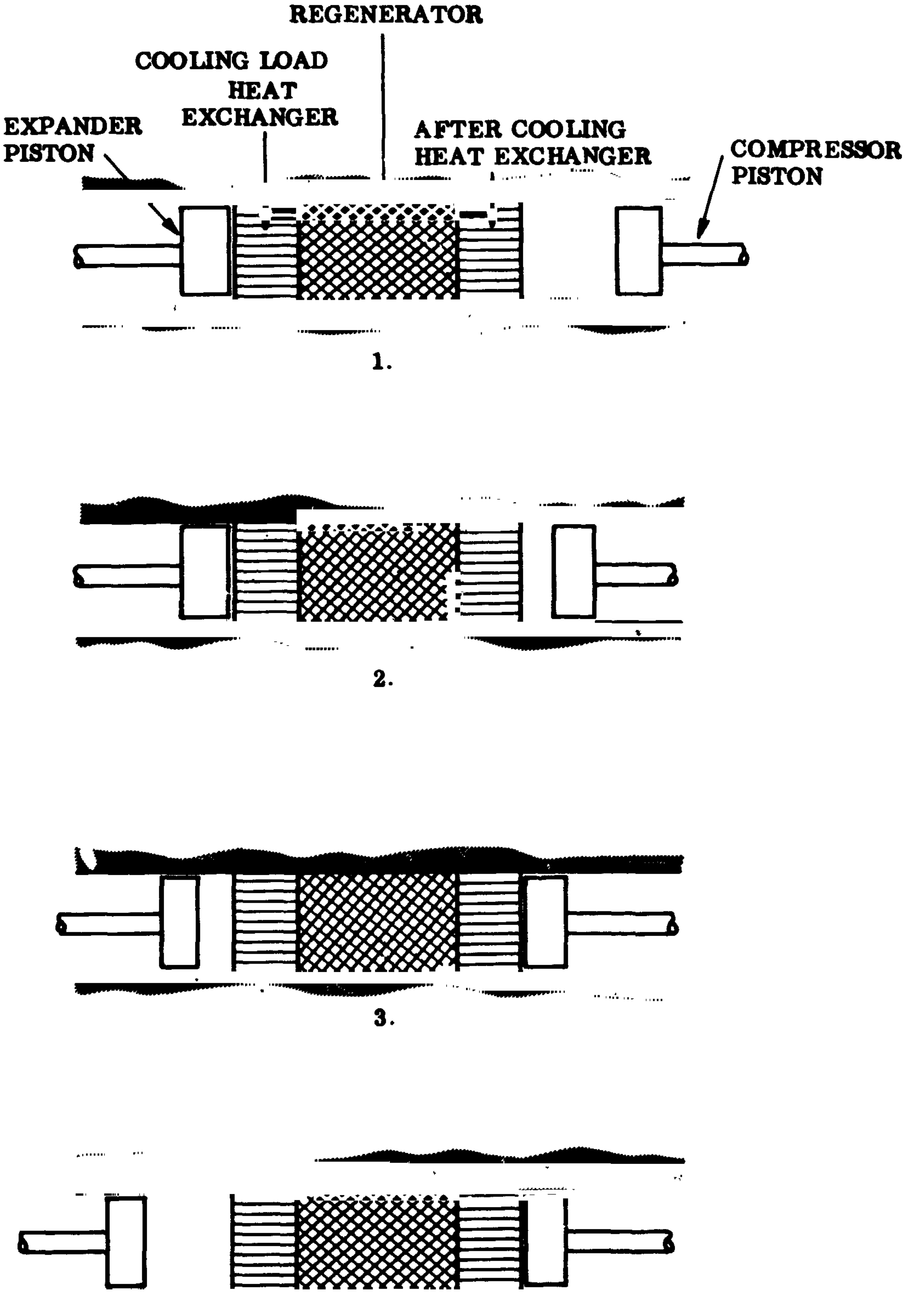

Fig. 3-6 The Practical Stirling Refrigerator

end to the ambient end at constant volume by equal increment of both pistons. During this transfer, the lost energy of expansion is replaced in the load exchanger and the temperature is raised to the ambient temperature in the regenerator.

This cycle can equally well be executed using just one piston to perform both expansion and compression processes, and using a passive displacer to move the fluid from one space to another. This configuration of refrigerator is shown in Figure 3-7.

In practice, it is not practical to move either the two pistons or the piston and displacer in the intermittent manner shown. It is customary to drive both components from the same crank shaft for practical convenience. Both components are thus continually in motion, but the cycle can be satisfactorily executed by phasing the piston or displacer motions such that compression occurs with most of the fluid in the warm space and expansion occurs with most of the fluid in the cold space.

Because of the cyclic operation of the practical Stirling refrigerator and the fact that working fluid will be distributed through several temperature regimes during compression and expansion, it is impossible to show the steady-state cycle processes on a temperature entropy diagram in the conventional way. It is consequently very difficult to perform a reliable thermal analysis of this type of system without resorting to quite complex digital and/or analog computational techniques.

Thermodynamic analysis can show that the Stirling cycle is as efficient theoretically as the Carnot cycle. In practice there are many inefficiencies, but the efficiency of the practical Stirling cycle refrigerator exceeds that of any other type of cryogenic refrigerator.

3.3.2 Vuilleumier Refrigerator

The Vuilleumier refrigerator is in essence a practical Stirling refrigerator in which compression and expansion of the working fluid is effected thermally instead of mechanically. This modification is best illustrated in connection with the Stirling refrigerator configuration of Figure 3-7. The working

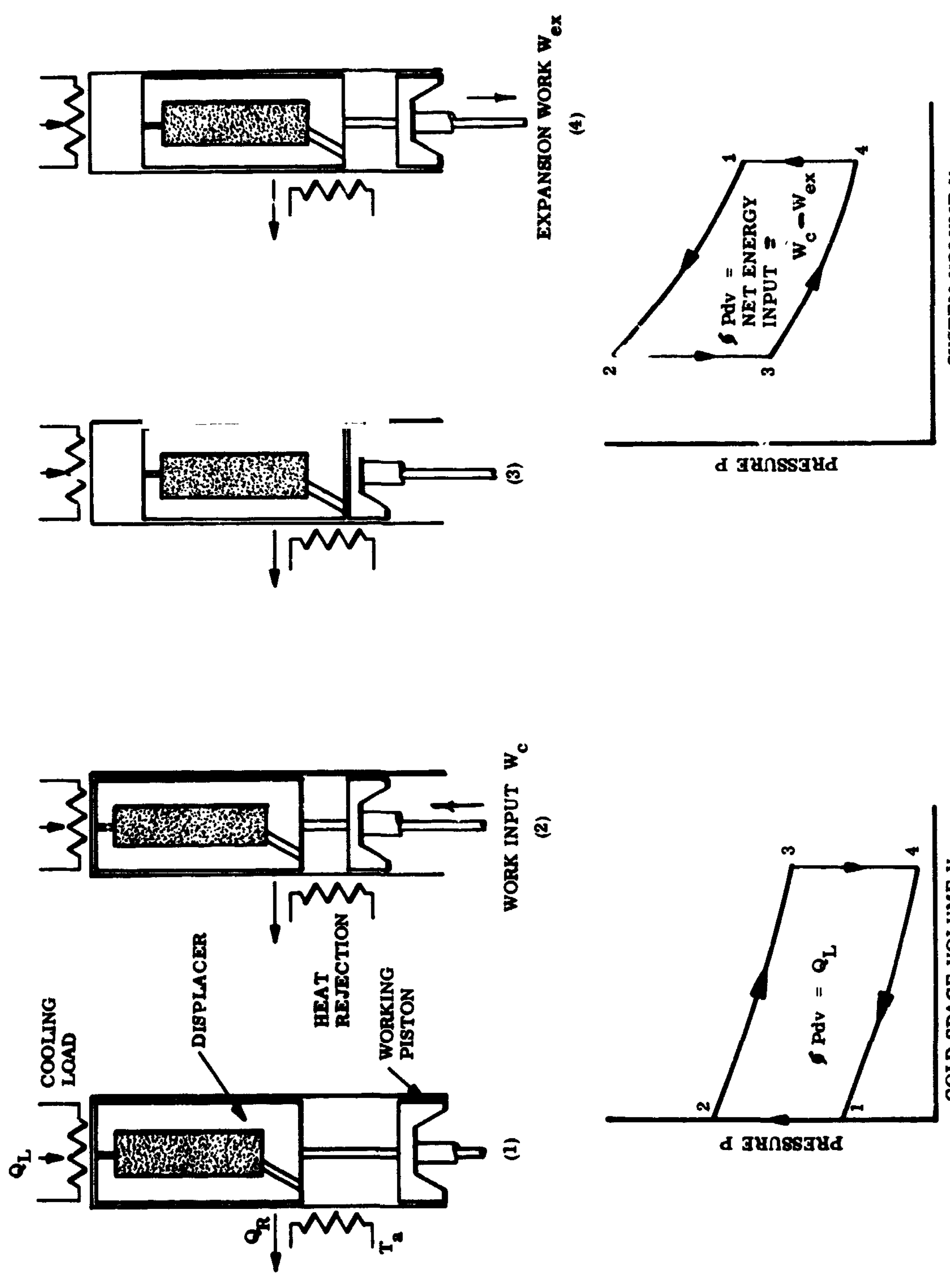

Figure 3-7 The Stirling Refrigerator

piston is removed and is replaced by a thermal compressor/expander consisting of a hot space, ambient space, regenerative heat exchanger, and displacer. The cycle of operations, shown in Figure 3-8, closely parallels that of the Stirling refrigerator. In position 1, the fluid is all in the ambient space. From 1 to 2, the compressor displacer moves from hot to ambient end, causing fluid to move from ambient to hot spaces at constant volume, resulting in an increase in system pressure and hence compression of the fluid remaining in the ambient space. From 2 to 3 the expander displacer is moved to displace this remaining fluid to the cold end. From 3 to 4 the pressure is reduced by displacing fluid from the hot space back to the ambient space, thereby expanding the fluid in the cold space. From 1 to 2 the cold gas is returned to the ambient space by movement of the expander displacer. The heat interactions in the exchangers are similar to those in the Stirling refrigerator. In addition to the load and after-cooler heat eschangers, however, there is also a power heat exchanger required at the hot end through which the energy required to compress the fluid is supplied. This energy will be higher than the actual work of compression since the device is in essence a combined engine and compressor, and thus the supplied energy must also include the necessary rejection heat besides the compressive work.

In practice the intermittent movement of the displacers is achieved by driving both of them from the same crankshaft, but displaced in pahse such that during compression most of the fluid is in the ambient space, and during expansion most of the fluid is in the cold space.

Thermal analysis of the VM refrigerator is very similar to that of the Stirling refrigerator. The VM refrigerator is a constant-volume device, whereas the Stirling refrigerator changes overall volume at a prescribed rate. Otherwise the same general approach is employed.

The fact that the cycle energy for the Veuilleumier refrigerator may be supplied in the form of heat rather than electrical power opens the possibility of utilizing radioisotope or solar collector heat sources directly -- without the intermediate step of conversion to electrical energy.

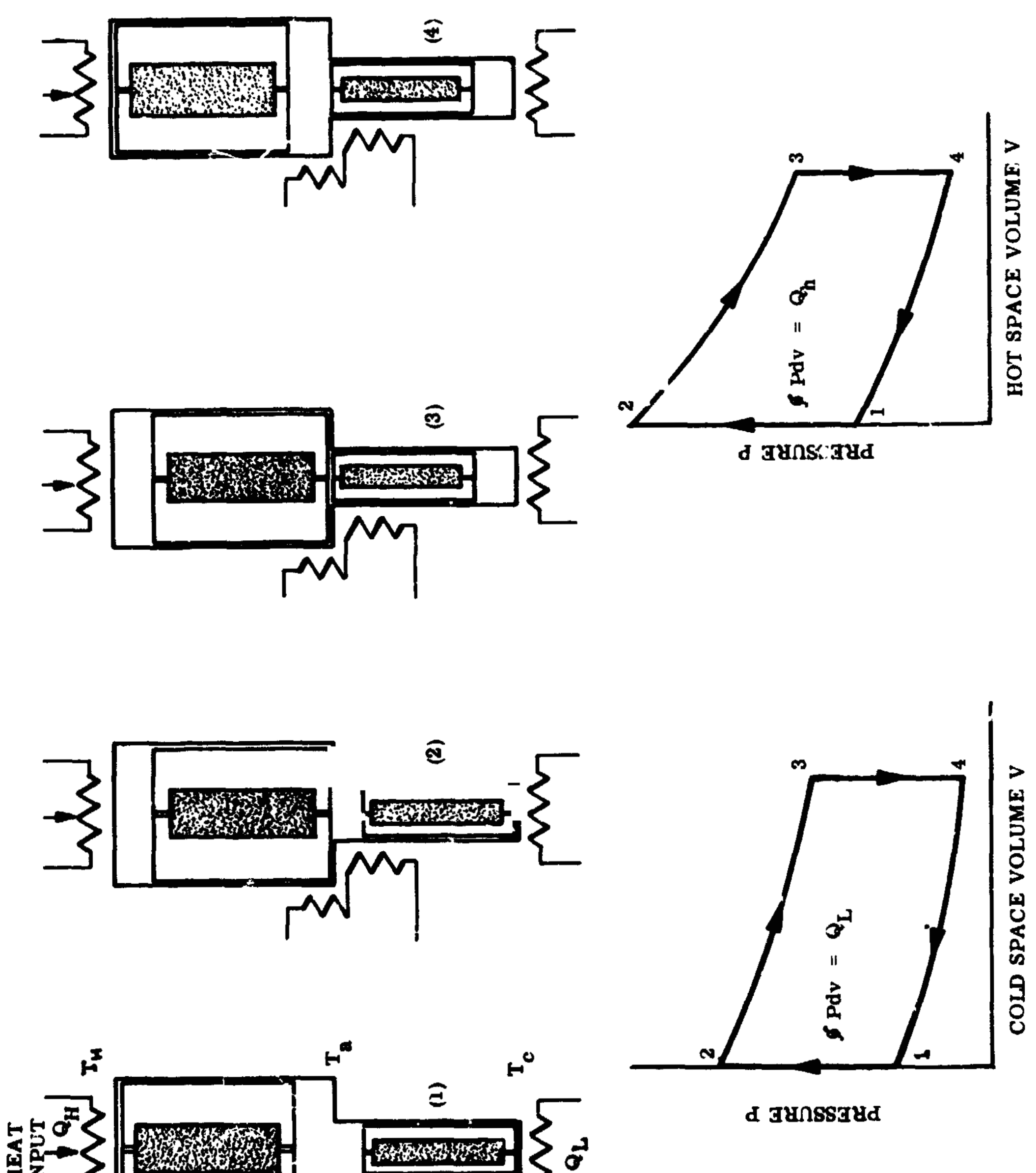

Fig. 3-8 Vuilleumier Cycle

3.3.3 Separable Component Systems (Gifford-McMahon, Solvay, and Taconis)

The practical Stirling and VM refrigerators achieve compression, expansion and heat transfer processes in a single mechanical unit. However, refrigerators can be built which use regenerative exchangers in which the compression, expansion, and heat exchange components are completely separate, if switching valves and surge volumes are used to isolate the time-dependent operation of the exchanger from the operation of the compressor and expander. Valves introduce irreversibility which cause more harm to system efficiency if they occur at the cold end than at the ambient end. It is therefore possible to conceive a refrigeration system in which the main regenerative heat exchanger, load exchanger, and expander operate as one unit, and the compressor as another. Such a system has many practical advantages in that separation of components is achieved, but no low temperature valving is required. Valves and surge tanks are used only at the ambient end. This arrangement admits many areas of design freedom by comparison with the Stirling or VM refrigerator. The compressor and heat exchanger-expander interface requirements are confined to working fluid flow rates and pressures. The type of compressor used to supply the working fluid at these rates and pressure can be selected optimally from all possible types - dynamic, positive displacement, or thermal.

The exchanger-expander unit will be very similar to the cold end of a Stirling or a VM refrigerator. With separation, however, there is greater freedom of choice of displacer drive and means of extracting expansion work. By changing the valve timing, the shape of the P-V diagram can be influenced to some degree.

In recent years the split component systems have gained a great deal of popularity. By separating the expander from the compressor, it is possible to construct a system consisting of a simple, lightweight, compact cooling unit which can be more easily integrated with the load, and a compressor which can be located remotely and connected to the expander with long flexible lines carrying the high- and low-pressure working fluid. Because of this remote location, the compressor design can be optimized for convenience and reliability rather than compactness. Because of the use of valves, the fluid flow is unidirectional and oil separators and filters can be inserted in the gas supply lines, permitting the use of reliable and proven oil-lubricated compressors instead of solid-lubricated compressors.

It was noted above that this type of refrigerator permits many design variations to be considered within the same basic concept. Because of this characteristic and the commercial attractiveness of the system, there are many varieties of split-component refrigerators on the market. These systems are basically the same in that they nearly all use modified hermetically sealed freon compressors, so that the system variations are confined to the method of operating the exchanger-expander unit. However, for reasons of commercial advertising and patent justification -- plus a certain amount of pedantry -- a profusion of names has been applied to the individual expander types. They include: Taconis, Solvay, and Gifford-McMahon, with and without the adjective "modified".

There are two major techniques for operating exchanger-expanders. One technique is exemplified by the basic Solvay process. In Figure 3-9 the expander consists of an expansion piston connected to the working fluid and the inlet and exhaust valves through a regenerator. In position 1, the inlet valve is open and the exhaust closed. The regenerator and other void volumes are filled to the higher pressure. From 1 to 2, the piston moves outward and working fluid enters the cylinder after first being cooled in the regenerator. At point 2, the inlet valve is closed and the fluid pressure falls until the piston reaches its outermost position. At position 3, the exhaust valve is opened and the fluid in the system expands irreversibly to 4. From 4 to 5, the piston moves inward, expelling the working fluid from the system after its first being warmed in the regenerator. At 5, the exhaust valve is closed and the piston continues to move until it reaches the innermost position at 6. At position 6, the inlet valve is opened and the fluid in the system is compressed irreversibly from 6 to 1. The valve timing points 2 and 5 can be selected such that compression and expansion are reversible, i.e., positions 3 and 4, and 6 and 1, are identical. Alternatively, the valve timing can be chosen so that 2 and 3, and 5 and 6, are identical, maximizing the area of the P-V diagram.

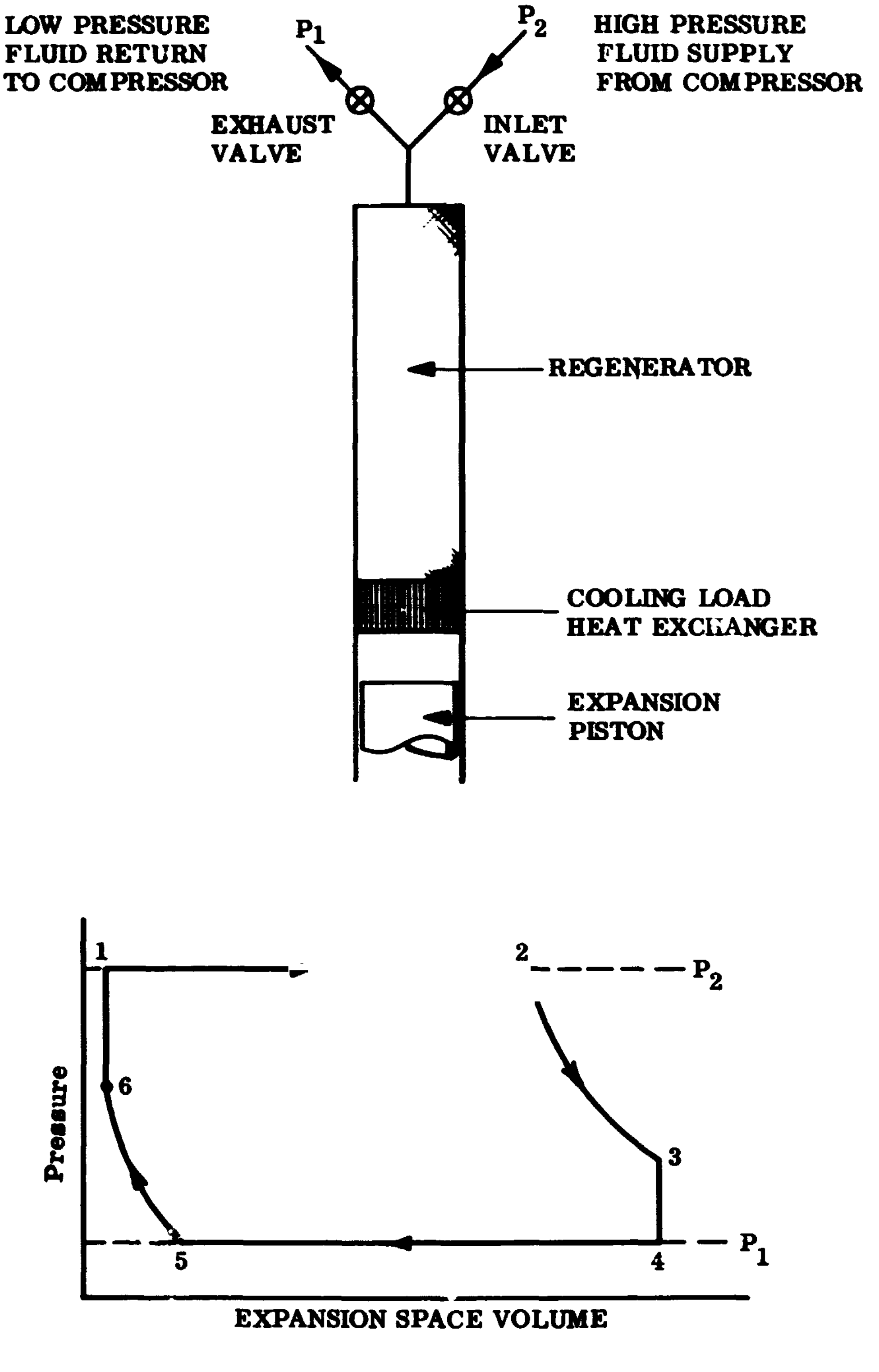

Fig. 3-9 The Solvay Expansion Process

In the Solvay process, the work of expansion can be extracted mechanically by connecting the piston to a crank mechanism. Alternatively, the opposite end of the expansion piston can be operated as a compression piston which consumes the expansion work either as work of compression, or in the form of heat by causing fluid to pass through a throttle valve and heat exchanger.

The other significant expansion technique is the Taconis process (Fig. 3-10). The system consists of a cylinder containing a movable displacer. Working f[illegible] can be introduced or rejected from the system via inlet and exhaust valves which communicate directly with the ambient temperature end of the cylinder, and with the cold end through a regenerative heat exchanger. In position 1, the inlet valve is open, the exhaust valve is closed, and the displacer is at the cold end. The ambient space and the regenerator contain high-pressure working fluid. From 1 to 2, the displacer is moved from the cold end to the ambient end and the cold space fills with high-pressure fluid. At point 2, the inlet valve closes and the displacer continues moving until it reaches the ambient end at 3. The pressure at 3 is lower than at 2 by virtue of the cooling which occurs when fluid is transferred from ambient to cold spaces. At 3, the exhaust valve is opened and the fluid expands irreversibly to 4. At point 4, the displacer is moved back towards the cold end, expelling low-pressure fluid, until the exhaust valve is closed at 5. From 5 to 6, the fluid is compressed by displacement from cold to ambient spaces. At 6, the displacer is at the cold end and the inlet valve is opened, compressing the gas in the ambient space irreversibly to point 1. As in the case of the Solvay cycle, the valve timing points 2 and 5 can be varied to maximize either cycle efficiency or unit performance.

In the Taconis process, the work of expansion is extracted from the system by a somewhat devious route. When the inlet valve is opened, the working fluid performs work as it flows into the expander to compress the fluid in the ambient space. When this fluid is displaced to the cold end, the heat of compression is deposited in the regenerator. During the exhaust phase this heat is picked up by the exhausting fluid and removed from the system.

The variations upon the Solvay and Taconis process usually involve valve timing method of operation of displacer or piston and geometric configuration.

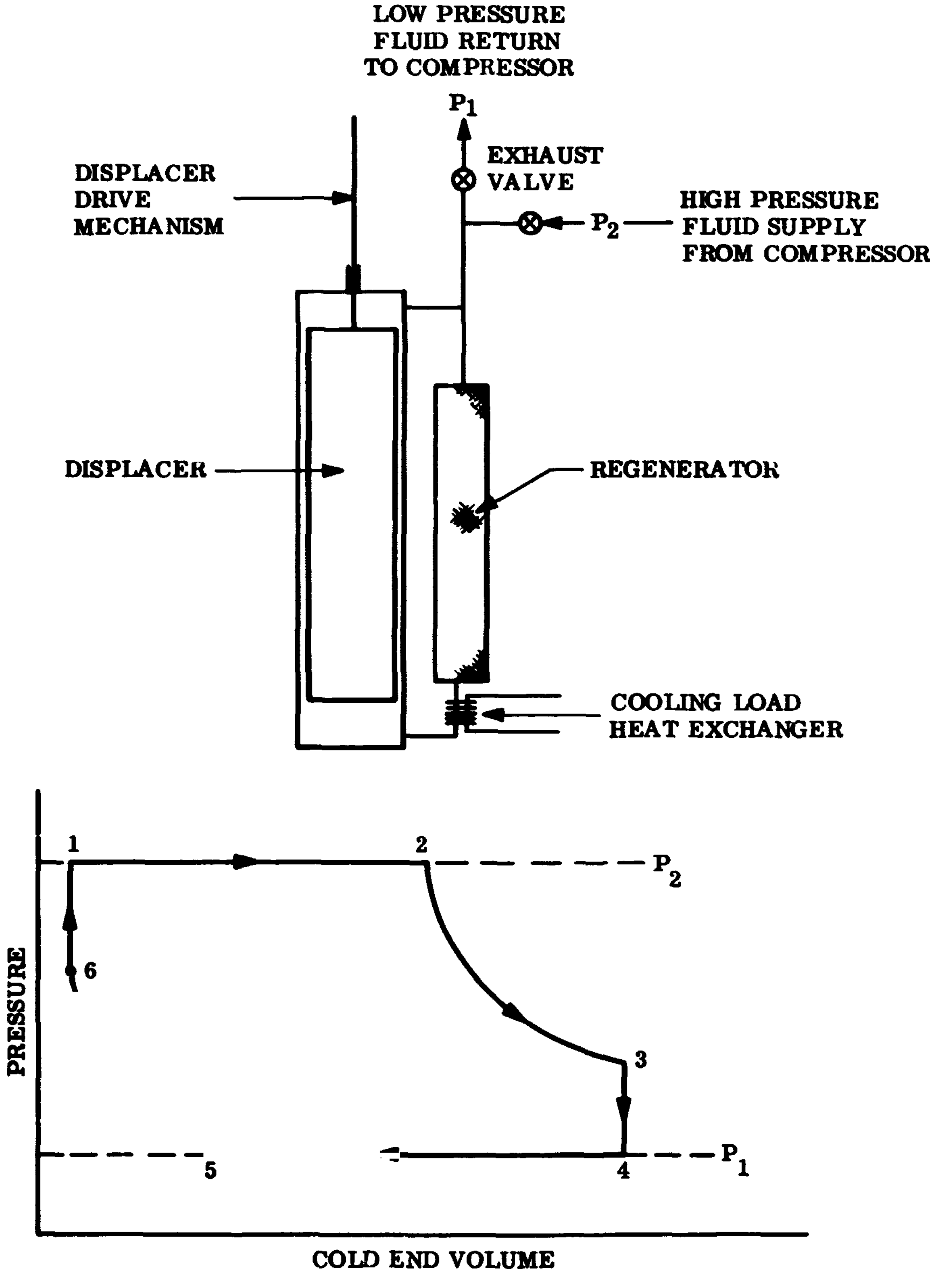

Fig. 3-10 The Taconis Expansion Process

The thermal analysis of the Taconis process is very similar to that of the Stirling and VM refrigerator in that remarks relating to the complex (differential) and simplified (integral) analysis approaches apply.

In the case of the Taconis expander, the boundary conditions differ in that the system is open and the condition of constant mass is replaced by the valve timing and flow rate equations, and the specified inlet and exhaust fluid pressures. The work required by the overall cycle comprising compressor and exchanger-expander is equal to the work needed to compress the fluid consumed by the expander.

The Gifford-McMahon cycle is essentially a version of the Taconis cycle, in which the regenerators are located inside the displacer to minimize the external piping.

These systems have been primarily developed utilizing large ground base compressor systems without attempts at weight reduction. Recently, however, a few units have been developed utilizing dry lubricated compressors in which the size and weight were minimized for airborne use.

3.3.4 Brayton Refrigerator

A practical Brayton-cycle refrigerator is shown in Figure 3-11. Gas is compressed with some increase in entropy from 1 to 2. The heat of compression is rejected to the ambient-temperature heat sink in an after-cooler from 2 to 3. The high-pressure fluid is cooled from 3 to 4 in the main heat exchanger. The pressure at 4 is slightly less than at 2, due to the flow losses in the two heat exchangers. The fluid is expanded from 4 to 5 with some entropy increase, and is then warmed to 6 by passage through the load heat exchanger. The fluid is warmed from 6 to 1 in the main heat exchanger as it returns to the inlet side of the compressor. The pressure at 4 is slightly higher than at 1 because of pressure losses in the heat exchangers.

Analysis of the cycle is performed by selecting high and low fluid pressures, load and sink temperatures, and either choosing mass flow rates and component dimensions from which efficiencies can be determined (as described in Section 4),

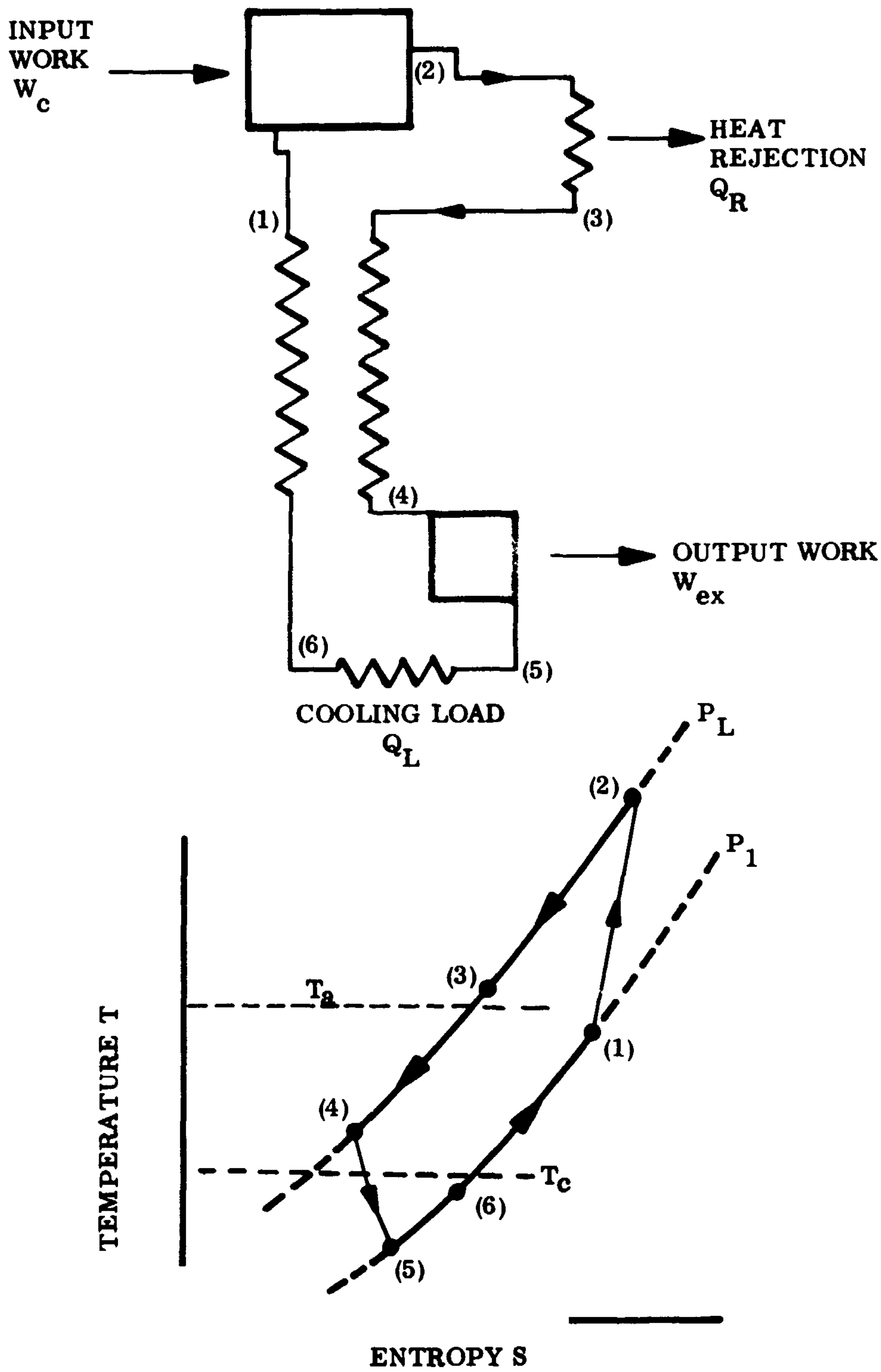

Fig. 3-11 The Reverse Brayton Cycle

or assuming efficiencies from which required component dimensions may be found in a separate calculation. The analysis begins by assuming a value for T, and hence, h_2 is found from the assumed or calculated compressor isentropic efficiency,

$$\eta_{isc} = \frac{h\,(P_2, S_1) - h_1}{h_2 - h_1}$$

T_2 is found from h_2 and P_c .

$$T_2 = T\,(P_2,\ h_2)$$

P_3 is found from the assumed or calculated after-cooler loss coefficient K_a

$$P_3 = P_2 - \frac{P_2 + P_3}{2} \quad K_a$$

h_3 is found from the assumed or calculated after-cooler effectiveness ϵ_a , T_2, and the sink temperature T_a

$$\epsilon_a = \frac{h_2 - h_3}{h_2 - h\,(P_3, T_a)}$$

T_3 is found from the fluid equation of state

$$T_3 = T\,(P_3,\ h_3)$$

h_4 is found from the assumed or calculated main heat exchanger effectiveness, ϵ_m

$$\epsilon_m = \frac{h_3 - h_4}{h_3 - h_6}$$

P_4 is found from the assumed or calculated main heat exchanger high-pressure side pressure loss coefficient, K_{mh}

$$P_4 = P_3 - \frac{(P_3 + P_4\ )}{2} \ K_{mh}$$

T_4 is found from the fluid equation of state

$$T_4 = T(h_4, P_4)$$

P_6 is found from the assumed or calculated load heat exchanger pressure loss coefficient, K_L

$$P_6 = P_5 - \left[\frac{P_6 + P_5}{2}\right] K_L$$

h_5 is found from the assumed or calculated expander isentropic efficiency, η_{isc}.

$$\eta_{isc} = \frac{h_4 - h_5}{h_4 - h\,(P_5, S_4)}$$

T_5 is found from the fluid equation of state

$$T_5 = T\,(P_5, h_5)$$

h_6 is found from the assumed or calculated load heat exchanger efficiency, ϵ_e

$$\epsilon_e = \frac{h_6 - h_5}{h(P_6, T_c) - h_5}$$

T_6 is found from the fluid equation of state

$$T_6 = T(P_6, h_6)$$

P_1 is found from the assumed or calculated main heat exchanger low-pressure side loss coefficient, K_{me}

$$P_1 = P_6 - \left[\frac{P_1 + P_6}{2}\right] K_{me}$$

h_1 is found from the assumed or calculated main heat exchanger effectiveness ϵ_m

$$\epsilon_m = \frac{h_1 - h_6}{h_3 - h_6}$$

T_1 is found from the fluid equation of state

$$T_1 = T\,(P_1, h_1)$$

The calculated values of P_1 and T_1 will not, in general, agree with the assumed values. Adjustments are made in the assumed expander pressure ratio and the cycle is recalculated using the new T_1. The process is repeated until a consistent set of figures is obtained. If component efficiencies rather than dimensions were assumed, then the component sizes and flow rates required to provide this performance must then be determined.

The cooling capacity of the refrigerator, q, is the heat absorbed by the load heat exchanger.

$$q_c = \dot{m} \, [h_6 - h_5]$$

The power required by the refrigerator, W, is the work of compression

$$W = \dot{m} \, [h_2 - h_1]$$

It is apparent that the analysis of continuous flow Brayton-cycle refrigerators is relatively straightforward. Performance data can be prepared quite readily as a function of component efficiencies, and the results of two extensive parametric studies are reported in the literature (21) (22).

This system has been developed in small scale versions employing high-speed turbomachinery operating on gas bearings. The gas bearings experience negligible wear since there are no rubbing surfaces. Experience with these machines is very limited in the small cooling ranges, but an operating time of 30,000 hours has been predicted by some investigators. At low flow rates, the inefficiency of the turbomachinery results in a relatively low overall system efficiency. Also, the high rotation speeds of the compressor require a high-frequency power supply to operate the system.

3.3.5 Claude Refrigerator

As the operating temperature of the Brayton refrigerator is lowered, point 5 (Fig. 3-11) will enter the two-phase region of the working fluid, and the fluid will leave the expander as a two-phase mixture. Up to the present time, it has not been considered good engineering practice to permit expanders to operate in the two-phase region because of possible mechanical damage to the expander.

For refrigeration at temperatures within the two-phase region of the working fluid, it has therefore become accepted practice to perform the expansion process isenthalpically through a throttle valve as in the Joule-Thomson cycle, rather than in an expansion engine.

As explained in Section 3.3.6, this process will not produce net refrigeration unless the value of $(\partial h/\partial P)_T$ is negative at the effective sink temperature. For helium, hydrogen, and neon, this means that the effective sink temperature must be reduced by use of an auxiliary heat exchanger. The Claude cycle is effectively a Joule-Thomson cycle in which the effective sink temperature is lowered by a Brayton-cycle refrigerator. It is designed so that the two systems share the same working fluids.

Figure 3-12 shows a practical Claude cycle. The cycle closely resembles the Brayton and Joule-Thomson cycles, Figures 3-11 and 3-13; and the cycle description is similar. The difference is that upon reaching point 4, the flow divides and a portion of the flow is expanded as in a Brayton refrigerator, and is returned to the compressor via a combined load and precooling exchanger, and the main exchangers. The remaining portion of the stream at 4 is passed through the other side of the load/precooling refrigerator and is cooled to T_{4a}. The system $4 - 4_a - 4_b = 5_a - 5_b - 5 - 6$ is a standard Joule-Thomson refrigerator and functions like the system $3 - 4 - 5 - 6 - 1$ in Figure 3-13. The fluid is cooled in the main Joule-Thomson heat exchanger, 4a to 4b, after which it is expanded isenthalpically to 5a. From 5a to 5b, the fluid is warmed in the Joule-Thomson load heat exchanger and then is reheated in the main exchanger to point 5 where the two flows are united and pass back to the compressor via the load/precooling exchanger and main exchanger.

It can be seen that the Claude cycle is essentially more complex and less efficient than the Brayton cycle, inasmuch as a Joule-Thomson refrigerator has been added, and that because of this, the cooling effect at the load is produced by isenthalpic expansion, which produces a greater increase in entropy than even the most inefficient expander. These implications are considered desirable if a two-phase mixture in the expander is to be avoided. Recently a reciprocating expander has been operated successfully in the two-phase

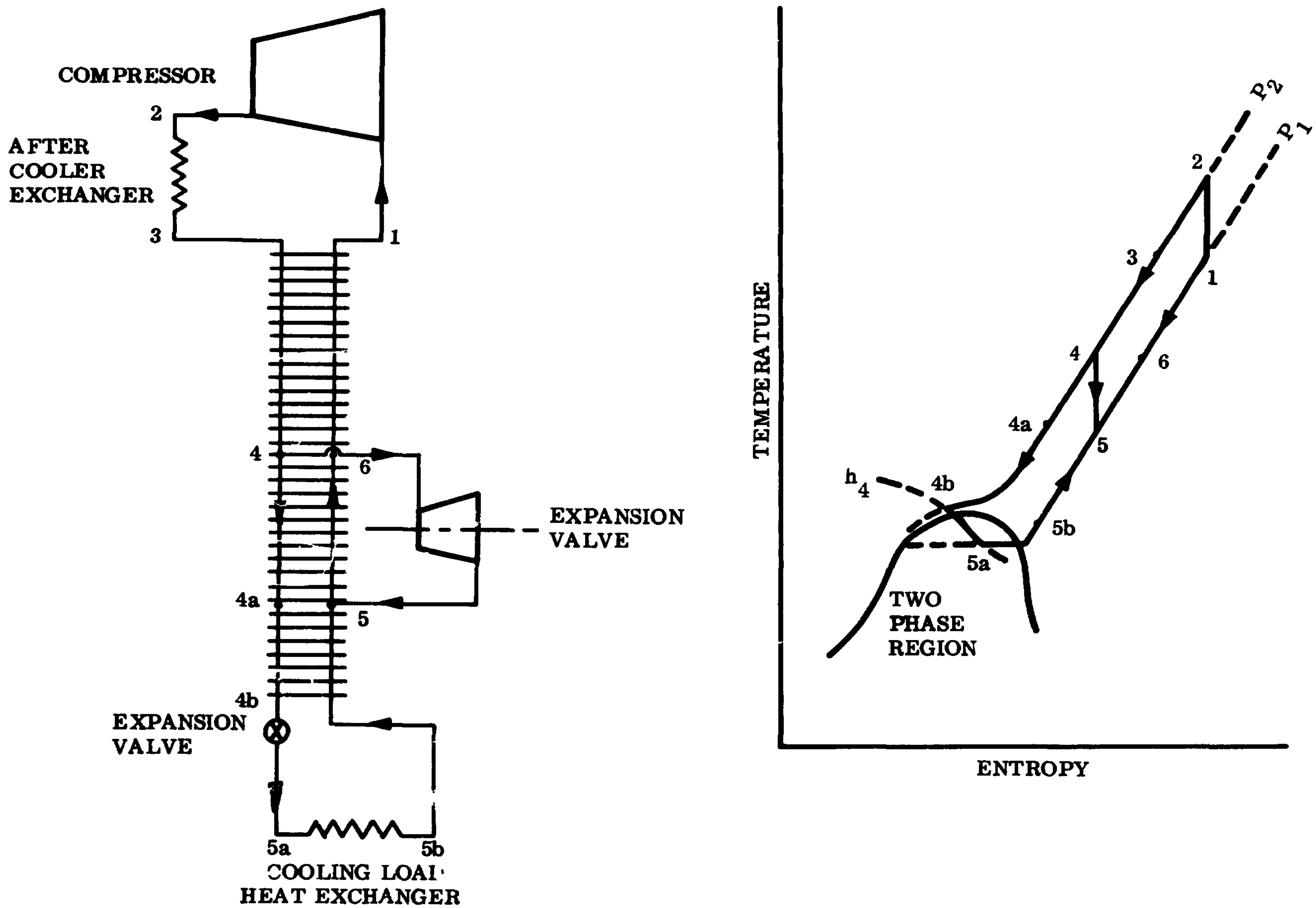

Fig. 3-12 The Claude Refrigeration Cycle

tion (3-24). If it proves possible to develop expander technology to the point where such expanders become generally available, the technical advantage of the Claude cycle would be eliminated.

The Claude cycle can be analyzed in a manner analogous to the Brayton-cycle and Joule-Thomson cycle analyses. For the temperature range of interest to this program, 20°K - 110°K, the possible working fluids are helium, neon, hydrogen, and nitrogen. Because of the low condensation temperature of helium, there is no necessity for adding a Joule-Thomson stage to a helium Brayton refrigerator. Neon or hydrogen Claude systems would be appropriate for the 20°K - 30°K range. A Claude system using nitrogen could be used in the 75°K - 85°K range, where its efficiency would be higher than that of a single-stage Joule-Thomson system.

An extensive parametric study of a helium Claude cycle refrigerator for use in the temperature range of 4.2K is presented by Muhlenhaupt and Strobridge[22].

3.3.6 The Joule-Thomson Refrigerator

A practical Joule-Thomson refrigerator is shown in Figure 3-13. The cycle is identical to the Brayton cycle of Figure 3-11 except for one important modification. The expansion process, 4 to 5, is accomplished by isenthalpic expansion through a throttling valve rather than by expansion in a work-producing device. Since no expansion work is produced, no heat addition is required in the load exchanger to replenish the lost internal energy of the working fluid. The cycle produces refrigeration by virtue of a useful side effect of non-ideal behavior at the sink temperature. The cooling effect is given by

$$q_c = \dot{m}\,[h_6 - h_5]$$
$$= \dot{m}\,[h_6 - h_4]$$

A heat balance on the main heat exchanger yields

$$h_1 - h_6 = h_3 - h_4$$

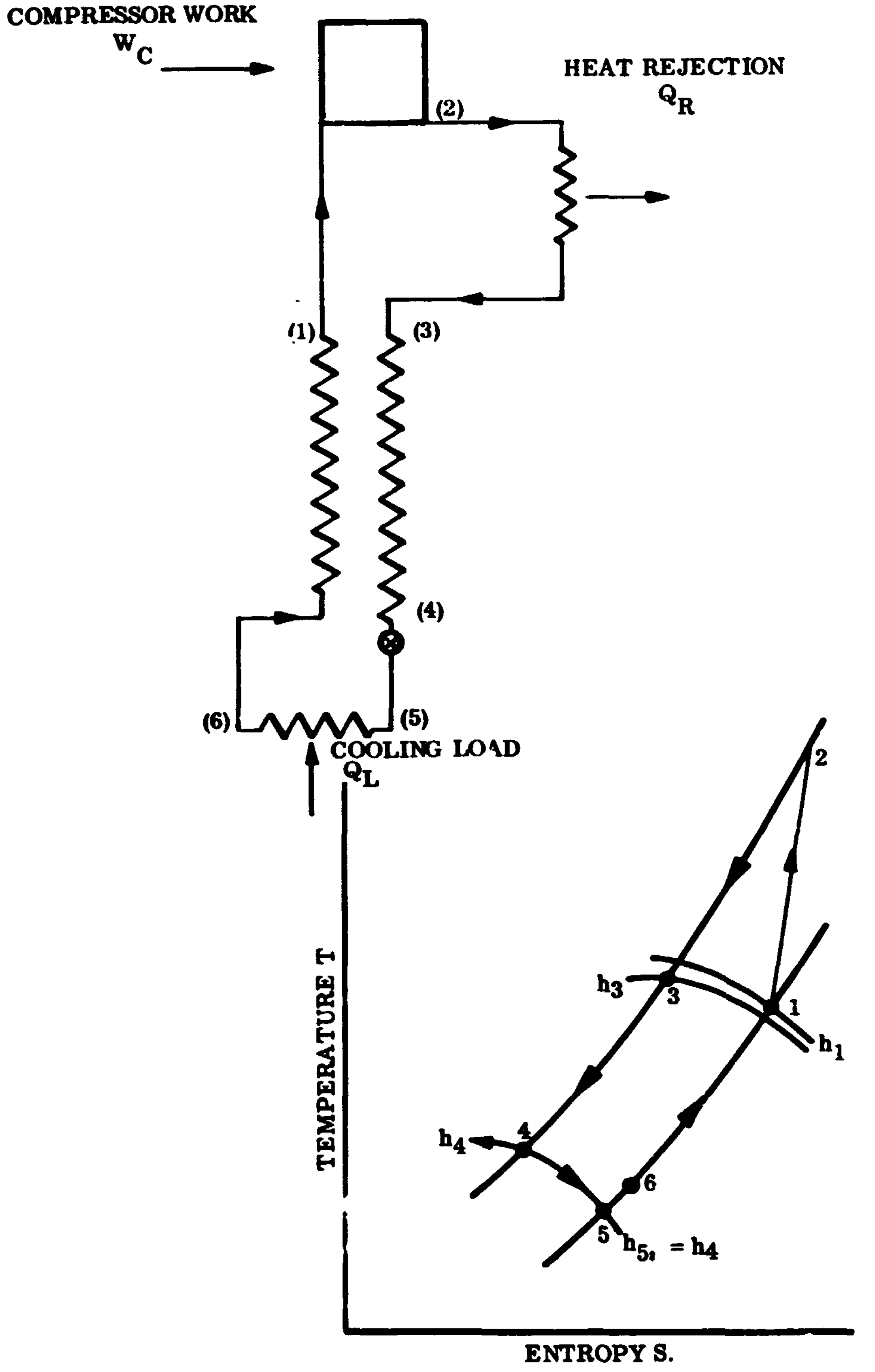

Fig. 3-13 Joule-Thomson Cycle

Hence

$$q_c = \dot{m} \quad h_1 - h_3$$

For q_c to be positive $(\partial h/\partial p)_{T_3}$ must be negative.

With a 100 percent efficient main heat exchanger $T_1 = T_3$

and the maximum value of q_c is given by

$$q_c(\max) = \dot{m} \left[h(P_1 T_3) - h(P_2, T_3)\right]$$

With less than 100 percent efficiency, q_c is given by

$$q_c = \dot{m} \left[h(P_1, T_1) - h(P_2, T_3)\right]$$

As T_1 is reduced due to less efficient heat exchange, h $(P_1 T_2)$ will decrease and q_c will eventually become zero. The performance of a Joule-Thomson system is therefore limited by the sign and magnitude of $(\partial h/\partial P)_{T_3}$, and by the ability of the main heat exchanger to permit utilization of this effect.

For the present application only nitrogen has both a negative value of $(\partial h/\partial P)_{T_3}$ at normal ambient temperature and is still a vapor in the temperature range of interest. Those fluids which condense at temperatures lower than nitrogen - neon, hydrogen and helium - can be used for very low temperature Joule-Thomson refrigerators if T_3 is reduced to a point where $(\partial h/\partial P)_{T_3}$ is negative. This can be done by precooling the fluid using another type of refrigeration system. Thus, Joule-Thomson systems can be used in double or triple cascade to obtain cooling in the range of liquid hydrogen or liquid helium temperatures.

The cooling capacity, q_c, of a single stage Joule-Thomson system is given by

$$q_c = \dot{m} (h_1 - h_3)$$

The power required, W, is given by

$$W = m\left(h_2 - h_3\right)$$

The significant parameters for assessing the performance of a Joule-Thomson refrigerator are the compression ratio, the gas properties at the warm end and the heat exchanger effectiveness. Dean and Mann [20] present values of W/q_c as a function of these quantities for Joule-Thomson refrigerators using nitrogen, hydrogen and helium as working fluid.

The irreversibility of the expansion process makes the Joule-Thomson cycle inherently less efficient than other cycles, and the required high operating pressure of the compressor may severely limit the potential for long life. These factors make the J-T cycle generally unattractive for long term space flight usage.

3.4 DEVELOPMENT STATUS OF REFRIGERATORS

Table 3-1 presents a brief summary of the development status of the various cycles discussed.

3.5 SUMMARY OF PERFORMANCE DATA FOR VARIOUS CYCLES

In this section the weight, size and power requirements of the various cycles considered is presented. In general, the characteristics are included for cooling in the range of 5-100 watts at $20^\circ K$ to $110^\circ K$ which is the range of parameters specified for the study. Additional data is included outside these parameters, both for the purpose of providing better curve fits in the primary range of interest, and to broaden the scope of use for the handbook. A partial list of the areas of application of cryogenic cooling, and the general range of parameters is shown in Table 3-2.

The performance curves which follow are primarily a result of an extensive literature survey which was conducted during the contractual period, in

Table 3-1

DEVELOPMENT STATUS OF CLOSED CYCLE CRYOGENIC REFRIGERATORS

SYSTEM SYSTEM	MAINTENANCE FREE OPERATING LIFE HRS	NUMBER OF UNITS MANUFACTURED	DEVELOPMENT STATUS	PRIMARY MANUFACTURERS
Stirling	1000	< 2000	Fully developed and operational for 6 years in aircraft. Mose efficient thermally. Lightweignt, small volume. Applicable to space flight with minor modifications	U. S. Philips Hughes Aircraft Malaker
Vuilleumier	1000 hrs. demonstrated to date	9	Recently developed, no operational experience, little life test data. Utilizes heat source directly for power. Efficiency approaching that of Stirling, significant development activity for space usage.	Phillips Laboratories Hughes Aircraft Stirling Electronics Garrett AiResearch
Solvay, Taconis Gifford-McMahon	5000	< 400	Fully developed system operational on aircraft for several years. Recently developed for airborne use utilizing dry-lube compressor. Longest maintenance free operating life. Efficiency substantially below Stirling cycle.	Cryogenic Technology, Inc. Air Products U. S. Phillips Cryomech
Joule-Thomson	300	<2000	Fully developed, extensively used on aircraft for cooling infrared systems for ≈6 years. Efficiency of system among the lowest. Does not appear to have potential for long life.	Garrett AiResearch Air Products Hughes Aircraft
Brayton	≈ 1000	2	Limited development in 77°K versions. Components have been developed for lower temperature usage, but have not been run as a complete system. Limited development activity at this time. May have potential for long life because of gas lubricated bearings.	Garrett AiResearch General Electric Arthur D. Little

which the performance data of various units was obtained. The operating characteristics of specific units which exist, or have been proposed, are tabulated in Tables 3-3 to 3-8. In curve fitting the data from existing units, the intended use of the unit was taken into consideration, since it is the purpose of this study to present data for units applicable to space-flight in which weight, volume, and required input power are at a premium. Data for units which are intended for application where weight and volume are not important were modified, where possible, for space use or discarded in obtaining the curves which follow. Sources of data utilized to make the curve fits follow.

1. Operating data on existing units intended for space-flight or aircraft use.
2. Predicted performance characteristics for space-flight systems from detailed studies by potential manufacturers.
3. Characteristics predicted by LMSC based upon more general data, on individual components; for example, component weights were added for some cycles to obtain system weights.

In general, all three techniques were utilized to obtain the performance curves, but where possible the methods were selected in order of preference. Consideration of the maturity of the development of the cycles was also made. For example, the Vuilleumier and small Brayton cycle machines have not reached the same state of maturity in their development as the Stirling and Gifford-McMahon units. This consideration led to some instances where a curve fit through the best points for the newer cycles was made while for the more mature units a least squares fit was made. The individual data points are not shown on the cycle performance curves for ease of reading. In addition, Tables 3-3 to 3-8 show the characteristics of existing units and also includes the tabulated data of the performance parameters.

TABLE 3-2

AREAS OF APPLICATION OF
CRYOGENIC COOLING

Application	Temp. Reqmts. °K	Cooling Reqmts. W
Extra terrestrial propellant reliquefaction (contract application)	20 to 110	5 to 100
Masers	2 to 5	≈ 1
Parametric amplifiers	20 to 78	1 to 2
Superconducting circuits	4.2 to 12	0.5 to 2
Superconducinng applications	2 to 16	> 1
γ-ray detector devices	77 to 120	0.2 to 1
Infrared devices	4.2 to 77	0.1 to 2

	Manufacturer	Malaker Corp.	Malaker Corp.	Malaker Corp.	Malaker Corp.
	Trade Name	Cryomite	Cryomite	Cryomite	Cryomite
	Model	Mark VII-C	Mark XIV-A	Mark VII-R	Mark XX
	I.D. Number	1	2	3	4
	Refrigeration Range	17.5 - 80°K	44 - 100°K	40 - 125°K	40 - 120°K
	Cycle	Stirling	Stirling	Stirling	Stirling
	Working Fluid	Helium	Helium	Helium	Helium
	High Pressure	NI	NI	NI	NI
	Low Pressure	17 atm Fill	NI	NI	NI
	Minimum Temp	17.5°K	44°K	40°K	40°K
	Cool-Down Time	8 min	7 min	3.8 min	7.4 min
	Expander RPM	NI	NI	NI	NI
	Volts-Phase-Frequency	208 - 3/4 - 400/60	208 - 3 - 400	208 - 3 - 400	208 - 3 - 400
	Cooling Means	Air or Water	Air	Air	Air or Liquid
	Ambient Temp Reqmts				
	Required Attitude	Any	Any	Any	Any
	Cryostat Dimensions	4.8"D x 11.5"L	2.9"D x 13"L	6 1/2"D x 23 1/2"L	19" x 18" x 15 1/2"
	Compressor Dimensions				
	System Volume	209 in.^{3}	86 in.^{3}	781 in.^{3}	1500 in.^{3}
	System Weight	15.5 lb	5.5 lb	40 lb	65 lb
	MTBF	40,000 hr	40,000 hr	40,000 hr	40,000 hr
	Maintenance Interval	1,000 hr	1,000 hr	1,000 hr	1,000 hr
	System Cost	$5,195	$9,000	$17,500	$24,000
15°K	Refrigeration				
	Power Input				
	COP				
	% Carnot				
	Lb/Watt				
	In.^{3}/Watt				
20°K	Refrigeration	1 watt			
	Power Input	480W			
	COP	.00208			
	% Carnot Eff.	2.92%			
	Lb/Watt	15.5			
	In.^{3}/Watt	209			
77°K	Refrigeration	17.7W	2.8W	60W	110W
	Power Input	395W	108W	1220W	1990W
	COP	.0448	.0259	.0492	.0553
	% Carnot	13%	7.5%	14.3%	16%
	Lb/Watt	0.876	1.97	0.667	0.591
	In.^{3}/Watt	11.81	30.8	13.0	13.6
110°K	Refrigeration	23.7	5W	90W	164W
	Power Input	395	96W	1220W	1860W
	COP	.073	.0522	.0738	.0883
	% Carnot	12.6%	8.25%	11.7%	14%
	Lb/Watt	0.654	1.10	0.445	0.396
	In.^{3}/Watt	8.8	17.2	8.7	9.15

FOLDOUT FRAME 2

TABLE 3-3

EXISTING STIRLING CYCLE REFRI

	Phillips Lab.	Phillips Lab.	Hughes Aircraft	Phillips Lab.	Malaker Corp.	Malaker Co
	None	Prototype	Prototype	Cryogem	Cryomite	Cryomite
	A-20	X-20		42100	Mark XV	Mark XVII-
	5	6	7	1- S	2- S	3-S
	12 - 300°K	12 - 300°K	45°K up	20°K up	54 - 100°K	77°K
	Stirling	Stirling	Stirling	Stirling	Stirling	Stirling
	Helium	Helium	Helium	Helium	Helium	Helium
	427 psia	NI	NI	125 psig	NI	NI
		NI	NI	NI	NI	NI
	12°K	12°K	45°K	20°K	54°K	54°K
	40 min	15 min	3 min	12 min	8 min	9 min
	1450 - 1750	1750	NI			
	400 - 3 - 50/60	2000 VA - 3 - 50/60	115 - 3 - 400	208 - 3 - 400	24V DC	24V DC
	190 gal/hr H_2O	Air or Liquid	Air or Liquid	Air	Air	Air
			-55 to +71°C			
		Any (g = 0)	Any	Any	Any	Any
1/2"	43.5" x 37.4" x 19.7"	4"D x 7.5"L	8" x 6" x 6"	5.87" x 4.81" x 10.9"	2.9"D x 12.2"L	3.2"D x L
		18.5" x 13.8" x 13"				
	15,000 in.^{3}			119 in.^{3}	66 in.^{3}	88 in.^{3}
	660 lb	112 lb	10 lb	12 lb	5 lb	13 lb
		NI	NI	1000	40,000 hr	40,000 hr
	500 hr	4,000 hr	500 hr		1000 hr	1000 hr
		NI	NI	NI	$9,000	
	20W	5W				
	8300W	1750W				
	.0024	.00286				
	4.5%	5.4%				
	33.0	22.4				
	100W	10W		1W @ 25°K		
	8300W	1750W		350		
	.0121	.00572		.0029		
	17%	8%		3.2%		
	6.60	11.2		12		
				119		
		36W	14W		1W	4.3W
		1750W	500W		29.5W	280W
		.0206	.0280		.034	.015
		6%	8.1%		9.9%	4.35%
		3.12	0.715		5	3.02
					66	20.4
		NI			1.9W	
					29.5	
					.064	
					11%	
					2.63	
					34.7	

TABLE 3-3

EXISTING STIRLING CYCLE REFRIGERATORS

FOLDOUT FRAME 3

ips Lab.	Malaker Corp.	Malaker Corp.	Malaker Corp.	Phillips Lab.	Phillips Lab.
m	Cryomite	Cryomite		Prototype	Micro-Cryogen
	Mark XV	Mark XVII-1	Mark XVI-3		
	2- S	3-S	4-S	5-S	6- S
up	54 - 100°K	77°K	77 - 110°K	7 - 300°K	40-300°K
	Stirling	Stirling	Stirling	Stirling	Stirling
m	Helium	Helium	Helium	Helium	Helium
	NI	NI	NI	6 atm	8.5 ATM
	NI	NI	NI	3.7 atm	4.5 ATM
	54°K	54°K	77°K	7°K	40°K
n	8 min	9 min	7 min	15 min	3 min
				600 RPM	1800 RPM
3 - 400	24V DC	24V DC	24V DC	320-3-60	24 VDC
	Air	Air	Air	Water	Air or Liquid -55°C to 75°C
	Any	Any	Any	Any	Any
x 4.81" x 10.9"	2.9"D x 12.2"L	3.2"D x 14"L	3.5"D x 15.5"L	6" x 12" x 24"	4" x 4" x 8"
in.³	66 in.³	88 in.³	137 in.³		128 in³
	5 lb	13 lb	10 lb	35 lb	3 lb
	40,000 hr	40,000 hr	40,000 hr		
	1000 hr	1000 hr	1000 hr		250 to 500 Hr
	$9,000				$4,000 to $6,500
5°K				1.3W (est.)	
				700W	
				.00186	
				26.9	
	1W	4.3W	8.2W		1.5W
	29.5W	280W	208W		90W
	.034	.015	.039		.0167
	9.9%	4.35%	11.3%		4.8%
	5	3.02	1.22		2.0
	66	20.4	16.7		95.5
	1.9W		12.5W		
	29.5		195W		
	.064		.064		
	11%		11.1%		
	2.63		0.8		
	34.7		11.0		

PRECEDING PAGE BLANK NOT FILMED

FOLDOUT FRAME I

	Manufacturer	Hughes Aircraft	Hughes Aircraft	Hughes Aircraft
	Trade Name			
	Model	Prototype	Prototype	Prototype
	I.D. Number	11	12	13
	Refrigeration Range	≈ 77°K	≈ 77°K	15K - 75°K
	Cycle	Vuilleumier	Vuilleumier	Vuilleumier
	Working Fluid	Helium	Helium	Helium
	High Pressure		600 psi	
	Low Pressure			
	Minimum Temp			
	Cool-Down Time	30 min	10 min	30 min
	Expander RPM		600	
	Volts-Phase-Frequency	28 VDC	28 VDC	28 VDC
	Cooling Means	Air	Air	Liquid
	Ambient Temp Reqmts		-55°C to 71°C	
	Required Attitude	Any	Any	Any
	Cryostat Dimensions	7.15 x 7.15 x 8	6.5 x 5.7 x 5.1	10.5 x 13.6 x 7.8
	Compressor Dimensions			
	System Volume	410 in.^{3}	190 in.^{3}	1,110 in.^{3}
	System Weight		5.75 lb	
	MTBF		5,000 hr goal	
	Maintenance Interval	3,000 hr goal	1,000 hr	10,000 hr goal
Near 20°K	Refrigeration			0.15W at 15°K
	Power Input			370W
	COP			.000405
	% Carnot			0.77%
	Lb/Watt			
	In.^{3}/Watt			16,700
77°K	Refrigeration	0.6W	1.5W	
	Power Input	60W	200W	
	COP	.01	.0075	
	% Carnot	2.9%	2.2%	
	Lb/Watt		3.83	
	In.^{3}/Watt	683	127	

(1) Same units at two different operating conditions
(2) Based on 350°K ambient

FOLDOUT FRAME 2

TABLE 3-4

EXISTING VUILLEUMIER PROTOTYPE REFRIGERATORS (SMALL UNITS)

...hes Aircraft	Hughes Aircraft	Hughes Aircraft	Phillips Lab.	Phillips Lab.	Phillips L...
...totype	Prototype	Prototype X447550-100	Prototype	Prototype (1)	Prototype (...
	14	15	16	17	18
... - 75°K	25 - 75°K	30 - 75°K	77 - 200°K	77°K	77°K
...illeumier	Vuilleumier	Vuilleumier	Vuilleumier	Vuilleumier	Vuilleumie...
...lium	Helium	Helium	Helium	Helium	Helium
		400 psi	23 atm	30 atm	40 atm
	16°K		70°K		
min	30 min	30 min			
		240	450	600	600
VDC	115 - 3 - 400	28 VDC			
...quid	Liquid	Liquid	Air	Air	Air
...y	Any	Any	Any	Any	Any
....5 x 13.6 x 7.8	7.5 x 9.5 x 10"	10.5 x 13.6 x 7.8"	12 x 8 x 6	16.5 x 7.1 x 7.1"	16.5 x 7.1...
110 in.^{3}	712 in.^{3}	600 in.^{3}	580 in.^{3}	820 in.^{3}	820 in.^{3}
		18.1 lb	10.3 lb	15 lb	15 lb
...000 hr goal	1,000 hr	10,000 hr goal	800 hrs + demonstrated		
...5W at 15°K	2W at 25°K	0.4W at 20°K			
...0W	1,200W	550W			
...00405	.00167	.00073			
...77%	1.84	0.66%			
		45			
...,700	365	27[illegible] (2nd Stage)			
		6W	0.5W	1W	2W
		500W	70W	120W	191W
		(1st Stage)	.00715	.00833	.105
			2.07%	2.9% (2)	3.7% (2)
			20.6	15	7.5
			1,160	820	410

ERATORS (SMALL UNITS)

lips Lab.	Phillips Lab.	Hughes Aircraft	
		P/N X447525-100	
otype(1)	Prototype(1)	Prototype	
	18	19	
°K	77°K	77°K	
leumier	Vuilleumier	Vuilleumier	
um	Helium	Helium	
tm	40 atm	600 psi charge press.	
		64°K	
		7 min	
	600	600	
		28 VDC	
	Air	Air	
	Any	Any	
x 7.1 x 7.1"	16.5 x 7.1 x 7.1		
in.³	820 in.³	108 in.³	
b	15 lb	3.4 lb incl. inverter	
		744 hr +	
	2W	1.6W	
	191W	163W	
33	.105	.00983	
(2)	3.7%(2)	2.85%	
	7.5	2.12	
	410	67.5	

PRECEDING PAGE BLANK NOT FILMED

CLOSED

FOLDOUT FRAME 1

Manufacturer	Garrett AiResearch	Garrett AiResearch	Air Products	Air Products
Trade Name	None	None	None	None
Model	133488	144406	J-80-1000	J-30-3500
I.D. Number	21	22	23	24
Refrigeration Range	$\approx 77^{\circ}K$	$\approx 77^{\circ}K$	$\approx 77^{\circ}K$	$23^{\circ}K$
Cycle	J-T	J-T	J-T	J-T
Working Fluid	N_2	N_2	N_2	N_2 and He
High Pressure	155 atm	176 atm		
Low Pressure	1 atm	1 atm		
Minimum Temperature	$75^{\circ}K$	$75^{\circ}K$	$75^{\circ}K$	
Cool-Down Time	12 min	6.5 min	5 min	
Compressor RPM			3,850	3,850
Volts-Phase-Frequency	115/208 - 3 - 400	115/208 - 3 - 400		
Cooling Means	Air	Air	Air	Air
Ambient Temp. Reqmts.	$-40^{\circ}C$ to $56^{\circ}C$	$-40^{\circ}C$ to $71^{\circ}C$		
Required Attitude	Any	Any		
Cryostat Dimensions				
Compressor Dimensions	6.5"D x 12"L (3-stage)		5" x 8" x 12" (2-stage)	
Cryostat Wt.				
Compressor Wt.				
System Wt.	22.5 lb	19.5 lb	18 lb	
Compressor Volume				
Cryostat Volume				
System Volume	500 in.^{3} (est.)	0.45 ft.^{3} (777 in.^{3})		
MTBF	1,000 hr est	2,000 hr est		
Maintenance Interval	300 and 500 hr	400 hr	500 hr	500 hr
System Cost	$9,000	$8,000	$9,000	
$23^{\circ}K$ / 250K				
Refrigeration				0.35W ($23^{\circ}K$)
Power Input				1,050W
COP				0.000333
% Carnot				0.4%
Lb/Watt				
In.^{3}/Watt				
$77^{\circ}K$				
Refrigeration	5W	3W	2W	
Power Input	650W	450W	600W	
COP	.0077	.0067	.00333	
% Carnot	2.23%	1.9%	0.9%	
Lb/Watt	4.5	6.5	9	
In.^{3}/Watt	100	259		

Table 3-5

CLOSED CYCLE JOULE-THOMSON REFRIGERATORS (SMALL UNITS)

Products	Air Products	Santa Barbara Research Center	Hughes Aircraft	Fairchild Stratos Corp.	
e	None	None	Prototype	Prototype	
0-1000	J-30-3500				
	24	25	26	27	
7°K	23°K	≈79°K	77°K	≈30°K	
	J-T	J-T	J-T	J-T	
	N_2 and He	N_2	N_2	N_2 and He	
;		75°K	75°K	23°K	
in		5 min	5 min	50 min	
0	3,850				
	Air	Air		Air	
8" x 12" tage)		7"D x 12.5"L			
o		16 lb	40 lb	52 l[illegible]	
		0.35 ft.^{3} (603 in.^{3})		1765 in.^{3}	
hr	500 hr	500 hr			
0		$10,000		$15,[illegible]44	
	0.35W (23°K)			0.5W (25°K)	
	1,050W			1,000W	
	0.000333			.00050	
	0.4%			.6%	
				10[illegible]	
				3,[illegible]20	
		5W	12W		
		326W	750W		
3		.015	0.016		
		4.5%	4.8%		
		3.2	3.33		
		121			

PRECEDING PAGE BLANK NOT FILMED

FOLDOUT FRAME 1

Manufacturer	Cryomech, Inc.	Cryomech, Inc.	Cryomech, Inc.	Cryomech, Inc.	CTI	CTI	CTI	CTI
Trade Name	None	None	None	None	Cryodyne	Cryodyne	Cryodyne	Cryc
Model	AL01	AL02	GB02	GB12	350	355	1020	10
I.D. Number	30	31	32	33	34	35	36	38
Refrigeration Range	32 - 150°K	23 - 150°K	7.5 - 150°K	9 - 150 K	15 - 150°K	15 - 150°K	13 - 150°K	30
Cycle	G-M	G-M	G-M	G-M	G-M	G-M	G-M	G-M
Working Fluid	He	He	He	He	He	He	He	He
High Pressure	24 atm	24 atm	24 atm	24 atm	185 psi	275 psi	275 psi	300
Low Pressure	10 atm	10 atm	10 atm	10 atm	65 psi	75 psi	75 psi	10
Minimum Temp	23°K	23°K	7.5°K	9°K	15°K	15°K	13°K	25
Cool-Down Time	12 min	25 min	25 min	35 min	45 min	75 min	50 min	30
Expander RPM	144	144	144	144	72	82	82	82
Volts-Phase-Frequency	110/220 - 1 - 50/60	220 - 1 - 50/60	220 - 1 - 50/60	220 - 1 - 50/60	200/300 - 1 - 50/60	208/440 - 3 - 50/60	208/40C - 3 - 40/60	208/
Cooling Means	Air	Air	Air	Air	Air	Air	Air	Air
Ambient Temp Req	NI	NI	NI	NI	-25°F - +125°F	-25°F - +125°F	-25°F - +125°F	-25
Required Attitude	Cryostat any	Cryostat any	Cryostat any	Cryostat any	Cryostat any	Cryostat any	Cryostat any	Cryo
Cryostat Dim. (in.)	2.5 x 2.5 x 14.5	5 x 5 x 18	5 x 5 x 21	5 x 5 x 24	19 x 5 x 9	18 x 10 x 6	20 x 13 x 8	16.
Compressor Dim. (in.)		29W x 19 x 27H	29 x 19 x 27	29 x 19 x 27	28 x 17 x 16	41 x 27 x 26	41 x 27 x 26	41
System Volume ($in.^3$)		15,350	15,420	15,500	8,460	29,900	30,880	30,
Compressor Wt	125 lb	175 lb	175 lb	175 lb	175 lb	425 lb	425 lb	425
Cryostat Wt	5 lb	25 lb	25 lb	25 lb	22 lb	22 lb	33 lb	30
System Wt	130 lb	300 lb	200 lb	200 lb	229 lb (2)	468 lb (2)	488 lb (2)	480
MTBF	5000	5000	5000	5000	10,000	10,000	13,000	14,
Maintenance Interval (1)	3000/5000	3000/1500	3000/1500	3000/1500	3000/3000/6000	3000/3000/6000	3000/3000/6000	300
System Cost	$8,610	$10,290	$13,200	$13,200	$13,000	$16,000	$17,000	$18,
12°K Refrigeration			2.4W	3.4W				
12°K Power Input			3000W	3000W				
12°K COP			.0008	.00113				
12°K % Carnot			1.92%	2.5%				
12°K Lb/Watt			83	59				
12°K $In.^3$/Watt			6430	4560				
15°K Refrigeration			4.0W	6.0W		1.0W	4.6	
15°K Power Input			3000W	3000W		5600W	5600	
15°K COP			.0013	.0020		.00018	.00082	
15°K % Carnot			2.47%	3.8%		0.32%	1.45%	
15°K Lb/Watt			50	33.3		468	106	
15°K $In.^3$/Watt			3860	2580		29,900	6720	
20°K Refrigeration	1.0W @ 25°K		5.5W	8W	3W (2nd Stage)	5W (2ndStage)	11W (2nd Stage)	
20°K Power Input	900W		3000W	3000W	2100W	5600W	5600W	
20°K COP	.0011		.00184	.00267	.00143	.00089	.00197	
20°K % Carnot	1.2%		2.57%	3.7%	2%	1.2%	2.7%	
20°K Lb/Watt	130		36.4	25	76	93	44	
20°K $In.^3$/Watt			2800	1940	2820	5980	2810	
77°K Refrigeration	18W	75W			5W (1st Stage)	5W (1st Stage)	10W (1st Stage)	100
77°K Power Input	900W	3000W			2100W	5600W	5600W	560
77°K COP	.020	.025						.01
77°K % Carnot	5.8%	7.2%						5.4
77°K Lb/Watt	7.22	2.67						4.8
77°K $In.^3$/Watt								205
110°K Refrigeration	29	89W						
110°K Power Input	900W	3000W						
110°K COP	.0322	.0297						
110°K % Carnot	5.08%	4.7%						
110°K Lb/Watt	4.5	2.2						
110°K $In.^3$/Watt		172						

(1) Cryostat/compressor oil filter/compressor

(2) Total weight excludes instrument panel

(3) Expander/compressor/valve

(4) Valve assembly

FOLDOUT FRAME 2

EXISTING

	CTI	Air Products	Air Products	Air Products	Air Products	Cryom..h, Inc.	Cryomech, Inc.	CTI	
e	Cryodyne	Displex	Displex	Displex	Displex	None	None	Cryodyne	
	10077	CS-102	CS-202	(Airborne)	CS-1003	DT01	GB05	0120	
	38	38	30-S	31-S	32-S	33-S	34-S	35-S	
150°K	30 - 150°K	30 - 300°K	12°K - 300°K	77°K - 150°K	77°K - 150°K	15°K - 150°K	15°K	17.5°K - 150°K	
	G-M	Mod. Solvay	Mod. Solvay	Mod. Solvay	Mod. Solvay	G-M	G-M	G-M	
	He	He	He	He	He	He	He	He	
i	300 psi	320 psig		290 psi	NI	24 atm	24 atm		
i	100 psi	115 psig		90 psi	NI	10 atm	10 atm		
	25°K	30°K	12°K	NI	NI	23°K	NI	17.5°K	
	30 min	20 min	45 min	5 min	5 min	NI	NI	10 - 15 min	
	82	144		385	400	144	144	Ref. 200 - 3 - 400	
- 3 - 40/60	208/440 - 3 - 50/60	208/440 - 3 - 60	115V - 50/60	NI	NI	220 - 1 - 50/60	220 - 1 - 50/60	Comp 208 - 3 - 400	
	Air	Air	Air	Air	Air	Air	Air	Air	
- +125°F	-25°F - +125°F	40 - 110°F	40 - 110°F	65°C	80°F	NI	NI	-63°F - +131°F	
t any	Cryostat any	Cryostat any	Cryostat any	Any	Any	Cryostat any	Cryostat any	Cryostat any	
13 x 8	16.5 x 13 x 8	4D x 19L	4D x 17L	0.5"D x 3.0"L	0.5"D x 4.8"L			10 x 20 x 10	
27 x 26	41 x 27 x 26	22 x 17 x 15	22 x 17 x 15	1.7D x 5.7L (4) 5.0 x 5.5 x 7.2	2.5"D x 5.4"L (4) 15.2" x 21.8 x 11.1			10 x 4 x 8	
	30,500	5,600	5,700	202	3,720			270 in^3	
lb	425 lb	150 lb	150 lb	7.5 lb	65 lb	35 lb	75 lb	20 lb	
b	30 lb	10.6 lb	10.6 lb	3.5 lb	2 lb	4 lb	6 lb	5 lb	
lb[2]	480 lb[2]	161 lb	161 lb	11 lb	67 lb	39 lb	81 lb	25 lb	
	14,000	3000 - 5000 est	3000 - 5000 est	26312/8456/8493	NI	5000	5000	10,000	
/3000/6000	3000/3000/6000	3000/6000	3000/6000	1200	4500/4500	3000/1500	3000/1500	3000/500/2000	
	$18,000	$7,000						$10,000	
			0.7W				1.0W		
			1735W				900W		
2			.00040				.0011		
			0.77%				2.1%		
			230				81		
			8150						
(2nd Stage)			1.5W (load station)			0.5W @ 25°K		0.5W	
			1735W			600W		680W	
			.00086			.00083		.00073	
			1.2%			.92%		1.0%	
			107			78		50	
			3800					540	
(1st Stage)	100W	17W		1.5W	1.0W				
W	5600W	1700W		340W	500W				
	.0179	.01		.0044	.002				
	5.2%	2.9%		1.28%	.58%				
	4.8	9.5		7.3	67				
	205	330		135	3720				
		22W							
		1700W							
		.013							
		2%							
		7.3							
		255							

TABLE 3-6

EXISTING GIFFORD-McMAHON REFRIGERATORS

FOLDOUT FRAME 3

Cryomech, Inc.	CTI	CTI	CTI	Phillips	British Oxygen	
Kone	Cryodyne	Cryodyne	Cryodyne	Airborne	None	
G2C5	0120	0110	20	P/N 46021.	IR16 - Mk II	
34-S	35-S	36-S	37-S	38-S	39-S	
15°K	17.5°K - 150°K	6.5°K - 150°K	19.0° - 150°K	16 - 100°K	12 - 22°K	
G-M	G-M	G-M	G-M	Solvay	Mod. Taconis	
He	He	He	He	He	He	
24 atm					20 atm	
10 atm					10 atm	
NI	17.5°K	6.5°K	19.0°K	16°K	12°K	
NI	10 - 15 min	240 min	less than 15 min	20 min (75 gms cu)	40 min	
144	Ref. 200 - 3 - 400	Ref. 130 - 1 - 50/60			166 RPM	
220 - 1 - 50/60	Comp 208 - 3 - 400	Comp 208/230 - 1 - 50/60	115/100 - 1 - 60/50	115 - 3 - 400	240 - 1 - 50	
Air	Air	Air	Air	Air	Air and Water	
NI	-63°F - +131°F	-25 - +125°F	+40 to +110°F	NI	30°C	
Cryostat any	Cryostat any	Cryostat any	Cryostat any	Any	Cryostat any	
	10 x 20 x 10	10 x 20 x 31	3.5D x 7 x 11.2	3" x 5" x 12"	8"D x 13"L	
	10 x 4 x 8	26 x 17 x 17	13 x 13 x 19	5 x 7.5 x 9"	36" x 21" x 27"	
	270 in^3	7600 in^3	3280	517 in^3	21,000 in^3	
75 lb	20 lb	175 lb	70 lb	9.5 lb	240 lb	
6 lb	5 lb	30 lb	11 lb	5.5 lb	20 lb	
[illegible] lb	25 lb	205 lb	81 lb	15.0 lb	260 lb	
5000	10,000	10,000	10,000	2,000		
3000/1500	3000/500/2000	3000/3000/6000	3000/3000/6000	2,000	NI	
	$10,000	$23,000			$9,100	
		1.6W				
		2100W				
		.000763				
		1.07%				
		128				
		4750				
1.0W		2.4W			0.7W	
900W		2100W			2640W	
.0011		.00114			.000265	
2.1%		2.2%			0.51%	
81		117			372	
					30,000	
	0.5W		0.2W	0.4W	2.5W	
	680W		1000W	639W	2640W	
	.00073		.0002	.000627	.000950	
	1.0%		0.27%	.85%	1.3%	
	50		405	37.5	104	
	540		16,400	1300	8400	
				3.8W		
				639W		
				.00595		
				1.73%		
				3.95		
				136		

PRECEDING PAGE BLANK NOT FILME'

Table 3-7

PROTOTYPE BRAYTON-CYCLE REFRIGERATORS

Manufacturer	Garrett AiRes	Hymatic	A.D. Little	A.D. Little	A.D. Little
Trade Name	None	None	None	None	None
Model	Prototype	Prototype	Prototype	Prediction(2)	Prototype
I.D. Number	40	42	44	45	46
Refrigeration Range	≈80°K	19 - 28°K	3.6°K	77°K	90°K
Cycle	Brayton	Brayton	Brayton	Brayton	Brayton
Working Fluid	N_2	He	He	He	He
High Pressure	0.72 atm	20 - 30 atm			
Low Pressure	0.30 atm	1 atm			
Minimum Temperature	≈75°K	19°K			
Cool-Down Time	≈6 hr	30 min			
Expander RPM		1500			
Volts-Phase-Frequency	115 - 1 - 60				
Cooling Means	Water		Radiative	Radiative	
Ambient Temp. Reqmts.	NI	-40°C to 70°C	NI		
Required Attitude	NI	NI	NI	Any	Any
Cryostat Dim. (in.)	8.5 x 10.6 x 28.3	6 x 4 x 15	8 D x 60 L	6.5"D x 32"L	7.8"D x 32"L
Compressor Dim. (in.)		NI	5.5 D x 52 L		
System Volume	2,500 in.^{3}		7,700 in.^{3}	1,060 in.^{3}	1,530 in.^{3}
Compressor Wt.	15 lb	NI	72 lb		
Cryostat Wt.		20 lb	52 lb		
System Wt.	15 lb	NI	124 lb	20 lb	90 lb
Min. Temp. — Refrigeration		0.3W at 28°K	1W at 3.6°K		
Min. Temp. — Power Input			1310W		
Min. Temp. — COP			.000763		
Min. Temp. — % Carnot			6.25%		
Min. Temp. — Lb/Watt			124		
Min. Temp. — In.^{3}/Watt			7700		
As Indicated — Refrigeration	2W at 80°K			2.5W @ 77°K	2.1W @ 84°K
As Indicated — Power Input	375W			100W	125W
As Indicated — COP	.00533			.025	.0168
As Indicated — % Carnot	1.5%			7.25%	4.9%
As Indicated — Lb/Watt	7.5			8	42.8
As Indicated — In.^{3}/Watt	1,280			425	727

(1) Excluding vacuum case.
(2) Based on extrapolation from prototype tests to refined spacecraft unit.

It should be apparent from these comments that some significant extrapolations were required in making these curve fits and the authors judgment was used in many cases. For these reasons it is suggested that the following performance data be used as a guide in performing trade-off studies and not as an absolute indication of the characteristics of units intended for space-flight cryogenic cooling.

3.5.1 Coefficient of Performance vs Cooling Load

An indication of the thermal efficiency of the refrigerator is given by the coefficient of performance (COP) defined as the net refrigeration produced divided by the input power

$$COP = \frac{Q_{ref.}}{Q_{input}}$$

Figure 3-14 shows the COP data for five different cycles at 20°K as a function of the net refrigeration produced. In general, a large amount of applicable data was available for the various units. An exception was that of the Brayton cycle where predicted performance data was utilized. Data for large industrial units at higher cooling capacities are also shown, and the results of a previous study for the Stirling unit are in good comparison.

The value of COP for a reversible (Carnot) refrigerator is given by

$$COP = \frac{T_c}{T_h - T_c}$$

where T_c is the temperature at which cooling takes place and T_h is the temperature of the surroundings (300°K for these units). The values of COP for the carnot cycle at 20°K and 4.2°K are shown in Figure 3-14 for comparison with actual units.

The adverse effects of miniaturization are easily seen from Fig. 3-14. The COP decreases substantially as the unit becomes smaller. This is due to the fact that relatively higher heat leaks are present for the smaller units because of the unfavorable area to volume ratios, and some components of the system become more difficult to fabricate efficiently in small size.

PRECEDING PAGE BLANK NOT FILMED

FOLDOUT FRAME 1

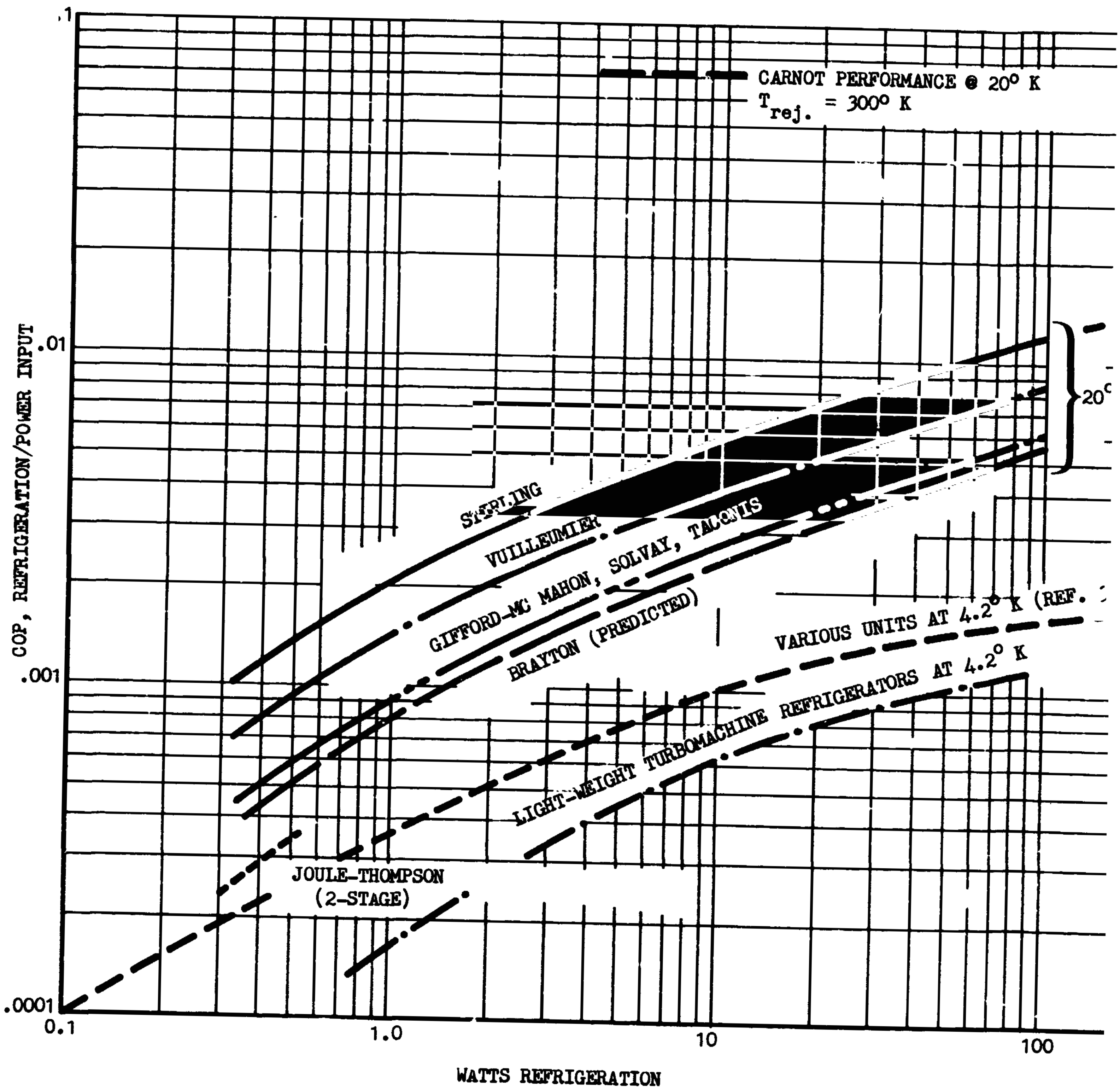

FOLDOUT FRAME 2

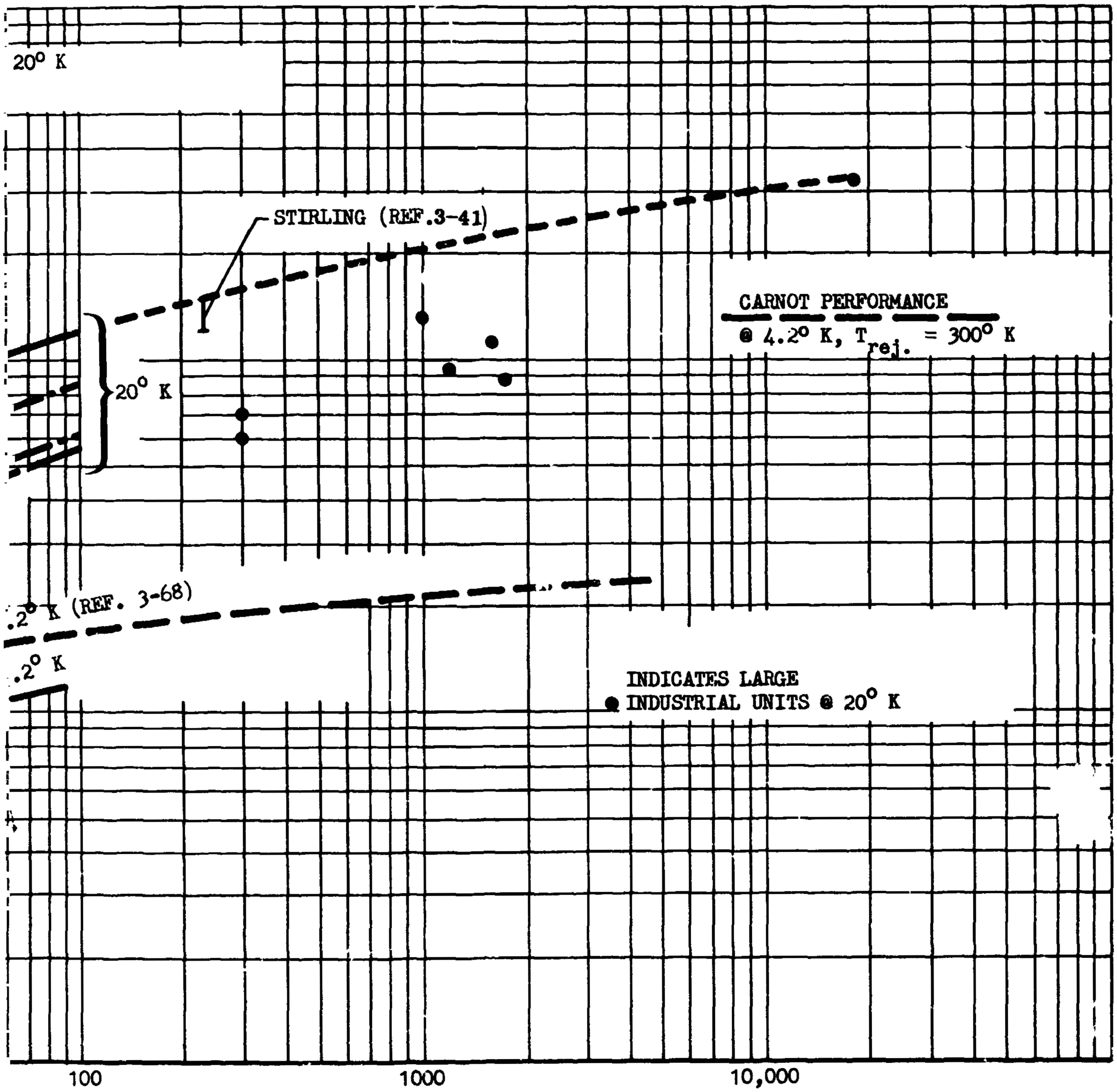

FIGURE 3-14 SUMMARY OF REFRIGERATOR COEFFICIENT OF PERFORMANCE FOR VARIOUS CYCLES AT 20°K AND 4.2°K

Frictional losses are also proportionally higher.

The relative efficiency of the various cycles has been fairly well established with the exception of the Brayton cycle for which only predictions were available in the range of interest here. It is expected that if the performance of actual Brayton units is obtained, the values may be somewhat lower than shown since inefficiencies are generally higher than predicted. Performance for the Joule-Thompson unit is shown only in the area of 0.4 W where data is available, predictions or extrapolations were not made, since the interest in a J - T unit for application in this area is limited.

Data for various units operating at 4.2°K is also shown in the figure and is taken from reference 68. No attempt was made to show the relative performance of various cycles at this temperature, the curve being included only as a rough guide.

The units shown on the dotted curve represent for the most part ground based units where weight optimization was not performed. An additional curve is shown for lightweight turbo machinery refrigerators at 4.2°K, some of which were developed specifically for space flight. These reductions in weight are achieved with some loss in efficiency. As shown, the lightweight units are less efficient than the others.

Figure 3-15 shows COP data for the various cycles at 77°K, a temperature at which the majority of data is available. The same observations hold; the curve for the Brayton cycle is based on prediction plus one experimental point and the agreement with a previous study at higher cooling loads is satisfactory. The value for COP are substantially higher than at 20°K, and approximately parallels the increase for the carnot cycle.

3.5.2 Coefficient of Performance vs Temperature

Figure 3-16 and 3-17 show the effect of temperature on the COP at two cooling loads, 5W and 100W which correspond to the limit of the parameters for the study. The variation of COP with temperature is governed by two primary

PRECEDING PAGE BLANK NOT FILMED

FOLDOUT FRAME /

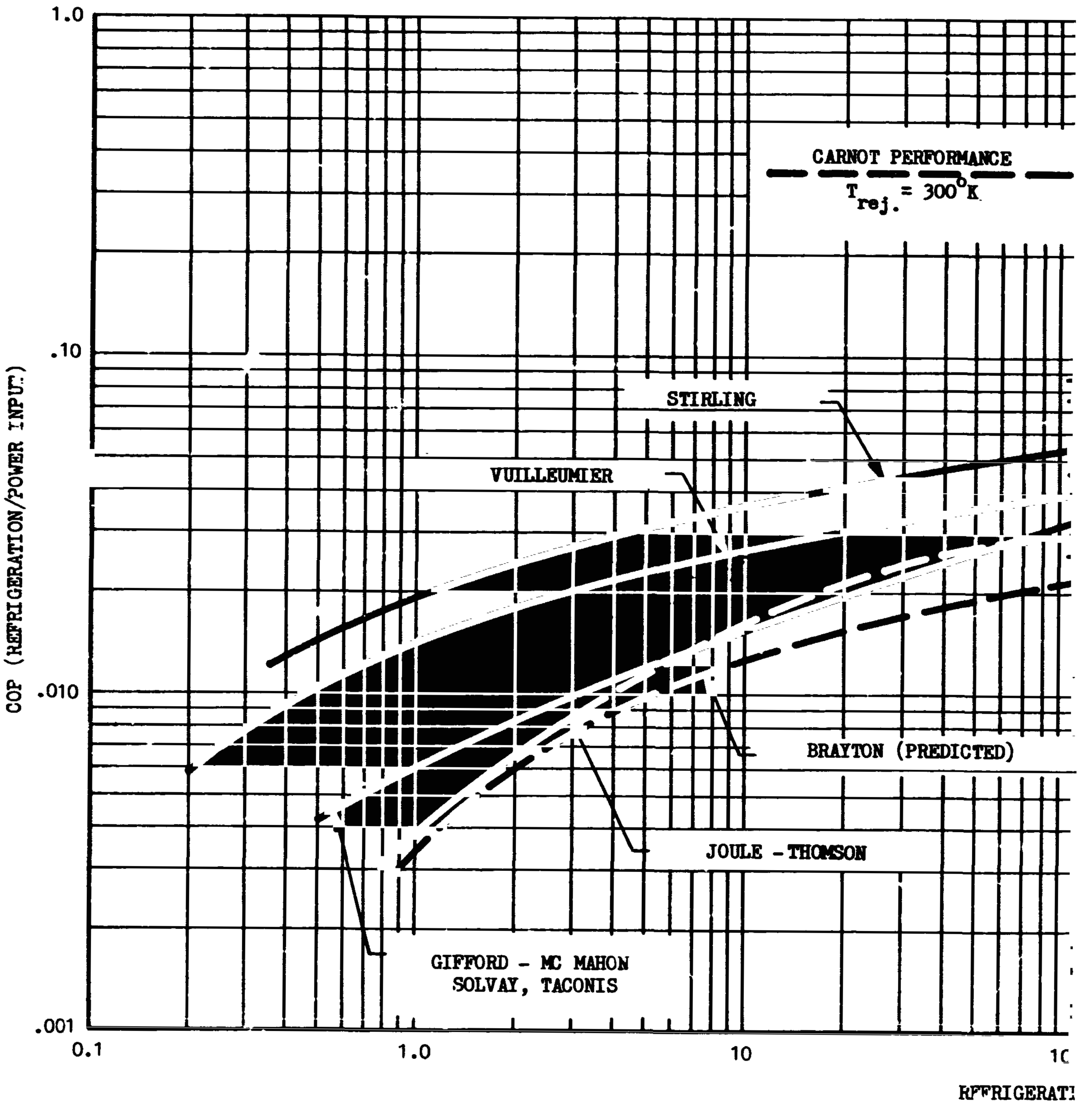

FOLDOUT FRAME 2

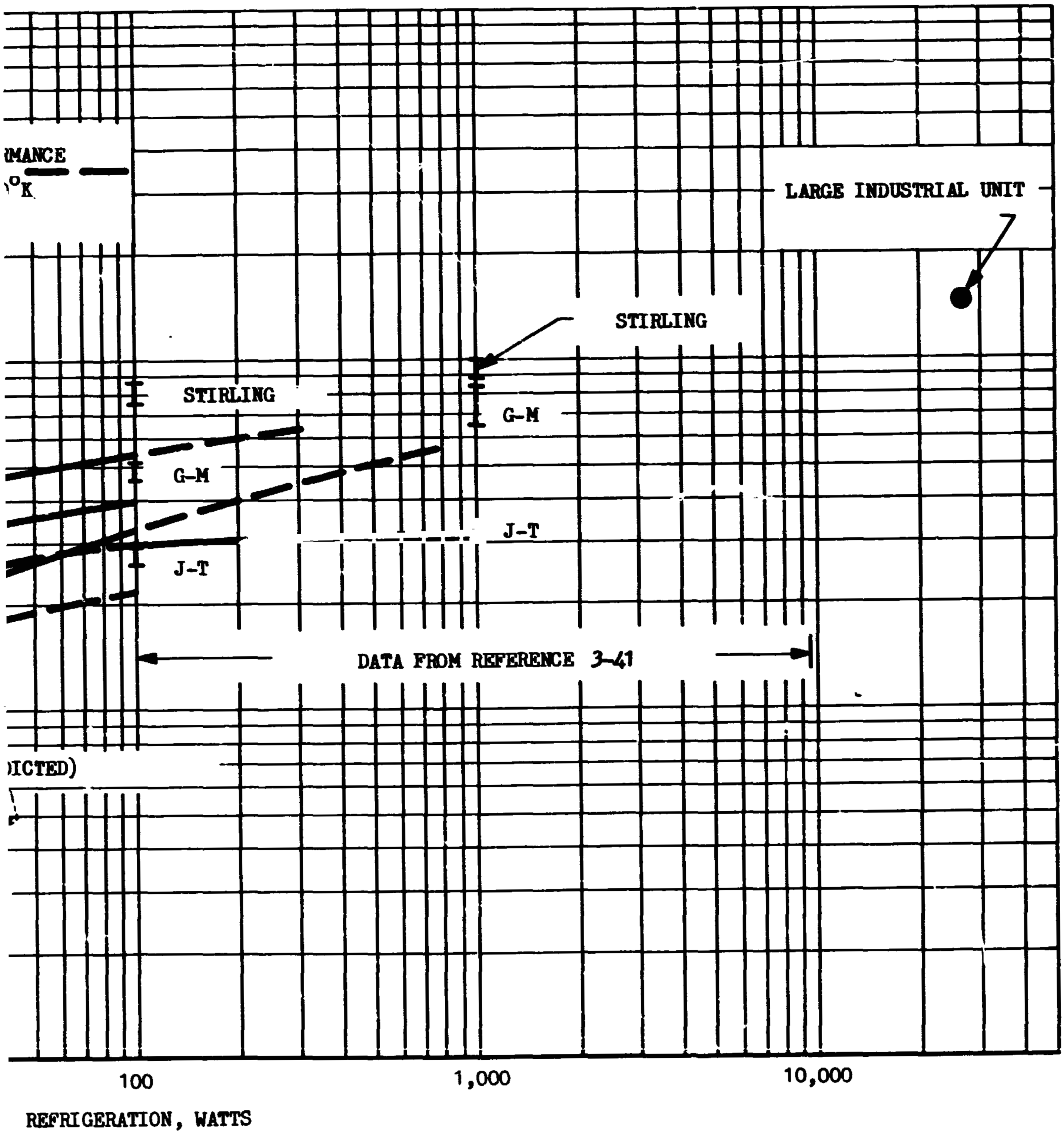

FIGURE 3-15 SUMMARY OF REFRIGERATOR COEFFICIENT OF PERFORMANCE VS. REFRIGERATION FOR VARIOUS CYCLES AT 77°K

PRECEDING PAGE BLANK NOT FILMED

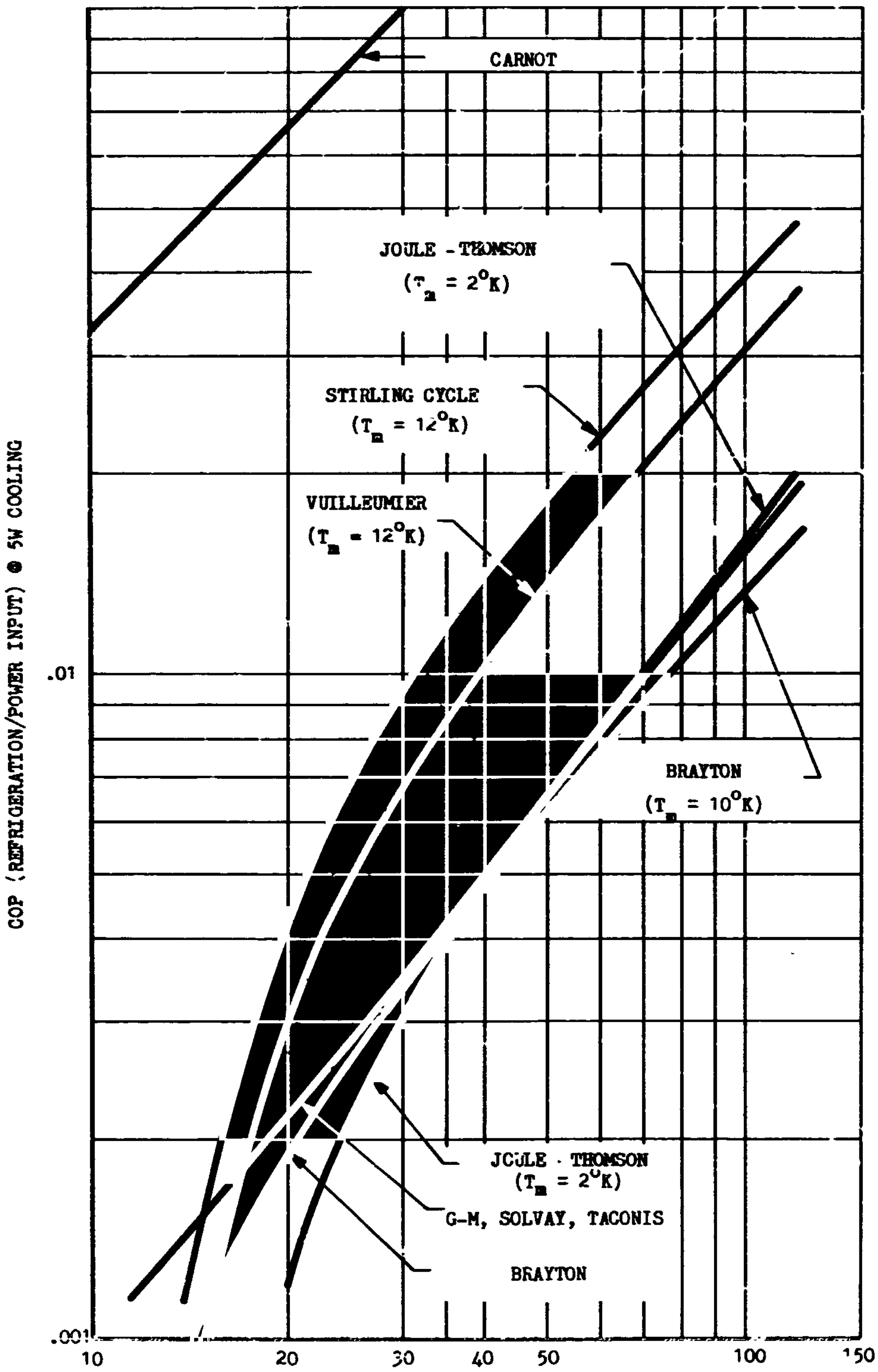

FIGURE 3-16 COEFFICIENT OF PERFORMANCE AT 5 WATTS VERSUS TEMPERATURE

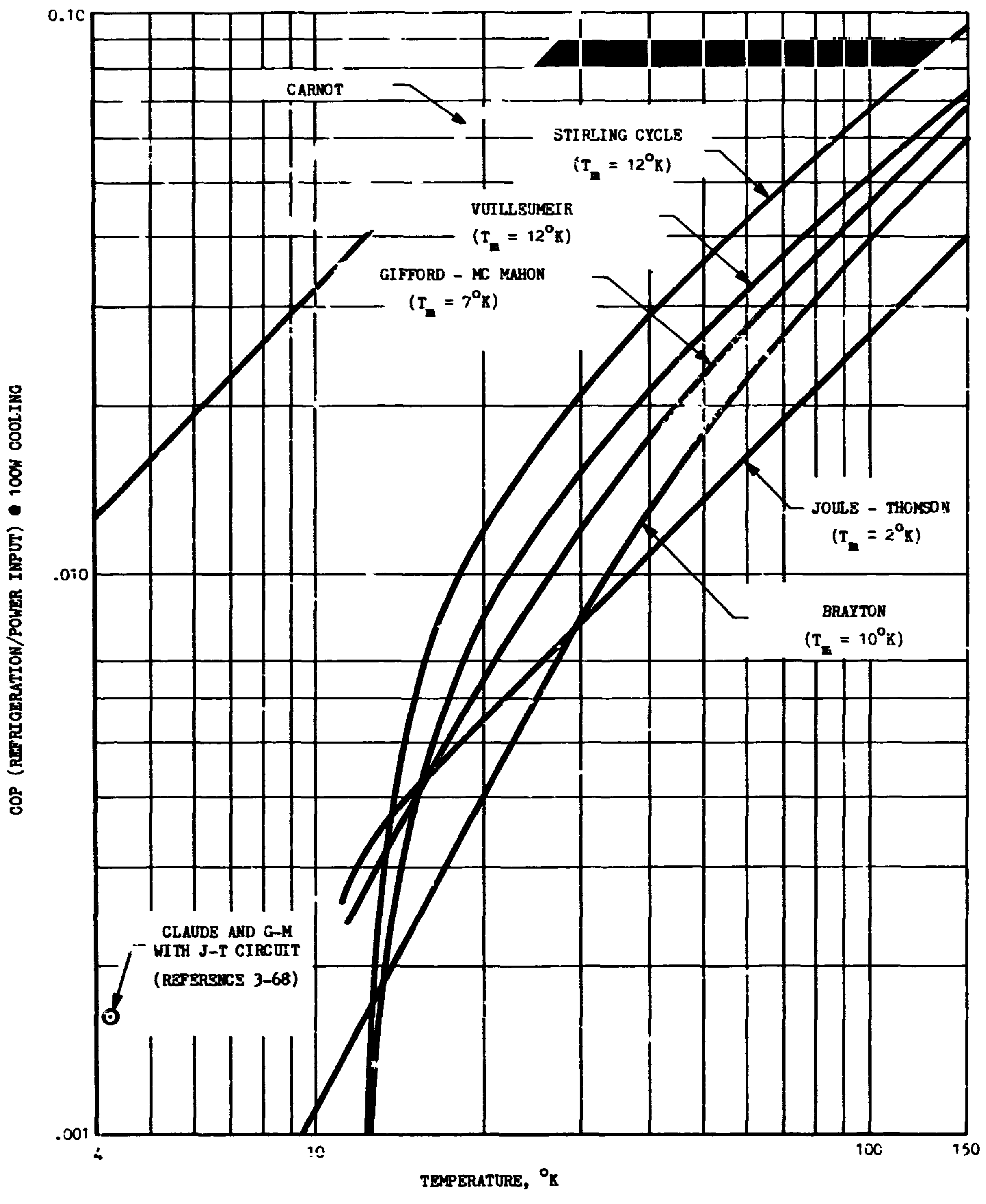

FIGURE 3-17 COEFFICIENT OF PERFORMANCE AT 100 WATTS VS. TEMPERATURE

effects. (1) The COP begins to decrease rapidly as the minimum temperature for the particular cycle is approached. For example, as approximately 12°K is approached for the Stirling unit, the COP begins rapidly decreasing due to the rapidly decreasing specific heat of the regenerator material and corresponding loss of efficiency. The approximate minimum temperatures (Tm) achieved are indicated on the curves for the various cycles. (2) The curves generally parallel the Carnot efficiency curve a. temperatures substantially higher than their minimum values, as shown on the Figures.

Also shown is the performance of 4.2°K Claude and G-M units which both employ a Joule-Thomson expansion circuit to reach 4.2°K, the normal boiling point of helium.

3.5.3 Refrigerator Weight vs Power Input

The weight of most machinery can be correlated quite successfully with the power input to the unit providing units with common design requirements are utilized. For example, if the machinery is designed for spaceflight where weight is a premium then this common basis will provide a consistent correlation. Data for compressors, motors, and complete refrigeration units was correlated on this basis. The complete results for compressors and motors are presented in the final report*. Figure 3-18 presents the correlation for refrigeration system weight as a function of input power. Some of the data for 400 cycle motors and dry lubricated compressors is also indicated in the figure to help discern the relative contribution of the different components which make up the total system weight. Various cycles are indicated, and no differentiation was made as to cycle in fitting the curves except for those cycles employing rotating machinery. These machines were considered separately from those employing reciprocating machinery. The curve fits were made through minimum weight systems rather than through the mean of the data to indicate the expected best weight that is currently attainable for weight optimized systems.

*Investigation of External Refrigeration Systems for Long Term Cryogenic Storage - Final Report LMSC-A981632, 22 February 1971.

PRECEDING PAGE BLANK NOT FILMED

FOLDOUT FRAME 1

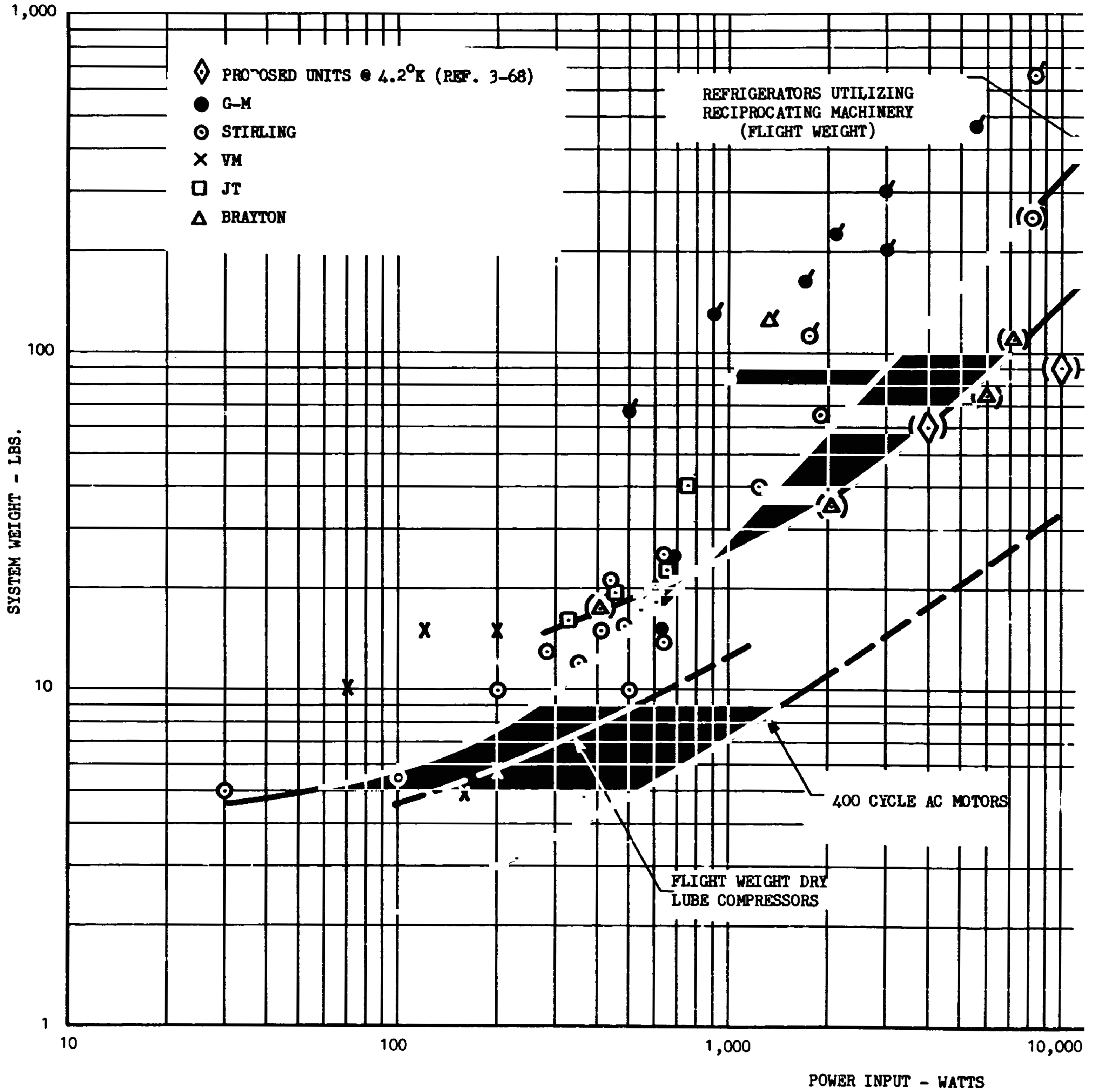

FOLDOUT FRAME 2

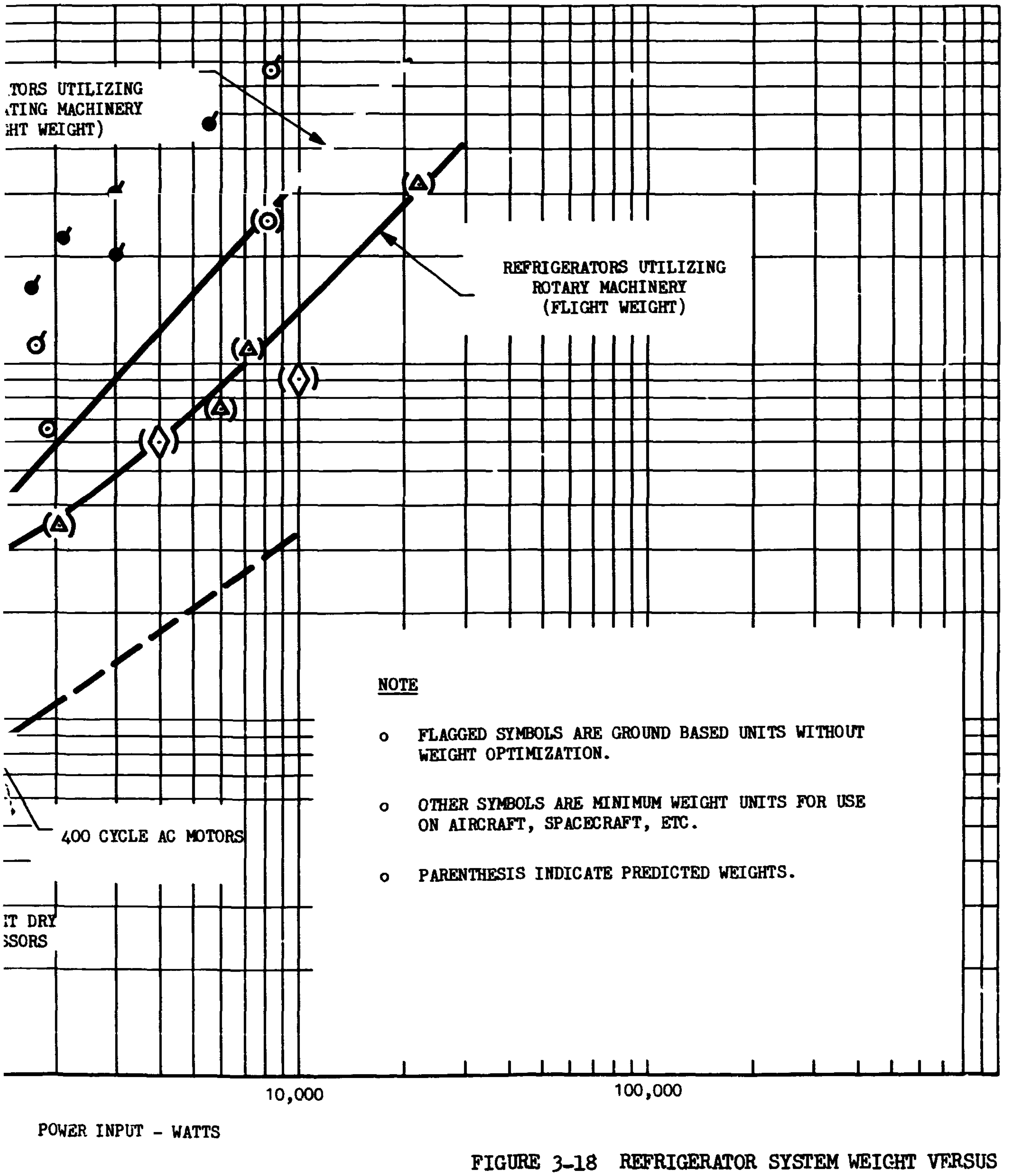

FIGURE 3-18 REFRIGERATOR SYSTEM WEIGHT VERSUS POWER INPUT FOR VARIOUS MACHINES

Data points are shown for units which are obviously designed for ground use with no weight minimization as flagged points, and are shown for general interest, although they were not used in the curve fits.

The curves presented in Figure 3-18 can be utilized in predicting weights of various units for which weight data is not available, and this technique was used in some instances where important data was lacking. The data also show the importance of obtaining a high coefficient of performance in order to minimize weight. For the higher power inputs, little data on weight optimized systems was available, and some extrapolations were necessary to cover the desired range. For the Brayton cycle systems employing turbomachinery a combination of predicted values and a few experimental points were used.

The results show a weight advantage for the turbo-machinery units for power inputs in excess of about 800-900 watts.

3.5.4 Weight vs Cooling Capacity

Figure 3-19 shows the comparison of weights for the various cycles at 20°K. Wherever possible data for operating flight weight systems was utilized. For those cases where sufficient data was lacking, weights were estimated based on a combination of the curve fits for COP previously described and the system weights vs power input. As might be expected the lower weight cycles are those with the highest thermal performance (COP) values, the Stirling units being the lightest weight systems, while the Brayton cycle shows a relatively improved position at the higher cooling rate. Comparison with a previous study (Ref. 41) at higher cooling rates is again shown. The weight of heavy units for ground use (wet lubricated compressor, etc.) is shown for the G.M., Taconis and Solvay units for comparison with what is expected for a weight optimized unit for those cycles. Weight optimized versions of the Solvay and G.M. cycle units have been built and are operating in the cooling range near one watt.

PRECEDING PAGE BLANK NOT FILMED

FOLDOUT FRAME 1

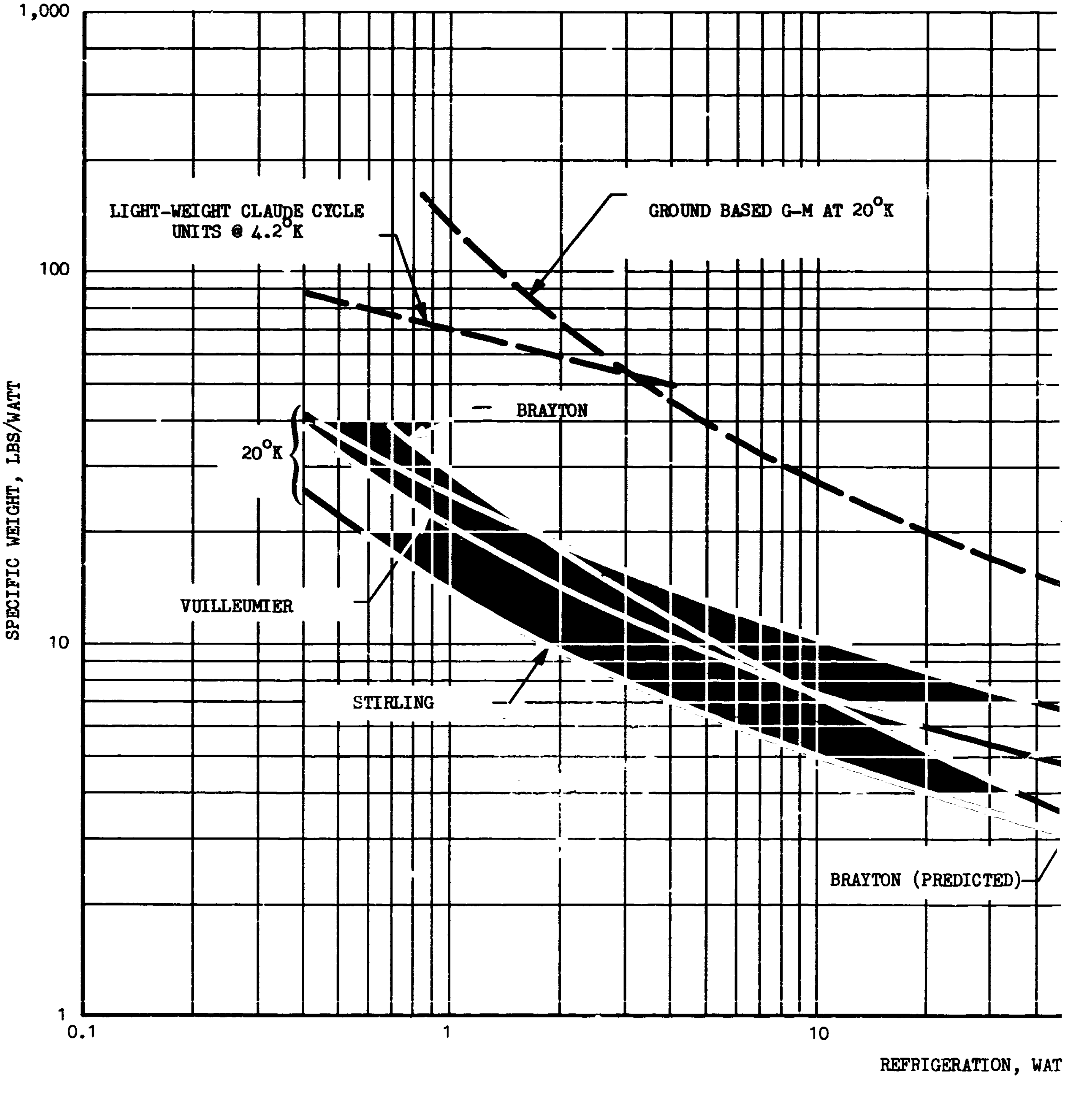

FOLDOUT FRAME 2

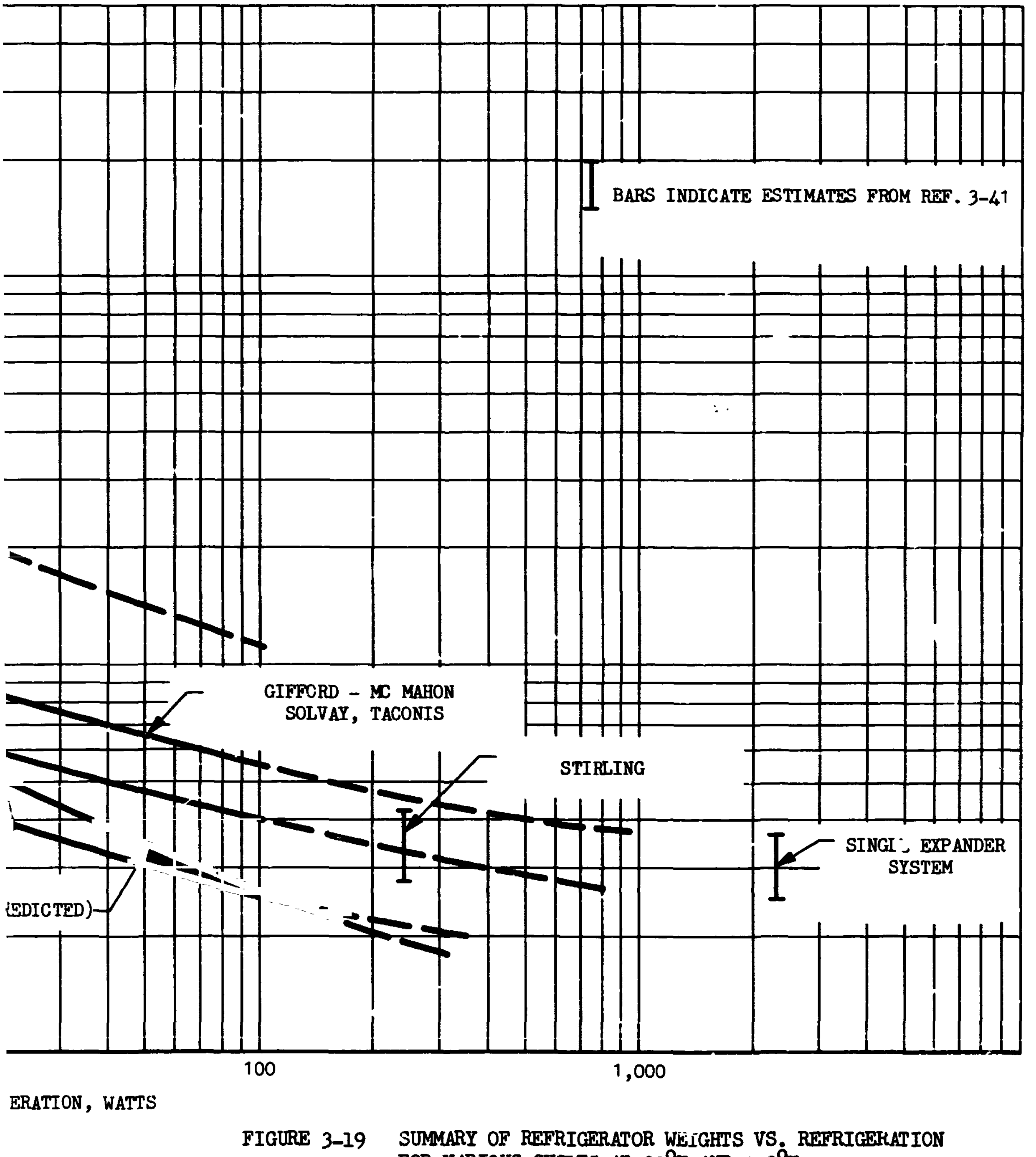

FIGURE 3-19 SUMMARY OF REFRIGERATOR WEIGHTS VS. REFRIGERATION FOR VARIOUS CYCLES AT 20°K AND 4.2°K

In addition, a curve is shown for lightweight Claude cycle refrigerators at 4.2°K. This curve is based primarily on predicted values and requires experimental verification before it can be used with any degree of confidence.

All of the curves show a reduction in specific weight as the refrigeration level is increased. This tendency is primarily a consequence of the variation of the coefficient of performance vs vooling rate, and the character of the curves is similar to the COP vs refrigeration curves.

Figure 3-20 shows the specific weight data for the 77°K cooling level. More operating data on actual units was available for this case than at 20°K. The same general comments are applicable to this curve as for the 20°K case. The weight of the units is substantially less than at 20°K.

3.5.5 Weight vs Temperature

The specific weight vs temperature is shown in Figures 3-21 and 3-22 for cooling levels of 5 watts and 100 watts. The characteristics of the curves are similar to the COP vs temperature curves.

As the minimum temperatures are approached the weights rapidly increase as the thermal efficiency rapidly decreases, while at the higher temperature the slope becomes nearly constant. These curves can be utilized to make estimates of weight requirements at intermediate temperatures. Additional cross-plotting will be necessary to assess weight penalties at other cooling rates than the 5 watts and 100 watts selected here.

3.5.6 System Volume

The volume of the refrigeration systems showed the greatest spread and least correlation of the various parameters. One reason for this is that volume data was not readily available for most units. Reported data did not specify if actual (displaced) volume was reported or if the volume envelope was specified. In the majority of cases the drawings of the units were utilized to calculate the volumes. The system volumes for

PRECEDING PAGE BLANK NOT FILME

FOLDOUT FRAM. /

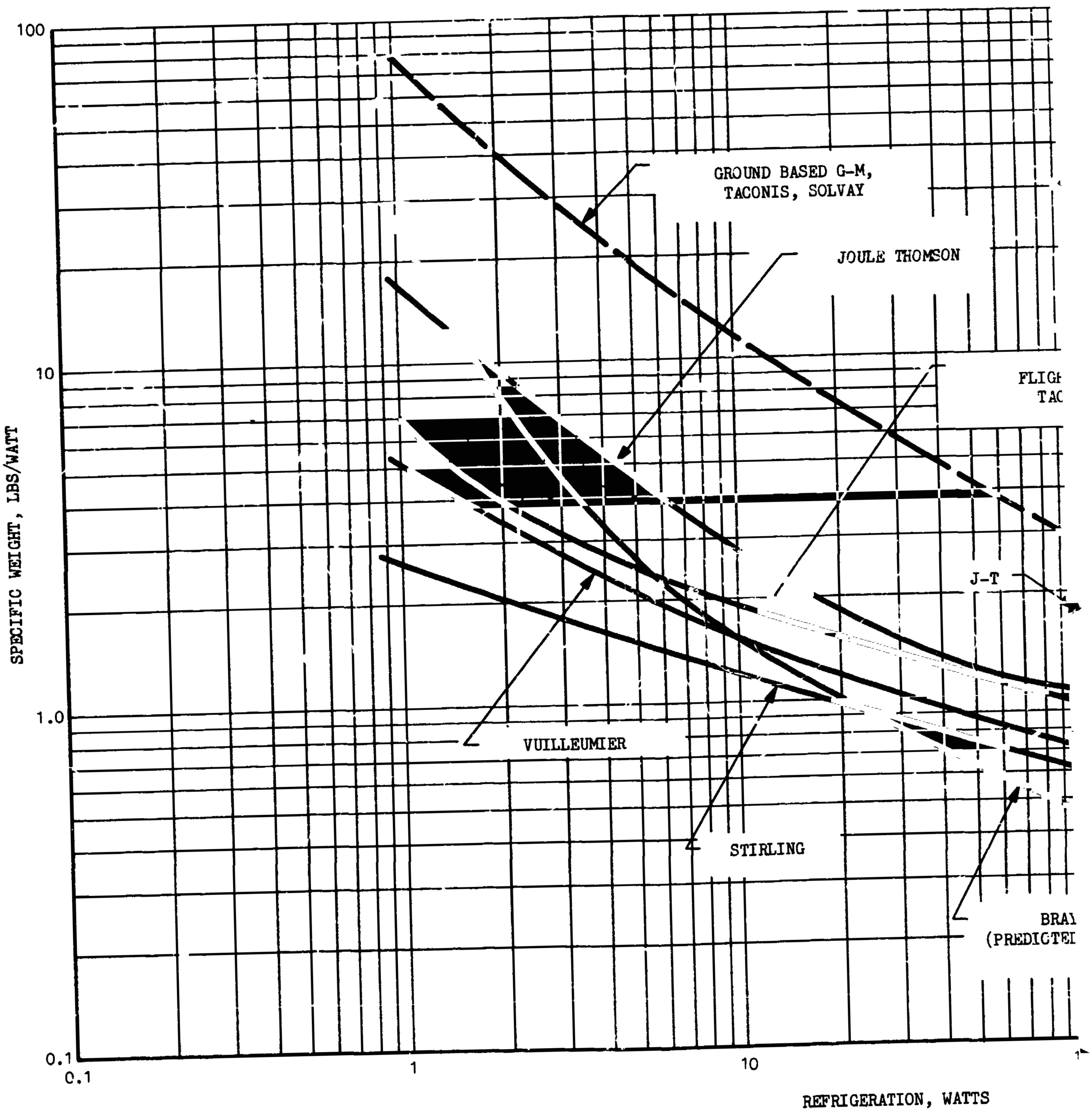

FOLDOUT FRAME 2

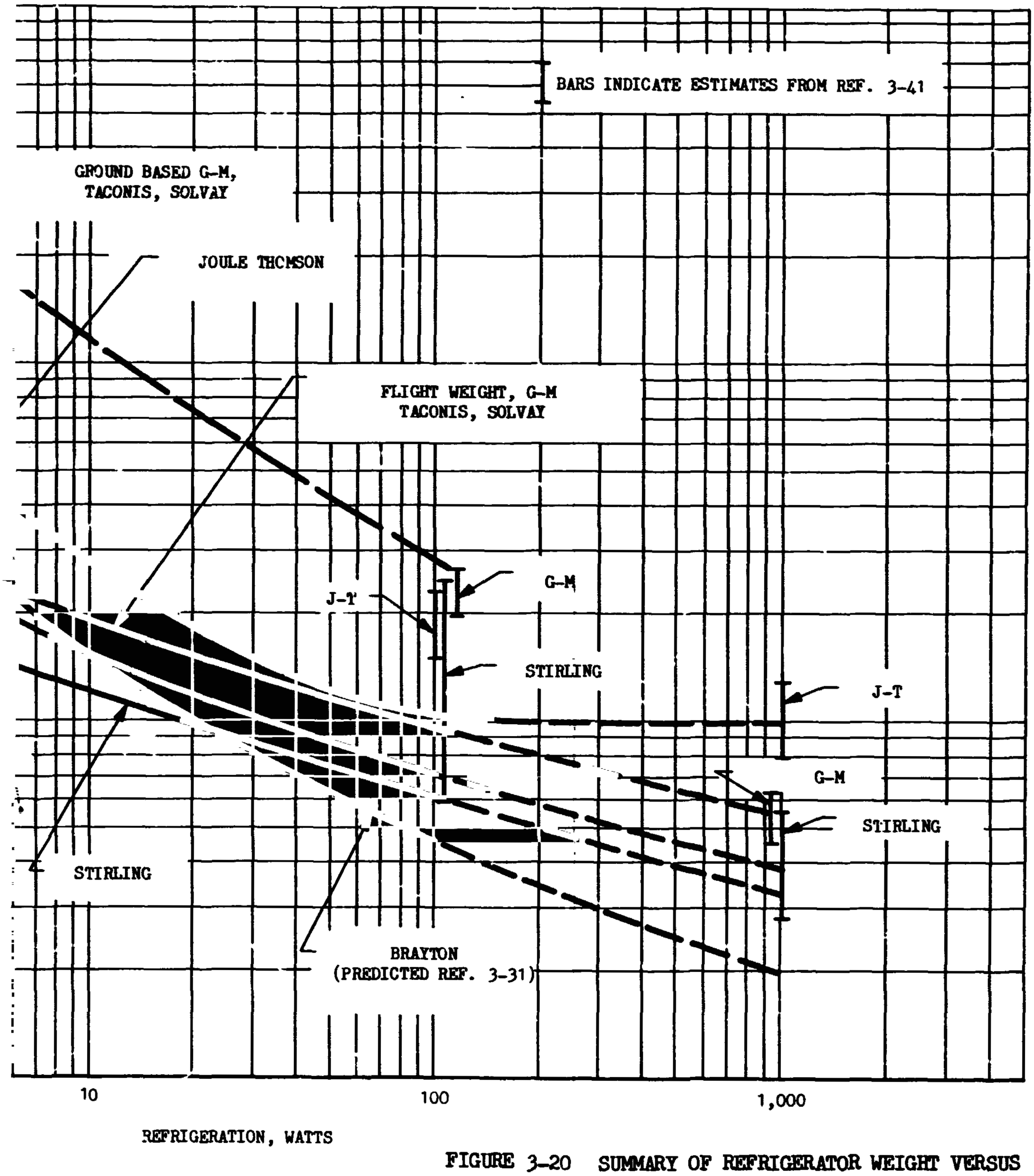

FIGURE 3-20 SUMMARY OF REFRIGERATOR WEIGHT VERSUS REFRIGERATION FOR VARIOUS CYCLES AT 77°K

PRECEDING PAGE BLANK NOT FILMED

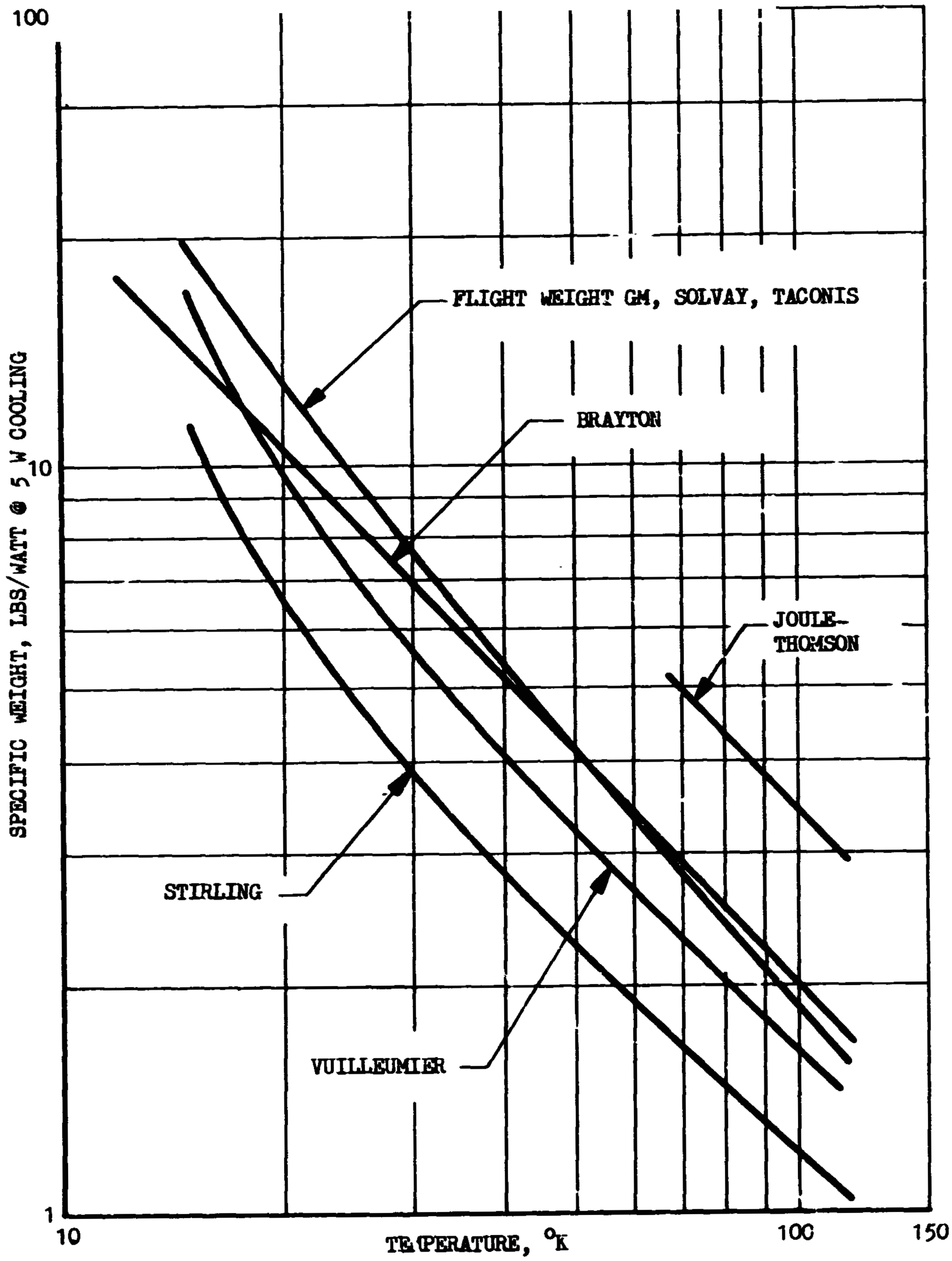

FIGURE 3-21 SUMMARY OF REFRIGERATOR WEIGHTS VS. TEMPERATURE AT 5 WATT COOLING CAPACITY

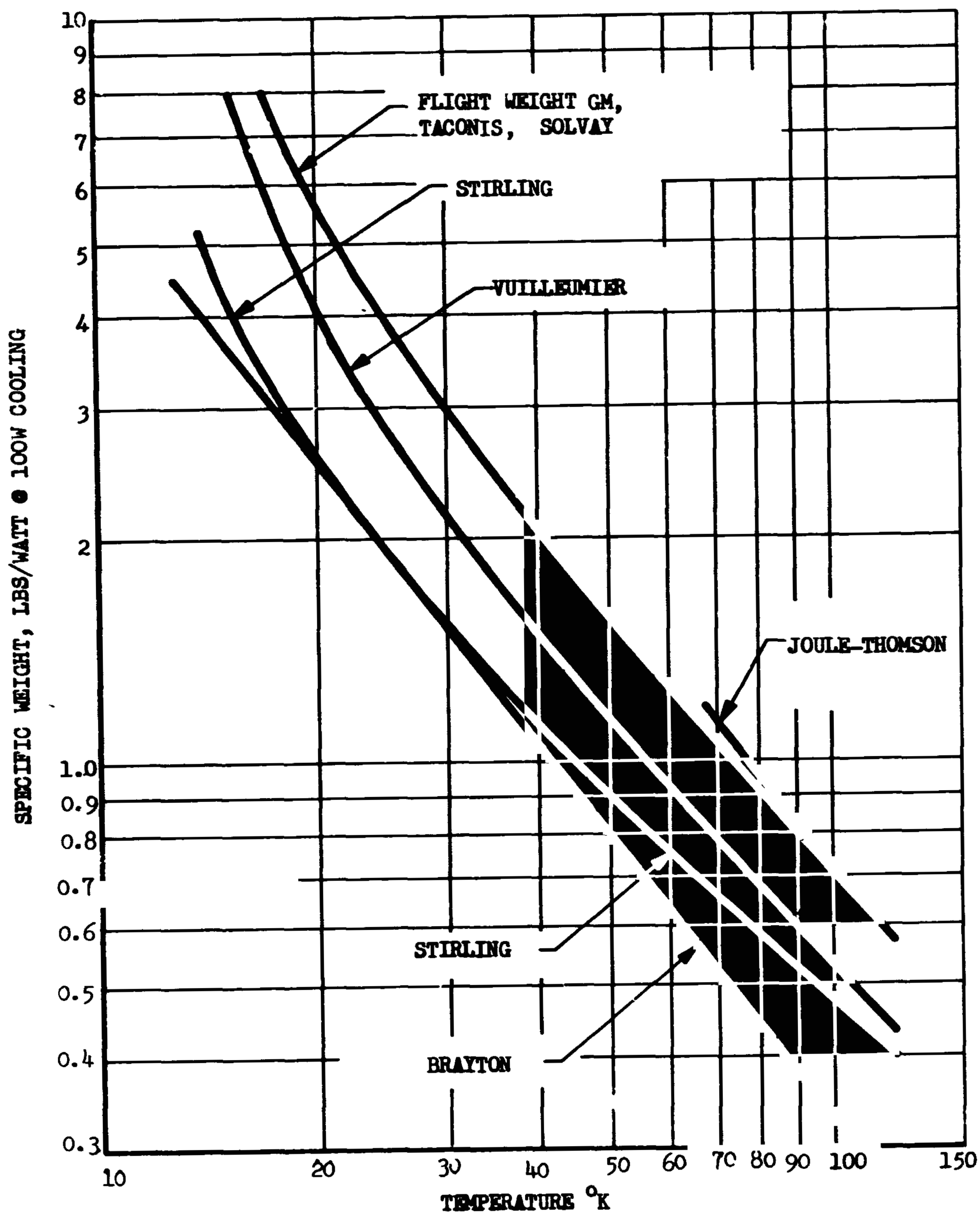

FIGURE 3-22 SUMMARY OF REFRIGERATOR WEIGHTS VS. TEMPERATURE AT 100 WATT COOLING CAPACITY

specific units are shown in the tables. Some cycles are inherently more compact than others.

For example, the Stirling cycle can be conveniently fabricated in a single unit and lends itself to compact packaging. The Solvay cycle on the other hand may consist of two or three separable units (compressor, cryostat, valve assembly) in which the overall volume is somewhat higher. The Solvay or Gifford McMahon unit on the other hand, offers greater flexibility since the cryostat is quite small and can be more easily integrated into a cryogenic system, while the compressor can be mounted in a remote location, connected to the cryostat only by the gas supply and return lines.

Several correlations of the volume data were attempted, the first being system volume vs power input. The result showed excessive scatter. A more successful correlation is shown in Figure 3-23 which shows the system density as a function of system weight. The data show considerable scatter. Also shown on the curve is data on large industrial units which provide cooling at $4.2^{o}K$ (Reference 3-68). The following trends are in evidence from the data.

1. The density of lightweight units intended for flight is quite low. This is felt to be due to the greater use of lightweight materials such as aluminum in place of the more commonly utilized steel.
2. The lightweight Stirling units seem to form a separate trend at a higher density. This may be due to the basic character of the cycle which lends itself to very efficient packaging compared with the other units.
3. The data appear to show a reduction in density with increased weight. A possible explanation for this is that the larger units were specifically intended for terrestral use in which the design goals were ease of installation and servicing of components. A greater potential for volume reduction therefore exists for the large units.

PRECEDING PAGE BLANK NOT FILMED

FOLDOUT FRAME 1

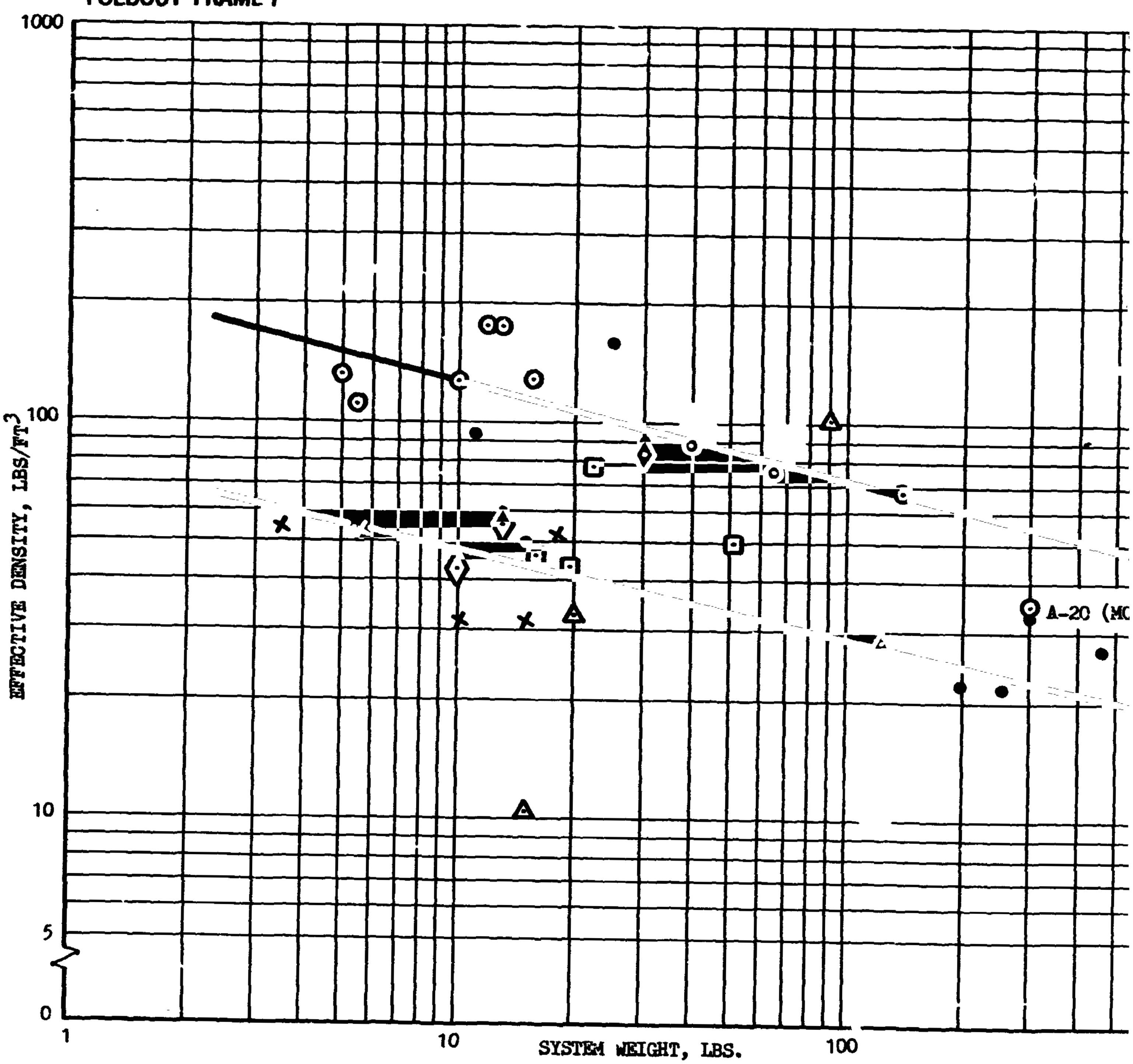

FOLDOUT FRAME 2

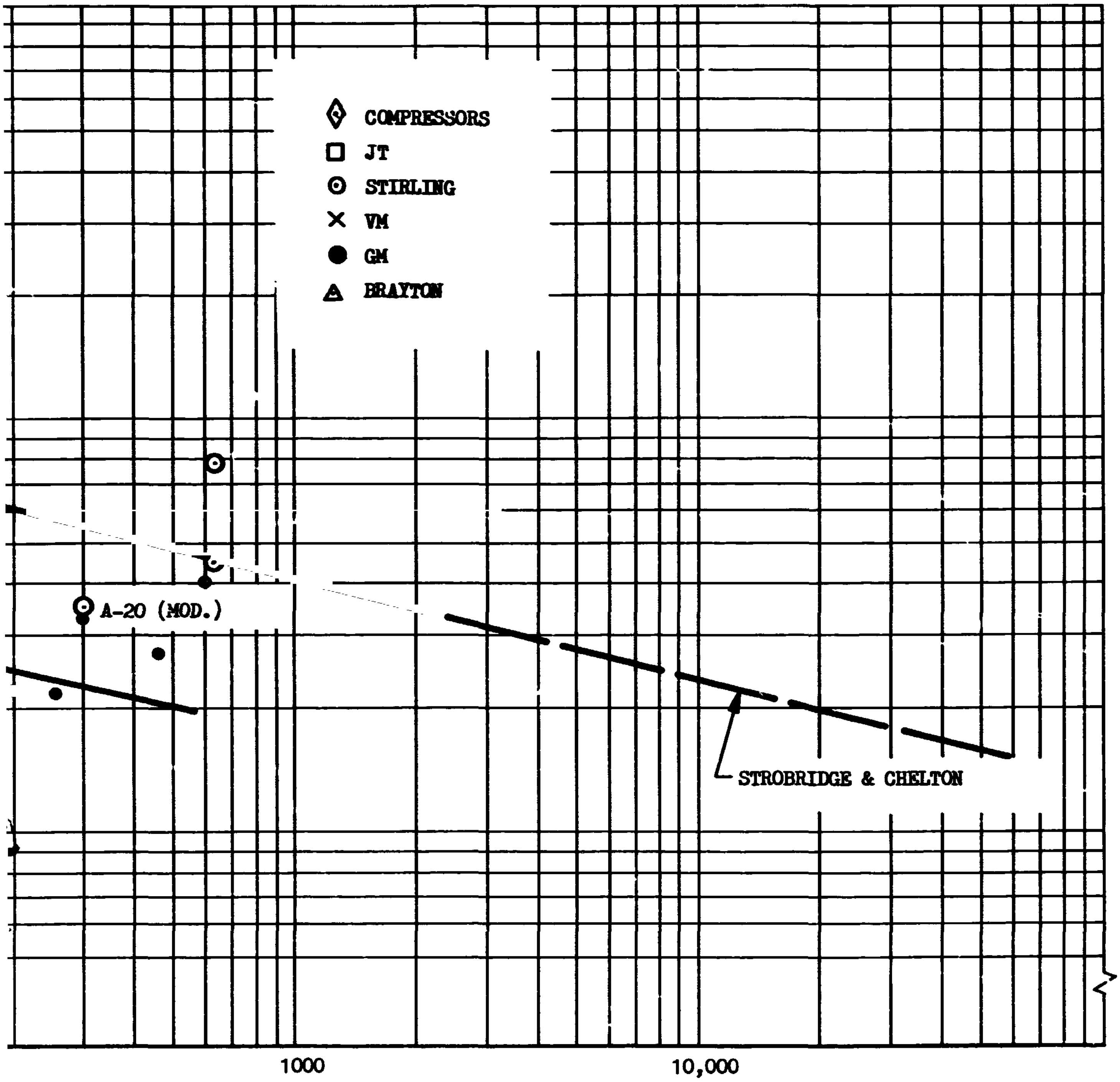

FIGURE 3-23 REFRIGERATOR SYSTEM DENSITY
VERSUS SYSTEM WEIGHT

It is suggested that in the absence of better volume data for a unit the two density lines should be utilized; one for the Stirling units and one for the other units as shown on the figure.

The system volume data which follows is based on Figure 3-23 in the absence of more specific data on units.

3.5.7 System Volume vs Cooling Rate

Figures 3-24 and 3-25 present the curve fits for specific volume as a function of cooling rate at 20°K and at 77°K for the cycles considered. The general character of the curves is again similar to the COP and weight curves. The volume curves represent the largest uncertainty of the various parameters and a substantial reduction in volume should be obtainable with proper design techniques. Most of the units have provisions for either air or water cooling included in the volumes, which may be eliminated, or at least reduced for space application.

3.5.8 System Volume vs Temperature

Figures 3-26 and 3-27 present a cross plot of the data for specific volume as a function of temperature at cooling rates of 5 and 100 watts. The same general considerations govern the character of these curves as for the COP and weight data.

3.6 COOLDOWN TIME OF REFRIGERATORS

Data have been included, where available, on the cooldown times of the various refrigerators in the data tabulations. The cooldown times of the units specified by the manufacturers are generally for conditions of minimum heat load and little or no mass attached to the cold head of the unit. The primary usage of the smaller units has been in cooling infrared detectors in which the mass of the focal plane assembly unit is small, generally in the range of 50-100 gms. In addition, the heat load to the cold finger is minimized to levels often in the area of 100-200 mw. As a result, most of the data available on cooldown of the closed cycle units is for those conditions where the heat to be removed is minimal.

PRECEDING PAGE BLANK NOT FILMED

FOLDOUT FRAME 1

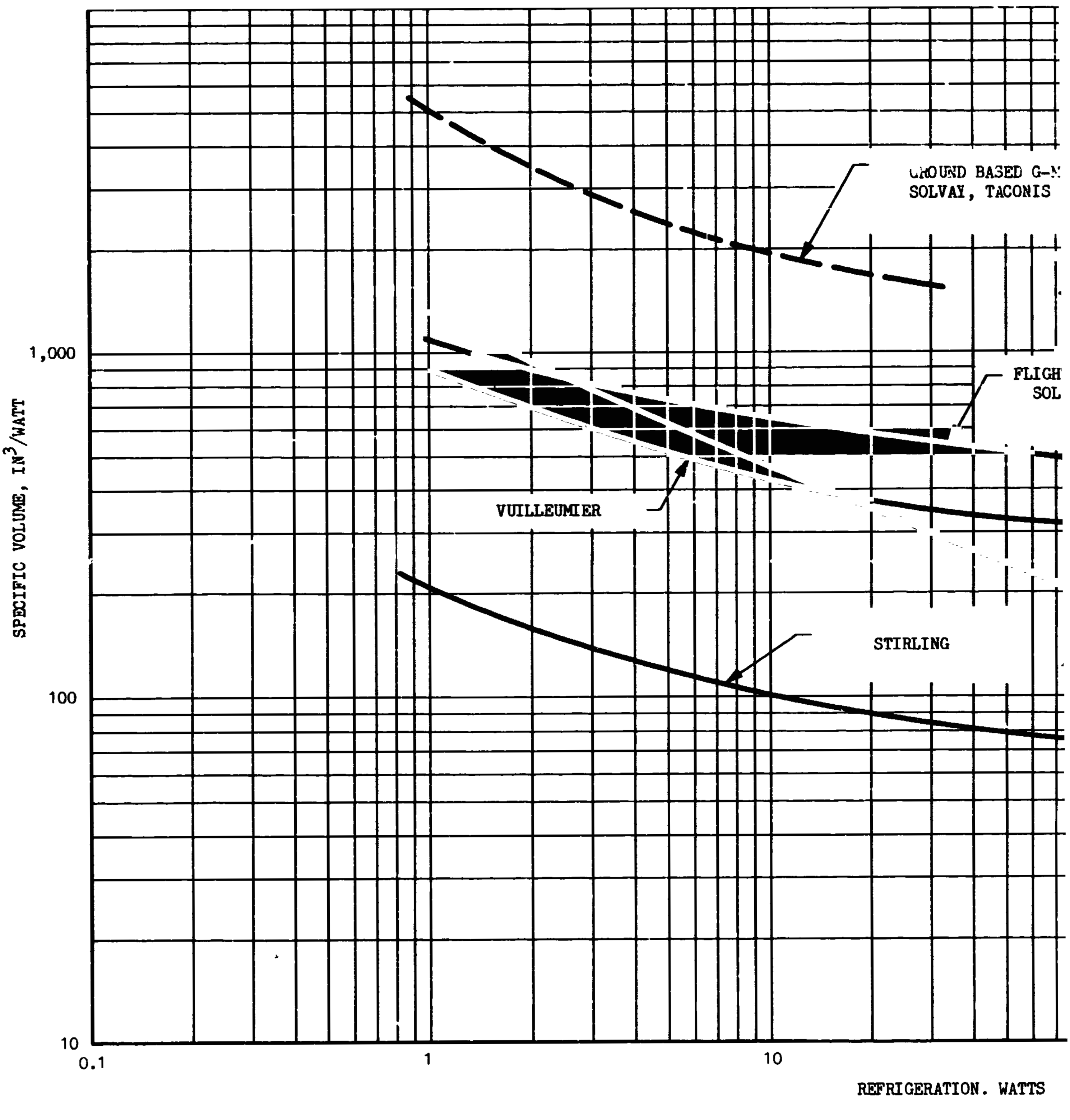

FOLDOUT FRAME 2

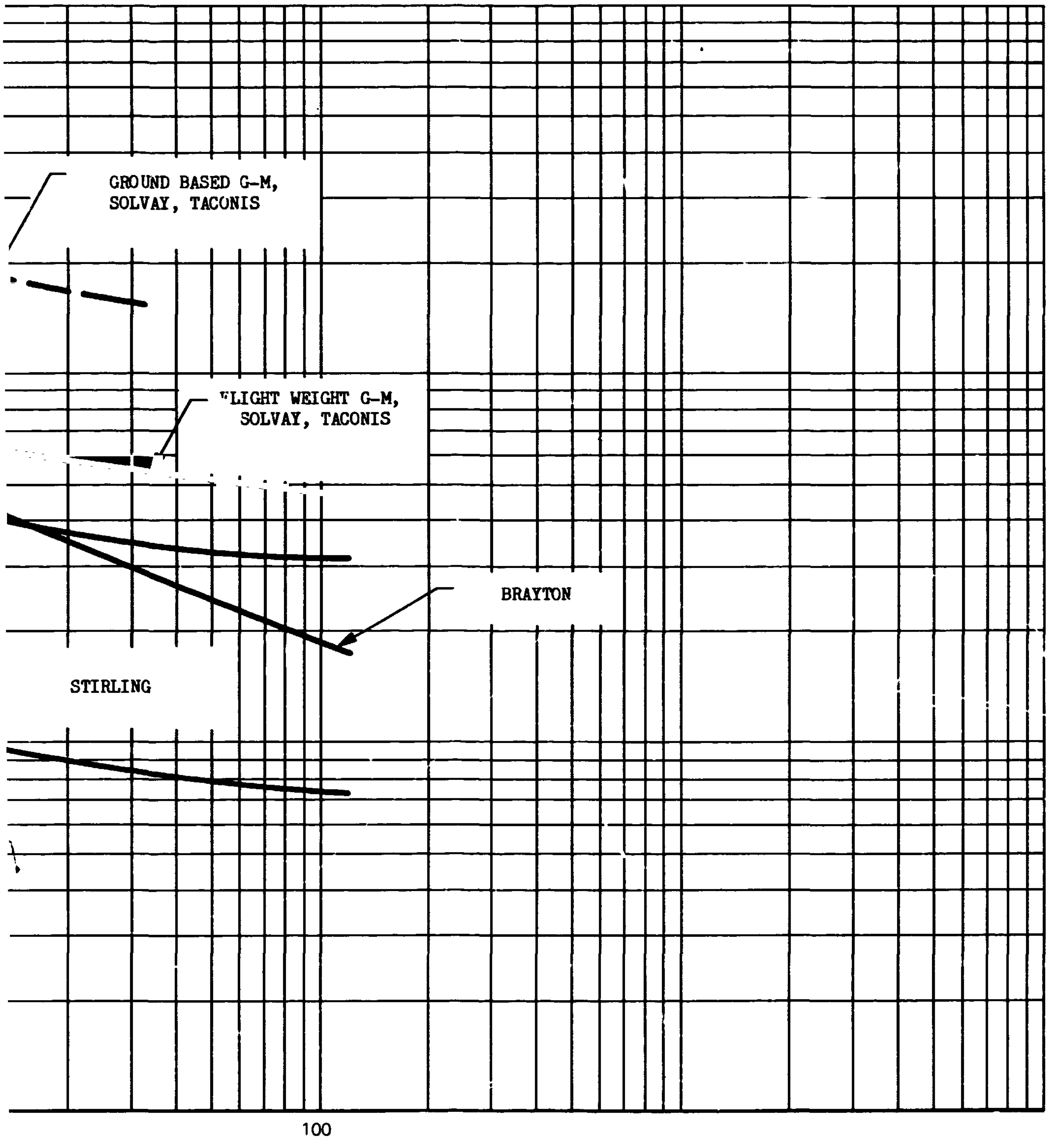

FIGURE 3-24 SUMMARY OF REFRIGERATOR SPECIFIC VOLUME VERSUS REFRIGERATION AT 20°K

PRECEDING PAGE BLANK NOT FILMED

FOLDOUT FRAME 1

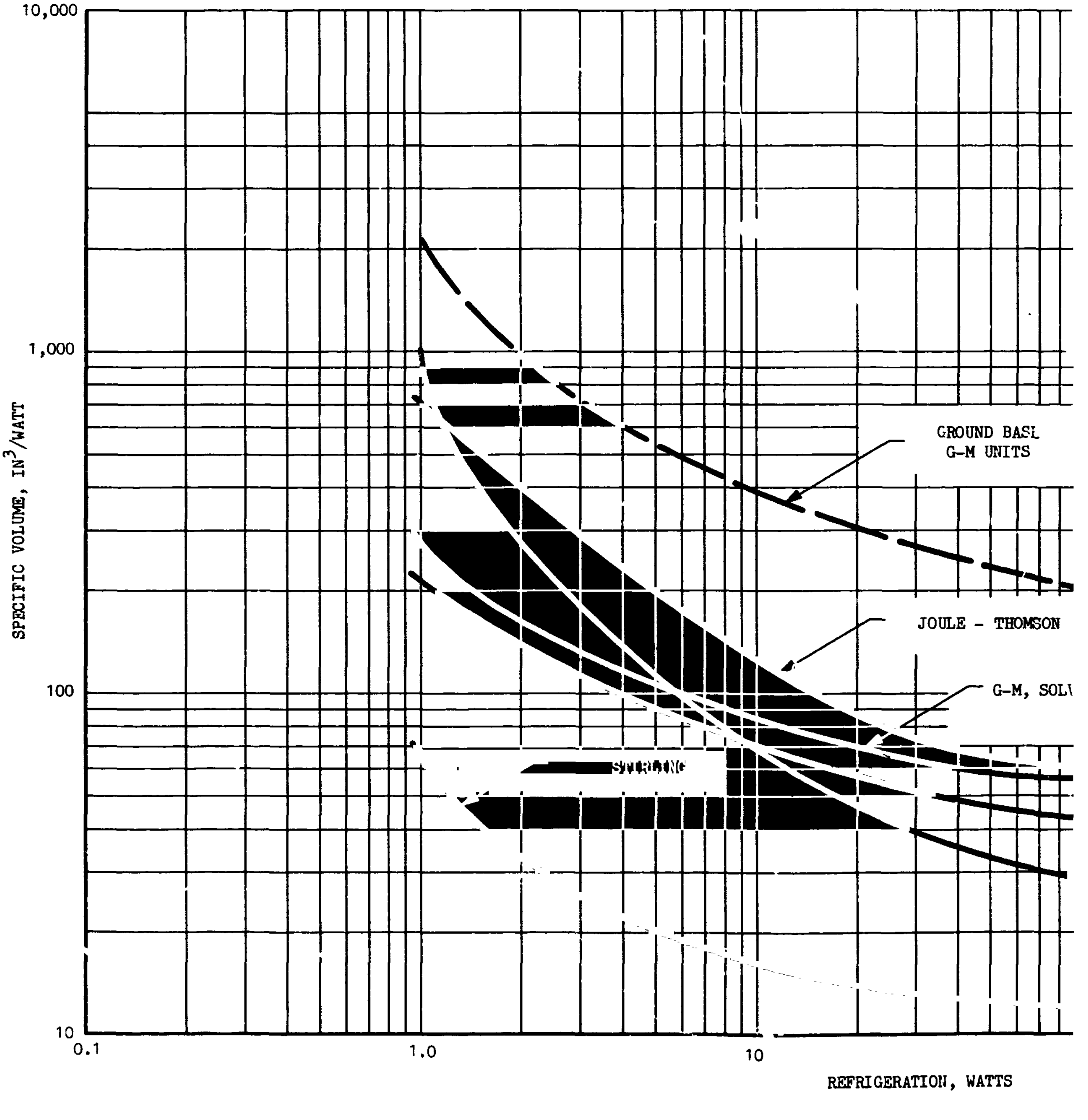

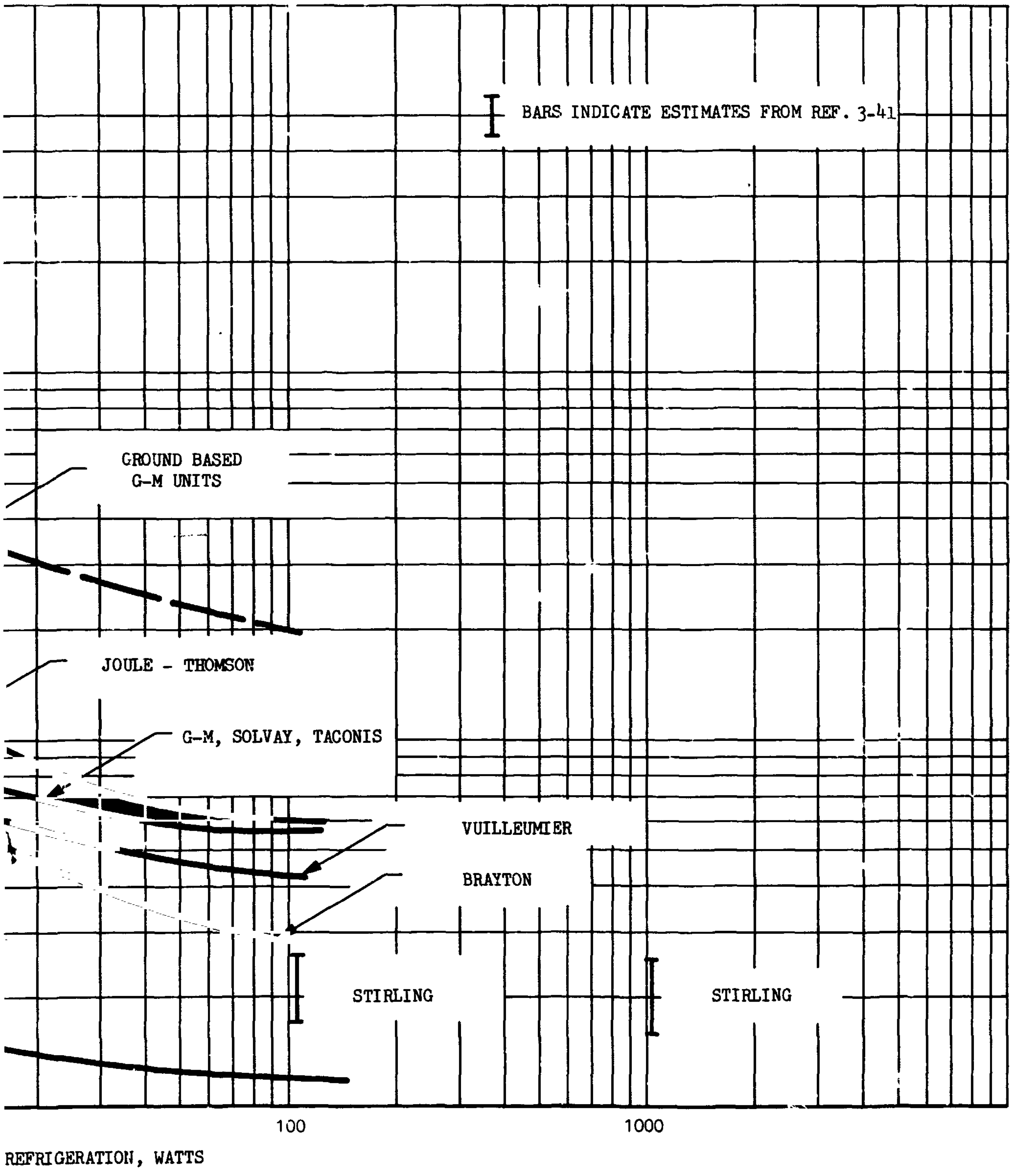

FIGURE 3-25 SUMMARY OF REFRIGERATOR SPECIFIC VOLUME VERSUS REFRIGERATION AT 77°K

PRECEDING PAGE BLANK NOT FILMED

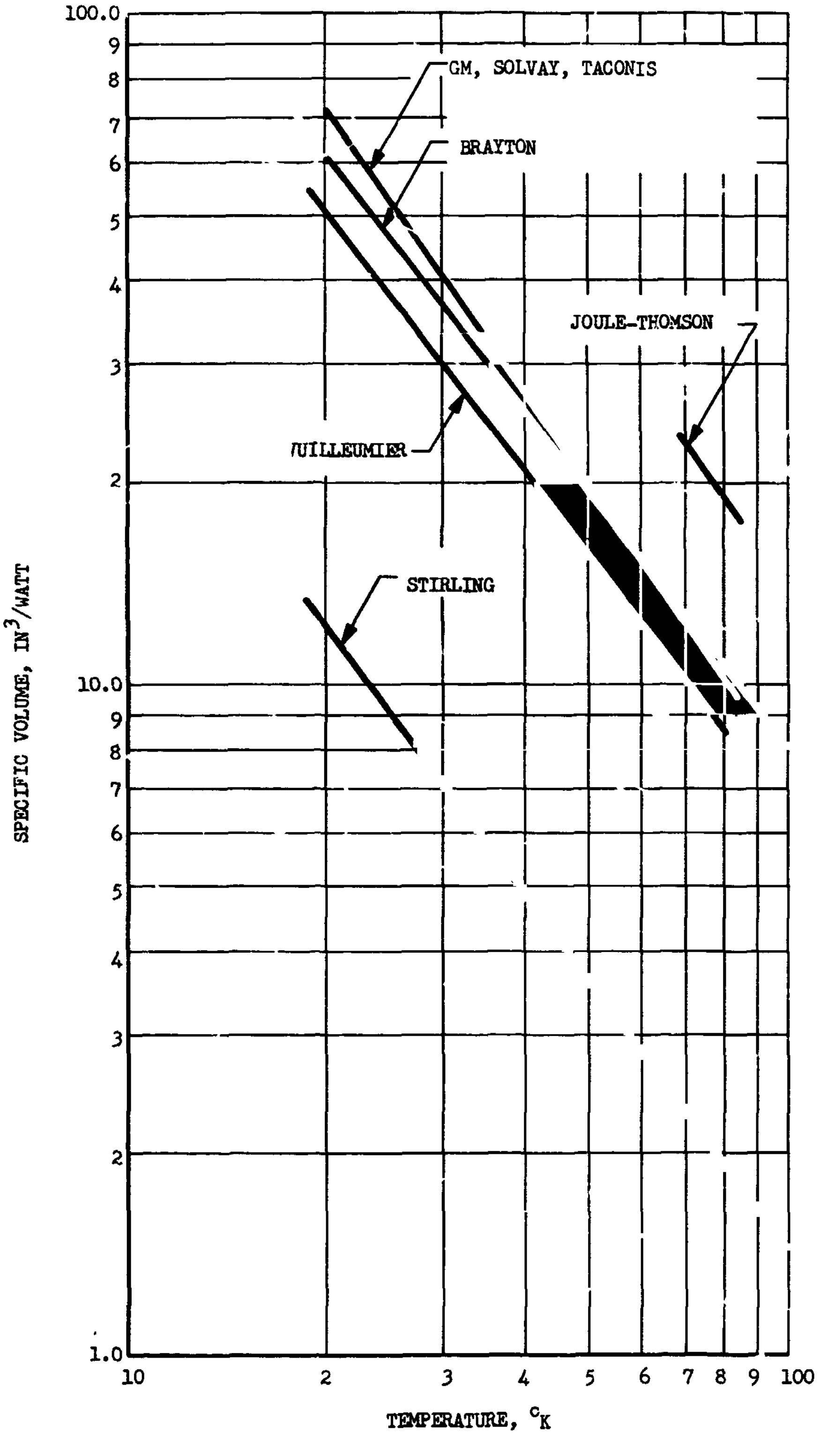

FIGURE 3-26 SUMMARY OF REFRIGERATOR SPECIFIC VOLUME VERSUS TEMPERATURE FOR VARIOUS CYCLES AT 5 WATTS

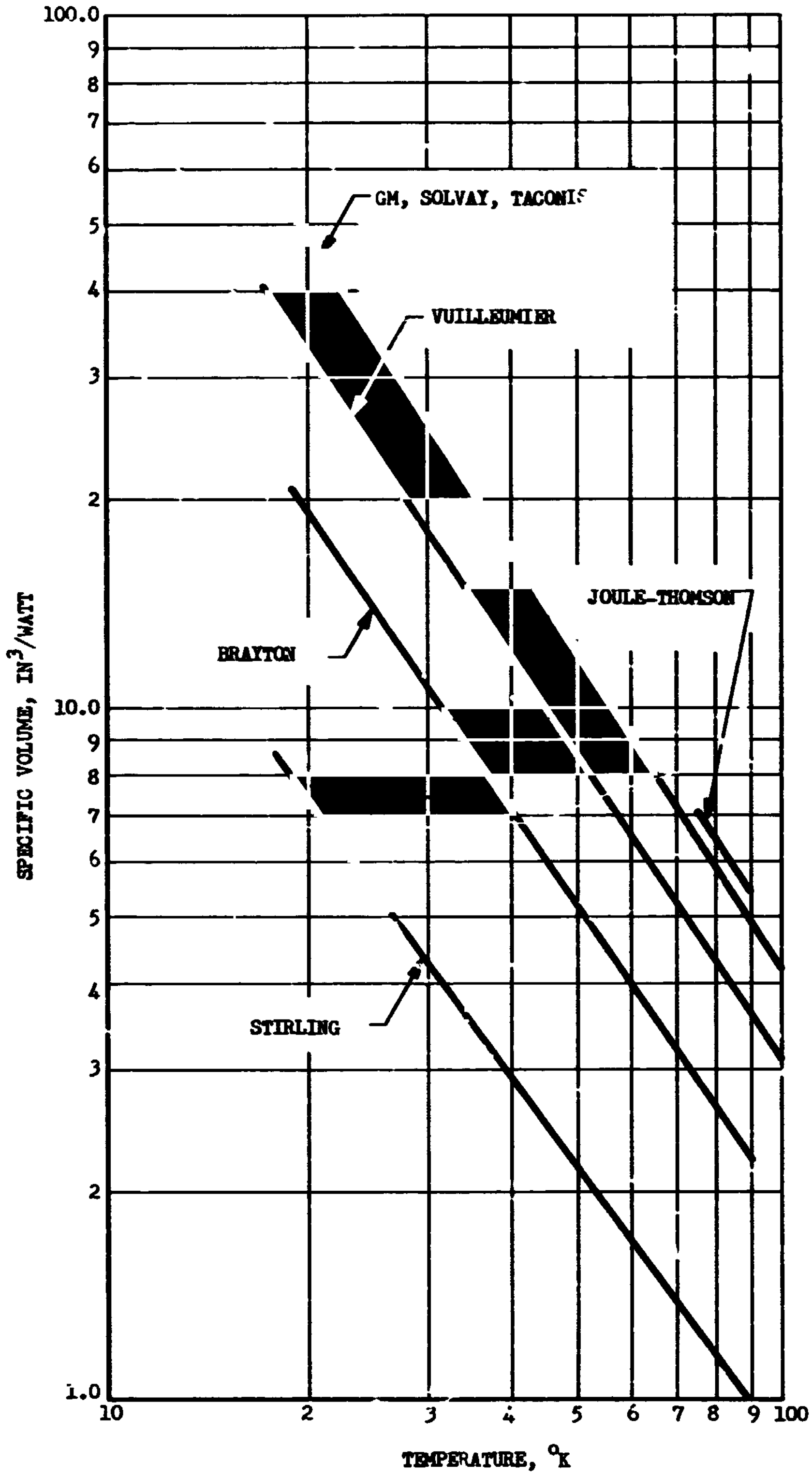

FIGURE 3-27 SUMMARY OF REFRIGERATOR SPECIFIC VOLUME VERSUS TEMPERATURE FOR VARIOUS CYCLES AT 100 WATTS

For applications where the mass to be cooled is substantially higher and where intermittent operation is desirable, the time for the refrigerator to cool down to its required operating condition can be an important design consideration. One example is an infrared telescope where the barrel and optical elements, which represent a significant mass, must be cooled. Another is the case of intermittent refrigeration of propellant tanks in which it is desired to eliminate venting of the tank. In this case, heat exchanger elements and/or secondary fluid coolant systems must be cooled down to operating conditions prior to efficient propellant refrigeration.

The required information to determine the cooldown rate for various systems is the net refrigeration as a function of temperature for the unit being considered. If this information is available, then a transient analysis can be made which accounts for both external heat inputs and heat removal from items being cooled. Unfortunately, most of the manufacturers specify refrigeration rate versus temperature only in the general region of the operating temperatures, and cooling rates up to the ambient temperatures near 200°K to 300°K are not generally available. It is felt that analysis techniques of predicting cooldown rates are extremely complex and not suitable. A discussion of analytical techniques for cool-down prediction is described in Ref. 3-67.

In order to form a rough guide in estimating the general cooldown characteristics of various refrigerators Figs. 3-28 and 3-27 were prepared. They show the cooling rate at temperature T normalized to the cooling rate at a specific temperature of interest as a function of temperature. As expected, the various units show a wide variation. It is suggested that in order to make an order of magnitude estimate the conservative or lower curves be used for design tradeoff purposes. It should be noted that a lengthy extrapolation of data to 300°K is required for all units except a Stirling unit for which data to 250°K was obtained. Manufacturers should be contacted for more specific data.

A useful technique in obtaining general cooldown data is to obtain the time required to cool two different masses on the end of the cold finger to a desired temperature. The cooldown time is proportional to the mass attached to the cold finger, and this proportionally can be determined from the two measurements. Data obtained in this manner is normally for initial temperatures of 300°K and limits the utility of the data when lower initial temperatures exist, for example, on a space application. An example of this type of data is shown in Fig. 3-30. The cooldown time versus mass of copper is shown for various units, primarily for the Cryogenic Technology Inc. units for which these data are available, and for a single Stirling unit. The cooldown time is naturally a strong vunction of the steady state cooling rate and the minimum temperature. Figure 3-30 is shown only as an illustration, unfortunately sufficient data is not available to generate general curves of this nature for design purposes. This data is for a mass of copper at the cold finger; copper is normally utilized to minimize temperature gradients in the cooled block. The heat removed in cooling copper from 300°K to 40°K is 12,700 J/lb as noted on Fig. 3-30.

3.7 EFFECT OF HEAT REJECTION TEMPERATURE ON REFRIGERATOR PERFORMANCE

Refrigeration systems in use at this time reject heat at temperatures near ambient ($\sim$ 300°K). This is due primarily to the convenience of rejecting the waste heat by air or water circulation to the atmosphere. No systems are known which reject heat at temperatures significantly different than this. It is felt that significant efforts would be required to develop systems which operate at temperatures substantially different from ambient. Lower temperatures leading to improved thermal efficiency may require modified sealing techniques for the working gas (rubber O-rings are used in most present systems) and wear characteristics of rubbing surfaces would undoubtedly change with temperatures. Let it suffice to say that this area has not been explored to a significant degree.

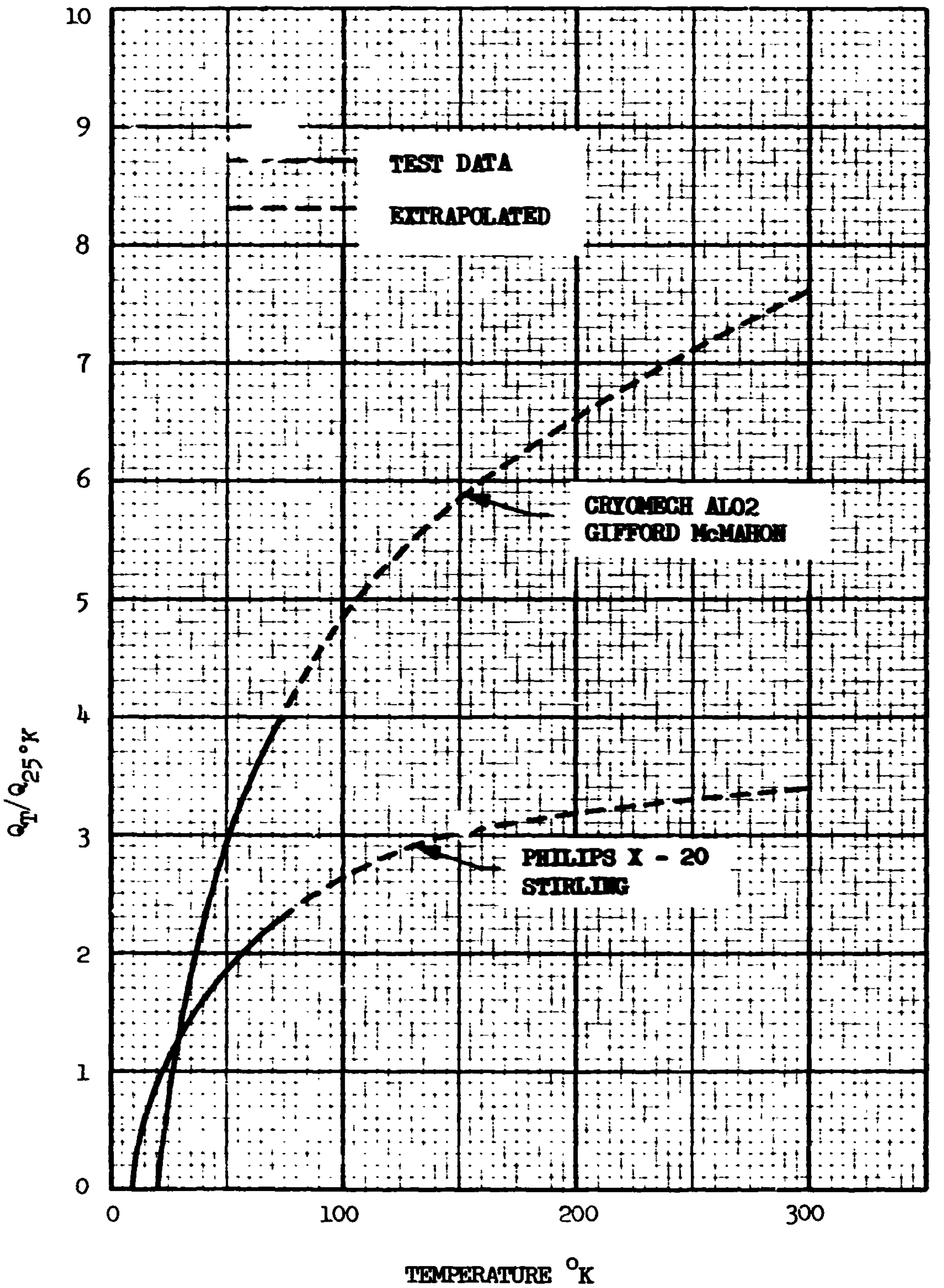

Figure 3-28. Estimated Cool-Down Characteristics of Various Refrigerators for 25°K Cooling

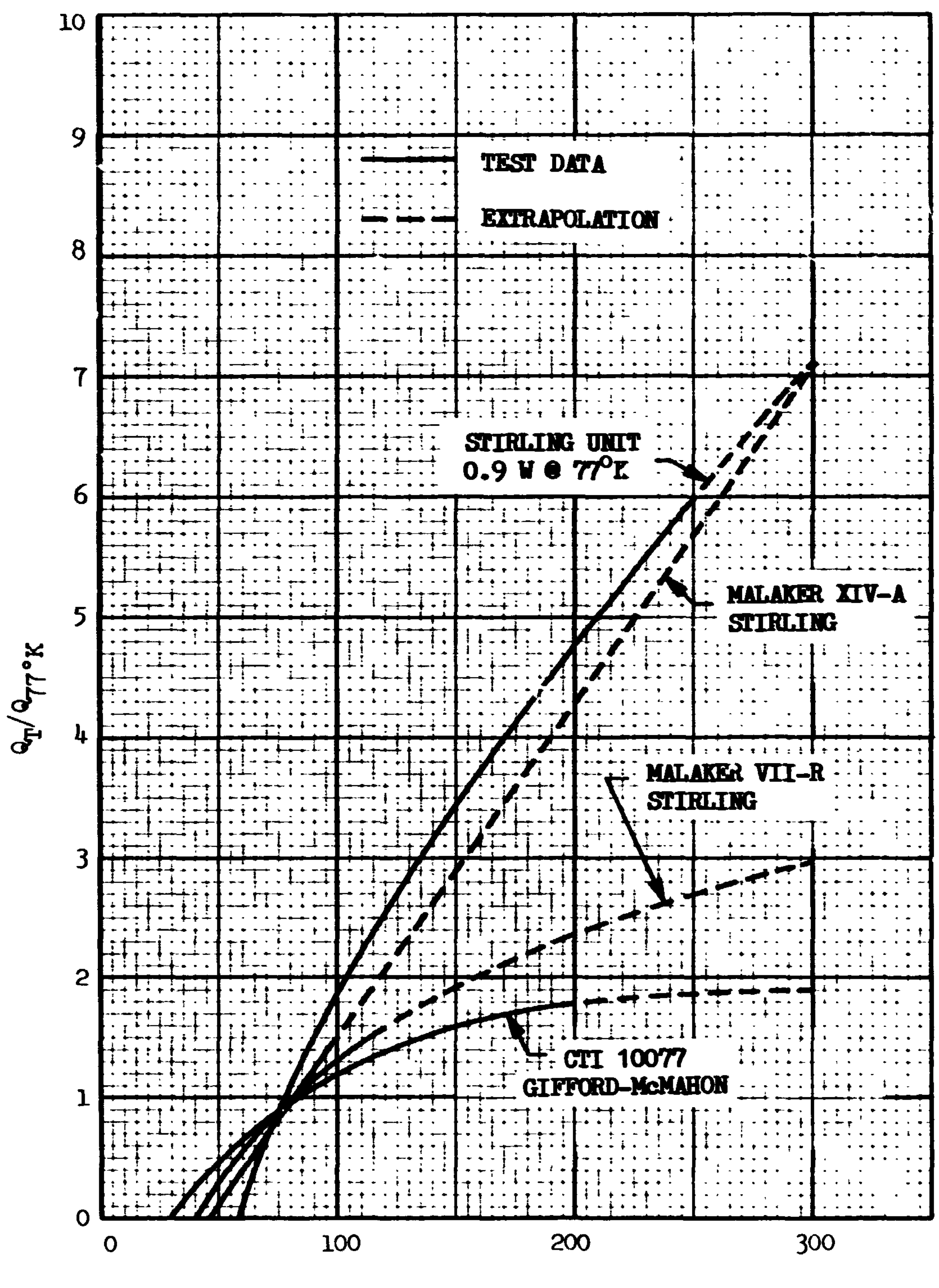

Figure 3-29. Estimated Cool-Down Characteristics of Various Refrigerators for 77°K Cooling

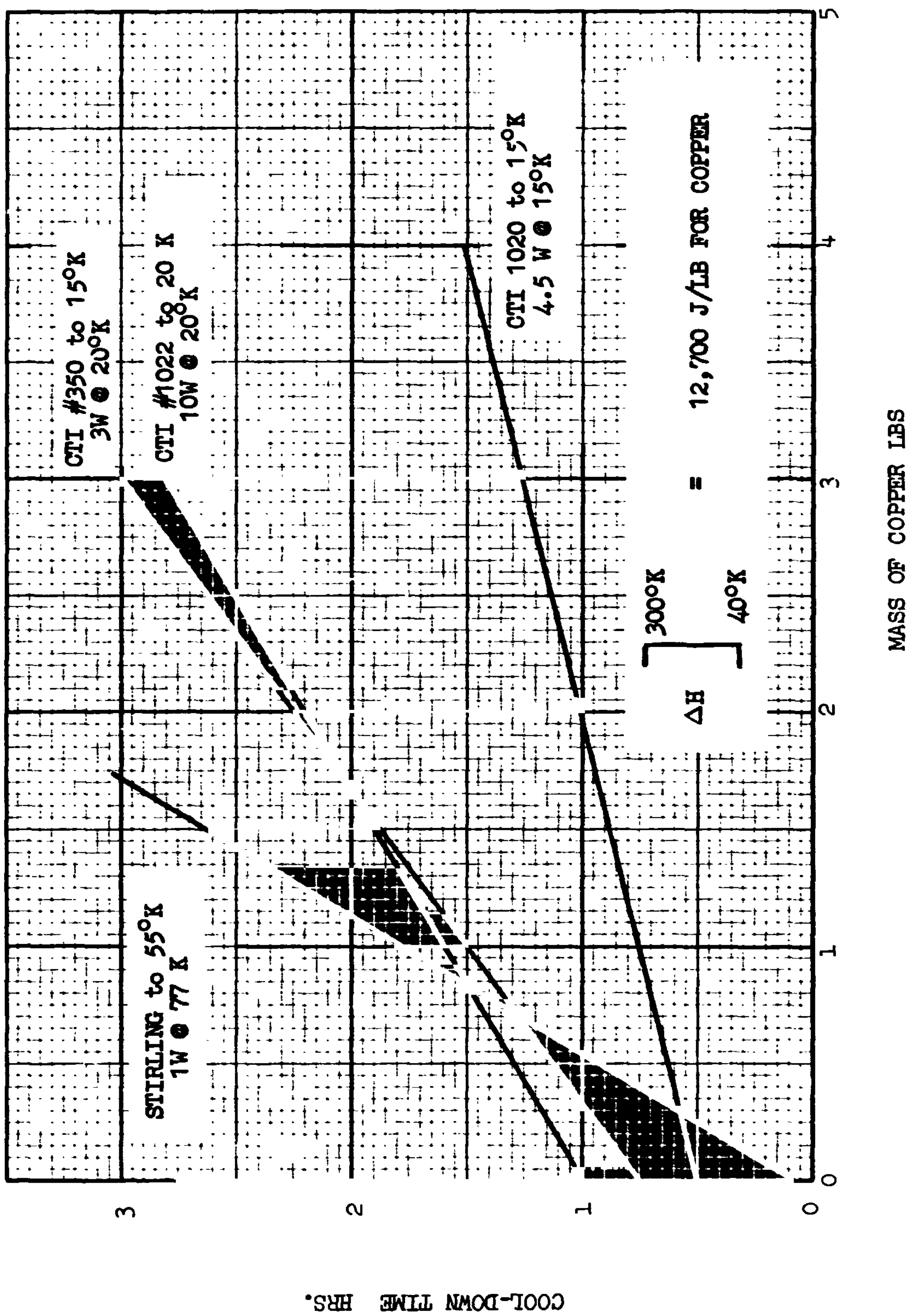

Figure 3-30. Cool-Down Times for Various Refrigerators (from 300°K)

The advantage of reducing the heat rejection temperature of the refrigerator is to improve the thermal performance. The thermal performance of the ideal Carnot cycle is given by:

$$\frac{\text{refrigeration output}}{\text{power input}} = \text{C.O.P.} = \frac{T_c}{T_h - T_c}$$

As indicated in the previous sections, the actual performance of operating systems is a fraction of the Carnot performance. In order to make system tradeoff studies where it is desired to study the effect of variations in the heat rejection temperature it is recommended that the actual performance (COP) of a unit being considered at ambient temperature be modified, according to the Carnot efficiency for various temperatures.

$$(\text{COP})_{T_h} = (\text{COP})_{300^\circ\text{K}} \times \frac{300^\circ\text{K} - T_c}{T_h - T_c}$$

For a given cooling rate, the required power input can be reduced by rejecting heat at a lower temperature as given by the Carnot relationship. Contrarily, an increased heat rejection temperature requires greater power input than the 300°K base point, but leads to a more efficient, lighter radiator for waste heat rejection.

Data correlations for refrigeration systems and compressors investigated in this contract indicate that the weight and size of these units can be correlated as a function of their power input. Other investigators have shown this correlation (Ref. 3-68). An example of this correlation for the units considered is presented in Fig. 3-18.

Figures 3-16 and 3-23 may be used to find the change in refrigeration system weight and volume as a result of a change in the heat rejection temperature.

In summary, the following procedure is recommended to perform tradeoff studies for a perturbation of heat rejection (radiator) temperature:

(1) Establish the characteristics (i.e., cooling load, weight, size, and power input) of the refrigerator rejecting heat at 300°K.

(2) Modify the COP of the unit corresponding to the new rejection temperature (assuming the required refrigeration level remains constant) using equation (3-29).

(3) Determine the power input for the new rejection temperature.

(4) Find the new weight and size of the unit for the new power input utilizing Fig. 3-18 and 3-23.

Some studies have been performed to determine the effect of the heat rejection temperature on the total system weight (refrigerator, power supply, and radiator) and the results have indicated the optimum to be near 300°K and fairly flat (Ref. 3-69, 3-70) for the particular conditions assumed. For other conditions the effect of heat rejection temperature may be more significant.

3-8. LIST OF REPORTS AND REFERENCES

3-1. Zefex, Inc., Bulletins 114-2, 114-118-1, 118-1, 118-3

3-2. Gast Manufacturing Corp., Bulletin ROC-169

3-3. Tecumseh Products Company, Bulletin 108-8

3-4. Bendix-Westinghouse Automotive Air Brake Company, Form No. BWE-581-9.

3-5. Copeland Refrigeration Corporation, Form No. 5907-R-10

3-6. Maddocks, F. E., "3.6°K Closed-Cycle Turborefrigerator" AFFDL-TR-67-134, Air Force Flight Dynamics Laboratory, Wright-Patterson Air Force Base, Ohio, October 1968

3-7. Breckenridge, R. W., "Exporatory Development of a 1 watt, 3.6°K Reciprocating Refrigerator for Space Applications", AFFDL-TR-68-59, Air Force Flight Dynamics Laboratory, Wright-Patterson Air Force Base, Ohio

3-8. Colyer, D. B., "Miniature Cryogenic Refrigerator Turbo alternators", Advances in Cryogenic Engineering, Vol. 14, Plenum Press, New York, (1969.)

3-9. Kohler, J. W. L., "The Stirling Refrigeration Cycle", Scientific American, April 1965, Vol. 212, No. 4, pp. 119-127.

3-10. Kohler, J. W. L., "Principles of Gas Refrigerating Machines", Advances in Cryogenic Engineering, Vol. 2, Plenum Press, New York (1960), pp. 243-249

3-11. Kohler, J. W. L., "Refrigeration Below -100°C", Advances in Cryogenic Engineering, Vol. 5, Plenum Press, New York (1960), pp. 518

3-12. Prast, G., "A Modified Philips Stirling Cycle for Very Low Temperatures", Advances in Cryogenic Engineering, Vol. 10, Plenum Press, New York (1964), p. 40-45

3-13. Cowans, K. W., Walsh, P. J., "Continuous Cryogenic Refrigeration for Three to Five Micron Infrared Systems", Advances in Cryogenic Engineering, Vol. 10, Plenum Press, New York (1964), pp. 468-476

3-14. Rios, P. A., Smith, J L., Jr., "An Analysis of the Stirling-Cycle Refrigerator", Advances in Cryogenic Engineering", Vol. 14, Plenum Press, New York (1968), p. 332

3-15. Qvale, E. B., "An Analytical Model of Stirling-Type Engines", PhD Thesis, Massachusetts Institute of Technology, Jan. 1967.

3-16. Rios, P. A., "An Analytical and Experimental Investigation of The Stirling Cycle," PhD thesis, Massachusetts Institute of Technology, Sept. 1969.

3-17. Malaker Laboratories, "Miniature Stirling Cycle Cooler", AFAL-TR-65-15, July 1964

3-18. Pitcher, G. K., DuPre, F. K. "Miniature Vuilleumier Cycle Refrigerator", Advances in Cryogenic Engineering, Vol. 15, Plenum Press, New York (1969)

3-19. Magee, F. N., Doering, R. D., "Vuilleumier Cycle Cryogenic Refrigerator Development", AFFDL-TR-68-67, August 1968.

3-20. Dean, J. W., Mann, D. B., "The Joule-Thomson Process in Cryogenic Refrigeration Systems", NBS TN 227, National Bureau of Standards, Feb. 1965

3-21. Muhlenhaupt, R. C., Strobridge, T. R. "An Analysis of the Brayton Cycle as a Cryogenic Refrigerator", NBS TN 366, National Bureau of Standards, August 1968

3-22. Muhlenhaupt, R. C., Strobride, T. R., "The Single-Engine Claude Cycle as a 4.2°K Refrigerator." NBS TN 354, National Bureau of Standards, June 1967

3-23. Wilson, D. J., d'Arbeloff, B. J., "The Performance of Refrigeration Cycles Below 100°R." Advances in Cryogenic Engineering, Vol. 11, Plenum Press, New York (1965), pp. 160-170.

3-24. Johnson, R. W., Collins, S. C., "A Hydraulically Operated Two-Phase Helium Expansion Engine", Advances in Cryogenic Engineering, Vol 16, Plenum Press, New York, 1970 (E-4)

3-25. Wapato, P. G., "Design and Development of a Miniature Non-Reciprocating Closed-cycle Cooler, TR AFFDL-TR-67-9, March 1967.

3-26. Maddocks, F. E., "3.6°K Closed-Cycle Turborefrigerator", AFFDL-TR-67-134, Oct. 1968

3-27. Breckenridge, R. W., "Development of a Miniature Reciprocating Cryogenic Refrigerator for Space Applications", AFFDL-TR-67-78, May 1967.

3-28. Breckenridge, R. W., "Exploratory Development of a 1 Watt, 3.6°K Reciprocating Refrigerator for Space Applications," AFFDL-TR-68-59, Oct. 1968.

3-29. Crawford, A. H., "Specifications of Cryogenic Refrigerators", Cryogenics, Vol. 10, No. 1, Feb. 1970, pp. 28-37.

3-30. Colyer, D. B., Gessner, R. L., "Miniature Cryogenic Refrigerator Turbomachinery", Advances in Cryogenic Engineering, Vol. 13, Plenum Press, New York (1967), pp. 485-493

3-31. Gessner, R. L., Colyer, D. B. "Miniature Claude and Reverse Brayton Cycle Turbomachinery Refrigerators, Advances in Cryogenic Engineering, Vol. 13, Plenum Press, New York, (1967), pp. 474-484.

3-32. Wapato, P. G., "Development of a 4.2°K Cryogenic Refrigerator System", AiResearch Manufacturing Corp. Rept. 66-0347, June 1966

3-33. Fleming, R. B., "A Compact Perforated-Plate Heat Exchanger", Advances in Cryogenic Engineering, Vol. 14, Plenum Press, New York (1968), pp. 197-204

3-34. Colyer, D. B., "Miniature Cryogenic Refrigerator Turboalternators", Advances in Cryogenic Engineering, Vol. 14, Plenum Press, New York (1968), pp. 405-415

3-35. "The Development of Closed-Cycle Cryogenic Coolers for Long Duration Continuous Operation", AiResearch Manufacturing Co., 1966

3-36. Schonewald, Roger, "Cryogenic Refrigeration Systems", Industrial Research, Vol. 7, No. 10, Sept. 1965, pp. 86-91

3-37. Rochkind, Mark M., "Long Duration Cooling Using Open-Cycle Joule-Thomson Refrigeration", Review of Scientific Instruments, Vol. 38, No. 8, Aug. 1967, pp. 1171-3

3-38. Daunt, J. G., Goree, W. S., "Miniature Cryogenic Refrigerators", Report to Office of Naval Research Contract Nonr-263(70) (Stevens Institute of Technology) and Contract N0014-67-C-0393 (Stanford Research Institute.) 1969

3-39. Gifford, W. E., "Refrigeration Below 20°K". Cryogenics, Vol. 10, No. 1, Feb. 1970, pp. 23-27

3-40. "Conceptual Design Study of Space-borne Liquid Hydrogen Recondensers for 10 and 100 Watts Capacity". Arthur D. Little, May 1962. Report No. 63270-11-02 NAS 5-664.

3-41. Malaker Laboratories, "Investigation of Gas Liquefiers for Space Operation." ADS-TDR-63-775, August 1963

3-42. Hagedorn, N. H., "Parametric Mass Analysis and Comparison of Two Types of Reactant Cooling- and-Storage Units for a Lunar-Based Hydrogen-Oxygen Regenerative Fuel Cell System." NASA TND-4386, February 1968

3-43. Stephens, S. W., "Advanced Design of Joule-Thomson Coolers for Infra-Red Detectors." The Hymatic Engineering Col. Ltd. Infrared Physics, Vol. 8, No. 1, 1968, pp. 25-35

3-44. Breckenridge, R. W., "Spaceborne Refrigeration Systems." Cryogenics and Infrared Detection Systems Technical Colloquium, Frankfurt, W. Germany, April 1969

3-45. McCormick, J. E., "Cryogenic Refrigeration Efficiency Nomograph." ASHRAE Journal, Vol. 8, No. 11, 1966, pp. 60-65

3-46. Strobridge, T. R., "Refrigeration for Superconducting and Cryogenic Systems." MBS., Particle Accelerator Conference, Washington, D. C., March 1969

3-47. Higa, W. H., "A Practical Phillips Cycle for Low-Temperature Refrigeration.", NASA TR-32-712, Nov. 1965

3-48. Kirkley, D. W., "A Thermodynamic Analysis of the Stirling Cycle and a Comparison with Experiment," SAE Paper 949B, Jan. 1965

3-49. Heffner, F. E., "Highlights from 6500 Hr of Stirling Engine Operation," SAE Paper 949D, Jan. 1965

3-50. Rios, P. A., "An Analytical and Experimental Investigation of the Stirling Cycle." PhD Thesis, Massachusetts Institute of Technology, Sept. 1969

3-51. Ackermann, R. A., and Gifford, W. E., "A Heat Balance Analysis of a Gifford-McMahon Cryorefrigerator", Advances in Cryogenic Engineering, Volume 16, 1970

3-52. Lucek, R., Damsz, G., Daniels, A., "Adaptation of Rolling Type Seal Diaphragms to Miniature Stirling Cycle Refrigerators." AFFDL-TR-67-96, July 1967

3-53. Curwen, P. W., "Recent Developments of Oil-Free Linear-Motor Resonant-Piston Compressors." ASME Publication 69-FE-36, June 1969

3-54. Meier, R. N., Currie, R. B., "A 4.°K Single-Engine Cycle Helium Refrigerator." Air Products and Chemicals, Inc., Advances in Cryogenic Engineering, Vol. 13, Plenum Press, New York, 1967, pp. 442-449

3-55. Higa, W. H., Wiebe, E., "A Simplified Approach to Heat Exchanger Construction for Cryogenic Refrigerators." Cryogenic Technology, Vol. 3, No. 2, March/April 1967, pp. 47-51

3-56. "Experimental Testing of Size 204 Ball and Roller Bearings for Use in Miniature Cryogenic Compressors." AFFDL-TR-66-223, January 1967

3-57. Walker, G., "Operations Cycle of the Stirling Engine with Particular Reference to the Function of the Regenerator." Journal Mechanical Engineering Science, Vol. 3, No. 4, 1969, pp. 394-408

3-58. Gifford, W. E., "Basic Investigation of Cryogenic Refrigeration Methods," AFFDL-TR-67-41, July 1967

3-59. Rios, P. A., Smith, J. L., Qvale, E. B., "An Analysis of the Stirling Cycle Refrigerator." Advances in Cryogenic Engineering, Vol. 14, Plenum Press, New York, 1968, pp. 332-342

3-60. Rule, T. T., Qvale, E. B., "Steady-State Operation of the Idealized Vuilleumier Refrigerator." Advances in Cryogenic Engineering. Plenum Press, New York, 1968, pp. 343-352

3-61. Walker, G., "Dynamical Effects of the Rhombic Drive for Miniature Cooling Engines." Advances in Cryogenic Engineering, Vol. 14, Plenum Press, New York, August 1968, pp

3-62. Stuart, R. W., Hogan, W. H., Rogers, A. D., "Performance of a 4.°K Refrigerator." Advances in Cryogenic Engineering, Vol. 12, Plenum Press, New York, June 1966, pp. 564-575

3-63. McMahon, H. O., Gifford, W. E., "A New Low-Temperature Gas Expansion Cycle." Advances in Cryogenic Engineering, Vol. 5, Plenum Press, New York, September 1959, pp. 354-367

3-64. Trepp, C., "Refrigeration Systems for Temperatures below 25°K with Turboexpanders." Advances in Cryogenic Engineering, Vol. 7, Plenum Press, New York, August 1961, pp. 251-261

3-65. Schulte, C A., Fowle, A. A., Heuchling, T. P., Kronauer, R. E., "A Cryogenic Refrigerator for Long-Life Applications in Satellites." Advances in Cryogenic Engineering, Vol. 10, Plenum Press, New York, August 1964, pp. 477-485

3-66. Gifford, W. E., "The Gifford-McMahon Cycle." Advances in Cryogenic Engineering, Vol. 11, Plenum Press, New York, August 1965, pp. 152-159

3-67. Suslov, A. D., "Starting Period of Microgenic Apparatus," Izv. Vuz, Mashimostroenie, No. 5, 1969, pp. 97-101 (In Russian)

3-68. Strobridge, T. R., Chelton, D. B., "Size and Power Requirements of 4.2°K Refrigerators," Advances in Cryogenic Engineering, Vol. 12, Plenum Press, New York, Aug. 1966, pp. 576-584

3-69. Leo, B., "Designer's Handbook for Spaceborne Two-Stage Vuilleumier Cryogenic Refrigerators", Technical Report AFFDL-TR-70-54, June 1970

3-70. Johnson, J. C., "Design and Selection of Miniature Cryogenic Refrigerators", Thesis, Ohio State University, 1969

3-71. Finkelstein, T., Joshi, T. J., and Walker, G., "Design Optimization of Stirling Cycle Cryogenic Cooling Engines by Digital Simulation", Advances in Cryogenic Engineering, Volume 16, 1970

3-9. REFRIGERATOR MANUFACTURERS

From the beginning of the program to the present a comprehensive survey of refrigerator development has been made. This has included establishing communication with the following specialist refrigerator manufacturers.

Arthur D. Little, Inc.
520 Acorn Park
Cambridge 40, Mass.
R. W. Breckenridge, Jr.

Cryogenic Technology, Inc.
Kelvin Park
266 Second Ave.
Waltham, Mass. 02154
John Sheppard

The Malaker Corporation
West Main St.
High Bridge, N. J. 08829
Jim Burr

British Oxygen Company
Cryoproducts Div.
Deer Park Road
London S.W. 19, England
J. B. Gardner

Garrett AiResearch Manufact. Co.
Cryogenic Systems
2525 West 190th St.
Torrance, Calif. 90509
R. Hunt

General Electric
Research and Development Center
P. O. Box 43
Schenectady, N. Y. 12301
R. B. Fleming

Hymatic Engineering (Pendix Representative)
Hickory Grove Rd.
Davenport, Iowa 52808
B. F. Gerth

U. S. Phillips Corporation
Norelco Cryogenic Div.
One Angell Road
Ashton, Rhode Island 02864
J. A. Halloran
Bob Smith
A. B. Austin, B. J. Ferro

Cryomech
314 Ainsley Dr.
Jamesville, W. V. 13078
W. E. Gifford

Sterling Electronics, Inc.
(Sub-Marine Systems Div.)
9174 DeSoto Ave.
Chatsworth, Calif.
Kenneth Cowans

Air Products and Chemicals
Allentown, Pa. 18105
R. F. Niehaus
J. V. Galdieri
R. L. Rerig
R. C. Longsworth

Wright-Patterson AFB
(Flight Dynamics Lab)
AFFDL (FDFE)
Wright-Patterson AFB, Ohio 45433
W. J. Uhl, Jr.
Ronald White

The Welch Scientific Company
840 Cherry St.
San Carlos, Calif.
Ted Crane

SECTION 4
REFRIGERATOR FAILURE CHARACTERISTICS

4.1 INTRODUCTION

In order to assess the influence of the refrigerator upon overall system reliability the engineer/planner must know the reliability of the refrigerator as a separate component. The reliability of the refrigerator is defined for a specific application as the probability that it will deliver a specified level of performance for a specified length of time while operating in a specified environment. The reliability of a refrigerator is not, however, a specifiable performance parameter. It is prediction as to the most probable future behavior of a given type of component which, at best, is based upon a statistical analysis of experimental failure rate of data obtained for identical components operating in an identical environment. Where such data do not exist, extrapolations must be made from data obtained for combinations of refrigerator and environment which resemble the specified systems. Alternatively if the refrigerator is made from commonly used components whose failure rate has been well established, the refrigerator reliability will have to be predicted from the resultant of the component reliabilities.

There are no failure rate data for any specific class of refrigerators in any specific spaceflight application. There are in fact only isolated instances of any refrigerator being used in space at all (e.g., open-cycle Joule-Thomson systems for planetary fly-by missions). Further, available refrigerators for either ground or airborne use do not necessarily resemble the refrigerators which will ultimately be used in space, inasmuch as maintenance will not be a design possibility. However, the engineer/planner must be provided with some estimate of the failure rates that could be expected from low temperature refrigerators in order to assess the feasibility of active refrigeration. During the assembly of this handbook many conversations were held with members of the refrigerator industry and personnel from Department of Defense refrigerator research sponsoring agencies. The information and opinions obtained from these sources showed considerable variation as to the failure rates that might be obtained from specially designed, fully developed spaceborne refrigerators, largely because of proprietary interests, it would seem. It is clear, therefore, that probable failure rates will remain a subject of argument until more experience is gained. The writers of this handbook have assessed these arguments and have suggested some lifetime figures which seem to reflect an average industry-wide opinion. The spacecraft designer is invited to use these estimated mean-time-to-failure figures given below for each refrigerator type in preliminary calculations. For more detailed and current information contact should be made with a manufacturer or sponsoring agency.

Section 2 shows how the falure rate data may be related to reliability for a given mission duration.

4.2 FAILURE RATE DATA

In Section 4.4 of the final report (1) a discussion of the important features of each type of refrigerator was presented and the major points stressed therein are as follows.

1. Existing refrigeration systems can be divided into conventional technology systems (Stirling, Vuilleumier, Gifford-McMahon/Solvay) and advanced technology systems (gas bearing Brayton refrigerators).

2. The conventional technology refrigerators are subject to component wear as well as random failures. For space use they can all be designed for reduced wear at the expense of other characteristics, such as weight. The Vuilleumier refrigerator is being developed for space use as a low wear unit. However, it is not clearly established that the Stirling and Gifford-McMahon/Solvay systems would not show equally extended lives were they to be redesigned in low wear form for space applications. All these systems can be expected to show predominantly adult failure rates in maintenance free form.

3. The advanced technology refrigerators should show very long lifetimes when fully developed. Their development is, by definition, considerably behind that of the conventional technology systems. The gas bearing systems should ultimately show constant failure rates although they may be expected to show

infantile characteristics because of their complexity.

Table 4-1 summarizes the projected lifetimes for all systems. The distinction between 5 watt/100°K and 100 watt/20°K refrigerators is to illustrate the effect of size. It is stressed that the figures are entirely conjectural and are to serve as a guide in preliminary calculations.

Table 4-1

ESTIMATED LIFETIMES

Load Range	5 Watt/100°K		100 Watt/20°K	
	Conservative	Optimistic	Conservative	Optimistic
Stirling	1000 hrs	2000 hrs	3000 hrs	6000 hrs
Gifford McMahon/Solvay	2000 hrs	4000 hrs	3000 hrs	5000 hrs
Vuilleumier	1000 hrs	2000 hrs	3000 hrs	5000 hrs
Gas Bearing Brayton	20000 hrs	30000 hrs	20000 hrs	30000 hrs

4.3 RELIABILITY PREDICTION

It is neither necessary nor feasible to present a condensation of reliability theory in the present context. It is possible, however, to present some basic considerations quite briefly in a manner which permits a rapid approximate assessment to be made of the relationship between refrigerator failure rate, mission duration, and reliability.

The fundamental data required for prediction of the reliability of a refrigerator in a mission of specified duration and environment is the failure rate of the refrigerator in that environment as a function of time. In general the failure rates of engineering components show a rate initially decreasing with time as "infantile" problems are rectified. The failure rate remains constant during the so-called useful life. At extended periods the rate increases with time as "adult" wearout occurs.

In terrestrial and airborne systems the refrigerator would be operated in the region of constant failure rate. Infantile problems can be rectified by bench testing. Adult failure modes are eliminated by performing preventive maintenance on parts subject to wear or other forms of degradation at a time prior to the adult regime. In the spaceflight application it is assumed that maintenance cannot be expected. Thus adult mortality failure rate curves can be expected from those systems which incorporate wear components. In order to relate failure rate data to reliability use can be made of the Weibull failure rate function

$$\lambda(t) = \frac{b}{t_c^{\,b}} \; t^{b-1} \qquad 4\text{-}1$$

Here b and t_c are constants. The Weibull function has no theoretical justification. It is merely a convenient function for expressing the various types of failure rate by a single expression. Falling, constant, and rising failure rates can be obtained by choosing b to be less than, equal to, or greater than unity, respectively. The reliability, R (t), is found from:

$$R\ (t) = \exp.\left[-\int_0^t \lambda\ (t)\ dt\right] \qquad 4\text{-}2$$

Here t is the lifetime of interest. The absolute number of failures per unit time is equal to the product $\lambda(t)R(t)$. For $b = 3.44$ the failures are symmetrically distributed about a mean value, as might be expected for systems which fail due to a wearout. In order to illustrate the difference between constant and adult failure rates reliability R is plotted on Figure 4-1 for $b = 1.0$ and 3.44. The other variable is the ratio of lifetime to mean time to failure, MTTF. For $b = 1.0$, λ is constant and MTTF is equal to $1/\lambda$. For $b = 3.44$ the MTTF is the time at which the peak in $\lambda(t)R(t)$ occurs.

In summary reliability can be calculated from equation 4-2 once $\lambda(t)$ is known. Figure 4-1 shows R(t) plotted versus (lifetime/MTTF) for the special cases for which $\lambda(t)$ [illegible] expressed by equation 1 with $b = 1.0$ and 3.44. The difference [illegible] the two curves emphasizes the point that failure rate da[illegible] a time-dependent rather than time-average functio[illegible]

In order to increase the probability that the service demanded from a system for a given period is obtained, redundant systems can be used. In the cooling situation parallel redundancy in which more than one refrigerator is operating at a given time does not seem to be reasonable, since the storage vessel would be overcooled most of the time and power consumption would be excessive. Series redundance, however, appears to offer a very significant increase in reliability. In this case additional refrigeration systems are provided to be switched on if the operational unit fails. The reliability of such a system can be estimated with the help of Figure 4-1. Suppose an operational lifetime of 4,000 hours is required from a unit whose MTTF is 4,000 hours. Using the curve for b = 3.44 a reliability of 0.52 is obtained. Suppose two units were provided so that a lifetime of 2,000 hours was expected from each; the reliability of a 4,000-hour MTTF unit on a 2,000 hour task is found to be .95. Such an analysis is somewhat oversimplified, but an approximate comparison of multi-unit systems can be made in this manner.

---

(1) Investigation of External Refeigeration Systems for Long Term Cryogenic Storage, LMSC-A981632, 22 February 1971.

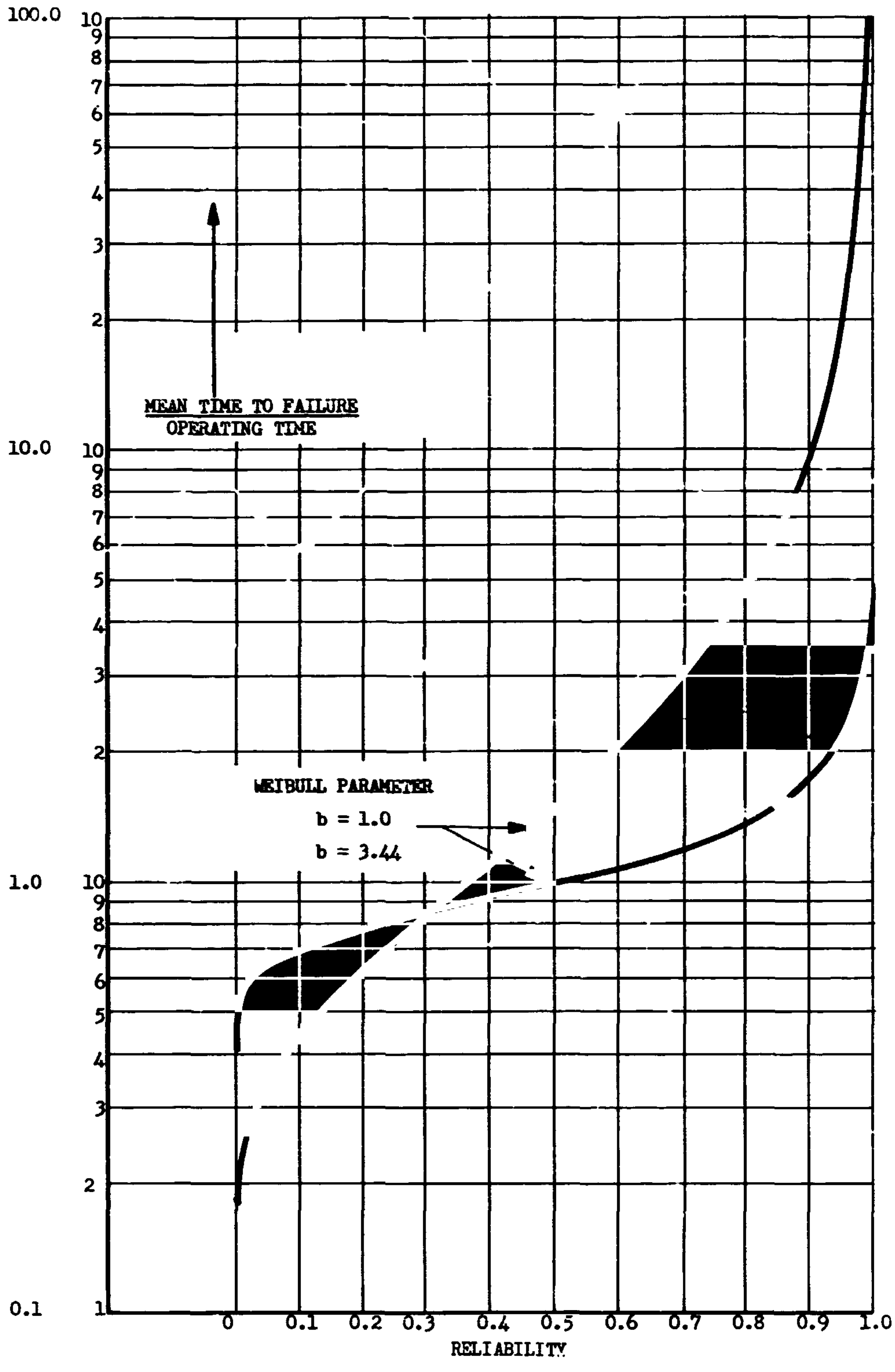

FIGURE 4-1 LIFE RATIO VERSUS RELIABILITY

Section 5
THERMAL ENVIRONMENTS

5.1 DEFINITION OF THERMAL ENVIRONMENT PARAMETERS

The objective of defining parameters describing refrigerator system thermal environments is to enable the system designer to make rapid preliminary estimates of average spacecraft surface temperatures and radiator heat rejection limits for a range of possible missions. For the purpose of this study, the maximum incident solar heat fluxes were taken to be as high as that experienced near Venus, and provisions were made for estimating absorbed heat fluxes for three mission groups. These groups are planetary orbit operations, Martian and Lunar surface operations, and deep space operation, such as translunar or transmartian flight.

The environmental parameters for these cases can be derived by considering the definition of the average net heat flux radiated by a surface in space or on an airless planetary surface. A general expression for this quantity may be written

Net radiated Flux Density	=	Emitted Flux Density	-	Absorbed Solar Flux Density	-	Net Absorbed Planetary or Lunar Flux Density	(5-1)

where the flux densities are regarded as steady-state values or are averaged over an appropriate time interval (such as an orbital period for an orbiting vehicle) It has been assumed that no thermal interchange occurs between the surface in question and other portions of the spacecraft. Symbolically, equation (5-1) can be written

$$\frac{q_{net}}{A_{eff}} = G_E T^4 - G_A - G_P, \quad \text{Watts/Ft}^2 \qquad (5\text{-}2)$$

where

$$G_E = \sigma \epsilon_I \qquad (5\text{-}3)$$

$$G_A = \alpha_s F_s G_s \tag{5-4}$$

and

$$G_P = \sigma \epsilon_I F_P T_P^4 \quad \text{for lunar or planetary surface operation} \tag{5-5a}$$

$$G_P = \epsilon_I F_P R_P + \alpha_s \bar{F}_{Ps} \rho_P G_s \quad \text{for orbital or near-planet operation} \tag{5-5b}$$

where

σ	=	Stefan-Boltzman Constant = 0.5267×10^{-8} W/Ft^{2}K^4
ϵ_I	=	Infrared Emittance
α_s	=	Solar Absorptance
F_s	=	View Factor for solar radiation
G_s	=	Solar Irradiation flux density, W/Ft^2
F_P	=	View Factor to planet surface
T_P	=	Planet temperature, ^{o}K
R_P	=	Planet Infrared Radiosity, W/Ft^2
$\bar{F}_{Ps}$	=	Time Average view factor for planet-reflected solar radiation
ρ_P	=	Planet Albedo

An upper limit of 500 W/Ft^2 for the sum $(G_A + G_p)$ is possible for near-Venus operation. These relations can be used to determine the average net heat rejection from a radiator having a known surface temperature, or the equilibrium surface temperature of a surface having a known net heat rejection.

5.2 DIRECT SOLAR HEAT FLUX

The value of G_A is the product of solar absorptance, view-factor to the sun, and local solar irradiance (i.e., the solar constant at a given distance from the sun). The view factor to the sun for a flat surface is the cosine of the angle between the outward normal to the surface and a line to the sun. The view factor for curved surfaces is the ratio of the area projected in the direction of the sun to the total surface area. The solar irradiance is given by

$$G_s = \frac{130}{r_p^2} \text{ , W/Ft}^2 \tag{5-6}$$

where r_p is the distance from the sun in astronomical units.

Values of solar absorptance and infrared emittance are tabulated in Table 5-1 for a variety of materials. Also shown are values of these properties after vacuum and simulated solar radiation exposure for 1000 equivalent sun hours (ESH).

5.3 PLANETARY HEAT FLUX

Evaluation of the planetary or lunar heat input, G_P, is somewhat more complex. For an object resting on or near the planetary surface the evaluation of the view factor to the planet's surface is usually straight forward. View factors from vertical and horizontal surfaces to an adjacent lunar or planetary surface are shown in Fig. 5-1. View factors to a hill and to a crater are plotted as a function of elevation angle to the top of the hill or crater. The hill is assumed to be of infinite extent in the direction parallel to the vertical side A_V of the vehicle. The crater is assumed to be circular, surrounding the surface A_V.

In order to determine Gp for a radiating surface passing or orbiting near a planetary surface the terms in (5-5b) must be evaluated. The view factor from a flat surface to the visible portion of a planet, F_P, can be evaluated using the data of Ref. 5-1. Referring to the geometry illustrated in Fig. 5-2, two cases can be distinguished:

1. <u>Entire Planet Visible from Surface</u>

   For this case $\lambda + \Phi \leq \frac{\pi}{2}$, where

   λ = Angle between surface normal and a line to the planet center

   Φ = $\sin^{-1}(R/H)$

   R = Planet radius

Table 5-1

Representative Values of Solar Absorptance and Infrared Emittance

Material	Solar Absorptance, α_S		Infrared Emittance, ϵ_I	
	Normal	After 1000 ESH Exposure	Normal	After 1000 ESH Exposure
Clad Aluminum	0.22 ± 0.04	0.24 ± 0.04	0.06 ± 0.03	No Change
Optical Solar Reflector	0.050 ± 0.005	No Change	0.80 ± 0.02	No Change
White Acrylic Paint	0.24 ± 0.04	0.40 ± 0.04	0.86 ± 0.03	No Change
White Silicone Paint	0.20 ± 0.03	0.34 ± 0.03	$0.90 {+0.03 \atop -0.06}$	No Change
Black Acrylic Paint	0.93 ± 0.03	No Change	0.88 ± 0.03	No Change
Solar Cell Assembly	0.78 ± 0.04	0.83 ± 0.04	0.80 ± 0.03	No Change

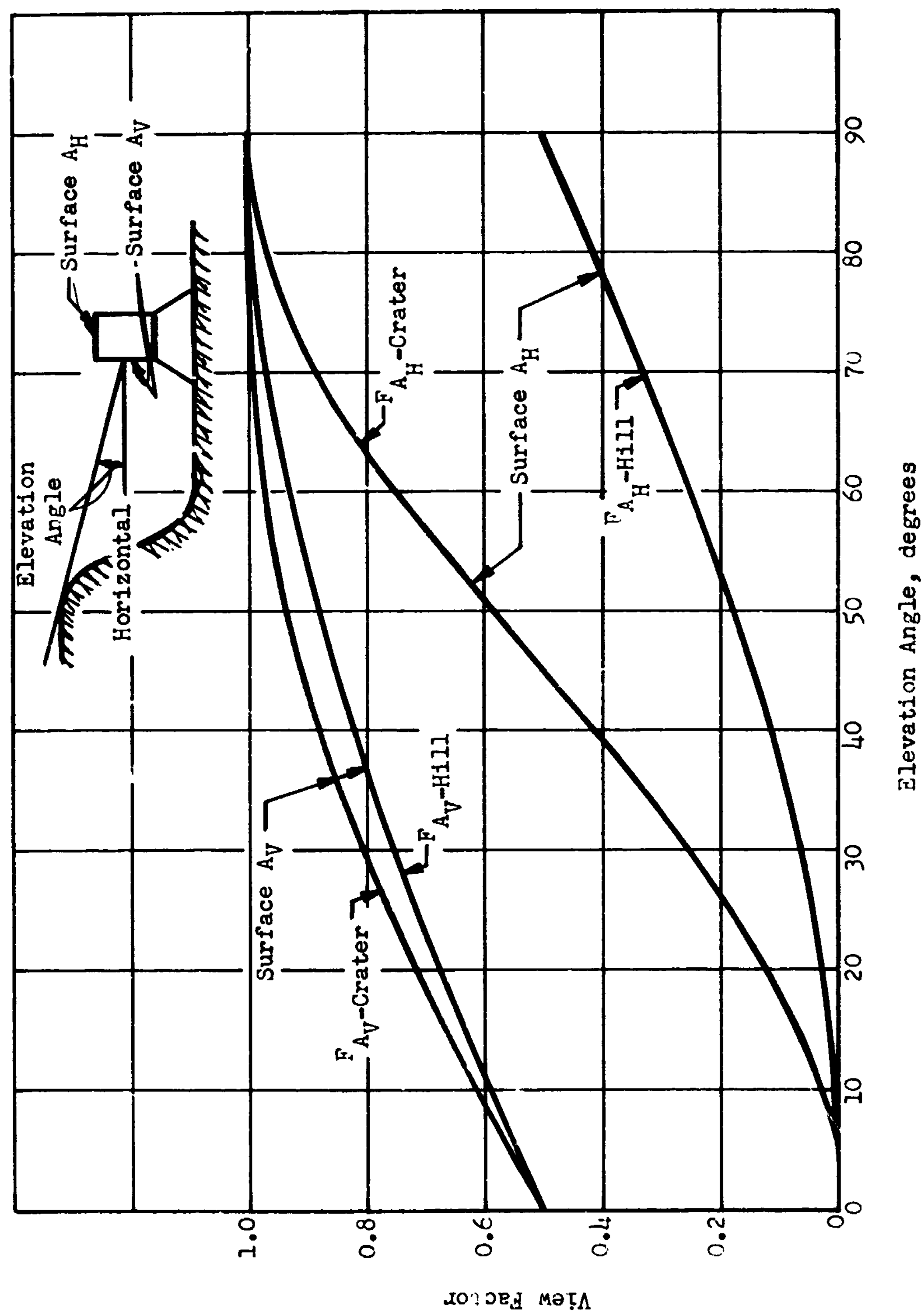

Fig. 5-1 View Factors from Vehicle Surfaces to Planetary Terrain

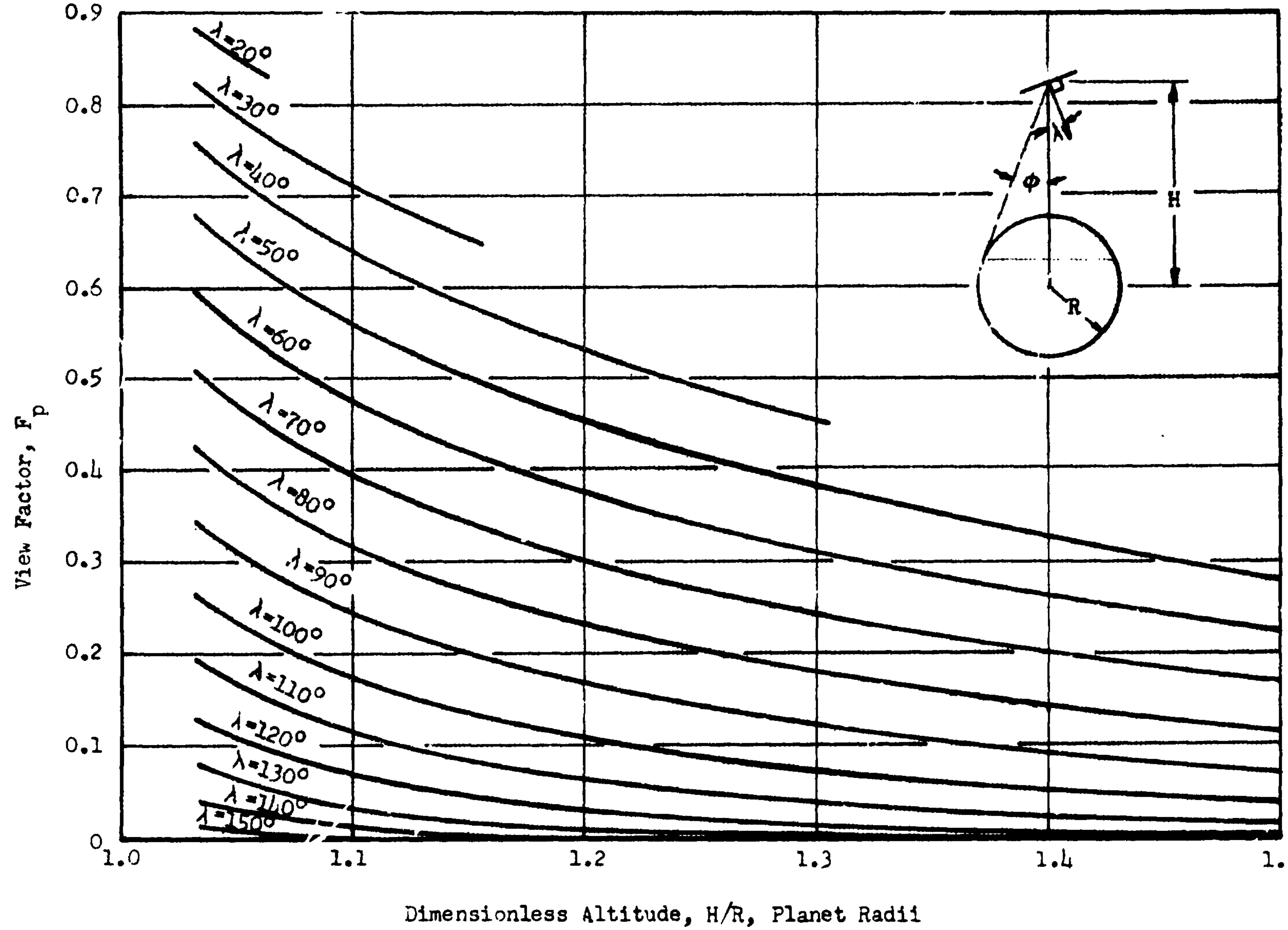

Fig. 5-2 Planetary View Factor for Infrared Exchange

H = Distance from planet center to spacecraft surface

The view factor is given by

$$F_P = \left(\frac{R}{H}\right)^2 \cos\lambda$$

2. Part of Planet Visible

For this case

$$\left(\frac{\pi}{2} - \Phi\right) < \lambda \leq \left(\frac{\pi}{2} + \Phi\right)$$

and the view factor is given in Fig. 5-2.

Average values of planetary radius, surface radiosity, and reflectance (albedo) are given in Table 5-2 for Earth's moon and the planets. Also shown in Table 5-2 are surface temperature ranges for each of the planets. Values of lunar surface temperature are shown in Fig. 5-3 as a function of sun elevation angle. Values of the surface temperature of Mars are shown in Fig. 5-4. The value of the time-average view factor for reflected solar radiation is obtained by integration of an instantaneous view factor. Thus,

$$\bar{F}_{Ps} = \frac{1}{2\pi} \int_0^{2\pi} F_{Ps}(\Theta)d\Theta \qquad (5\text{-}7)$$

where θ is the orbit position angle measured as shown in Fig. 5-5.

The value of the view factor $F_{Ps}(\Theta)$ may be approximated by the relation

$$F_{Ps} = C_R \cos\beta \cos\Theta \qquad (5\text{-}8)$$

where β is the angle between the orbit plane and a line to the sun, and C_R is a reflection coefficient given in Fig. 5-6.

5.4 TEMPERATURE OF NEAR-EARTH SATELLITES

Extremes in irradiation of a satellite are represented by the levels experienced on the six sides of a cube which always keeps the same side facing the

Table 5-2

PHYSICAL CHARACTERISTICS OF EARTH'S MOON AND THE PLANETS

Body	Mean Distance From Sun,[1] A.U.	Mean Radius		Orbital Period, Days	Period of Rotation, Days[3]	Gravitational Acceleration (Earth = 1)	Average Infrared Radiosity, W/Ft^2	Average Albedo	Surface Temperature Range, °K
		N.Mi.	Km.						
Mercury	0.3871	1263	2340	87.96	55.0	0.40	210	0.058	13 to 680
Venus	0.7233	3291	6100	224.70	(5)	0.89	60.5	0.76	240[6]
Earth	1.000	3438	6371	365.26	0.99769	1.00	21.8	0.39	220 to 320
Moon	(2)	938	1738	27.32	27.32	0.165	28.8	0.07	100 to 385
Mars	1.5237	1794	3324	686.98	1.02595	0.39	13.7	0.15	160 to 300
Jupiter	5.2037	37636	69750	4333.71	0.4115[4]	2.37	1.22	0.51	120 to 310
Saturn	9.5803	31387	58170	10829.5	0.4348[4]	0.90	0.355	0.50	100 to 225
Uranus	19.1410	12815	23750	30587.0	0.4458	0.97	0.0914	0.66	100 to 125
Neptune	30.1983	12087	22400	60612.3	0.5299	1.40	0.0404	0.62	100 to 125
Pluto	39.4387	1619	3000	90465.7	6.39	-	0.0204	0.16	~43

NOTES:
(1) Orbit semi-major axis.
(2) Mean distance of Moon from Earth = 384 405 Km.
(3) Mean solar days
(4) Approximate, varies with latitude
(5) Not known. Venus rotates very slowly if at all.
(6) Temperature of top of clouds. Surface temperature is about 700°K.

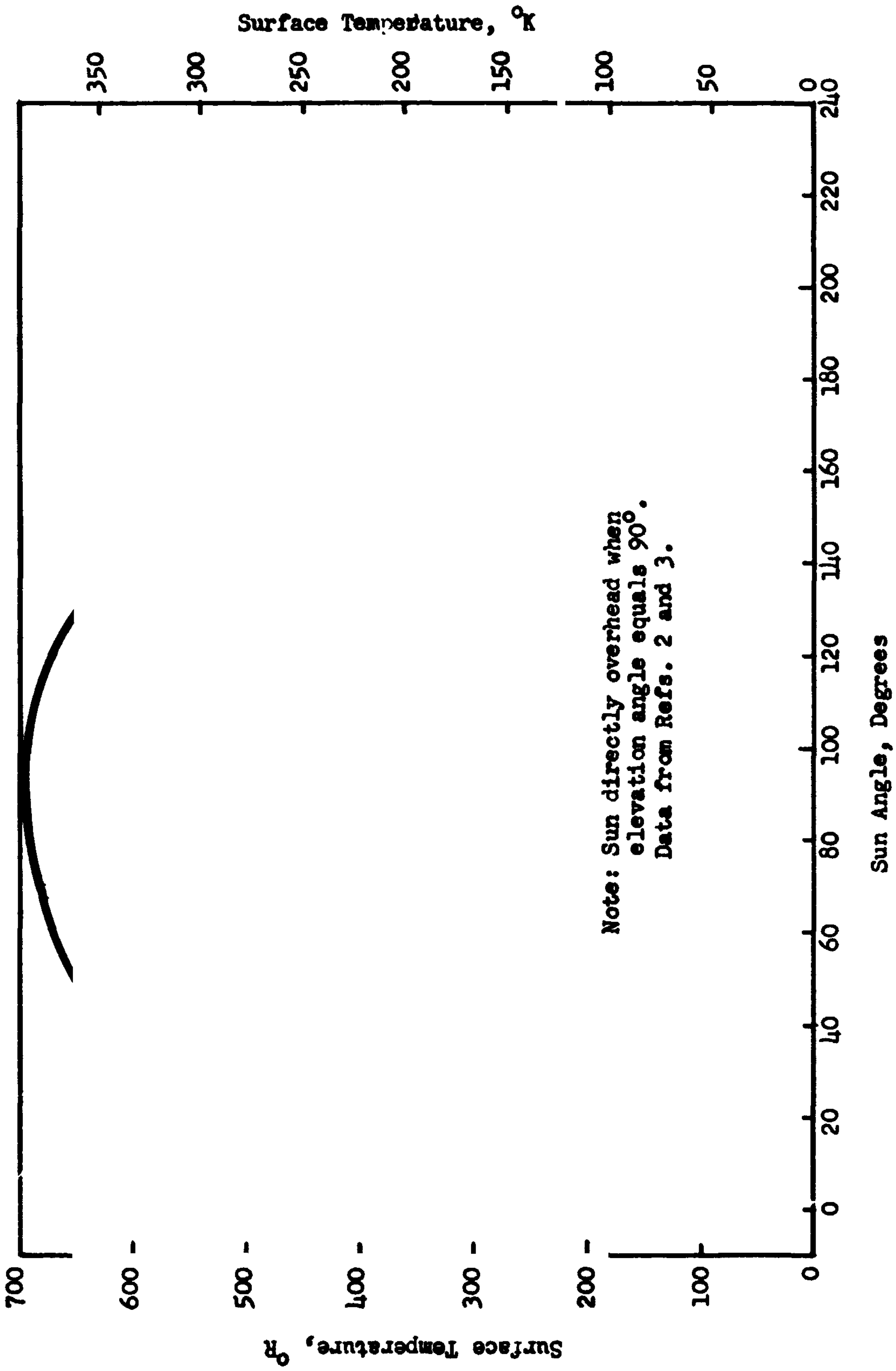

Fig. 5-3 Lunar Surface Temperatures

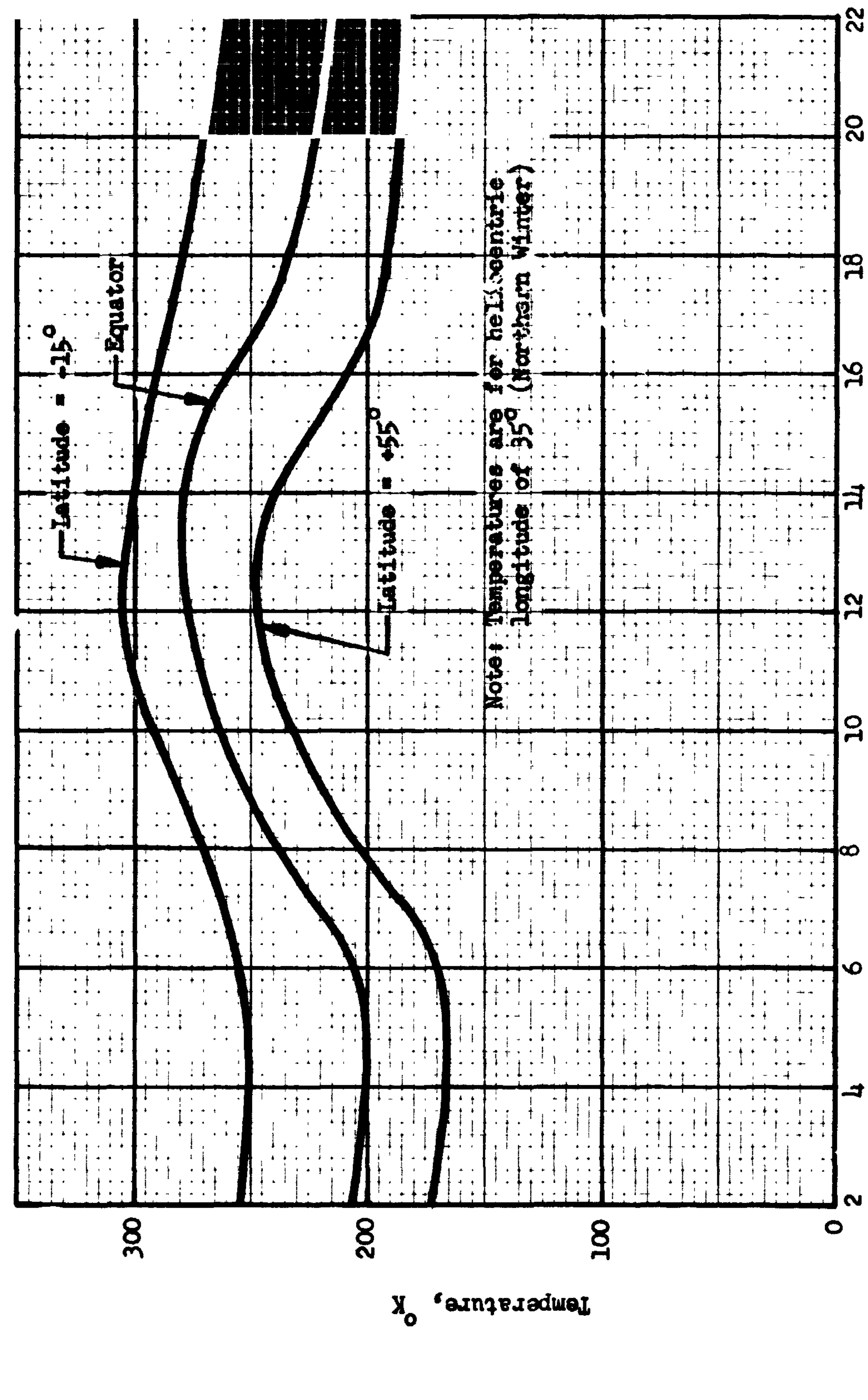

Local Time, Hours

Fig. 5-4 Diurnial Temperature Variation of the Surface of Mars

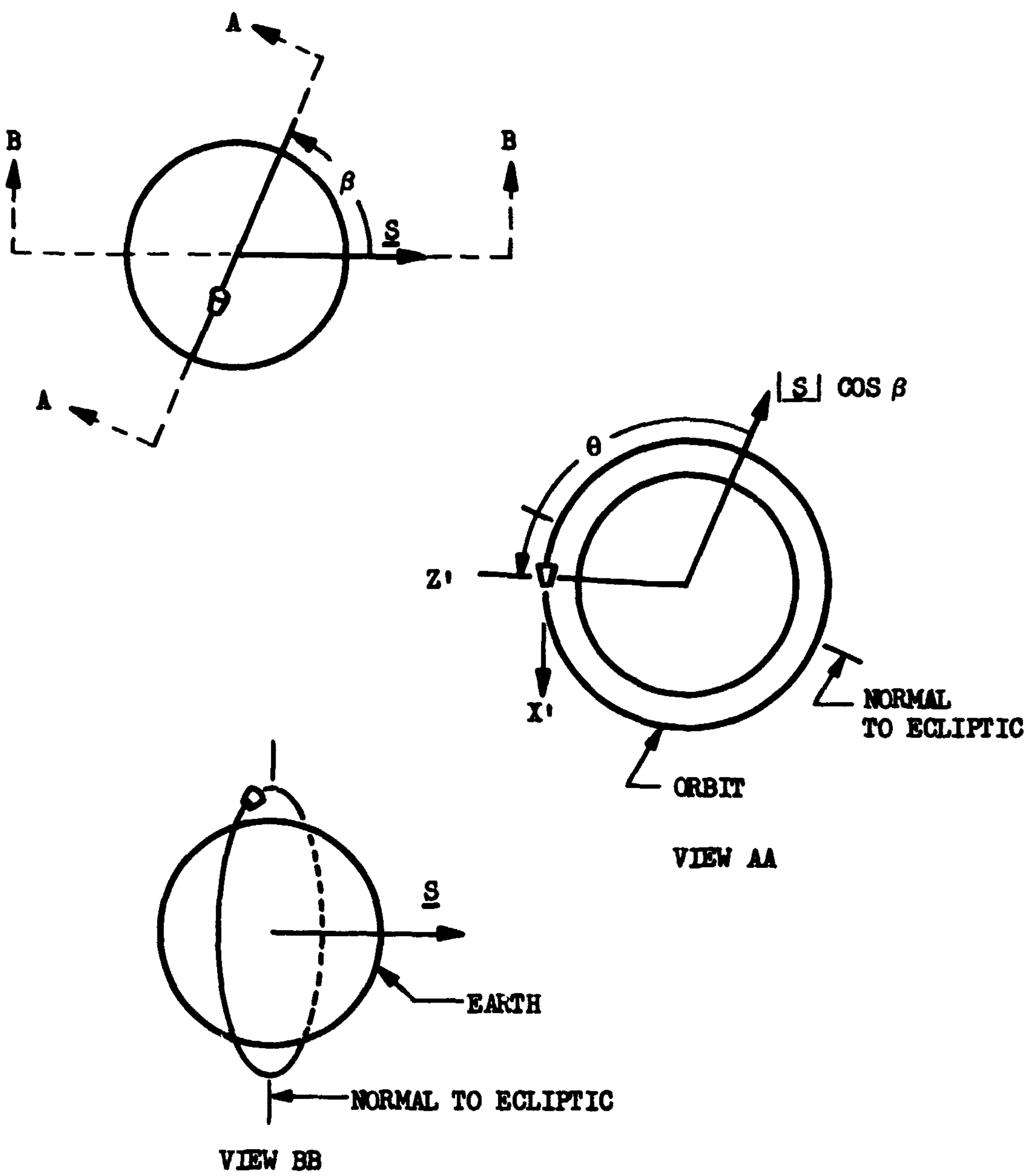

Fig. 5-5 Polar Orbit Geometry

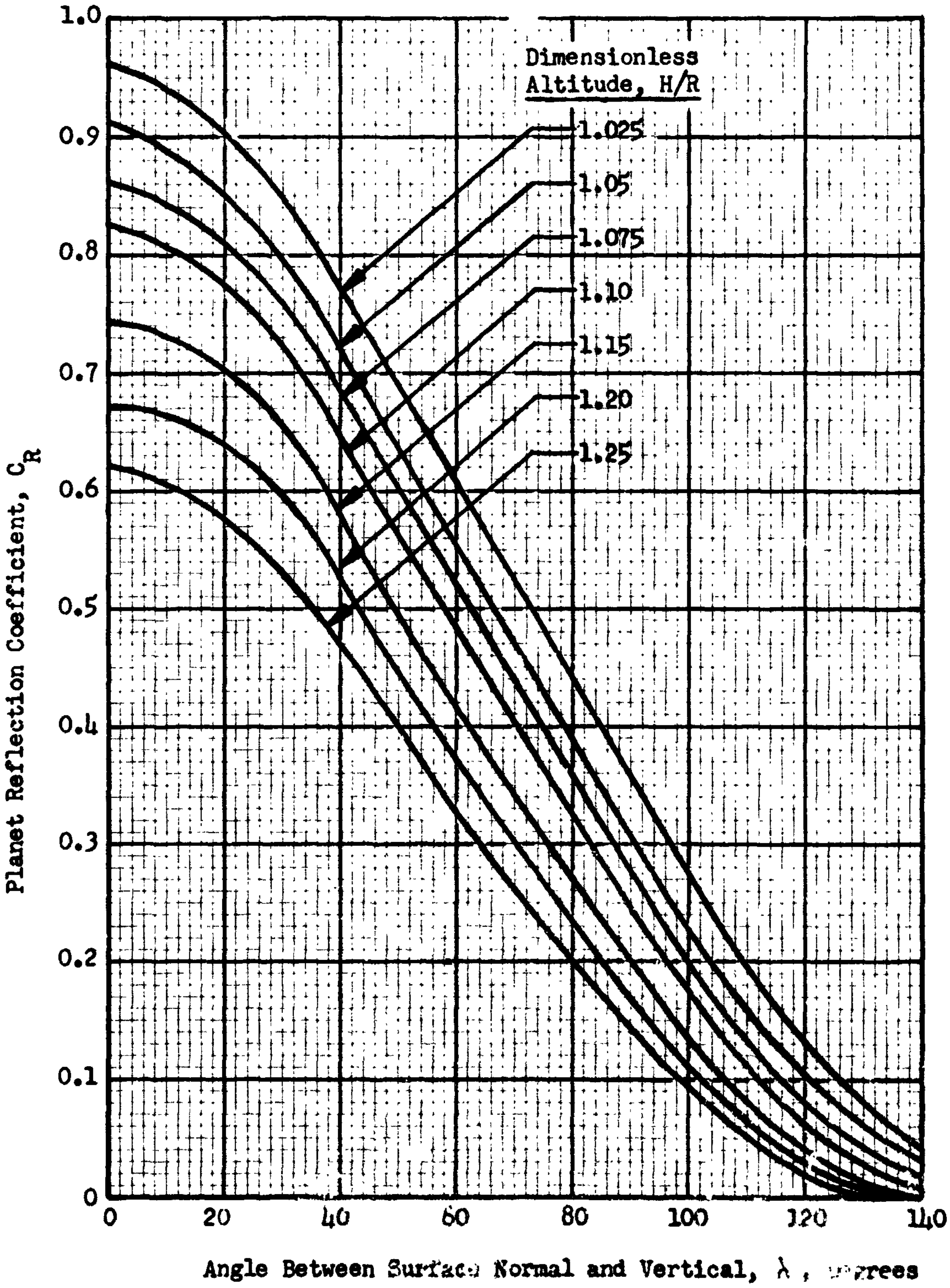

Fig. 5-6 Planet Reflection Coefficient for Flat Surf[illegible]

Earth, as shown here below. In the noon orbit illustrated, for which the

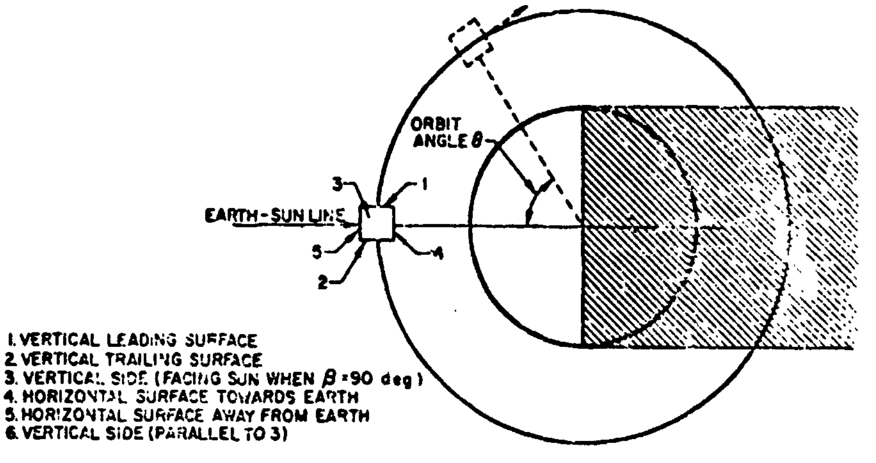

Oriented Cube in Noon Orbit

orbit solar incidence angle, β , is zero, the satellite passes through the Earth's shadow. As a result the various faces of the satellite are subjected to widely varying incident heat fluxes. When $\beta = 90^\circ$ (the twilight orbit, which is always normal to the Earth-Sun line), there are no time variations in the incident fluxes. Average orbital temperatures have been computed for each face of the cube, assuming they are thermally isolated from each other. These time-average temperatures are shown in Figs. 5-7 through 5-10, for orbits with $\beta = 0^\circ$ and $\beta = 90^\circ$ and various orbital altitudes and surface optical properties.

For a spherical tank covered with high performance insulation, the average surface temperature can be approximated by computing the average of the six surface temperatures of the cube.

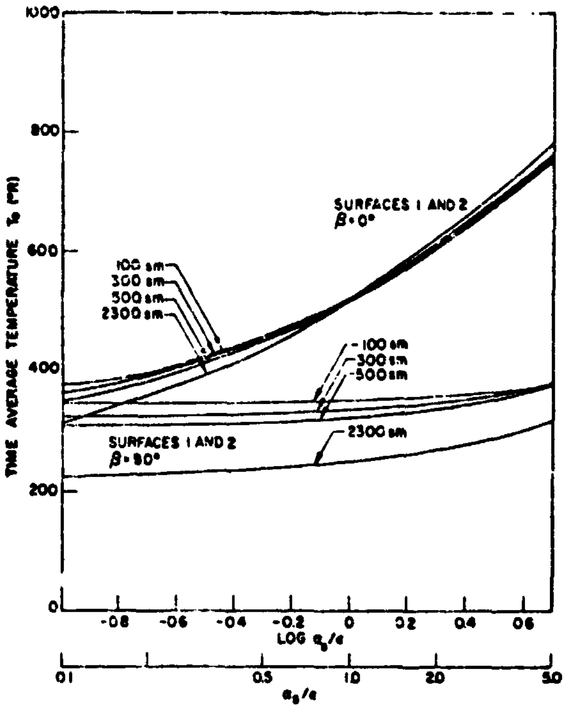

Fig. 5-7 Time Average Temperature as a Function of the α/ϵ Ratio (Surfaces 1 and 2)

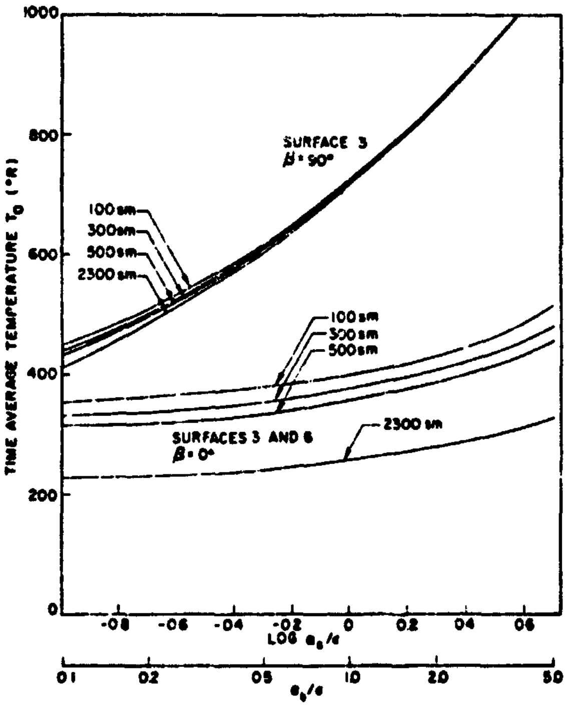

Fig. 5-8 Time Average Temperature as a Function of the α/ϵ Ratio (Surface 3)

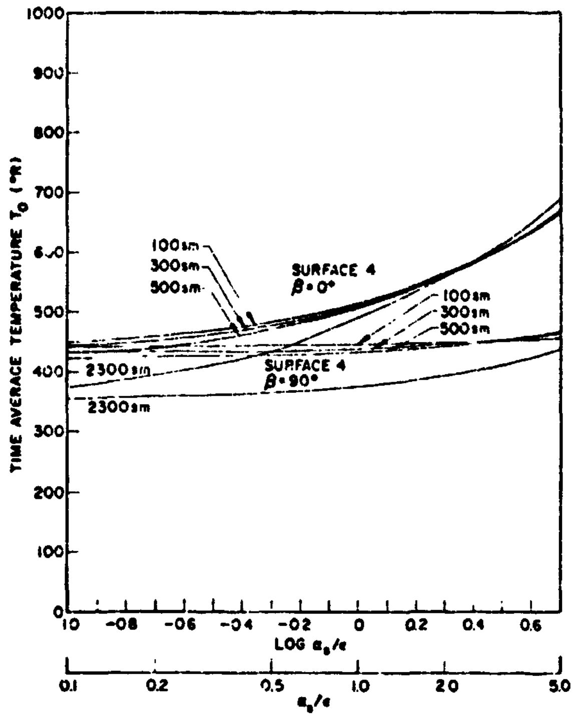

Fig. 5-9 Time Average Temperature as a Function of the α/ϵ Ratio (Surface 4)

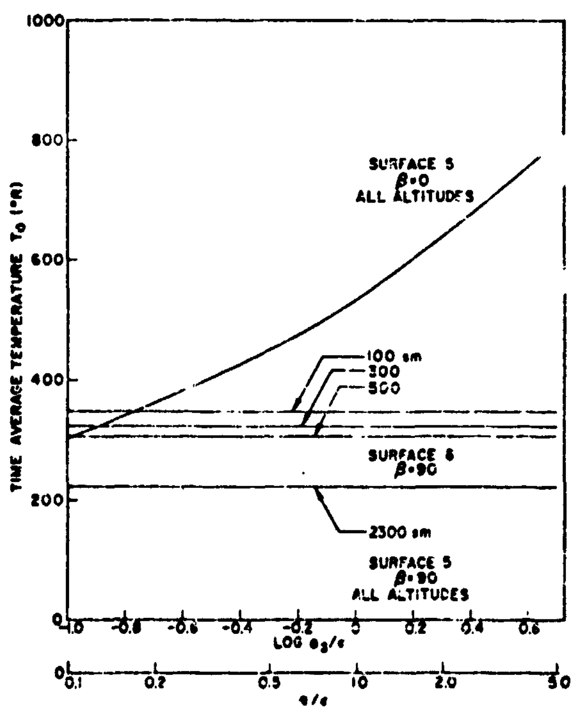

Fig. 5-10 Time Average Temperature as a Function of the α/ϵ Ratio (Surface 5)

Utilizing the data and methods outlined in this section the average surface temperature of an insulated tank was computed for several different space conditions. The conditions and temperatures are shown in Table 5-3.

Table 5-3

EQUILIBRIUM TANK SURFACE TEMPERATURES

<u>Case I - Low Earth Orbit, h = 200 n. mi.</u>

Circular, polar orbit

(Ia) 100% Sunlit Orbit - $\bar{T}$ = 214°K (385°R)

(Ib) 50% Sunlit Orbit - $\bar{T}$ = 204°K (365°R)

(Orbit plane parallel to sun's rays)

<u>Case II - Lunar Surface Operation</u>

(IIa) Lunar Noon (Sun Overhead) - $\bar{T}$ = 330°K (595°R)

(IIb) Lunar Night (Just before dawn) - $\bar{T}$ = 87°K (157°R)

<u>Case III - Deep Space Operation (2 A.U.)</u>

(IIIa) Unshielded Tank - $\bar{T}$ = 131°K (236°R)

(IIIb) Shielded Tank - $\bar{T}$ = 80°K (144°R)

External Solar Absorptance	=	0.10
Infrared Emittance	=	0.80

No Internal Heat Dissipation

Spherical Tank

REFERENCES

5-1 Cunningham, F. G., "Power Input to a Small Flat Plate from a Diffusely Radiating Sphere, with Applications to Earth Satellites," NASA TN D-710, 1961.

5-2 Lucas, J. W., et al, "Lunar Surface Temperatures and Thermal Characteristics," Surveyor V Mission Report, Technical Report 32-1246, Jet Propulsion Laboratory, Pasadena, California, 1 November 1967.

5-3 Lucas, J. W., et al, "Lunar Surface Temperature and Thermal Characteristics," Surveyor VI Mission Report, Technical Report 32-1262, Jet Propulsion Laboratory, Pasadena, California.

5-4 DeVaucouleurs, G., "The Physical Environment on Mars," Physics and Medicine of the Upper Atmosphere and Space, O.O. Benson and H. Strughold, Eds., John Wiley & Sons, Inc., New York, 1960.

5-5 Lockheed Missiles & Space Co., "Space Materials Handbook," C. G. Goetzel and J. B. Singletary, Eds., Contract AF 04(647)-673, January 1962.

Section 6
TANKAGE AND HEAT LEAKS

6.1 INTRODUCTION

To aid the designer or planner in computing the entire system weight for refrigeration trade-off studies, tank volumes, surface area, weights and heat transfer have been included. The tank weights are approximate and are mainly intended to provide weight increments for the trade studies. The heat rate to the tanks are based on a reasonable average for a large variety of multilayer insulations and supports. The heat rates through the multilayer insulation are based on calorimeter tests and modified by a factor of 2.8 to account for applications to real tanks.

The cryogens will be stored in pressure vessels of various sizes and locations dependent upon the application. Data on tank volumes of 20 to 280 ft^3 with hemisphical domes and cylindrical midsections are given in this section. The emphasis has been placed on single-walled tanks having multilayer insulation. However weights have been included for a vacuum jacket shells capable of withstanding 15 psi crushing pressure.

6.2 TANK VOLUME AND SURFACE AREA

The tank volume and surface area have been plotted parametrically as a function of diameter, D, and length of the cylindrical section to diameter ratio, L/D. The curves are shown in Figures 6-1 and 6-2. These same curves can be used to estimate the volume and surface area of a vacuum jacket by simply adding the vacuum annulus dimension to the pressure vessel diameter and reading the volume and area for the appropriate L/D.

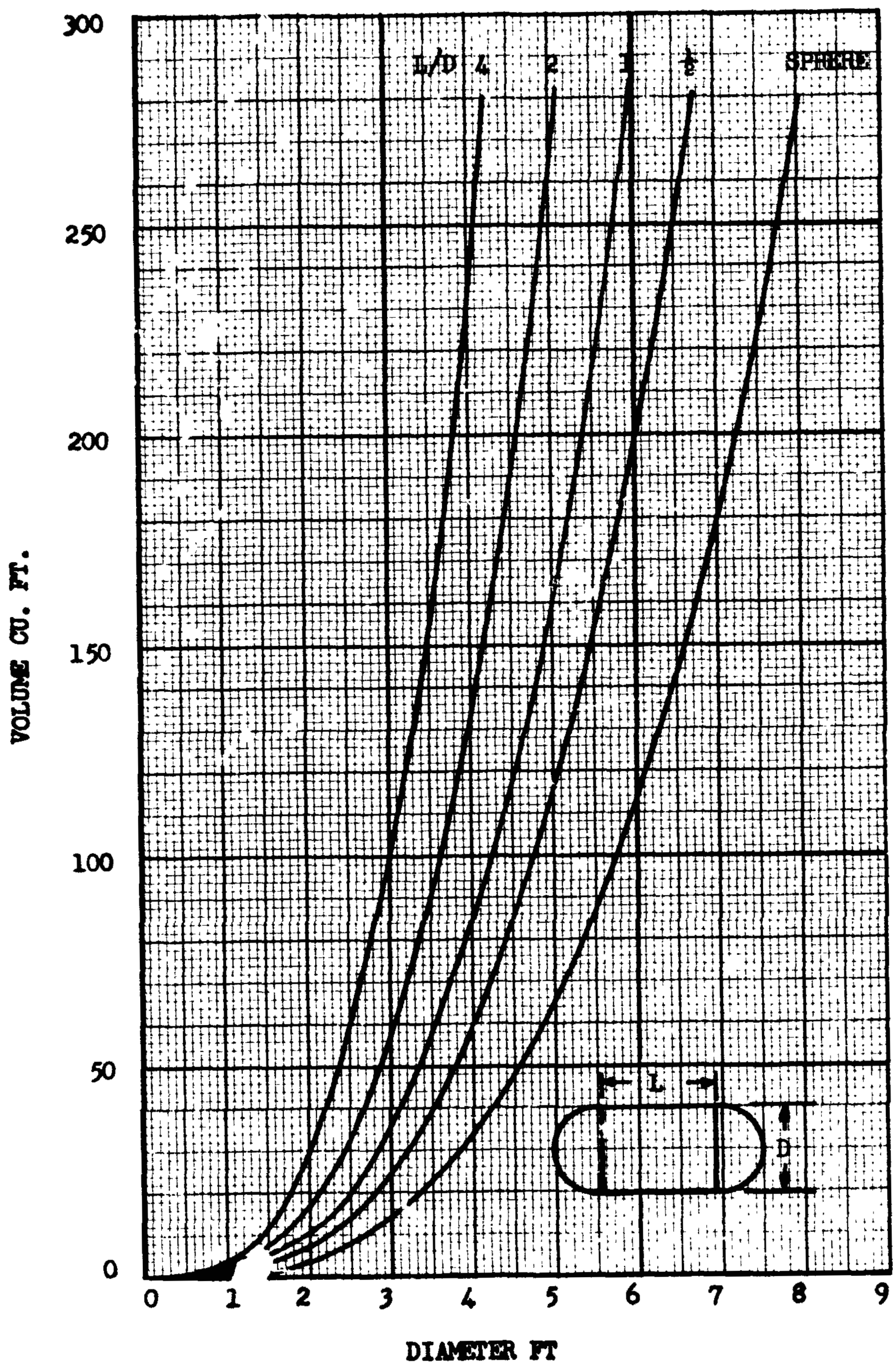

FIGURE 6-1 TANK VOLUME

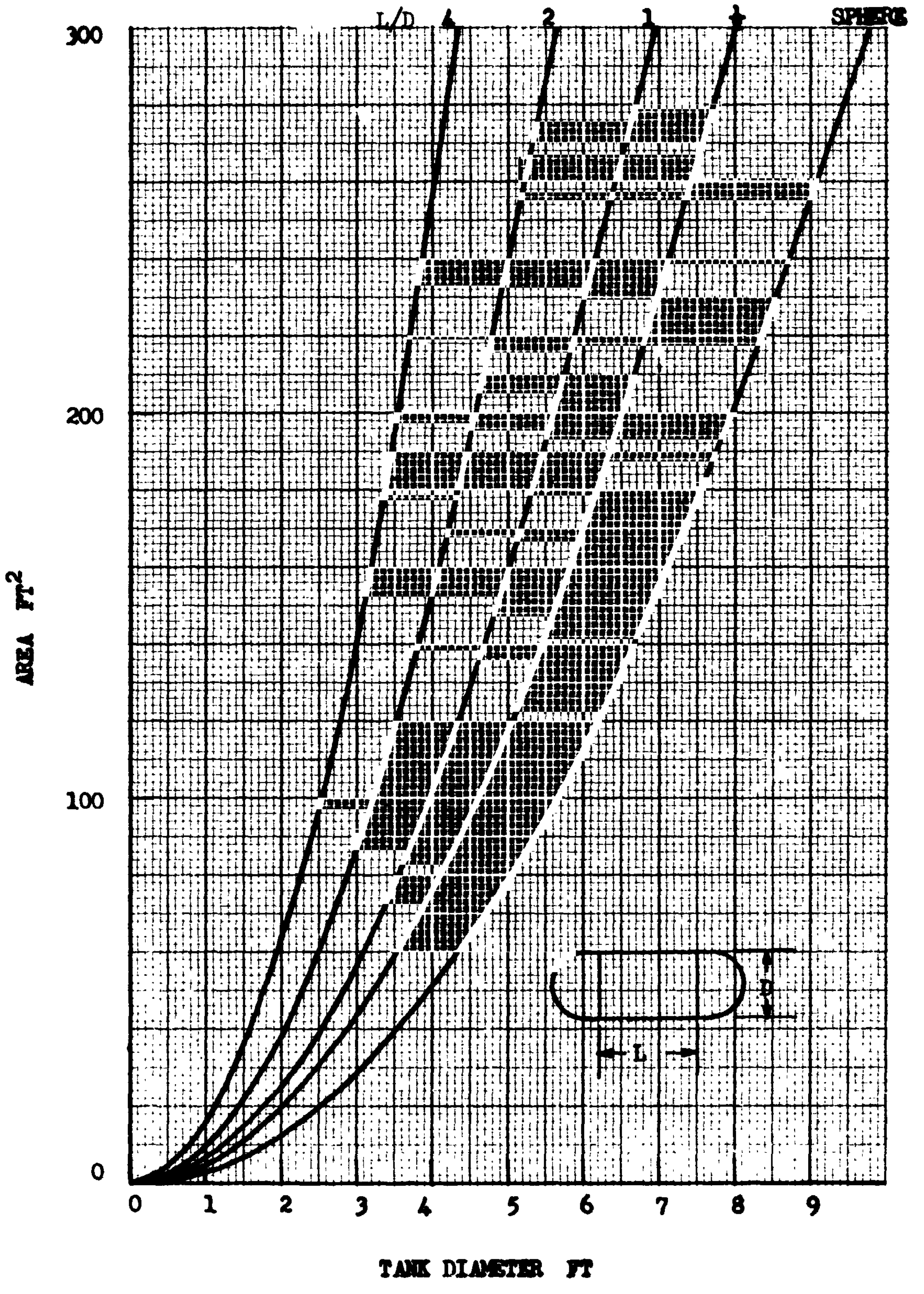

FIGURE 6-2 TANK AREA

6.3 WEIGHT ESTIMATE OF CRYOGEN TANKS

Figure 6-3 can be used to estimate the weights of propellant tanks. The curves shown are for aluminum tanks with a maximum operating pressure of 100 psi and a design allowable tensile stress of 40,000 psi. The following assumptions were made:

(1) The hemispheres used to fabricate the spherical tanks and the heads of the cylindrical tanks are one-piece with weld lands provided for assembly. If a gore construction is contemplated, additional weight should be introduced to provide adequate weld lands. For aluminum tanks, the weld lands were estimated to be twice the thickness of the membrane to take into account the reduced stress allowables in the weld and possible mismatch. Higher weld efficiency factors are obtained with stainless steel and nickel alloys and when that factor approaches 100% weld lands are not required.

(2) Weights of the tank support attachments, baffles, access covers and sumps are not included in the weights shown in the figure.

(3) The minimum weight curve is based on a minimum wall thickness of 0.040 in. and is shown for aluminum spherical tanks only. The variation of minimum weights between spherical and cylindrical tanks of the same volume is small if it is assumed the cylinder wall thickness to be twice that of the hemispherical heads.

The formulas used to evaluate the tank weights are as follows:

$$W_s = 0.785 \frac{\rho p}{\sigma} (D^3 + 3.82 D^2)$$

$$W_c = 0.785 \frac{\rho p}{\sigma} \left[2\left(\frac{L}{D}\right)D^3 + D^3 + 3.82 D^2\right]$$

where:

W_s = Weight of spherical tanks, lbs

W_c = Weight of cylindrical tanks with hemispherical heads, lbs

p = Maximum operating pressure, psi

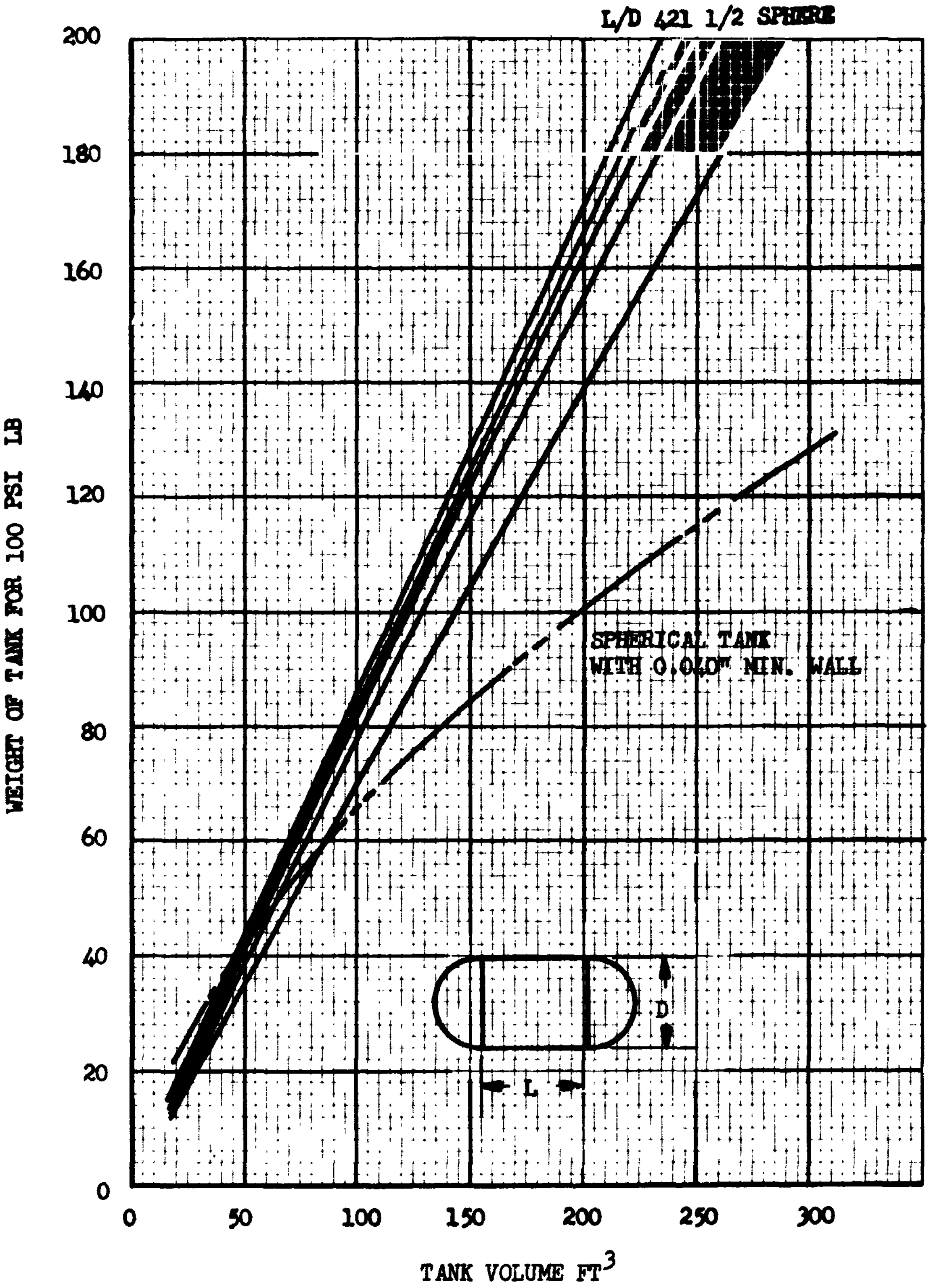

FIGURE 6-3 ALUMINUM TANK SHELL WEIGHT

ρ = Density of tank wall material, lb/in^3

σ = Tank wall material design allowable tensile stress, psi

D = Internal diameter of tank, in.

L = Length of cylindrical section of tank, in.

In order to use the data in Figure 6-3 for other conditions the following steps should be followed.

When the volume and $\frac{L}{D}$ ratio of the tank are known, find the weight of 100 psi operating pressure aluminum tank from the figure. For operating pressures other than 100 psi, design allowable tensile stresses other than 40,000 psi and material densities other than .101 lb/in^3 use the following formula:

$$W_a = W(\text{chart}) \times \frac{p_a}{100} \times \frac{40{,}000}{\sigma a} \times \frac{p_a}{.101}$$

where:

W_a = Actual weight of tank, lbs.

p_a = Actual tank maximum operating pressure, psi

σ = Actual material design allowable tensile stress, psi

a = Actual tank material density, lb/in^3

In all cases, but especially when the propellant density is high and the tank is submitted to high g-loads, the hydraulic head has to be added to the ullage pressure to determine the maximum operating pressure. If slosh is anticipated, another value depending on the shape of the tank and the number and shape of the baffles has also to be added.

6.3.1 Tank Support System Weights

Figure 6-4 shows a weight estimate of spherical tank support systems against the maximum propellant loading. These weights are based on axial loads of 4.5 g's forward and 1.0 g aft and a lateral load of $\pm$ 0.3 g's.

6.3.2 Baffles

The weight of baffles can be estimated between 2% of the tank weight for a 100 psi operating pressure for low density liquids and spherical tanks and 10% for high density liquids and long cylindrical tank with $\frac{L}{D}$ ratio of 4.

6.3.3 Vacuum Jackets

Figure 6-5 shows the estimated weights of aluminum self supporting vacuum jackets for spherical and cylindrical tanks. The weights are for vacuum jackets without reinforcing rings and the following formulas were used:

For spheres: $$\left(\frac{t}{D}\right)^2 = .685 \frac{P}{E_c}$$

For cylinders: $$\left(\frac{t}{D}\right)^3 = K \frac{P}{E_c}$$

where:

t = Thickness of shell, in.

D = Internal diameter of shell, in.

p = Critical external pressure, psi

E_c = Compression modulus of elasticity of shell material, psi

Weight savings can be obtained by incorporating stiffening rings to cylindrical shells having high $\frac{L}{D}$ ratios, and by using honeycomb shells.

6.3.4 Access Covers

If a manhole is required, a minimum of 20.0 lb should be added to the weights given by the chart. This weight is for an aluminum manhole ring and cover having a minimum access diameter of 19.5 inches and a design maximum pressure of 150 psi. A handhold access ring and cover with an opening of 8.0-in-diameter adds about 5.0 lb to the tanks.

6.4 Heat Leak to Tanks

In order to estimate the heat load that a refrigerator system would have to be designed for, estimates of heat transfer rates to the propellant tanks have been made. The heat leaks are generally broken up into three groups: the leak through the insulation; the leak through the supports; and the leak through lines and instrumentation.

6.4.1 Heat Leak Through Insulation

Several insulation systems have been under study over the last few years, (References 6-1 and 6-2). For cryogenic tanks in a space environment it

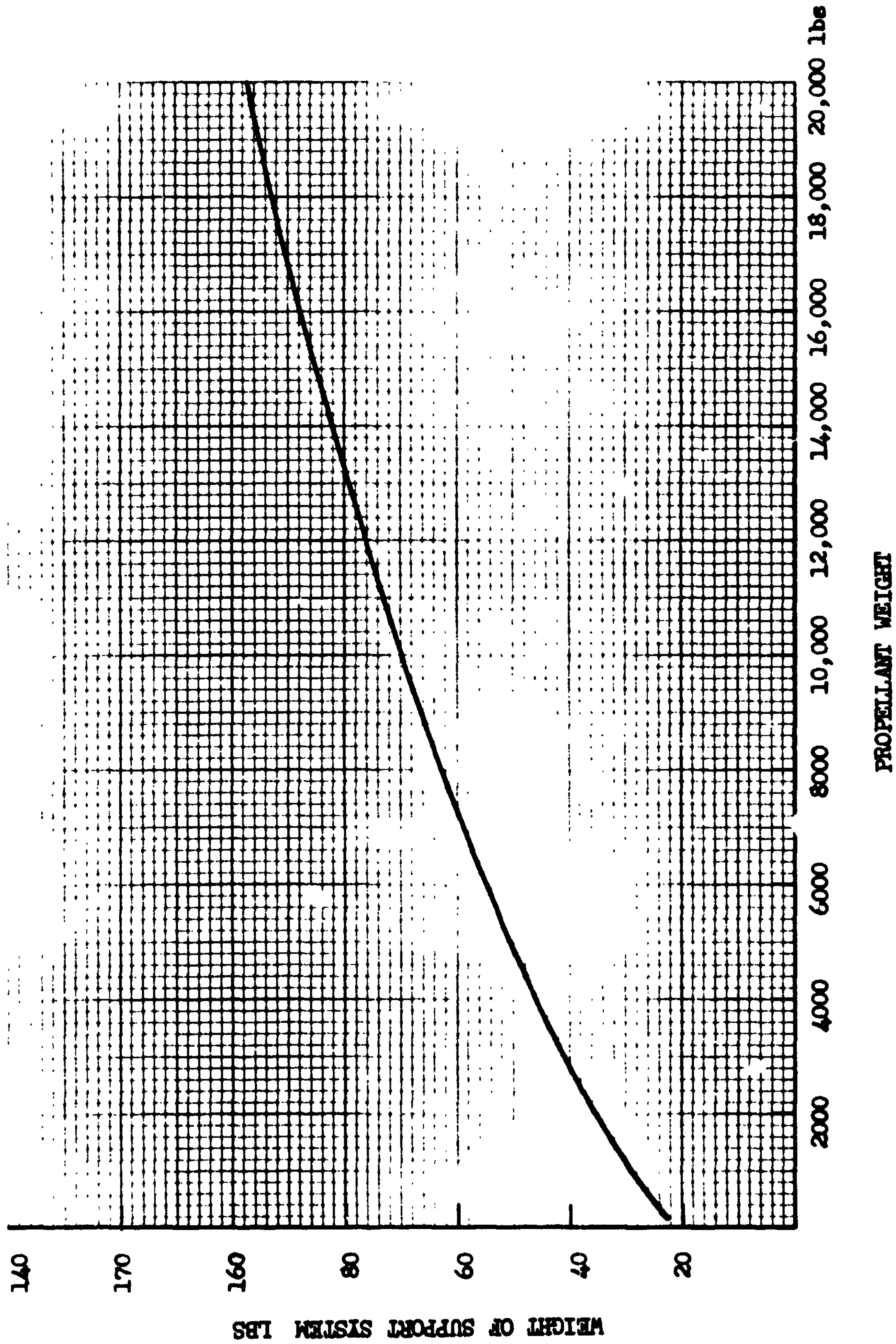

FIGURE 6-4 TANK SUPPORT WEIGHT

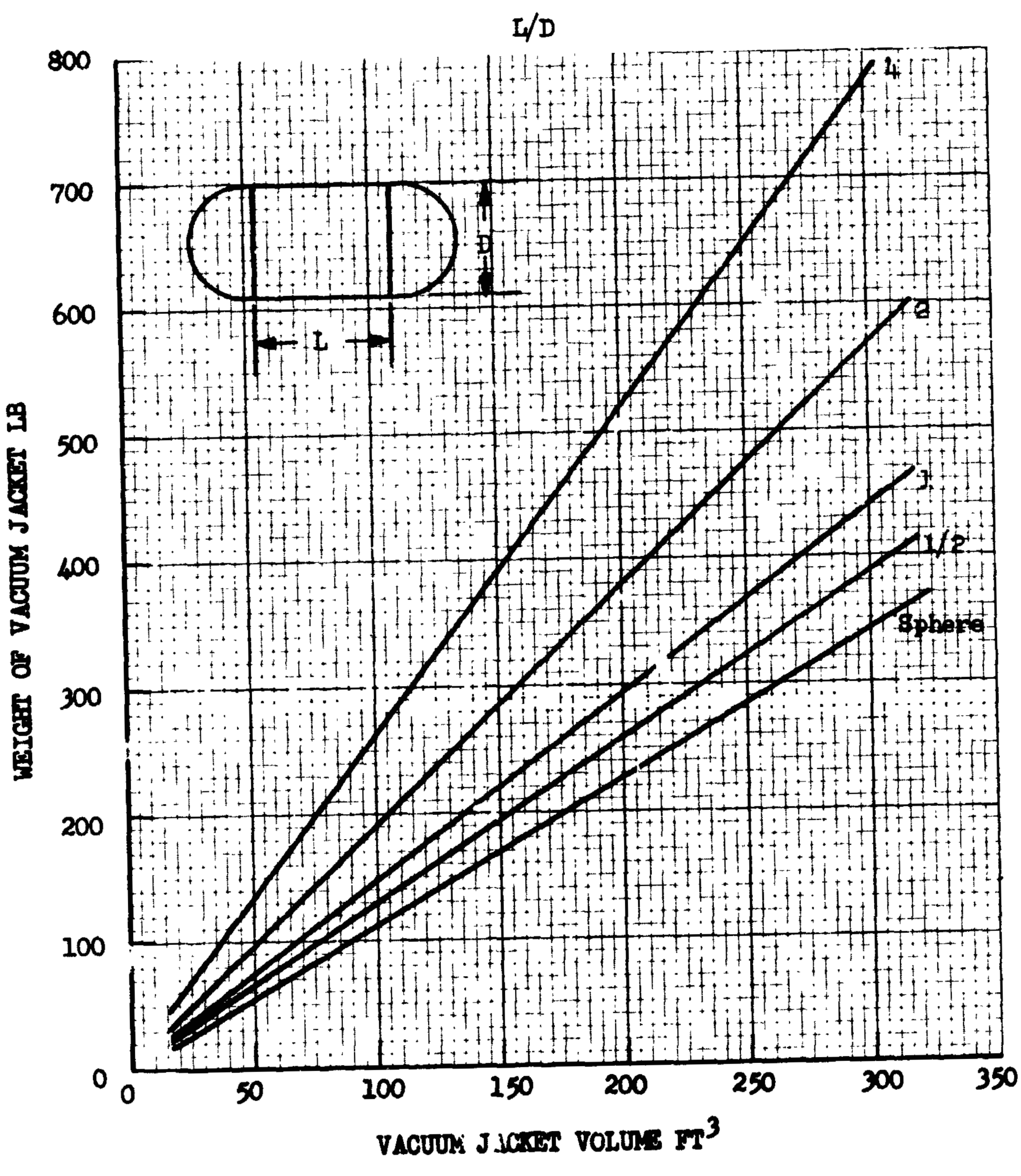

FIGURE 6-5 WEIGHT OF VACUUM JACKET

has been shown that multilayer insulation is among the better performers. A good candidate for insulation performance is a double-goldized mylar with silk net spacers. It gives good performance, as well as relatively low performance variation. Therefore, for estimates of heat transfer, this type of insulation was selected.

Analytical investigations of double-goldized mylar/silk net, coupled with empirical data from calorimeter tests have been employed to develop a relationship for the heat transfer as given by

$$q = .82 \frac{4.37 \times 10^{*} (N)^{3.27} TM(T_H - T_c)}{N_s + 1} + \frac{6.7 \times 10^{13} (T_H^{4.51} - T_c^{4.51})}{N_s}$$

where:

q = Heat rate Watts/Ft^2

N = Layer density No./in

N_s = Number of layers

T_H = Hot boundary temperature (^oR)

T_c = Cold boundary temperature (^oR)

$TM = \frac{T_H + T_c}{2}$ (^oR)

This relationship contains a multiplying factor of 2.8 to account for the degradation of the multilayer when it is applied to large tanks. This allows for fasteners, seams, and thermal degradation around supports. Utilizing this equation, heat rates were computed for several hot and cold boundary temperatures and are shown in Figure 6-6. This curve can be quickly used to determine the heat rate through the insulation if the total surface area and surface temperatures are known. The surface temperatures can be estimated from the procedures and data given in Section 5.0 if the surface is exposed to the external environment. If the tank is enclosed within a vehicle the environmental conditions of the vehicle are required. In most instances rough estimates can be obtained by evaluating the type of equipment that is in the vicinity of the tank.

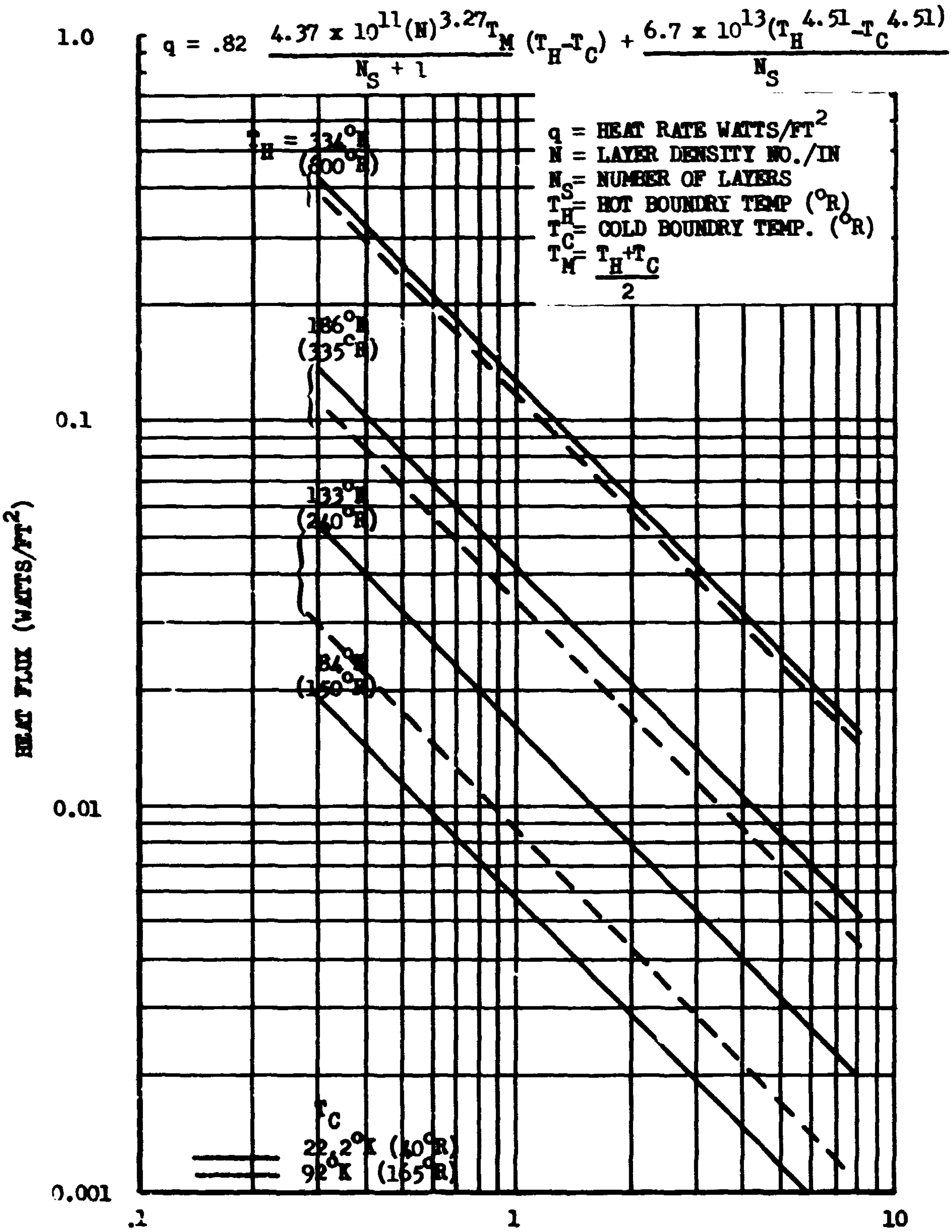

Figure 6-6 Heat Leak through Multilayer Insulation

6.4.2 Heat Leak Through Supports

Simple relationships can be developed to estimate the heat leak to a cryogen tank by computing the crossectional area required for the tank supports and estimating the solid conduction heat transfer. However, this approach generally results in much lower heat leak than is actually obtained in tests or as a result of detailed analysis which takes into account the radiation terms and the strut detail design and length. Therefore, several studies and tests performed over the years have been utilized to estimate the heat transfer to the cryogen tank. The data have been reviewed and normalized to put them in terms of the unit weight of the stored cryogens. In every case data were selected for fiberglass supports which were proven to be the best type of low heat leak support. For each case the design conditions include requirements for launch and ascent loads. The data are plotted in Figure 6-8, and a "best fit" curve has also been included. The identification of the data is given in Table 6-2. Most of the data fall into a fairly narrow band near the curve, with the exception of points 2, 5, and 8. Point 2 is for a slush hydrogen dewar that, due to the nature of the design, required the supports to be short compression members. This resulted in more than an order of magnitude increase in heat leak. Point 5 is a design for a cryogenic gas supply system where the supports were designed for oxygen loads due to commonality requirements. The point shown is for the case where hydrogen is used in the storage vessel, and therefore the heat leak per pound of hydrogen is high. Point 8 is for a propellant tank installation where the dense oxidizer could be supported in a near-ideal fashion. Also, the mission was such that the vehicle could be oriented away from the sun and the warm end of the supports were at a low temperature during steady-state operation. The combination of the good design conditions, mission profile, and the heavy propellant, gave a low value of heat leak per pound of cryogen.

It is suggested that for preliminary design estimates the curve shown in Figure 6-8 be used. For small hydrogen tanks, or for unusual design constraints the heat leak should be increased by as much as an order of magnitude, depending upon the installation.

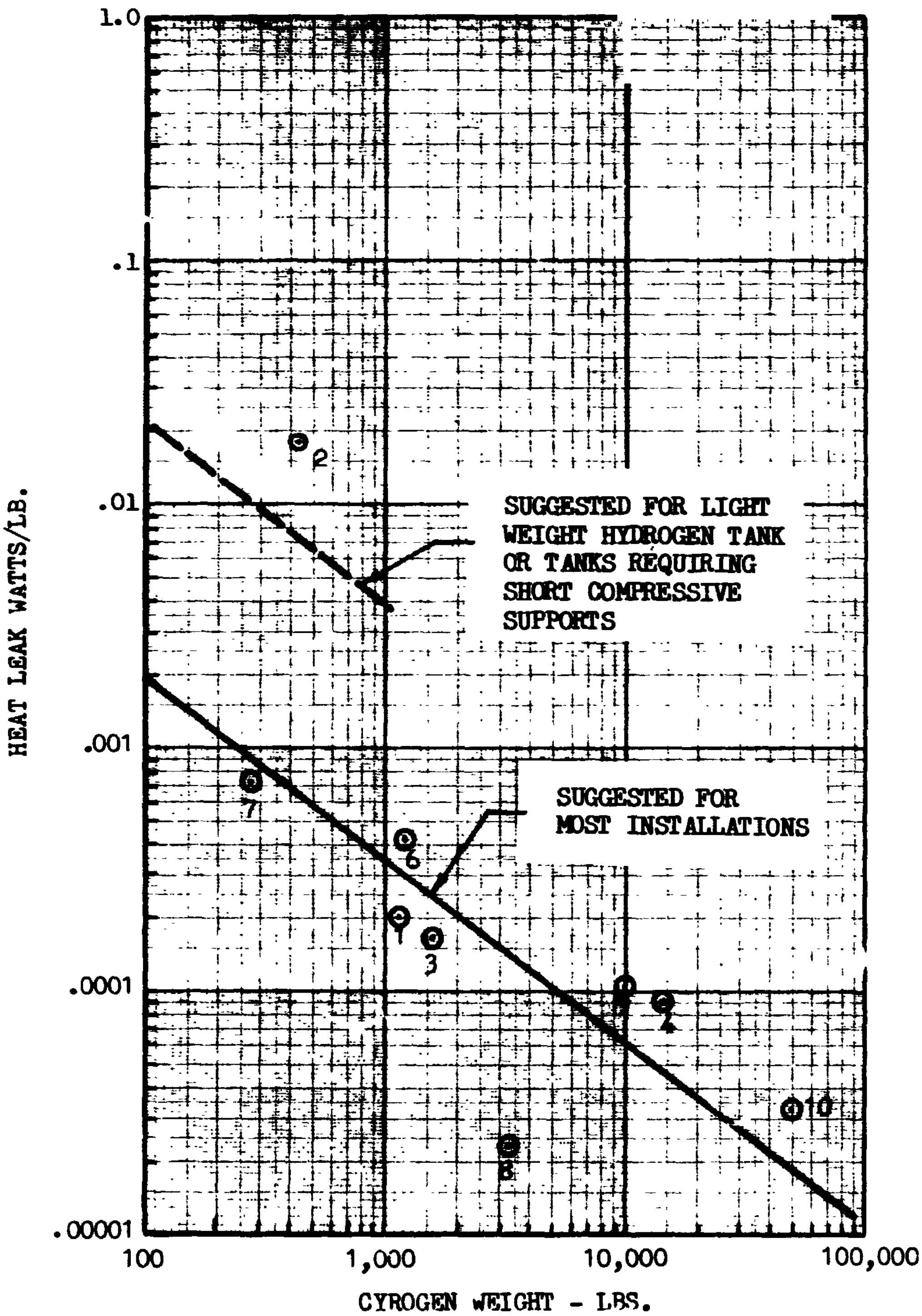

FIGURE 6-7 HEAT LEAKS THROUGH FIBERGLASS SUPPORTS

TABLE 6-1

HEAT LEAK THROUGH SUPPORTS AND LINES AND INSTRUMENTATION

Ident Point	Tank	Cryogen Wt Lb	--Heat Leak - Watts/Lb --- Supports	Lines & Instrumentation	Ref
1	109.7" Ellipsoidal LH_2	1,160	.0002	.00076	6-4
2	Slush H_2 Dewar	436	.018	.0033	6-5
3	Ellipsoidal LH_2	1,580	.00017	.00173	6-6
4	Ellipsoidal oxidizer	14,300	.000093	.000031	6-6
5	H_2 Dewar	75	.0088	.00034	6-7
6	O_2 Dewar	1,210	.00041	.00017	6-7
7	Ellipsoidal LH_2	275	.00071	.00021	6-8
8	Cylindrical + Hemisphere LF_2	3,300	.000024	.000012	6-8
9	Ellipsoidal LH_2	10,000	.000103	.00012	6-9
10	Ellipsoidal LO_2	50,000	.000033	.0000105	6-9

6.4.3 Heat Leak through Lines and Instrumentation

The same sources of data that were used to get the heat leak caused by the supports were used to get the heat leak caused by the lines and instrumentation. The term "lines and instrumentation" is used to include all sources of heat other ehan those caused by supports and insulation. However, it does not include the heat generated by the instruments themselves. A considerable amount of spread exists in the data as shown in Figure 6-8. This points up the fact that every design will have its own peculiarities that must be analyzed if a detail design is to be performed. However, to obtain rapid estimates of heat leak into the tank, the curve shown in Figure 6-8 can be used. The designer may want to adjust the heat upwards or downwards by an order of magnitude, depending upon his detail or peculiar design requirements.

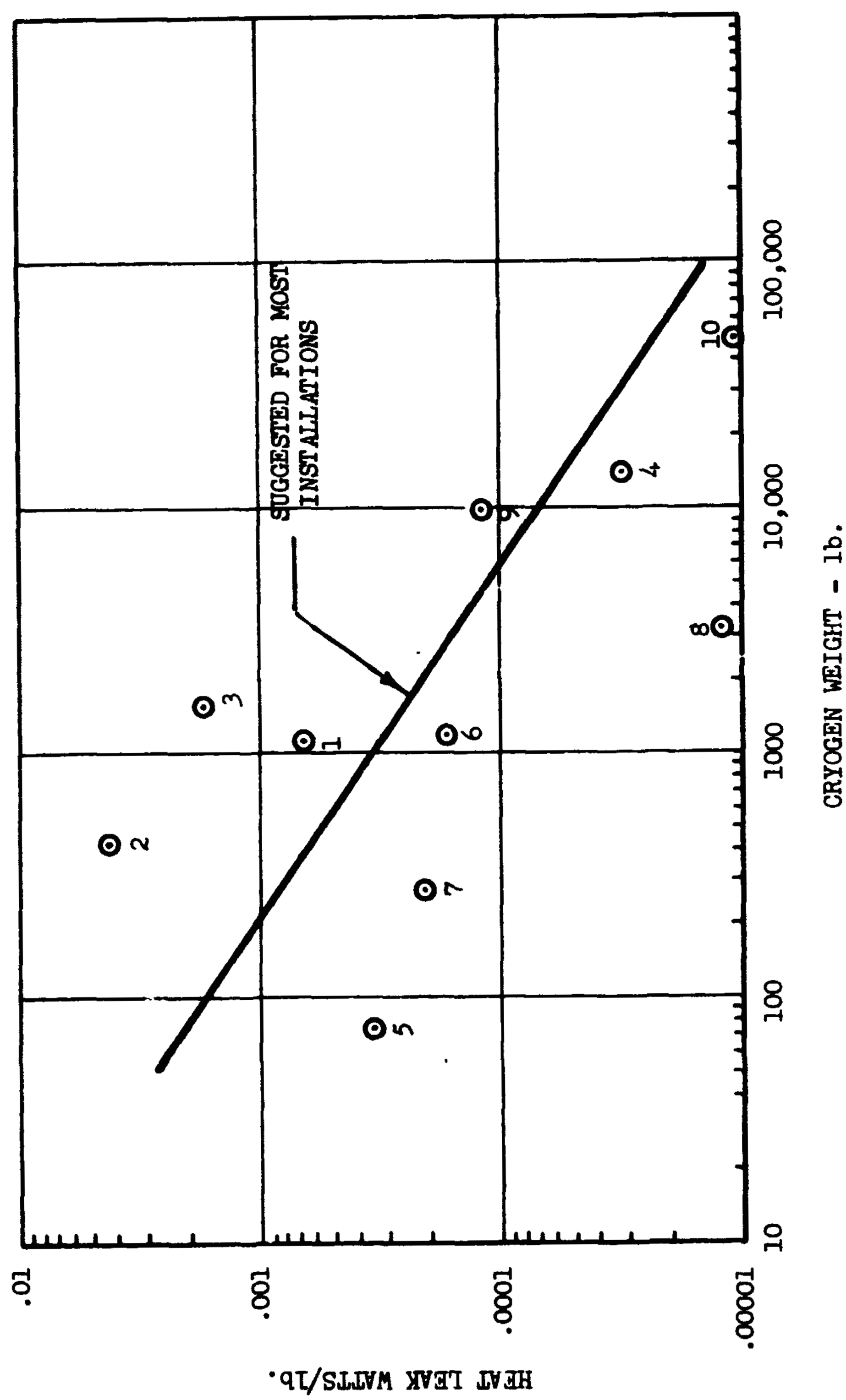

FIGURE 6-8 HEAT LEAK THROUGH LINES AND INSTRUMENTATION

REFERENCES

6-1 NASA-CR 54879, "Thermal Protection System for a Cryogenic Space craft Propulsion Module", Final Report for Contract NAS3-4199, Lockheed Missiles & Space Company, November 1966

6-2 LMSC K-17-68-5, "Investigations Regarding Development of a High-Performance Insulation System", Final Report for Contract NAS8-20758, July 1968

6-3 NASA-CR 72747, "Thermal Performance of Multilayer Insulations", Final Report for Contract NAS3-12025, Lockheed Missiles & Space Company, February 1971

6-4 LH_2 Storability in Space Propulsion Vehicles, Lockheed Missiles & Space Company, LMSC - 685104, 14 March 1968

6-5 LMSC K-11-68-1K, "A Study of Hydrogen Slush and/or Hydrogen Gel Utilization", Final Report for Contract NAS8-20342, Supplemental Program, Lockheed Missiles & Space Company, October 1968

6-6 Advanced Maneuvering Propulsion System. Lockheed Missiles & Space Company, LMSC-A960593, 31 January 1970

6-7 Cryogenic Gas Storage System. Lockheed Missiles & Space Company, LMSC 699613, 26 May 1967

6-8 Propellant Selection for Unmanned Spacecraft Propulsion Systems. Lockheed Missiles & Space Company, NASA CR 105202 NAS W 1644 15 September 1969

6-9 Improved Lunar Cargo and Personnel Delivery System. Lockheed Missiles & Space Company T-28-68-4 28 June 1968

Section 7
HEAT REJECTION SYSTEMS

7.1 INTRODUCTION

In order to estimate the heat rejection system characteristics the heat rejection rate must be known.

Values of required rates of heat rejection for a particular type of refrigeration system can be obtained using the definition of coefficient of performance presented in Section 3.

$$COP = \frac{\text{Cooling Load}}{\text{Power Input}} = \frac{q_c}{w}$$

The required rate of heat rejection is then

$$q = q_c + w = q_c \frac{(1 + COP)}{COP}$$

for mechanically powered refrigerators. For heat powered refrigerators,

$$q = q_h + q_c$$

where q_h is the rate at which heat is supplied to the refrigerator.

Values of coefficient of performance are given in Section 3 for a variety of refrigerators and operating conditions.

7.2 RADIATOR DESIGN

7.2.1 Preliminary Design of Radiators for Space Operation

The preliminary design procedure presented below is directed toward the steady-state operation of a radiator rejecting (or absorbing) heat solely by means of radiative transfer. It is assumed that the cross section of the surface between coolant ducts is trapezoidal or rectangular and that no change of phase occurs within the coolant ducts.

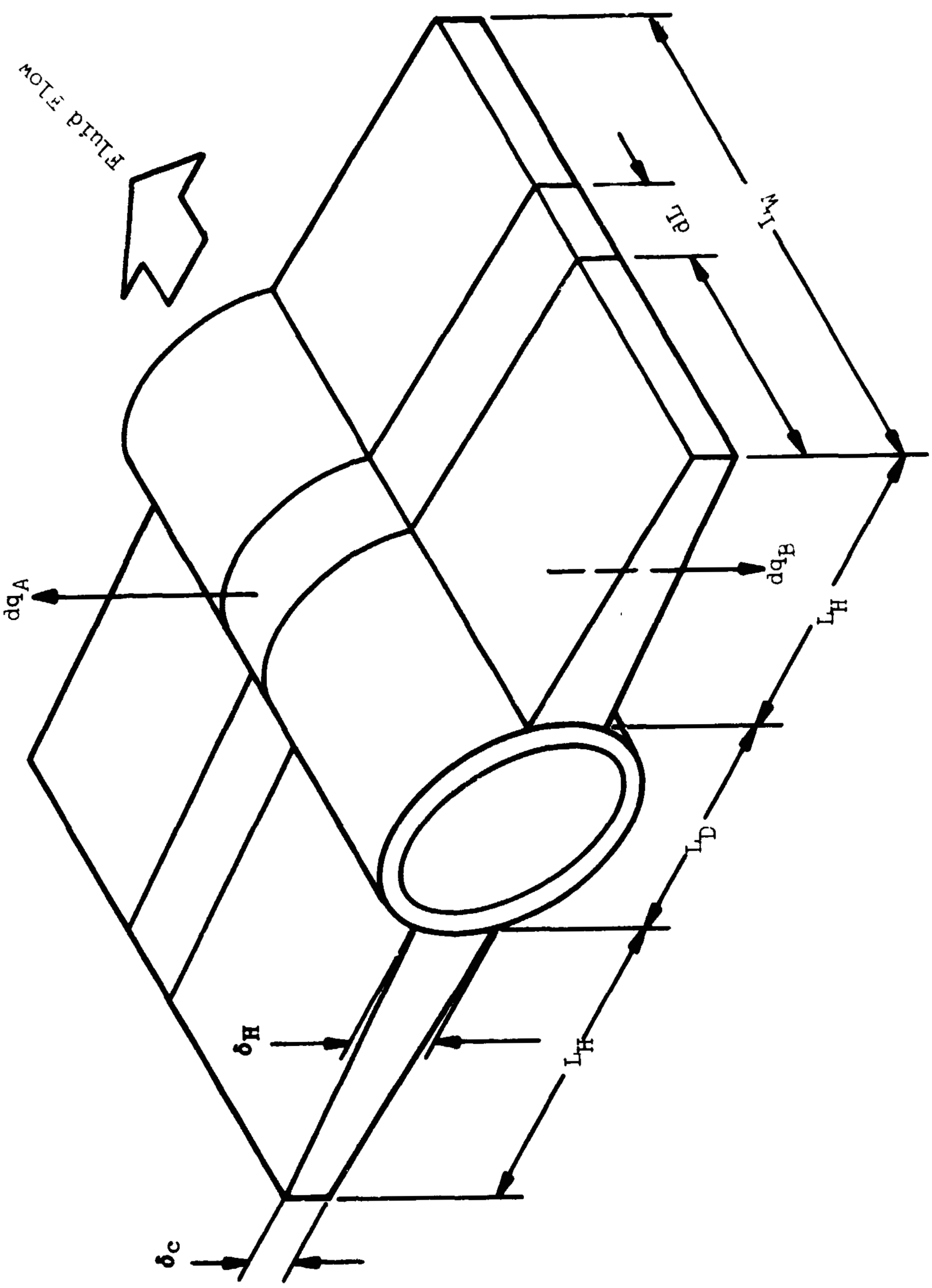

Figure 7-1 Radiator Duct with Trapezoidal Fins - Two Exposed Sides

A section of radiator using tapered fins is shown in Fig. 7-1. At the entrance to the radiator the fluid wall temperatures are T_{F1} and T_{W1}, respectively, at the exit the corresponding temperatures are T_{F2} and T_{W2}.

The values of the environmental factors G_E, G_A and G_P referred to below can be obtained by the procedure described in Section 5.

Radiators having a single active surface can be evaluated using the same equations provided the environmental factors are properly defined. For a two-sided radiator having different emittance values on each side,

$$G_E = \sigma (\epsilon_A + \epsilon_B)$$

and $G_A + G_P$ is the heat flux density from the environment reaching both surfaces. However, for a radiator having a single active surface (one side insulated) a value of zero is used for the underside surface emittance, ϵ_B, and $G_A + G_P$ is the environmental heat flux density incident only on the active surface.

7.2.1.1 Design Procedure

The usual design problem requires sizing a radiator to handle a given cooling load. Thus, given either q or the coolant flowrate, as well as coolant inlet and outlet temperatures, the length of a radiator having a given configuration is desired. The solution procedure for this case is outlined in stepwise fashion below.

1. Establish heat rejection rate for the given cooling load using the COP data in Section 3.
2. Select a fluid for the given inlet and outlet temperature range from Fig. 7-7.
3. Look up the fluid specific heat C_{P_F} from Table 7-1.
4. Compute the coolant flowrate from the known cooling load using

$$q = \dot{W}_F C_{P_F} (T_{F1} - T_{F2})$$

5. Solve for G_A, G_P and G_E using the data of Section 5.
6. Select values for the coolant duct dimensions and fin profile.

7. Solve for the heat transfer coefficient, h, using Fig. 7-3.
8. Assume the inlet and outlet tube wall temperatures, T_{W1} and T_{W2}, are equal to the adjacent coolant temperatures, T_{F1} and T_{F2}.
9. Obtain fin effectiveness values Ω_1 and Ω_2 from Fig. 7-4 with

$$P_1 = \frac{G_E T_{W_1}{}^3 L_H{}^2}{K \delta_H}$$

and

$$P_2 = \frac{G_E T_{W_2}{}^3 L_H{}^2}{K \delta_H}$$

10. Determine interradiation correction factors F_{R1} and F_{R2} from Fig. 7-2.
11. Compute equivalent lengths, L_{E1} and L_{E2}, at entrance and exit using the definition

$$L_E = F_R \left[L_D + \frac{2 \Omega L_H}{1 - \frac{(G_A + G_P)}{G_E T_W{}^4}} \right]$$

12. Use these values to compute "new" wall temperatures, T_{W1} and T_{W2}, by trial and error, using the heat balance resulting from the equations

$$\left[G_E T_{W_1}{}^4 - (G_A + G_P) \right] L_{E_1} = p\ h\ (T_{F_1} - T_{W_1})$$

and

$$\left[G_E T_{W_2}{}^4 - (G_A + G_P) \right] L_{E_2} = p\ h\ (T_{F_2} - T_{W_2})$$

13. With these wall temperatures steps 9 through 12 are repeated until consistent values of effectiveness and wall temperature are obtained.
14. Look up values of ϕ_F and ϕ_R from Figs. 7-5 and 7-6.

15. Compute required radiator length, L_W, from the equation

$$L_W = \frac{\dot{W}_F C_{P_F}}{ph} \left[\phi_F + \phi_R \left(\frac{ph}{G_E T_{W1}{}^3 \bar{L}_E} \right) \right]$$

where $\bar{L}_E$ is an average value of L_E over the length of the radiator.

7.2.2 Approximate Method for Radiator Design

The design procedure described above can be greatly simplified if the following assumptions are made:

- The heat transfer coefficient, h, is high so that there is a small temperature difference ($T_F - T_W$) between the coolant and the duct wall.
- The coolant duct width is small compared to the fin width.
- The tube-to-fin interradiation correction factor F_R is equal to one.
- An average effective width $L_{E_{AVG}}$ is defined based on the mean of the inlet and outlet temperatures.

7.2.2.1 Design Procedure Using Approximate Method

The solution for radiator length, using an approximate method based on the assumptions stated above, is given below in stepwise fashion.

1. Establish heat rejection rate for the given cooling load using the COP data in Section 3.
2. Select a fluid for the given inlet and outlet temperature range from Fig. 7-7.
3. Look up fluid specific heat C_{P_F} from Table 7-1,
4. Compute the coolant flowrate from the known cooling load using the equation

$$q = \dot{W}_F F_{P_F} (T_{F1} - T_{F2}) = \dot{W}_F C_{P_F} T_{F1} (1-Z)$$

where

$$Z = \frac{T_{F2}}{T_{F1}} = \frac{T_{W2}}{T_{W1}}$$

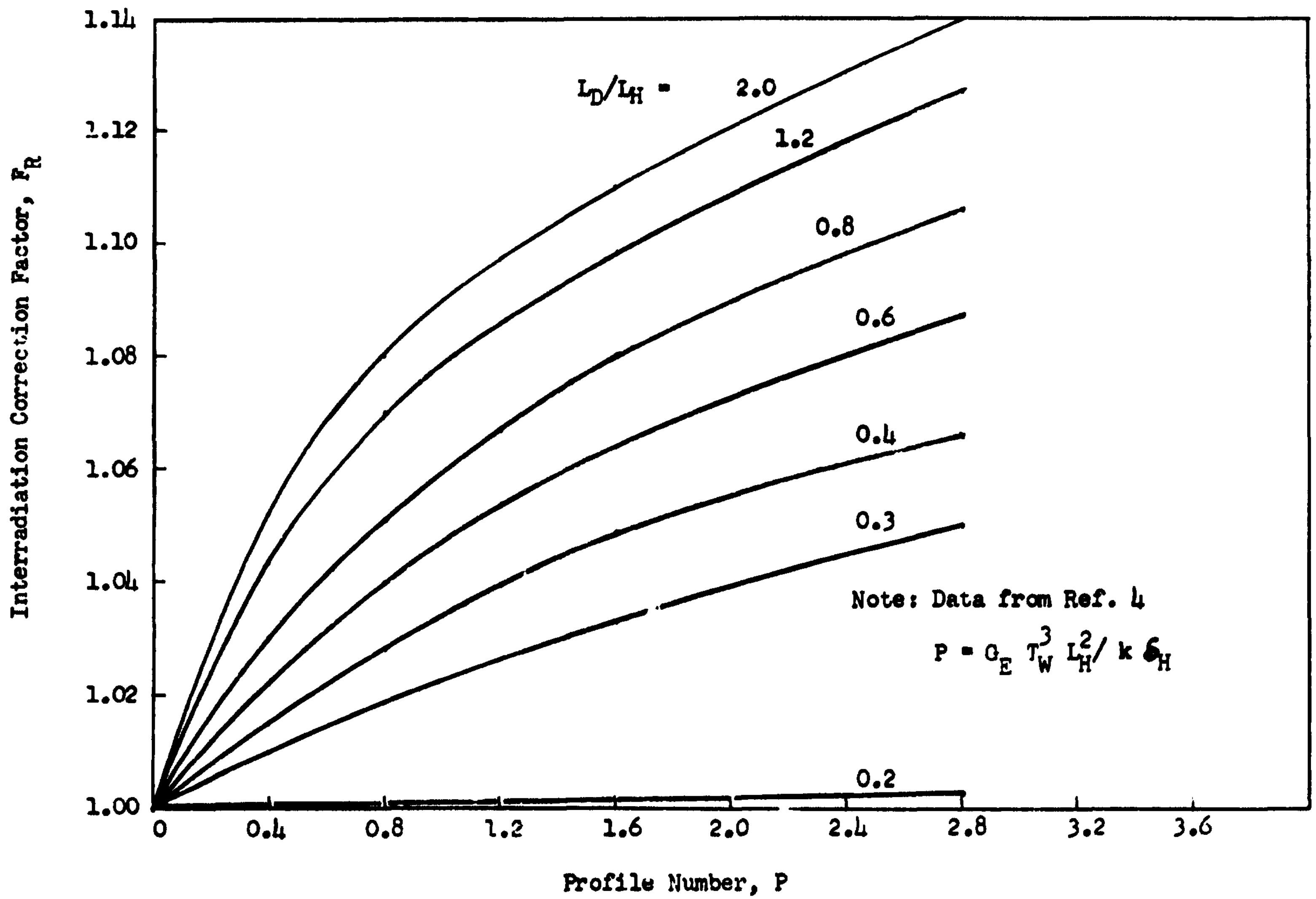

Figure 7-2 Correction Factor for Interradiation between Coolant Tube and Fins

FOLDOUT FRAME I

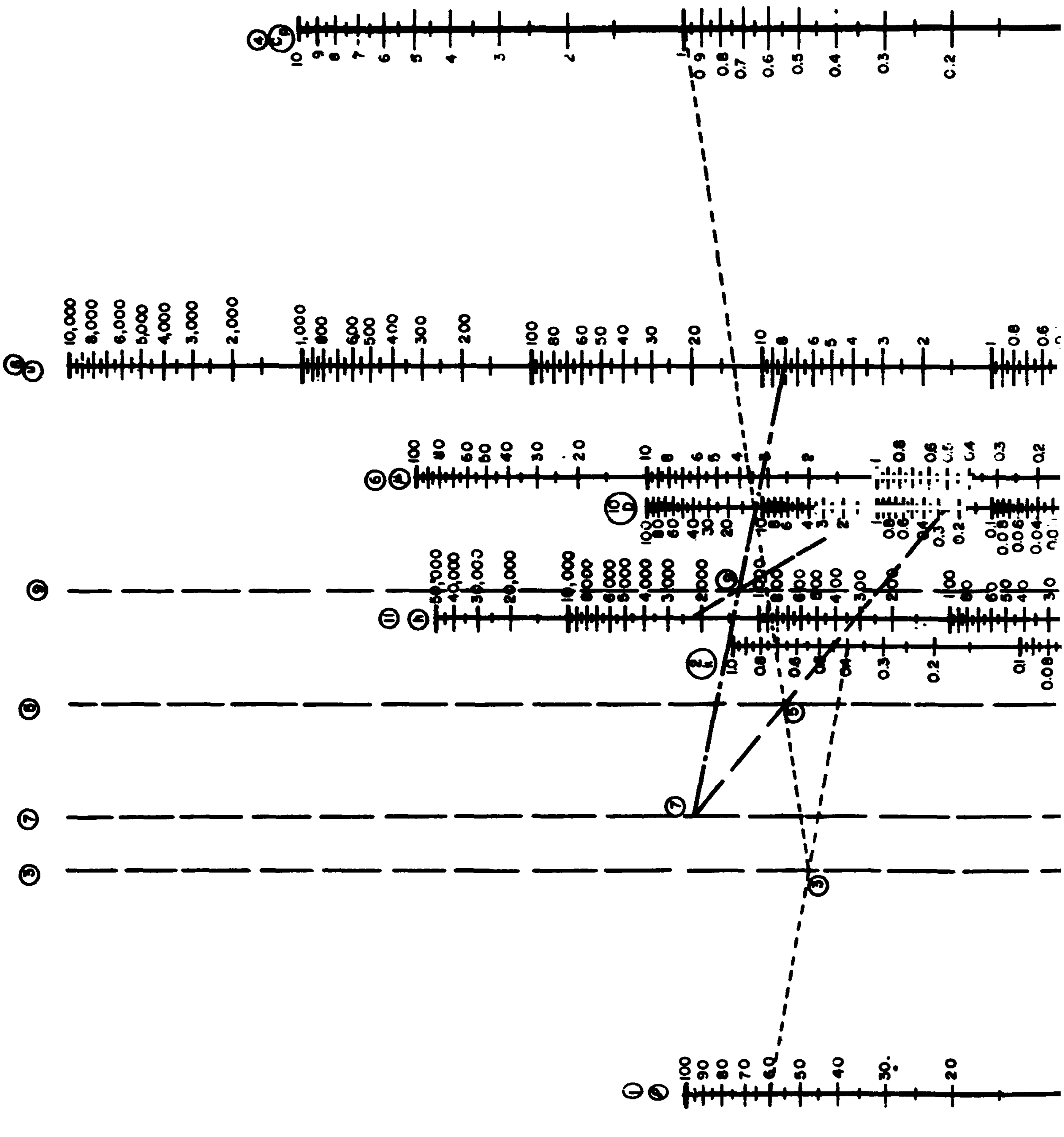

FOLDOUT FRAME 2

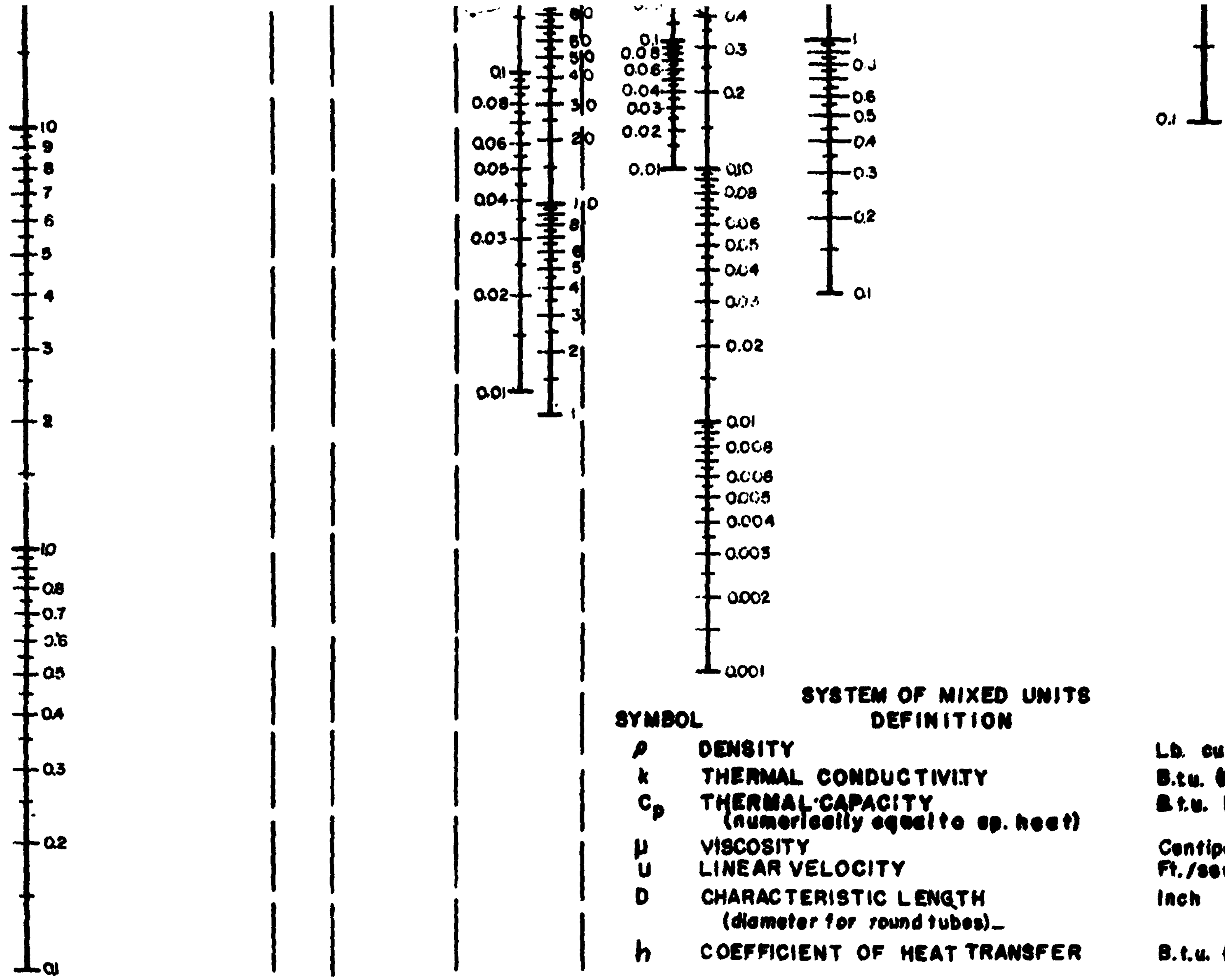

SYSTEM OF MIXED UNITS

SYMBOL	DEFINITION	UNIT
ρ	DENSITY	Lb. cu.ft.
k	THERMAL CONDUCTIVITY	B.t.u. (hr)(ft)(°F)
C_p	THERMAL CAPACITY (numerically equal to sp. heat)	B.t.u. lb.ft.
μ	VISCOSITY	Centipoise
U	LINEAR VELOCITY	Ft./sec.
D	CHARACTERISTIC LENGTH (diameter for round tubes)	Inch
h	COEFFICIENT OF HEAT TRANSFER	B.t.u. (hr.)(sq.ft)(°F)

Encircled numbers (e.g. 1 2----) indicate sequence of reference line usage

Fig 7-3 Nomogram for the DiHus-Boelter Equation

PRECEDING PAGE BLANK NOT FILMED

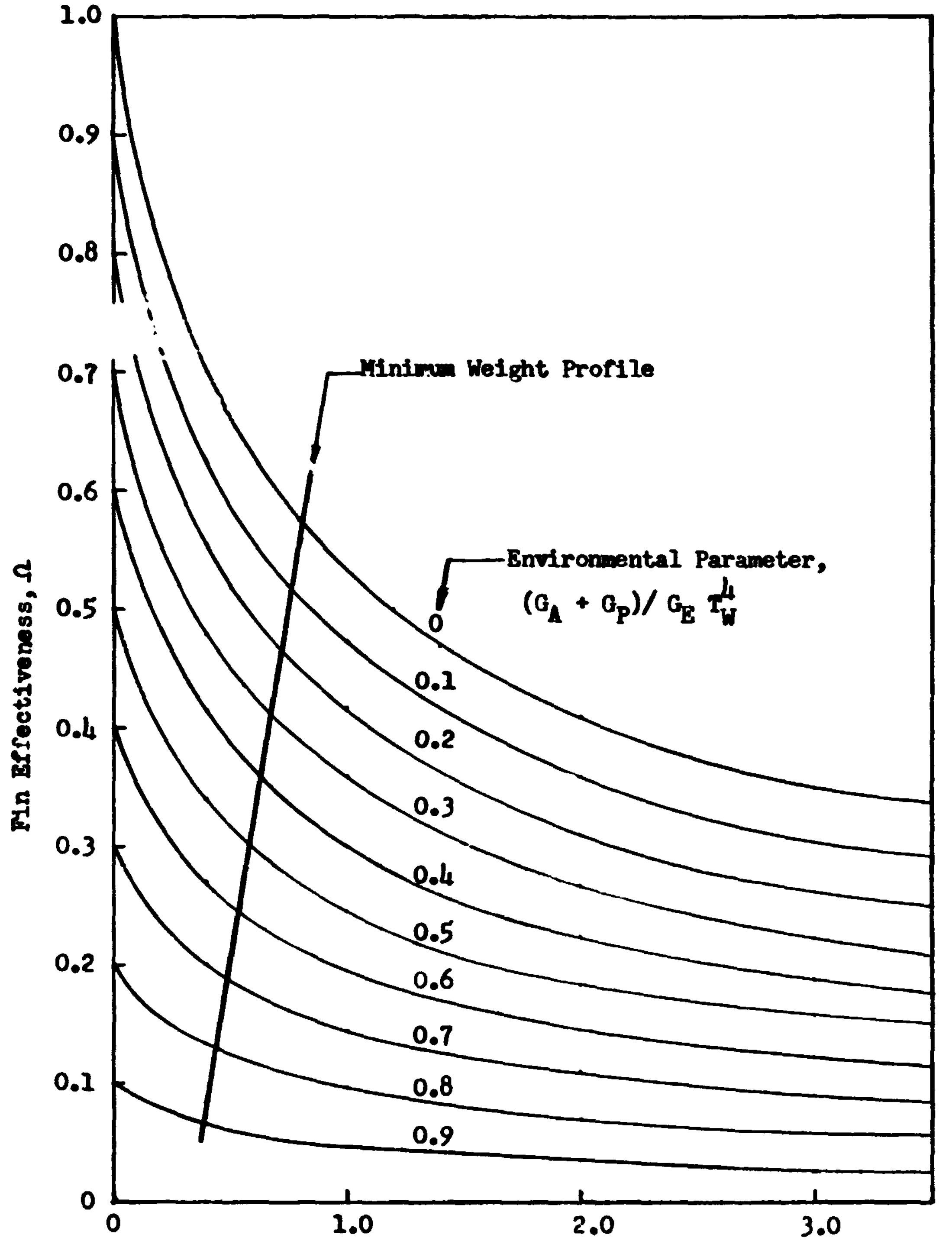

Figure 7-4 Fin Effectiveness for Rectangular Fins

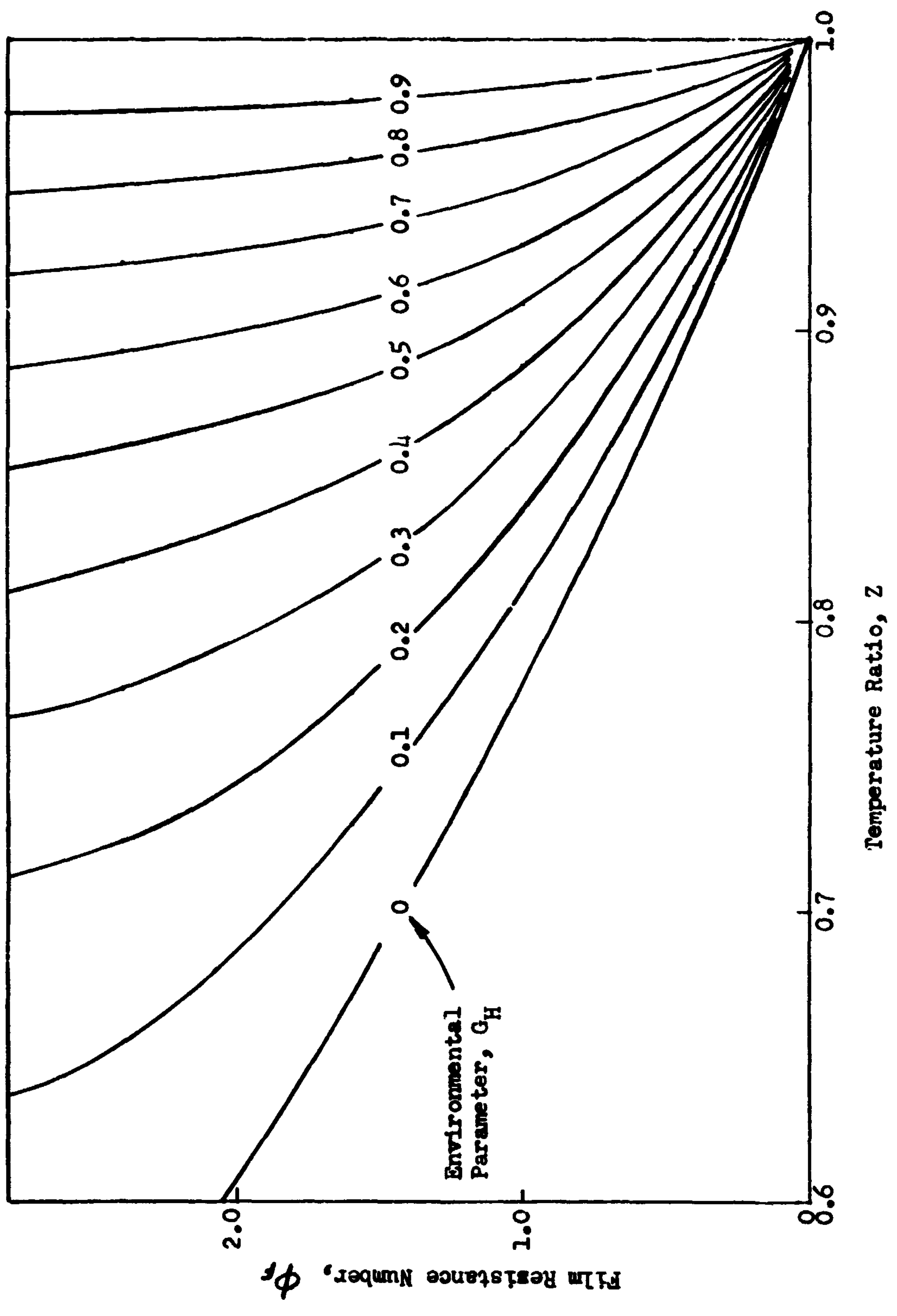

Figure 7-5 Film Resistance Number for Radiator Heat Rejection

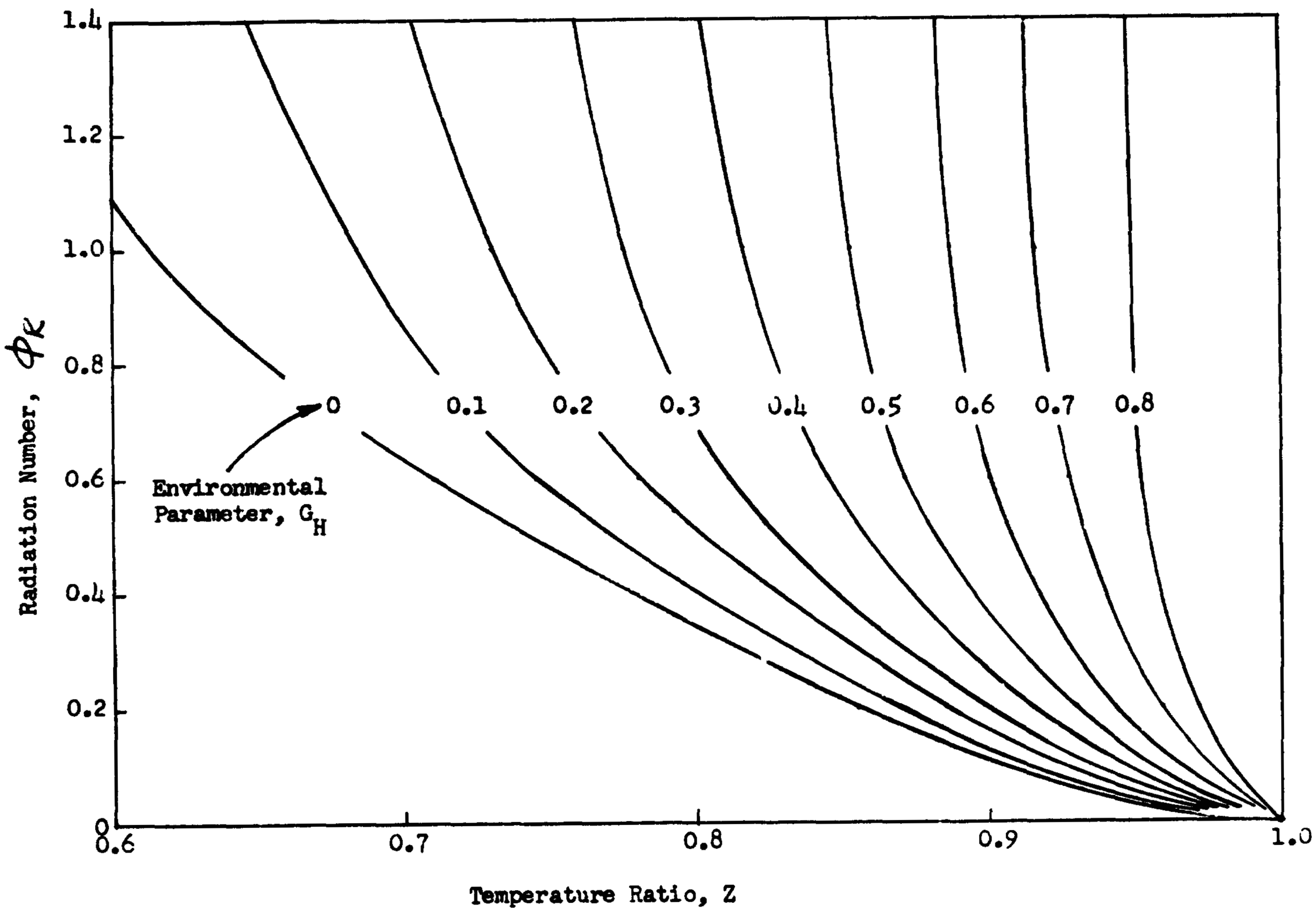

Figure 7-6 Radiation Number for Radiator Heat Rejection

5. Solve for G_A, G_P and G_E using the data of Section 5.

6. Assume a value for the inside diameter of the coolant tubing and solve for the heat transfer coefficient, h, using Fig. 7-3.

7. Select values for the coolant duct dimensions and fin profile.

8. Check that the following criterion is satisfied:

$$\frac{L_D}{L_H} > 0.01 \quad \frac{\left(\frac{T_{W1}}{100}\right)^3}{h}$$

If not, select revised values of L_D/L_H until the inequality is satisfied.

9. Compute average radiator temperature from

$$T_{AVG} = \frac{T_{F1} + T_{F2}}{2}$$

10. Compute the fin profile number using $T_W = T_{AVG}$ from the equation

$$P = \frac{G_E T_W^3 L_H^2}{K \delta_H}$$

where δ_H is the fin root thickness and K the fin thermal conductivity.

11. Look up fin effectiveness values corresponding to T_{AVG} from Figure 7-4.

12. Compute $L_{E_{AVG}}$ from

$$L_{E_{AVG}} = \left. \frac{2 L_H \Omega}{1 - \frac{G_A + G_P}{G_E T^4}} \right|_{T = T_{AVG}}$$

13. Look up value of ϕ_R from Fig. 7-6 using an average environmental parameter:

$$G_H = \frac{G_A + G_P}{\frac{G_E(T_{W_1}^4 + T_{W_2}^4)}{2}}$$

14. Compute required radiator length, L_W, from

$$L_W = \frac{\dot{W}_F C_P \phi_R}{G_E T_{F1}^{3} L_{E_{AVG}}}$$

7.2.3 Fluid Selection for Radiator Design

As described in the final report, the maximum rate of heat rejection is obtained, for a given radiator configuration, when the quantity

$$\psi_H = K \left(\frac{\rho}{\mu}\right)^{0.8} \left(\frac{C_p \mu}{K}\right)^{.33} = \frac{K^{0.67} \rho^{.8} C_p^{.33}}{\mu^{.47}}$$

is maximized.

Values of ψ_H are shown in Fig. 7-7 for several fluids of interest. Values of density, viscosity, specific heat and thermal conductivity are shown for these fluids in Table 7-1.

7.2.4 Pressure Drop in Coolant Ducts

The total frictional pressure drop of the fluid flowing in the coolant ducts can be estimated using the assumption that the tubing is smooth. The Fanning form of the pressure drop equation can be written

$$\Delta p = 2 \frac{fL}{D} \frac{1}{\rho} \left(\frac{\dot{W}_F}{A}\right)^2$$

or

$$\Delta p = 32 \frac{fL}{D} \frac{1}{\rho} \left(\frac{\dot{W}_F}{\pi D^2}\right)^2$$

where

f = Fanning friction factor
L = total tubing length
A = Tube cross-sectional area
D = Tube diameter
ρ = density
$\dot{W}_F$ = Mass flowrate

The friction factor, f, for smooth pipes is given by

$$f = 16/Re, \; 0 < Re \leq 3000$$

$$f = 0.0014 + 0.125\, Re^{-0.32}, \; 3000 < Re \leq 3 \times 10^6$$

where Re is the Reynold's number,

$$Re = \frac{\rho V D}{\mu}$$

The effect of bends or constrictions in the tubing (such as those due to valving) should also be added to the frictional pressure drop for an accurate estimate of the total Δp across the radiator.

7.2.5 Radiator Weight and Area Requirements

As an aid in estimating radiator weight and area requirements, values of these quantities have been computed for two extreme operating conditions:

(1) Operation in free space with no solar or planetary heat inputs.

(2) Operation on the lunar surface with the sun directly overhead.

Values of radiator weight and area were computed using the simplified procedure outlined in Section 7.2.2. No contingency was allowed to account for the weight of meteoroid protection or radiator headers. In all cases it was assumed that the rise in coolant temperature between inlet and outlet was 20°K. For operation in free space, fluid inlet temperatures of 110, 210 and 310°K were selected corresponding to feasible operating temperature ranges for methane, ethyl ether and water, respectively. Values of radiator area are shown in Fig. 7-8 as a function of net heat rejection rate. Only a single curve is shown for lunar surface operation since operation in the lunar environment with methane or ether was found to be unfeasible.

The computed radiator areas were converted to weight values using the appropriate relations for geometry of a triangular fin. For a trapezoidal radiator,

$$W = \rho L_W \left[\frac{\pi}{4} (D_o^2 - D_i^2) + L_H (\delta_c + \delta_H) \right]$$

Table 7-1

THERMOPHYSICAL PROPERTIES OF LIQUIDS AT ONE ATMOSPHERE

T (K)	ρ (Lb_m/ft^3)	C_p ($Btu/Lb_m R$)	$\mu \times 10^3$ ($Lb_m/ft.sec$)	K (Btu/HrFtR)	Pr
			WATER		
273	62.4	1.01	1.20	0.319	13.7
278	62.4	1.00	1.04	0.325	11.6
289	62.3	0.999	0.76	0.340	8.03
294	62.2	0.998	0.578	0.353	5.89
311	62.0	0.998	0.458	0.364	4.52
339	61.2	1.00	0.202	0.384	2.74
367	60.1	1.00	0.205	0.394	1.88
			AMMONIA		
244	42.4	1.07	17.6	0.317	2.15
256	41.6	1.08	17.1	0.316	2.09
273	40.0	1.11	16.1	0.312	2.05
300	37.2	1.17	14.5	0.293	2.01
322	35.2	1.22	13.0	0.275	1.99
			FREON 12		
233	94.8	0.211	28.4	0.040	5.4
256	91.2	0.217	23.[illegible]	0.041	4.4
273	87.2	0.223	20.0	0.042	[illegible].8
289	83.0	0.231	18.0	0.042	3.5
322	75.9	0.244	15.5	0.039	3.5
			NITROGEN		
114	55.0	0.479	0.202	0.0068	52
120	54.0	0.481	0.171	0.0072	41
130	52.35	0.486	0.135	0.0077	31
140	50.8	0.491	0.101	0.0082	22
			METHANE		
90	28.3	0.80	0.141	0.13	3.13
100	27.5	0.81	0.103	0.12	2.51
111	26.55	0.82	0.080	0.11	2.14
			ETHYL ETHER		
173	54.7	0.50	1.137	0.084	24.4
193	51.4	0.51	0.644	0.082	15.03
213	50.0	0.515	0.428	0.080	9.90
233	48.6	0.52	0.310	0.078	7.43
253	47.3	0.527	0.243	0.076	6.07
273	45.9	0.53	0.191	0.074	4.93
293	44.4	0.54	0.157	0.073	4.18
			FC-75		
233	119	0.25	5.11	0.038	121
278	113	0.25	1.58	0.038	37.4
322	106.5	0.25	0.686	0.038	16.3
367	100	0.25	0.355	0.038	8.42

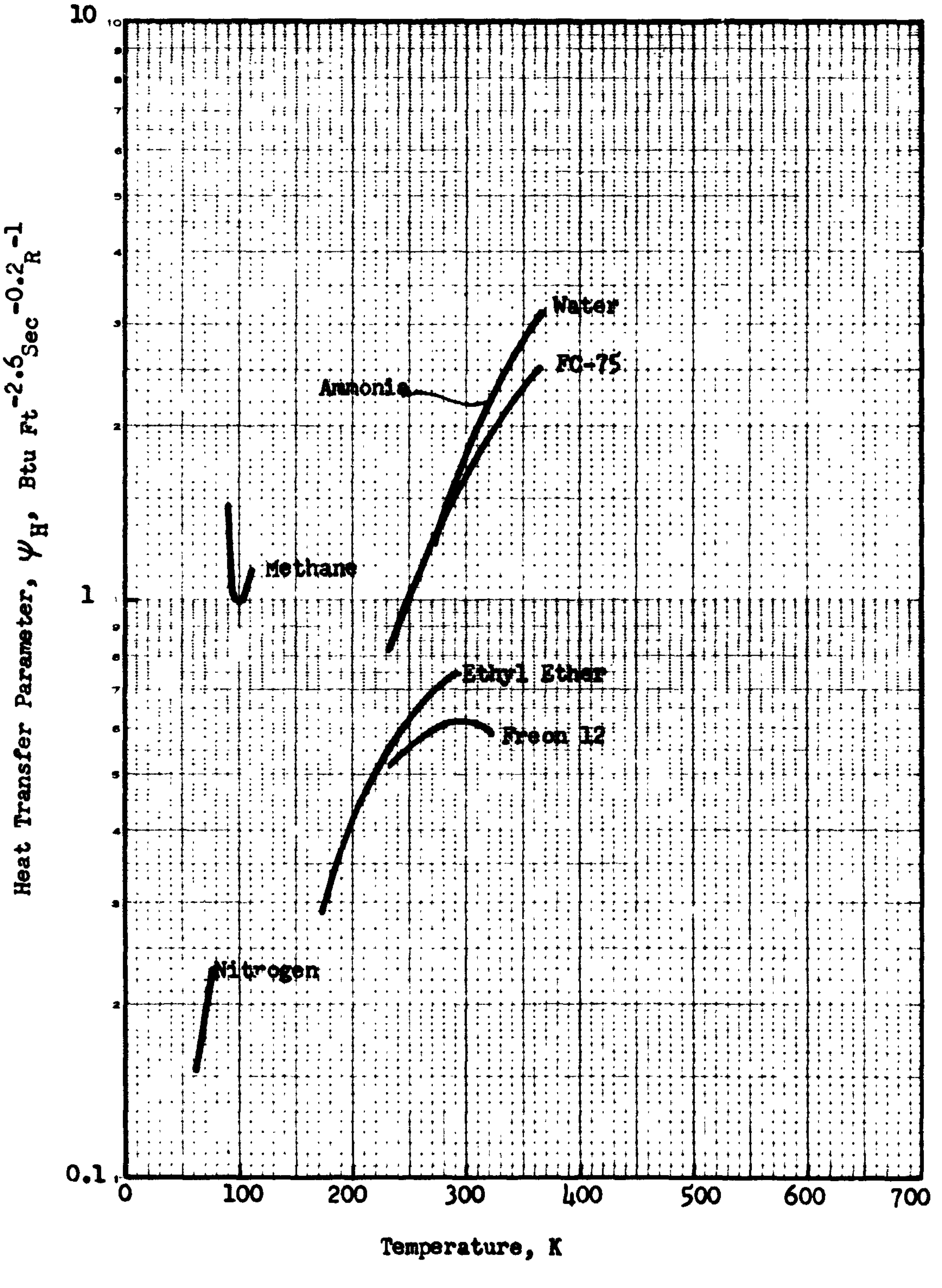

Figure 7-7 Heat Transfer Parameter for Various Liquids

where

L_W = radiator length
D_o = outside diameter of coolant tube
D_i = inside diameter of coolant tube
δ_c = fin tip thickness
δ_H = fin root thickness
L_H = fin width
ρ = fin material density

For a triangular fin, of course, $\delta_c = 0$. Values of radiator weight as a function of heat rejection rate are shown in Fig. 7-9 for the same conditions as those used for the data of Fig. 7-8.

7.3 DESIGN OF HEAT PIPE RADIATORS

The effectiveness of radiators for heat rejection systems can be increased considerably by replacing the coolant ducts with constant temperature heat pipes. Several possible configurations have been proposed for such a radiator (Refs. 7-5 to 7-8) and some experimental models have been built and tested (Refs. 7-5 and 7-9). A radiator design which has been successfully fabricated and tested is shown in Fig. 7-10. Since the condenser section of the heat pipe has a uniform temperature, the radiator design equations developed earlier may be used with T_W replaced by T_C. The required radiator area is then given by

$$A = \frac{q\,(L_D + 2\,L_H)}{F_R\,\left[\,(G_E T_C^{\,4} - G_A - G_P)\,L_D + 2\,G_E T_C^{\,4}\,\Omega L_H\,\right]}$$

where the symbols are defined in the nomenclature (Page 7-40). The condenser temperature T_C is determined by the thermal resistance of the heat pipe between the evaporator and condenser sections. Thus,

$$T_C = T_E - \frac{q\,R_{EC}}{N}$$

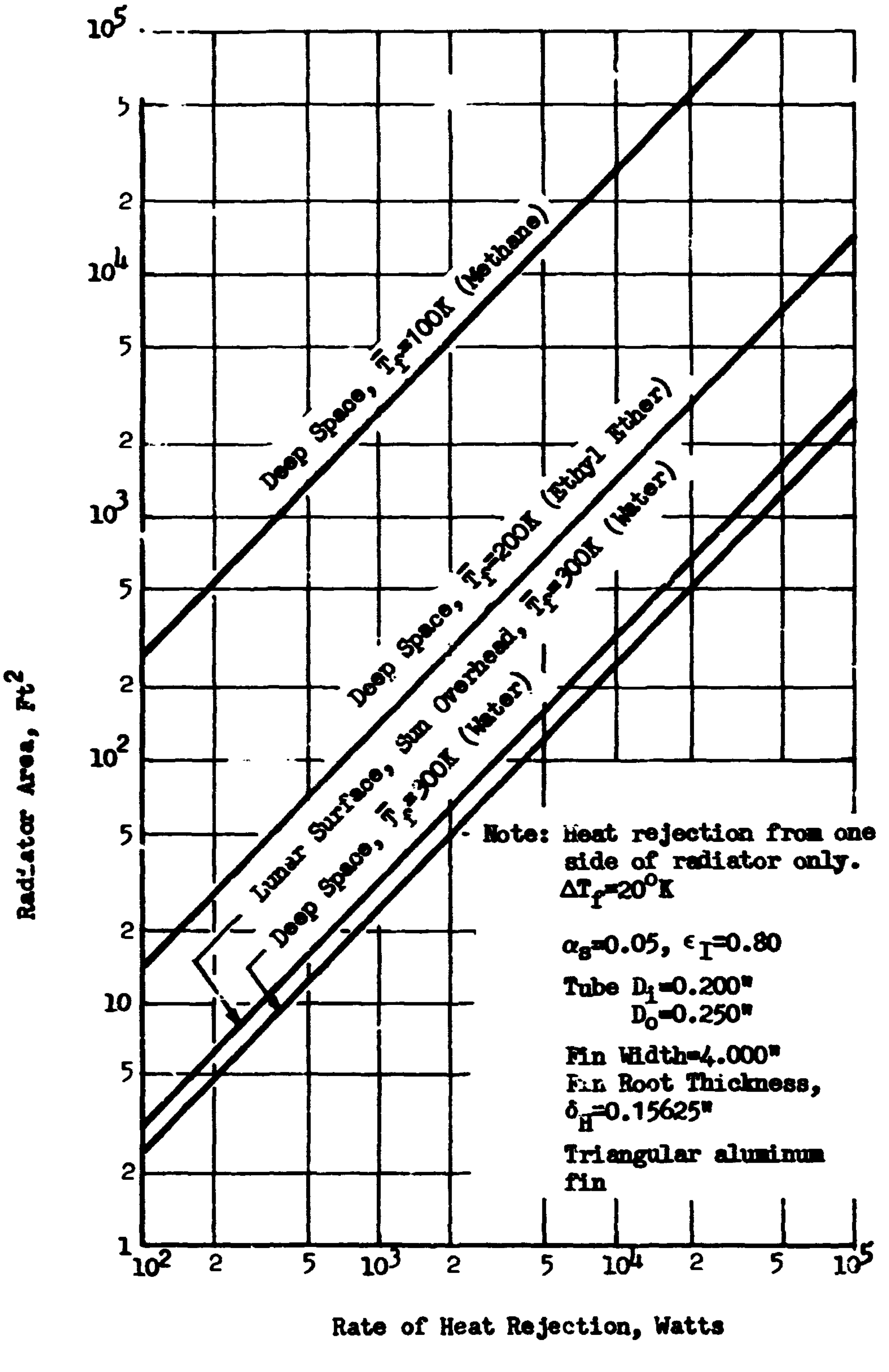

Figure 7-8 Radiator Area for Deep Space and Lunar Surface Operation

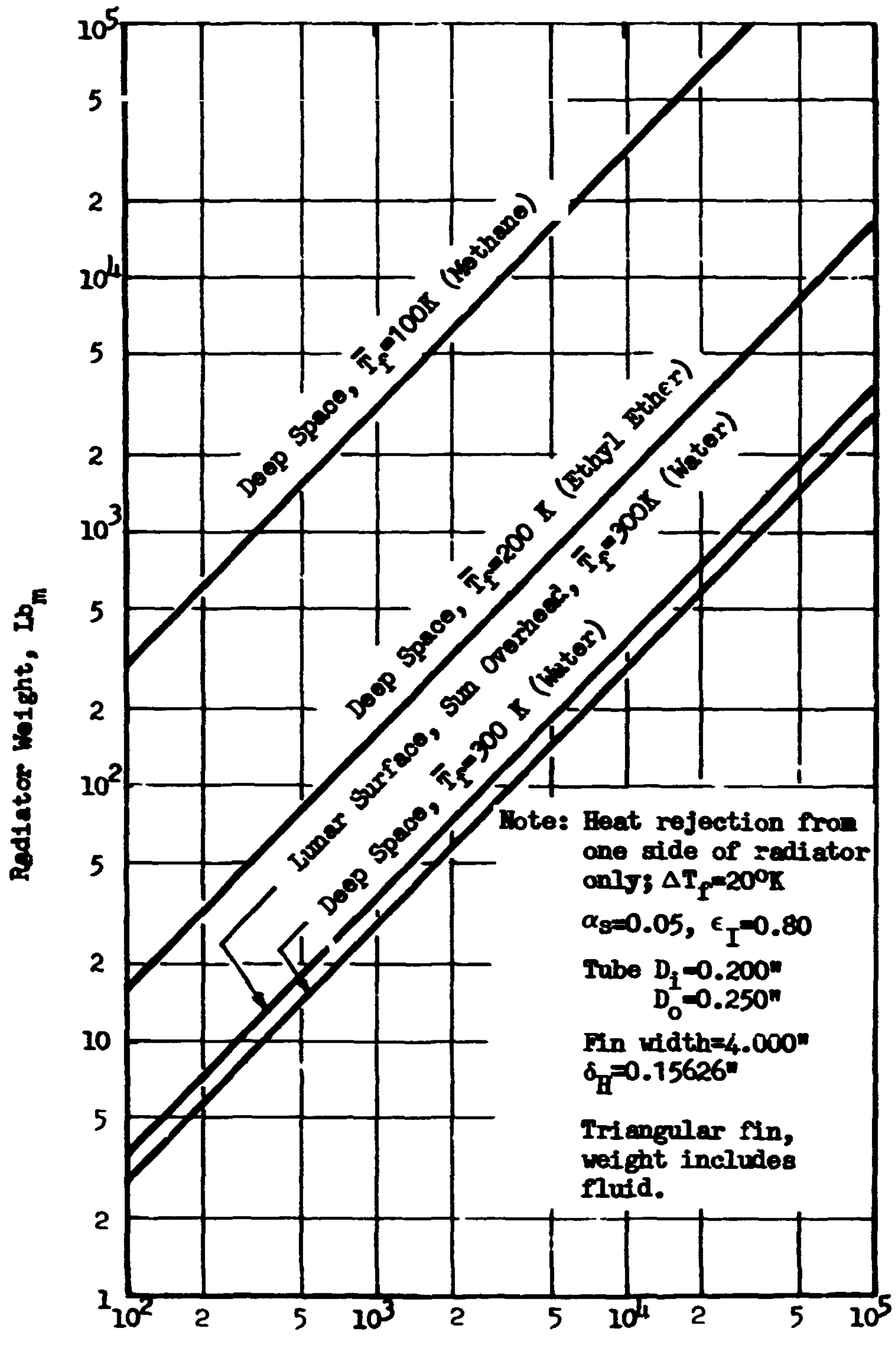

Figure 7-9 Radiator Weight for Deep Space and Lunar Surface Operation

where

T_E = temperature at evaporator end of heat pipe array, ^oK

R_{EC} = thermal resistance between evaporator and condenser, ^oK/watt

q = total rate of heat rejection, watts

N = number of heat pipes connected in parallel

The values of R_{EC} and the maximum value of heat flux per pipe, q/N, are evaluated using heat flux limits based on either the heat pipe evaporator heat flux limit or the capillary pumping limit. The overall thermal resistance between the evaporator and condenser is equal to the sum of the evaporator and condenser resistances, $R_{EC} = R_E + R_C$. The evaporator resistance is given by

$$R_E = \frac{t_e}{K_m A_e}$$

For homogeneous wicks, in heat pipes containing little or no excess fluid and having equal evaporator and condenser areas, $R_C \cong R_E$. However, in heat pipes having an excess fluid charge, the liquid layer thickness in the condenser may be up to twice that in the evaporator. Thus, in general

$$R_C = \frac{t_c}{K_m A_c}$$

where t_c may be up to twice the value of t_e.

7.4 FLUID CIRCULATION

In order to provide the designer with a complete set of data to evaluate refrigeration systems the weight and power of coolant circulating pumps have been included. The weight and power as a function of flow rate is shown in Figs. 7-11 and 7-12, respectively. These data are estimates based on data provided in Reference 7-4 by AiResearch for a small thermal conditioning circulation unit. The electric motor weight was based on a brushless D.C. unit running at 6000 RPM. The fluid circulated is water. A check for different fluids did not significantly influence the weights of the motor and pumps. For example if ethyl ether at a density of 45 lb/ft^3 were circulated instead

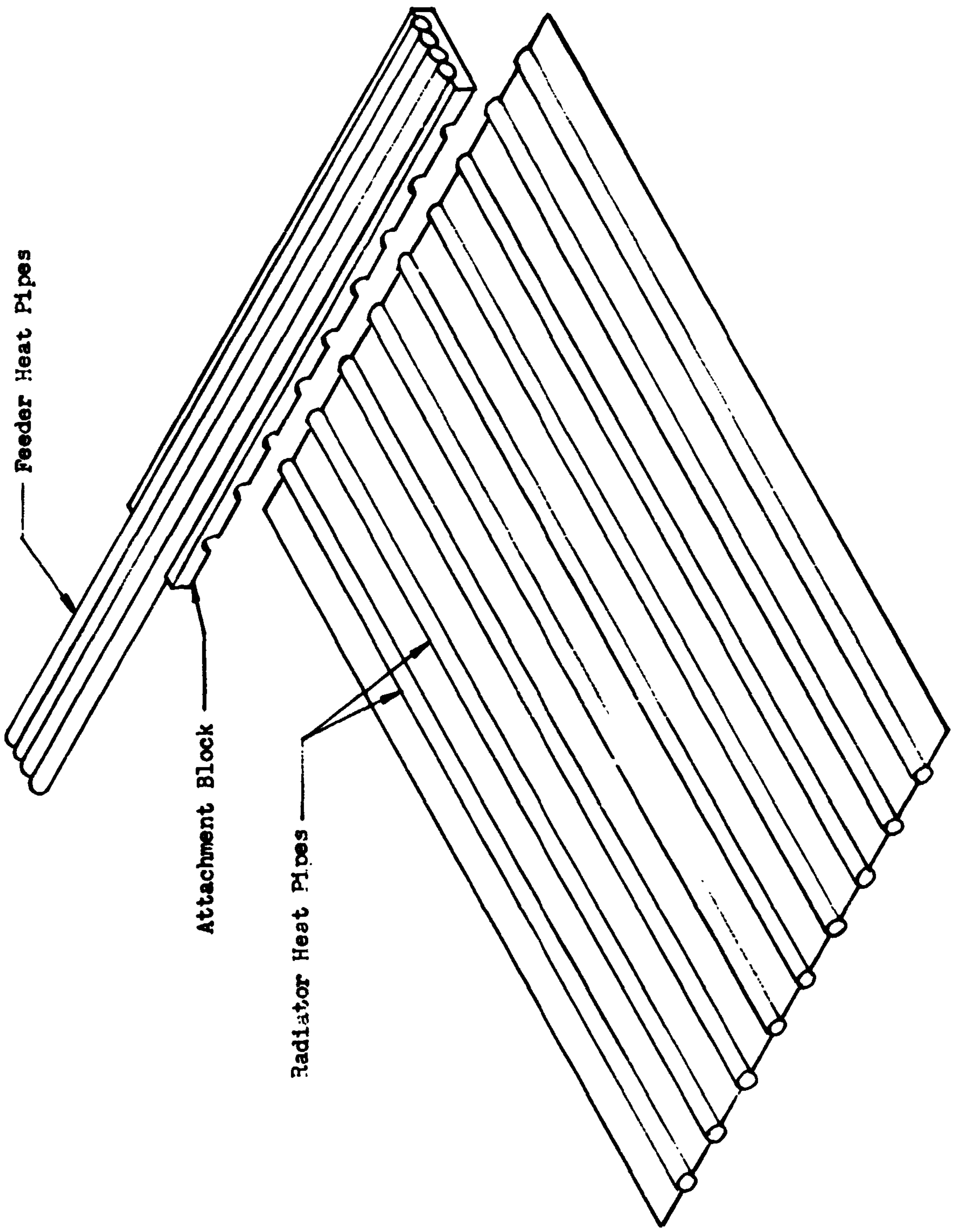

Figure 7-10 Rectangular Fin Radiator with Integral Heat Pipes

of water at a density of 62.4 lb/ft^3 the weight for a flow rate of 0.5 lb/sec and a pressure rise of 10 psi would increase to 6 lb from 5.75 lb for a water system. However, the power required should be proportionately increased by the ratio of the density of water to the density of the fluid to be circulated. The efficiencies of the pump and electric motor were assumed to be 0.80 and 0.85 respectively. The minimum weight of the case and supporting hardware was assumed to be 3.0 pounds.

7.5 HEAT PIPE DESIGN

The heat pipe is a self-contained passive device with an effective thermal conductance greater than that afforded by any solid material. The heat pipe is simply a closed, elongated tube containing a fluid, generally at low pressure, and a wicking material distributed along the inside of the tube. Heat is transferred from one end of the pipe to the other by continuous evaporation of the fluid at the hot end of the pipe and condensation at the cold end. Vapor flows from the hot end to the cold end as a result of the difference in vapor pressure between the two ends of the pipe; liquid condensed at the cold end is returned to the hot (evaporator) end as a result of capillary pressure developed within the wicking material. The heat pipe has been well established as a reliable device for long-life heat transport.

The normal operating range for a heat pipe fluid is between its triple point temperature and its critical temperature. Figure 7-13 shows the vapor pressure versus temperature for several liquids over a wide range of temperatures.

Previous investigations have shown that there are three major limitations on heat pipe operation. These limitations are: the wicking limit; the boilout limit; and the vapor choking limit.

The wicking limit is defined as that point at which the working liquid can no longer reach the evaporator through the wick in sufficient quantity to keep up with the required evaporation rate.

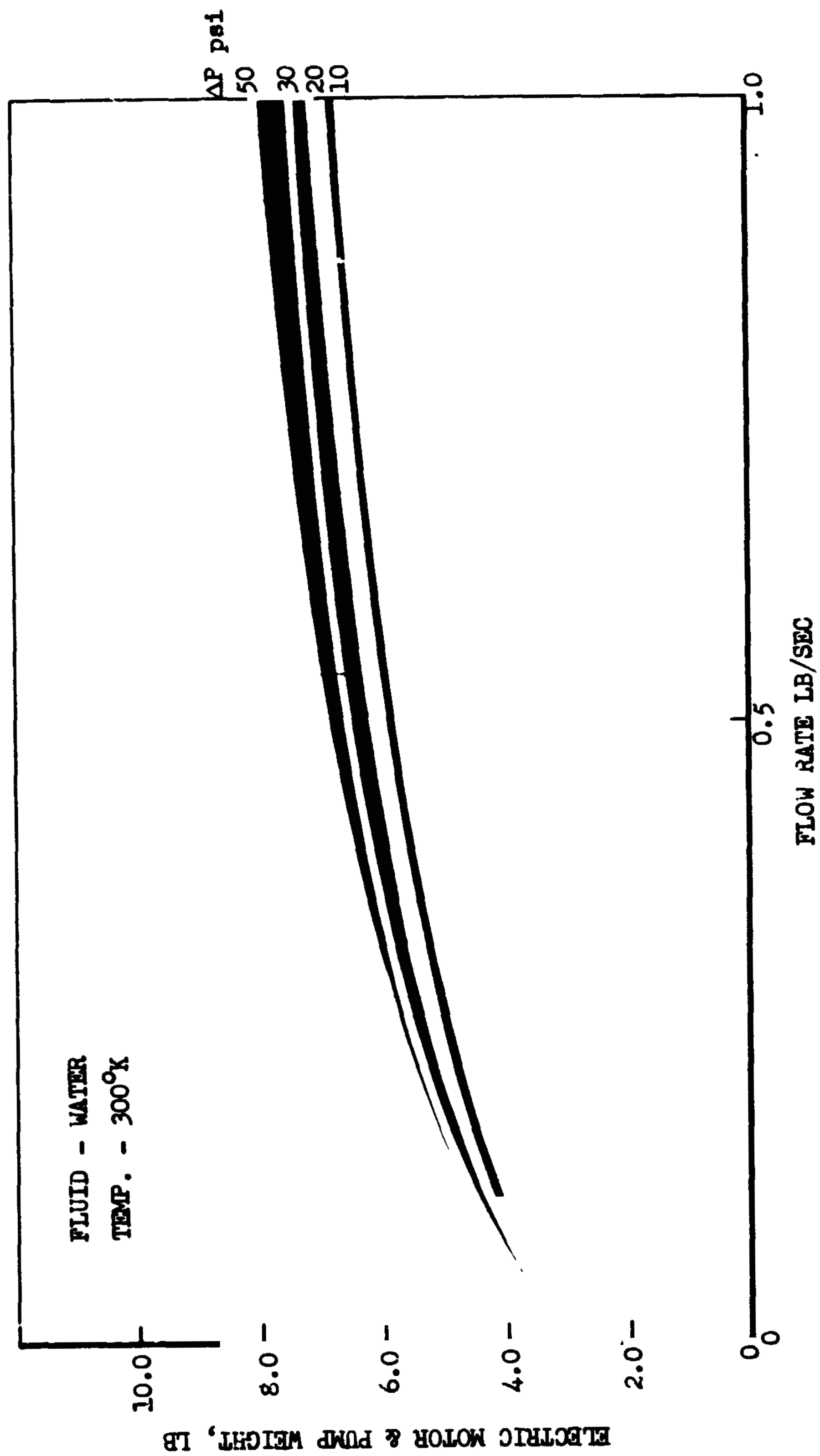

Figure 7-11 Weight of Circulation Pump and Motor

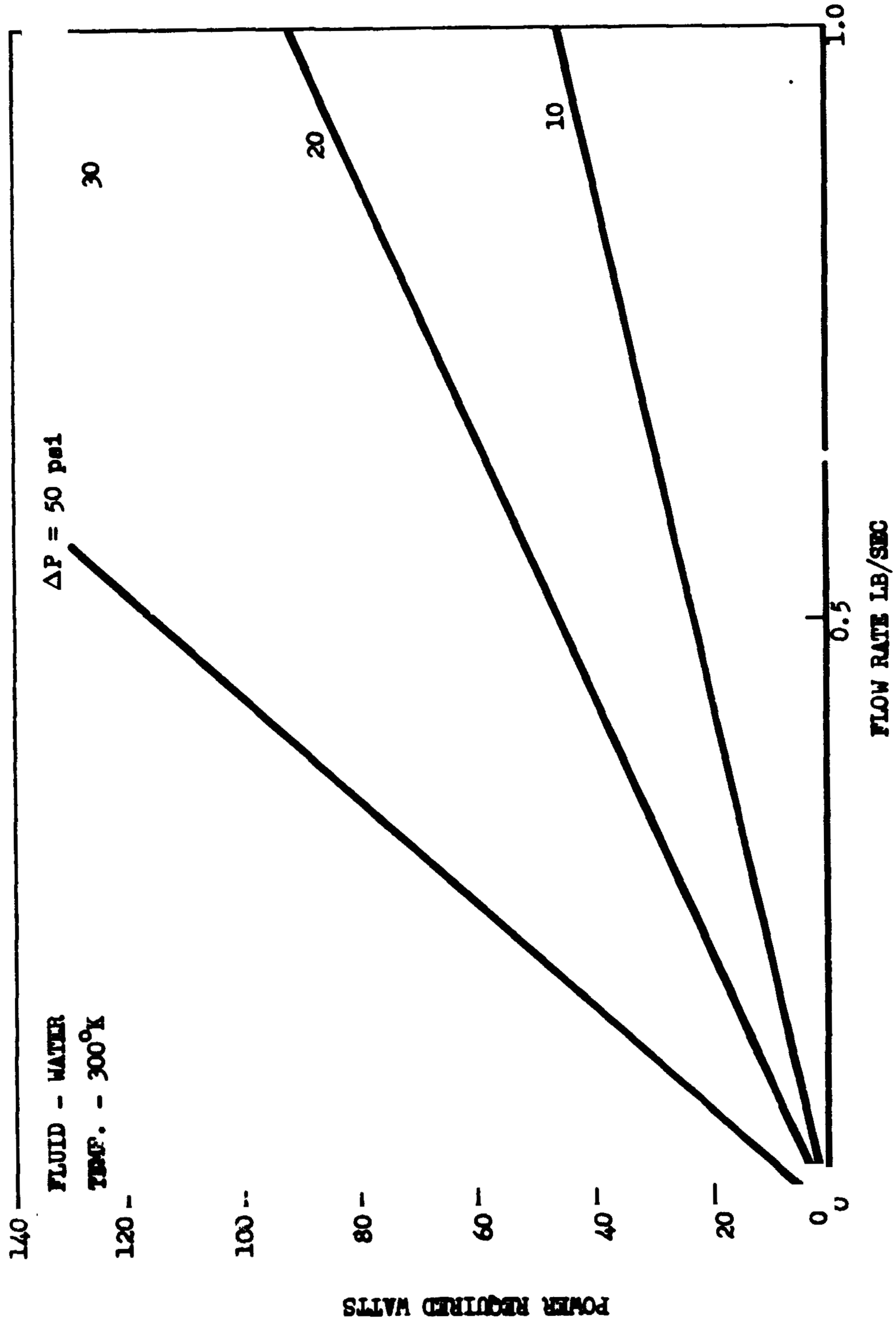

Figure 7-12 Power Required for Circulation Pump

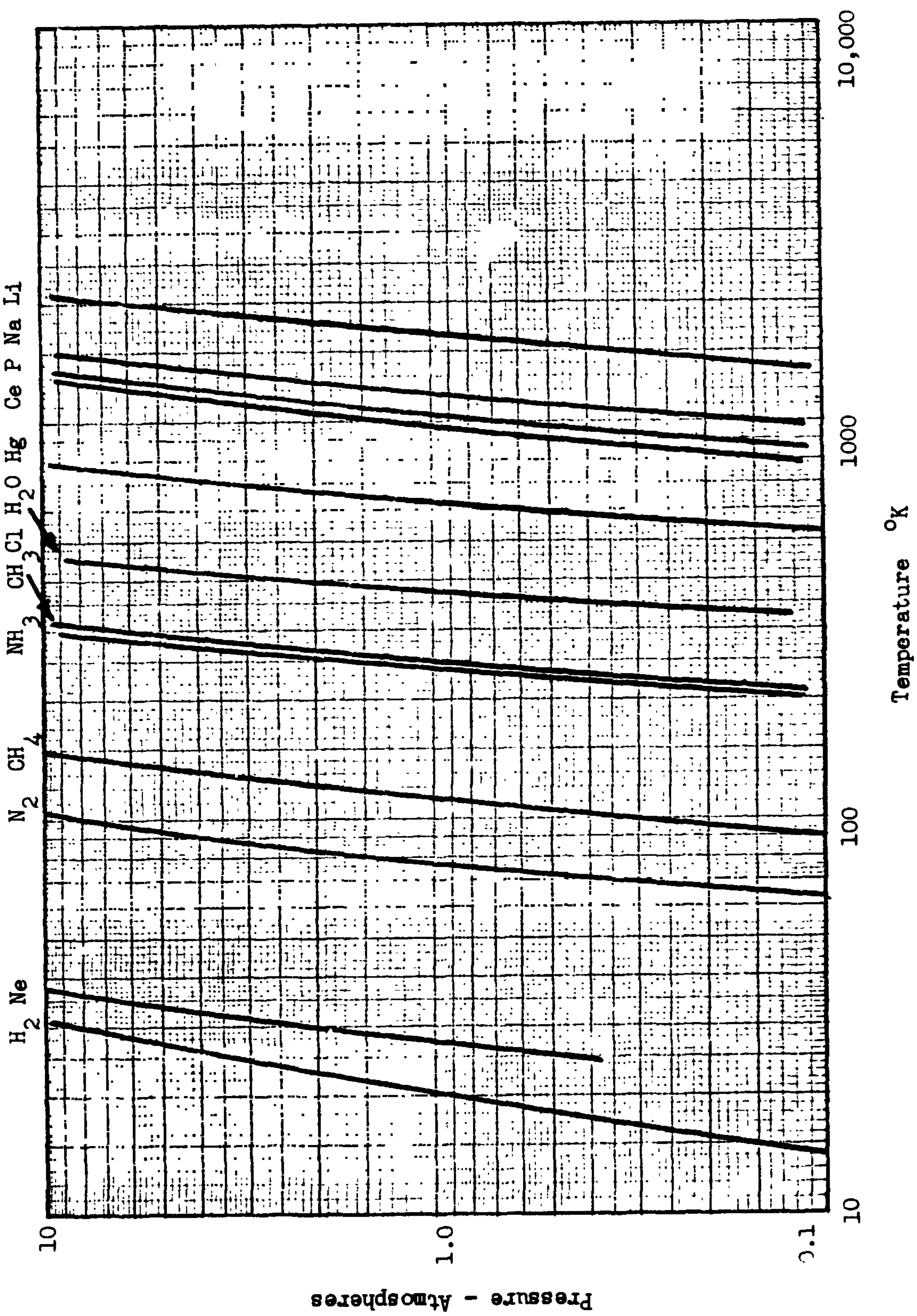

Figure 7-13 Vapor Pressure vs Temperature for Various Liquids

Cotter (Ref. 7-10) showed that in a zero-gravity field the maximum heat transfer rate for a cylindrical heat pipe with a homogeneous wick is given as:

$$Q_e = \frac{2\pi\sigma\lambda R_c \cos\theta}{(\ell + \ell_a)} \left[\frac{4 \nu_v R_c^2}{\rho_v R_v^4} + \frac{b \nu_\ell}{2\rho_\ell \epsilon (R_w^2 - R_v^2)} \right]$$

where the dimensions are shown in Fig. 7-14. This equation may be optimized with respect to the capillary radius R_c and the wick and vapor core radii R_w and R_v. Following the procedure, it is found that maximum heat flux is obtained when $R_v/R_w = \sqrt{2/3}$

To maximize Q_e with respect to the **wicking limit,** it is desirable to have a large value of $G_1 = \frac{\sigma\lambda}{\sqrt{\nu_v \nu_\ell}}$. Figure 7-15 gives values of G_1 for water and ammonia. Such a comparison is helpful in the initial cryogen selection, but it is not the only criterion to be considered during preliminary design considerations. It is also desirable to maximize the wick property group $\sqrt{\epsilon/b}$, which must be determined experimentally since it is a function not only of the wick material but of geometry as well.

The boilout limit is reached when the liquid in the evaporator vaporizes in the wick structure and forms an insulating vapor film which disrupts liquid flow. The result is a rapidly increasing evaporator temperature with little or no increase in heat transfer rate.

Neal (Ref. 7-11) has determined that the onset of nucleation, which limits the maximum radial heat flux, is proportional to the fluid property group

$$G_2 = \frac{\sigma K_\ell T_s}{\lambda \rho_v}$$

Values of G_2 are also plotted in Fig. 7-15 for water and ammonia. It is desirable to select a fluid with large values of this parameter. This selection must be made with due consideration given to providing satisfactory values of G_1.

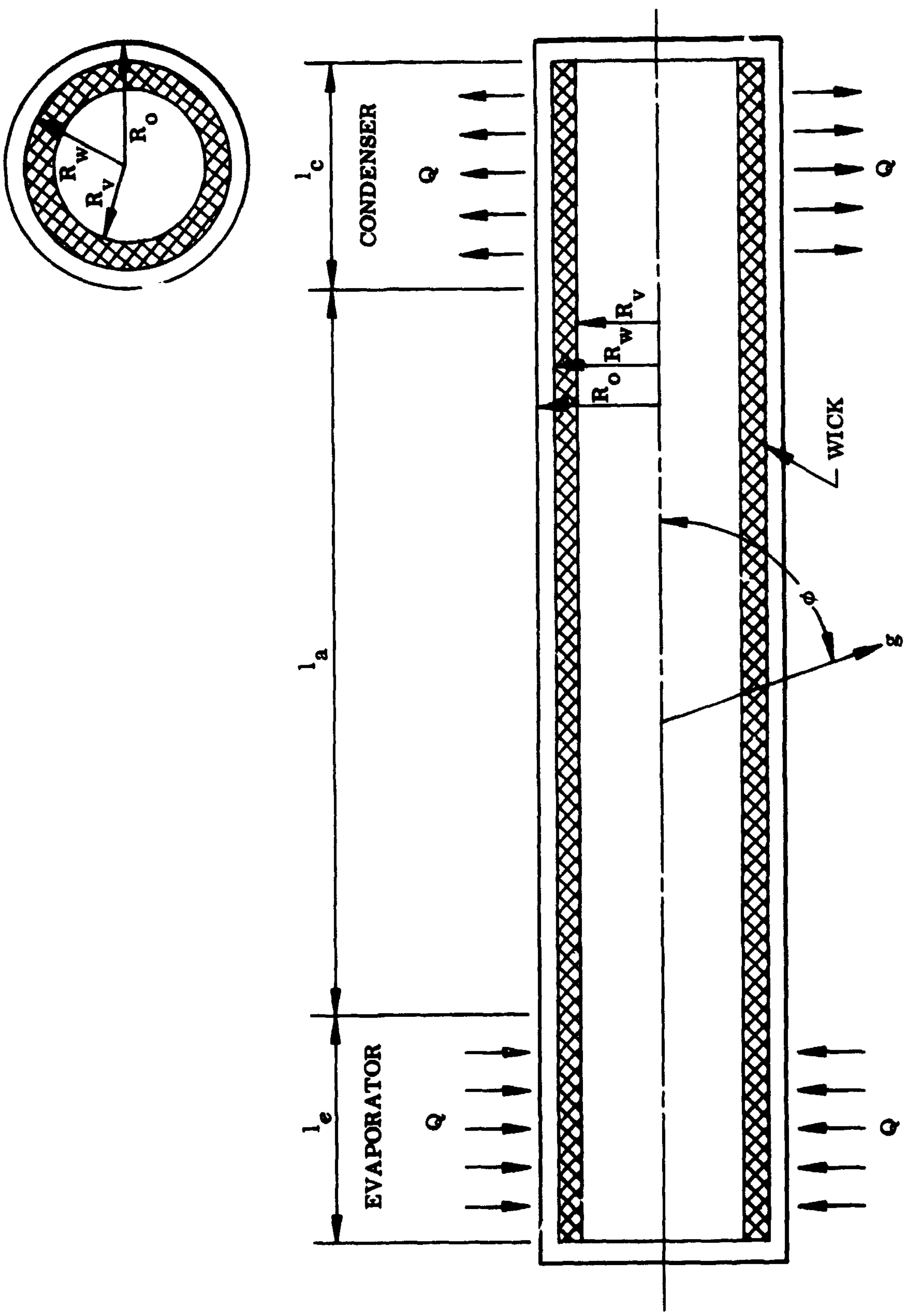

Figure 7-14 Heat Pipe Schematic

The third heat pipe performance limit is that due to choking of the vapor flowing from the evaporator to the condenser. Levy (Ref. 7-12) has predicted that at low vapor pressures, such as operation near the triple point temperature, the vapor flow can reach sonic velocities and thus prevent an increase in the heat transfer rate. He showed that the choking limit is given by:

$$Q_{e_{max}} = \frac{\rho_v \lambda V_a \pi R_v^2}{\sqrt{2(\gamma + 1)}}$$

where

$$V_a = \sqrt{\gamma g_o RT}$$

Q is a function of a fluid property group ($\rho_v \lambda \sqrt{g_o RT}$) and the dimensions of the heat pipe. This fluid property group, designated G_3, can be used in optimizing the fluid to be used in the heat pipe and is plotted on Fig. 7-15.

Predictions of maximum liquid flow rate capability are based on analytical characterizations of the various pressure drops and losses in the heat pipe system. A schematic representation of the sources of these pressure drops is shown in Fig. 7-16. During evaporation the vapor pressure decreases in the axial flow direction as mass is added to the vapor stream. An additional slight drop in pressure is observed in the adiabatic section due to wall friction. In the condenser section the pressure increases in the direction of fluid motion due to partial dynamic recovery of the decelerating flow. The liquid condensate is then pumped back to the evaporator by means of the induced capillary driving pressure. The liquid pressure drop in the wick structure is due to internal friction between the fluid and the porous wick material.

For low temperature heat pipes the net vapor pressure loss is very small and may be neglected. Thus the fluid circulation rate is essentially fixed by a balance between the liquid pressure loss flowing in the wick structure and the available capillary pumping pressure. The maximum capillary pumping pressure, Δp_c, is expressed as follows:

$$\Delta p_c \Big|_{max} = \frac{\sigma}{R_c} \Phi$$

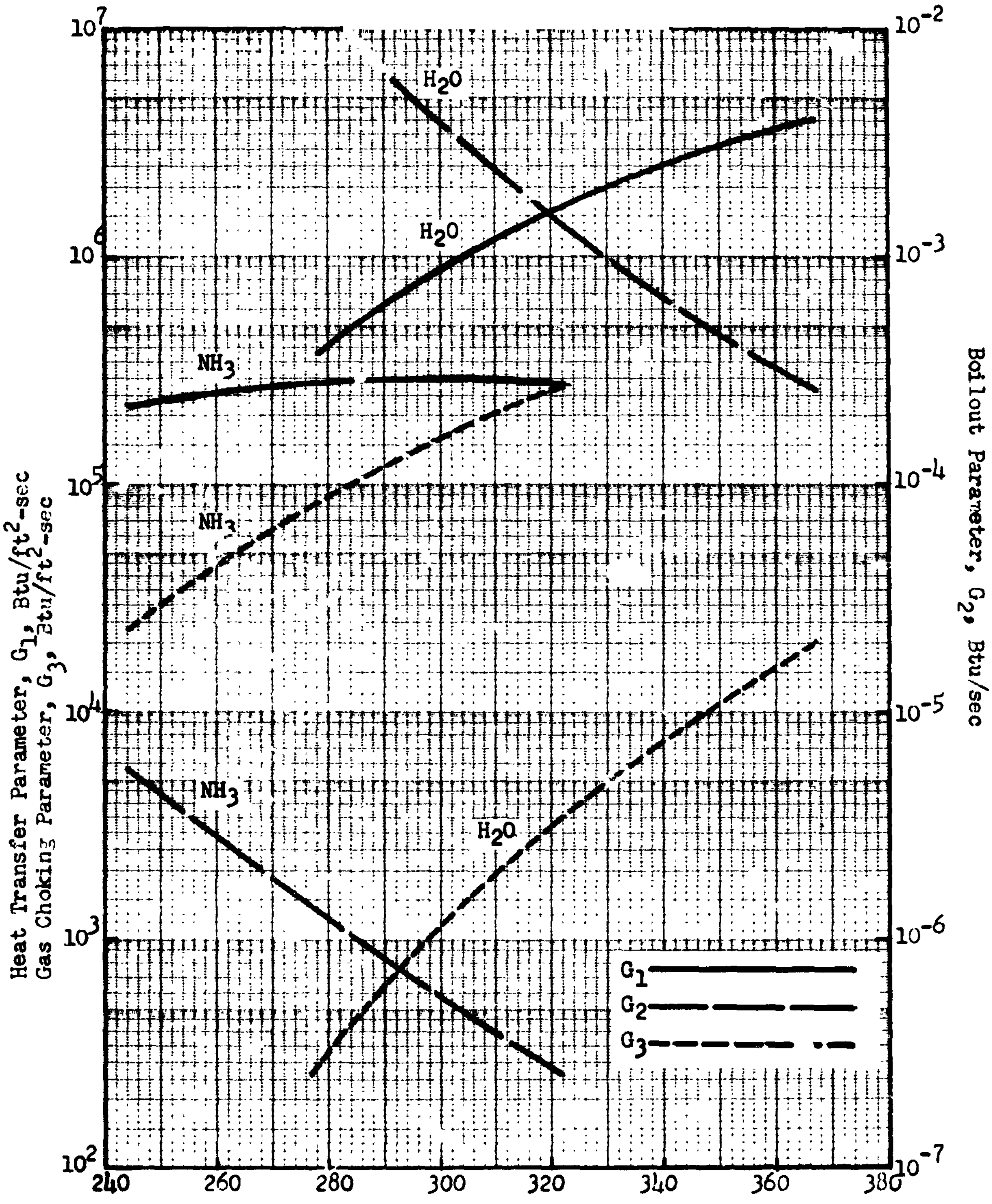

Figure 7-15 Fluid Property Groups at Moderate Temperatures

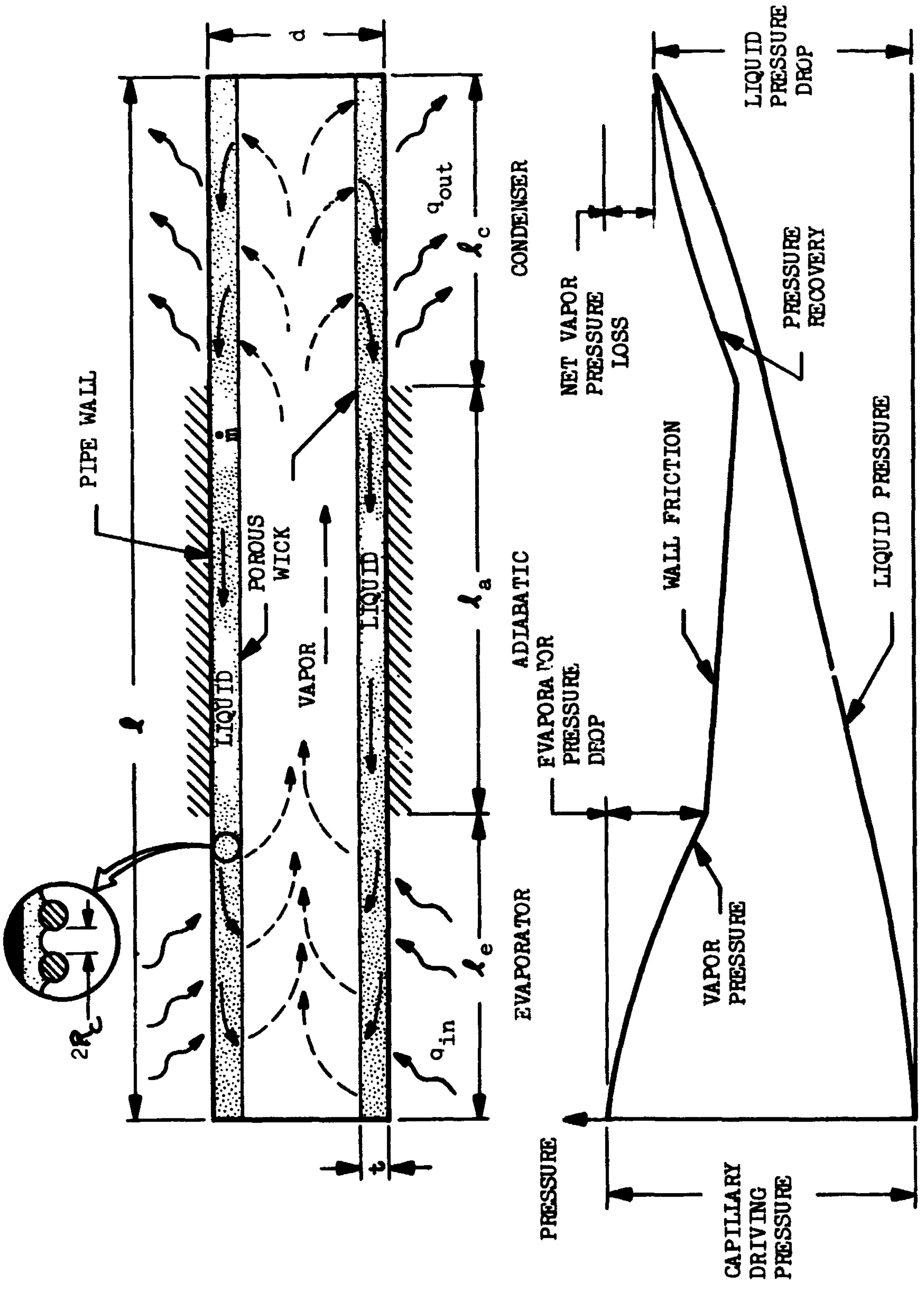

Figure 7-16 Heat pipe Schematic and Pressure Diagram

where R_c is the radius of holes in the wick (or $\frac{1}{2}$ hole size in a square weave mesh)

σ is the working fluid surface tension.

The quantity Φ is an empirical constant related to the meniscus shape in the pores of the wick. Hollister, (Ref. 7-15) determined values for Φ a number of liquid and solid capillary systems. For conservatism a value of $\Phi = 1.5$ is recommended in this regard.

The liquid pressure loss due to flow through a wick structure is highly dependent on the wick geometry from the standpoint of both its gross dimensions and configuration and the flow geometry within the wick structure. Expressions for pressure loss due to liquid flow within a wick structure are usually based on Darcy's Law or the Blake-Kozeny equation for flow in porous media and packed beds. Darcy's law is

$$\Delta P_L = \frac{\dot{m} \, \nu_L \ell}{A_w K_p}$$

This expression shows that wick pressure loss is minimized for maximum wick permeability values. Sample values of wick permeability, K_p, are listed in Table 7-2.

7.5.1 Size and Weight

The size and weight of a heat pipe are dependent on a combination of design factors.

V 'ues of $Q_{e_{max}}$ $(\ell + \ell_a)$ have been calculated for a zero-g heat pipe. These values are plotted in Fig. 7-17 for two fluids, water and ammonia, operating at 300°K. The wick parameters $\epsilon = 0.8$ and $b = 20$ were used in obtaining the results plotted in Fig. 7-23 (a typical value for K is about 1.5).

Corresponding values of heat pipe weight are plotted in Figure 7-18.

7.5.2 Design Procedure for Optimized Homogeneous Wick Heat Pipes

In the following, it is assumed that the required maximum heat flux, Q_e, the adiabatic length, ℓ_a and the nominal operating temperature are given. The heat pipe design procedure is then expressed in stepwise fashion below.

Table 7-2
WICK PERMEABILITY VALUES

Wick	K_p (Ft^2)	Source	
100 mesh screen (more than 3 layers)	0.16×10^{-8}	Kunz, et al	(Ref. 7-13)
200 mesh screen (more than 3 layers)	0.08×10^{-8}	Kunz, et al	
200 mesh screen			
o 1 layer, flat meniscus shapes	0.059×10^{-8}	Phillips	(Ref. 7-14)
o 1 layer, moderately curved meniscus shapes	0.04×10^{-8}	Phillips	
o 1 layer, highly curved meniscus shapes	0.014×10^{-8}	Phillips	
o 2 layers, flat meniscus shapes	0.062×10^{-8}	Phillips	
o 2 layers, curved meniscus shapes	0.045×10^{-8}	Phillips	
Nickle Foam porosity 0.9	2.5×10^{-3}	Phillips	
Felt Metal			
o porosity 0.9	0.5×10^{-8}	Phillips	
o porosity 0.8	0.05×10^{-8}	Kunz, et al	
o porosity 0.7	0.016×10^{-8}	Kunz, et al	

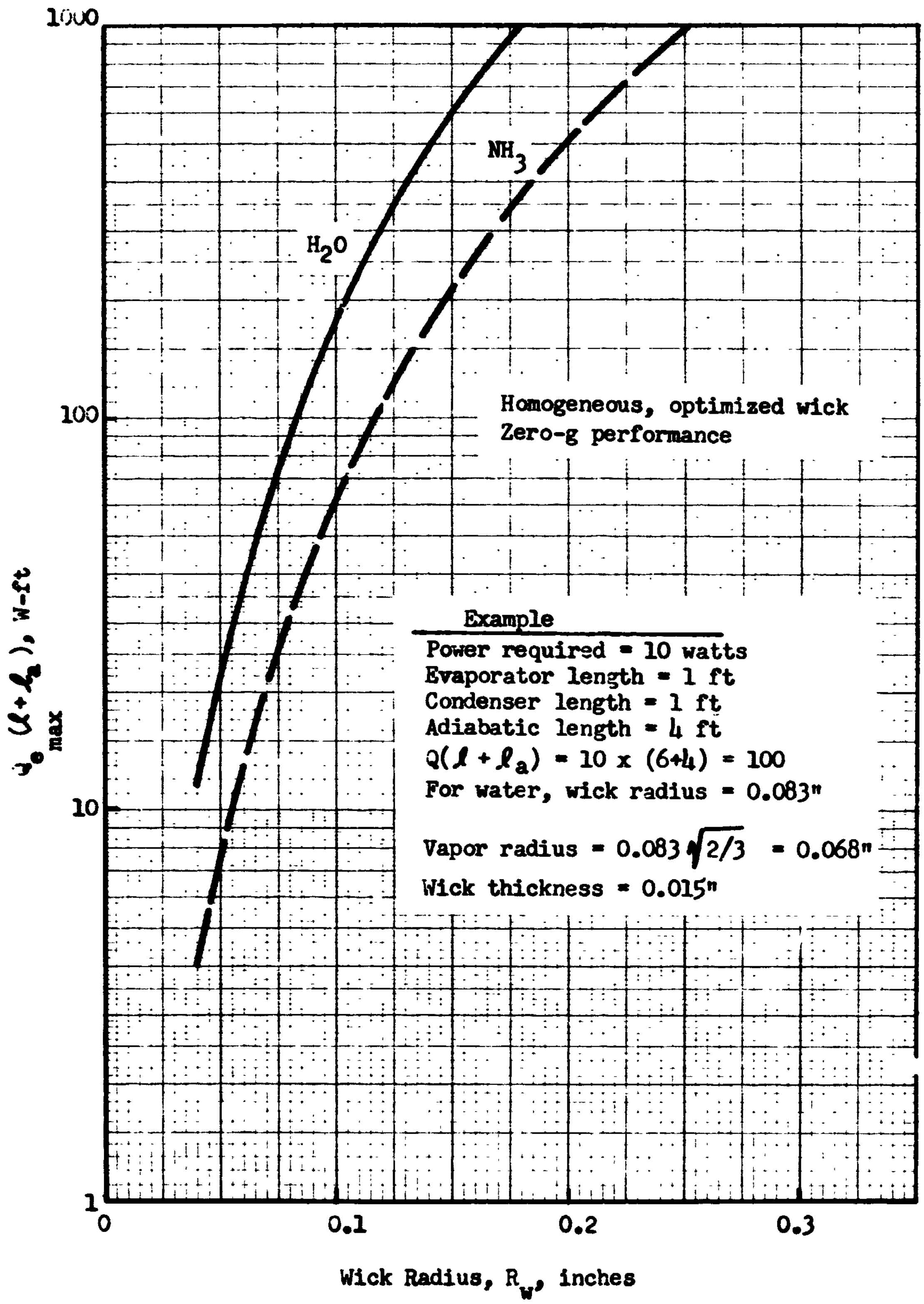

Figure 7-17 Heat Pipe Performance for Moderate Temperatures

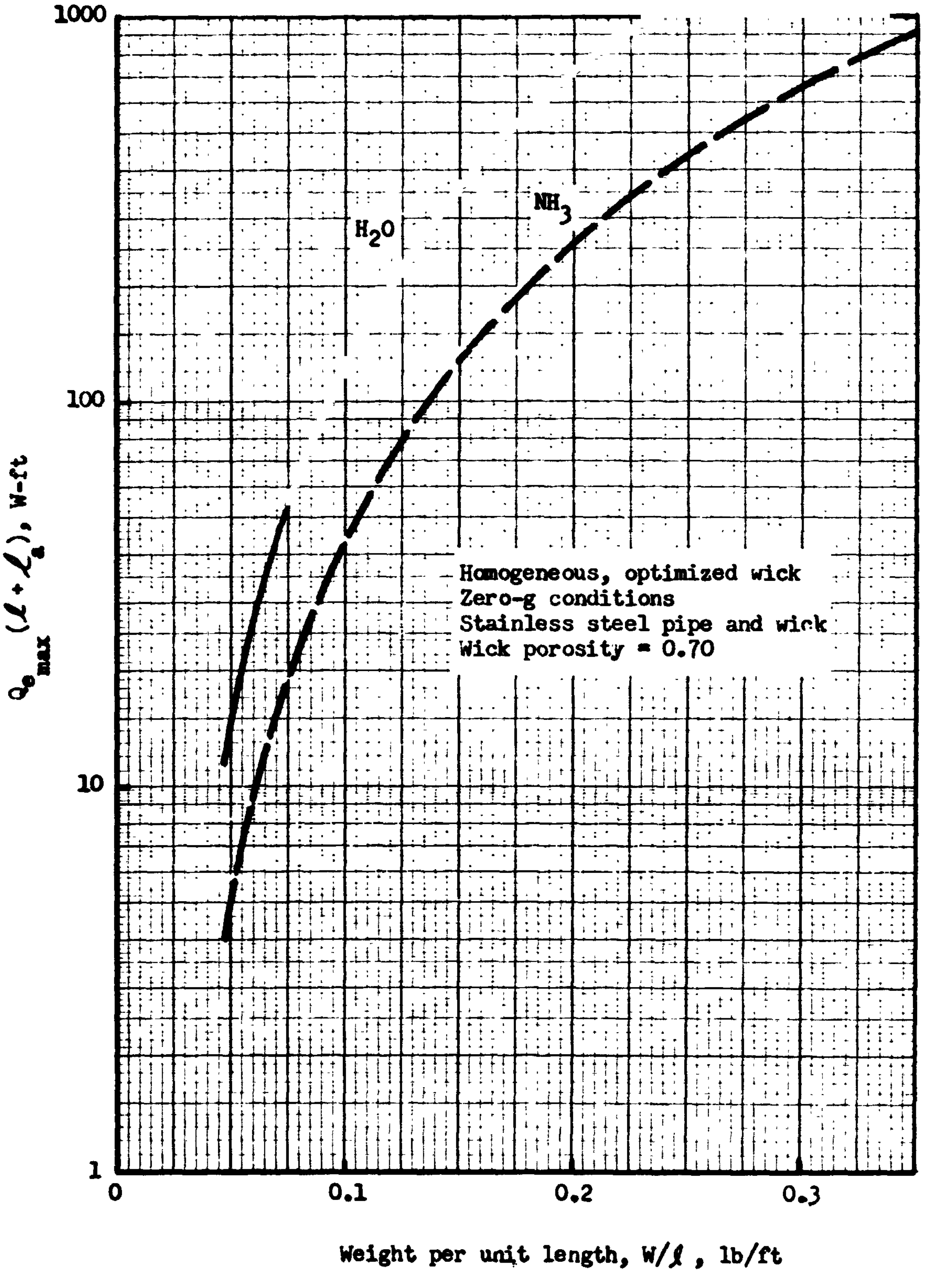

Figure 7-18 Weight of Moderate Temperature Heat Pipes

1. Select a fluid from Fig. 7-19 for the given operating temperature.
2. Select a wick material and assume a value of wick thickness, t.
   Look up wick permeability, K_p and poré radius, R_c.
3. Compute the mean fluid-wick conductivity,

$$K_m = \frac{K_s}{1 + \epsilon\left(\frac{K_s}{K_\ell} - 1\right)}$$

4. Look up the value of ΔT_{max} for the selected fluid from Fig. 7-20.
5. Compute the minimum allowable evaporator area from equation 7-44:

$$A_{e_{min}} = \frac{Q_e\, t}{K_m \Delta T_{max}}$$

6. Compute the required length of the evaporator section from

$$\ell e = \frac{A_{e_{min}}}{2\pi R_w}$$

7. Compute overall heat pipe length assuming equal evaporator and condenser lengths:

$$\ell = 2\ell_e + \ell_a$$

8. Look up the optimum wick radius, R_w, from Fig. 7-17.
9. Compute wick thickness for the optimized wick:

$$t = R_w - R_v = 0.1835\, R_w$$

10. Using this value of t repeat steps 5 through 10 until consistent values are obtained.
11. Compute wick cross-sectional area from

$$A_w = \frac{\pi}{3}\, R_w^{\;2}$$

12. Look up values for liquid heat of vaporization, λ, kinematic viscosity, ν_ℓ, and surface tension, σ .

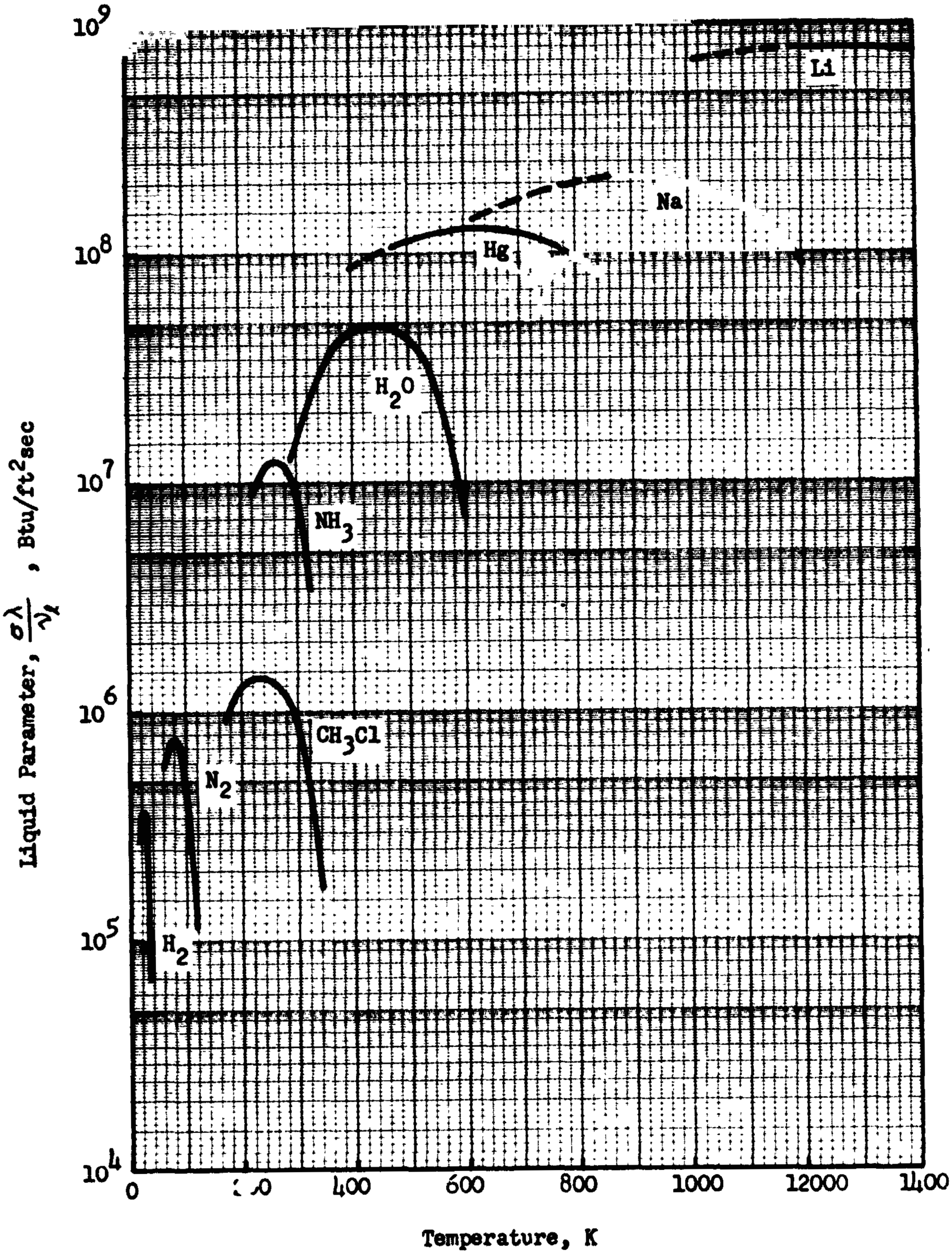

Figure 7-19 Liquid Parameter for Various Liquids

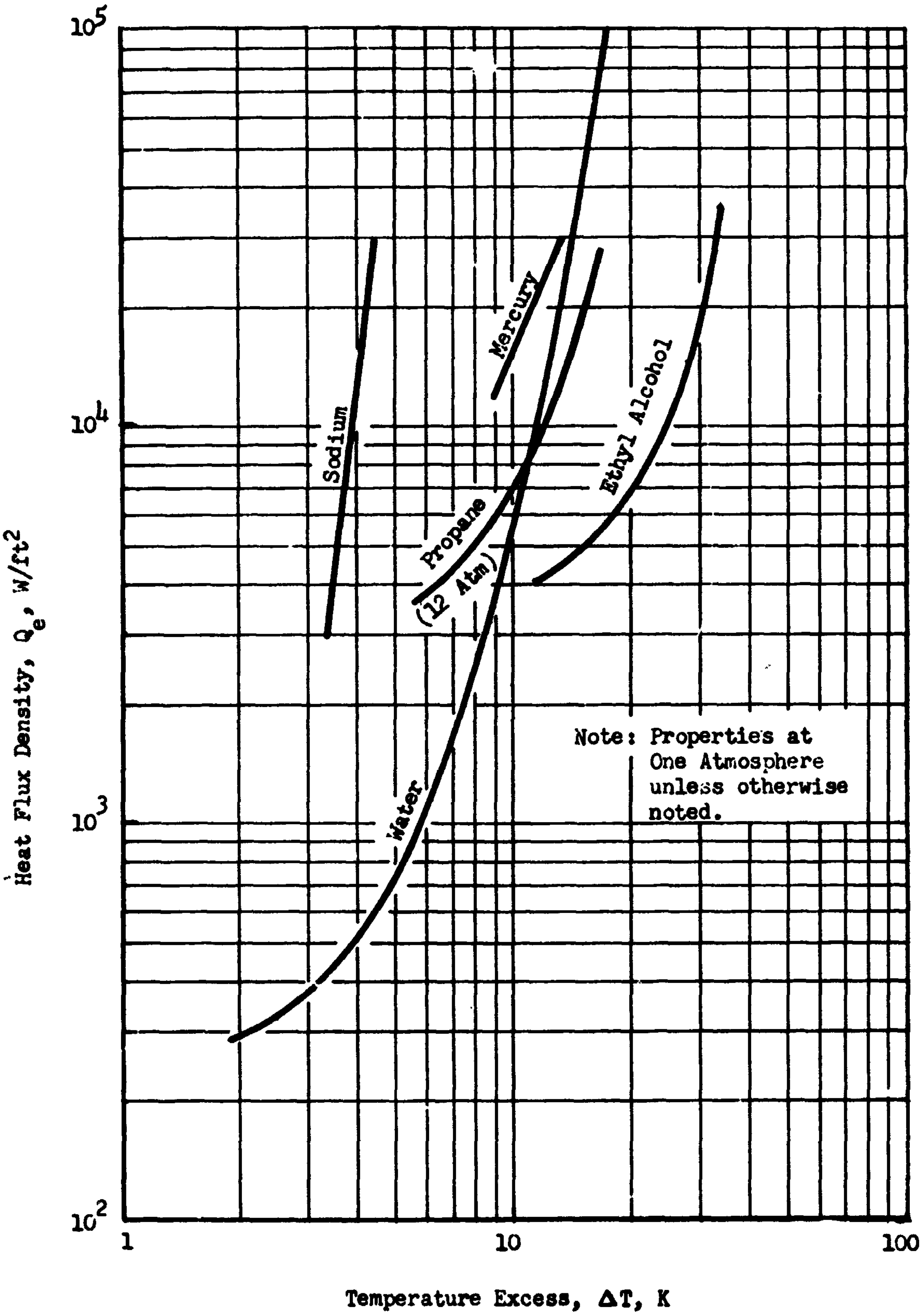

Figure 7-20 Nucleate Boiling Heat Fluxes for Moderate and High Temperature Fluids

13. Compute maximum liquid flowrate from

$$\dot{m}_{max} = \frac{Q_e}{\lambda}$$

14. Compute wick pressure drop from.

$$\Delta p_{L_{max}} = \frac{\dot{m}_{max} \nu_\ell \ell}{A_w K_p}$$

15. Compute capillary pumping Δp from

$$\Delta p_c = 1.5 \frac{\sigma}{R_c}$$

16. If $\Delta p_{L_{max}} > \Delta p_c$ select a new wick material having a higher permeability and/or a smaller capillary radius and repeat steps 13 and 14. Check that the mean conductivity for the new wick is not significantly different from that computed in step 3. If the new K_m is significantly smaller it will be necessary to repeat steps 4 through 16.

REFERENCES

7-1 Mackay, D. B., "Design of Space Power Plants," Prentice-Hall, Inc., Englewood Cliffs, N.J., 1963

7-2 McAdams, W. H., "Heat Transmission," 3rd ed., McGraw-Hill Co., Inc., New York, 1954

7-3 Sparrow, E. M., and Eckert, E. R. G., "Radiant Interaction Between Fin and Base Surface," A.S.M.E. J. Ht. Trans., V 84C, 1962, p. 12

7-4 Liquid Propellant Thermal Conditioning Unit - Interim Report, October 12, 1966, Airesearch Manufacturing Div., The Garrett Corp.

7-5 Lockheed Missiles & Space Company, "Heat Pipes for Active Thermal Control of Spacecraft, Report for 1969 Independent Development Program," LMSC/A965174, 13 February 1970

7-6 R. C. Turner, "The Constant Temperature Heat Pipe - A Unique Device for the Thermal Control of Spacecraft Components," AIAA Paper No. 69-632

7-7 H. C. Haller, S. Lieblein and B. G. Lindlow, "Analysis and Evaluation of a Vapor-Chamber Fin-Tube Radiator for High Power Rankine Cycles," NASA TN D-2836.

7-8 R. C. Turner and W. E. Harbaugh, "Design of a 50,000-Watt Heat-Pipe Space Radiator," ASME Aviation & Space Conference, Beverly Hills, California, June 1968

7-9 J. D. Hinderman, J. Madsen and E. D. Waters, "An ATS-E Solar Cell Space Radiator Utilizing Heat Pipes," AIAA Paper No. 69-630

7-10 Cotter, T. P., Theory of Heat Pipes, Los Alamos Scientific Laboratory Report No. LA-3246-MS, March 26, 1965

7-11 Neal, L. G., "An Analytical and Experimental Study of Heat Pipes," Report No. 99900-6114-R000, TRW Systems, Redondo Beach, California, June 1967

7-12 Levy, E. K., "Theoretical Investigation of Heat Pipes Operating at Low Vapor Pressures," Proceedings of ASME Aviation and Space Conference, PP 671-676, June 1968

7-13 Kunz, H. R., Langston, L. S., Hilton, B. H., Wyde, S. S., and Nashick, G. H., Vapor Chamber Fin Studies - Transport Properties and Boiling Characteristics of Wicks. NASA CR-812

7-14 Phillips, E. C., "Low Temperature Research Program" NASA CR 66792, June 1969

REFERENCES (Cont.)

7-15 Hollister, M. P., "Propellant Containment Utilizing Screen Mesh and Perforated Plate Surfaces," LMSC A665481, December 29, 1964

NOMENCLATURE

A - Area

A_w - Wick cross-sectional area

a - Land width divided by half the channel width

b - Geometric constant for homogeneous wicks, $b = 10$ to 20

C_{p_f} - Fluid specific heat

D - Diameter

F_R - Radiant interchange factor

g - Acceleration

G_A, G_E, G_H, G_P - Environmental Parameters

g_o - Gravitational constant

h - Heat transfer coefficient

k - Channel wick shape factor

K - Constant, thermal conductivity

K_ℓ - Thermal conductivity of liquid

K_m - Thermal conductivity of wick-liquid matrix

K_s - Thermal conductivity of solid wick material

K_p - Permeability

L_d - Width of fluid duct

L_e - Effective width of radiator

ℓ - Total length of heat pipe, $\ell_e + \ell_a + \ell_c$

ℓ_a gth of adiabatic section

$\dot{m}$ - Mass flow rate

P - Pressure, fin profile number

P_r - Reduced Pressure

P_c - Critical Pressure

P_r - Prandtl number

NOMENCLATURE (Cont.)

p	-	Perimeter of fluid passageway
Q_e	-	Axial heat transfer rate
q	-	Net rate of heat transfer
R	-	Gas Constant
R_c	-	Capillary radius
R_e	-	Reynold's number
R_o	-	Pipe outside radius
R_w	-	Outer wick radius
R_v	-	Vapor core radius
t	-	Wick thickness
t_c	-	Wick thickness in condenser section
t_e	-	Wick thickness in evaporator section
T	-	Temperature
T_c	-	Critical Temperature
T_F	-	Fluid Temperature
T_r	-	Reduced Temperature
T_s	-	Saturation Temperature
T_w	-	Wall temperature
V_a	-	Sonic velocity
V_ℓ	-	Volume of liquid in saturated wick
V_{tot}	-	Total open volume of heat pipe
$\dot{w}_F$	-	Rate of fluid flow in radiator duct
z	-	Vertical height in an acceleration field
Z	-	Compressibility factor, Ratio of fin root temperature at radiator outlet to that at inlet
α	-	Solar absorptance

NOMENCLATURE (Cont.)

β	-	Angle between orbit plane and planet-sun line
δ	-	Fin thickness
ϵ	-	Infrared emittance, porosity of wick
σ	-	Surface tension, Stefan-Boltzmann constant
λ	-	Heat of vaporization
μ_v	-	Vapor viscosity
μ_ℓ	-	Liquid viscosity
ρ_v	-	Vapor density
ρ_ℓ	-	Liquid density
ρ_s	-	Wick material density
ρ_w	-	Pipe wall density
ν_V	-	Vapor kinematic viscosity
ν_ℓ	-	Liquid kinematic viscosity
θ	-	Liquid-solid contact angle, orbit position angle
γ	-	Specific weight, ratio of specific heats
ψ_H	-	Heat Transfer Parameter
ϕ_F	-	Film Resistance number
ϕ_R	-	Radiation number
Ω_1	-	Fin effectiveness at fluid inlet
Ω_2	-	Fin effectiveness at fluid outlet

Section 8
HEAT ABSORPTION

8.1 INTRODUCTION

The material in this section has been prepared in order to provide the engineer with data and methods to quickly take into account the weight and performance of the devices required to transfer the heat from the cryogenic tank to the refrigerator. Many methods are possible to conduct the heat from the tank to the refrigerator and a few of them have been selected on which to provide data. Material is given in this section for on-tank heat exchangers, helium circulation devices, cryogenic heat pipes, and solid conduction devices. It is felt that a broad enough spectrum is covered by these devices that the engineer should be able to obtain a representative weight and performance estimate for nearly any space application that he may choose to analyze.

8.2 TANK WALL HEAT EXCHANGERS

A sketch of a typical heat exchanger installation is shown in Figure 8-1. It is assumed that the cold side fluid is helium at about 25 atmospheres pressure. The helium is pumped through a spiral wound tube which is fastened to the tank wall. It is assumed further that the cryogenic tank experiences an acceleration sufficient to mix the cryogenic liquid by natural convection, or that an internal mixer is provided as shown in Figure 8-1. The objective of preliminary design analyses is to find the heat exchanger wall area, the heat exchanger system weight, and the helium gas flowrate $\dot{W}_{He}$ required to maintain a prescribed temperature difference ΔT_{He} between inlet and outlet for a given heat transfer rate q.

8.2.1 Design Procedure

In order to size the heat exchanger wall area, the design equations presented in Section 8.2.1 of the final report can be used. A summary of representative helium properties is given in Table 8-1. The design procedure is outlined in

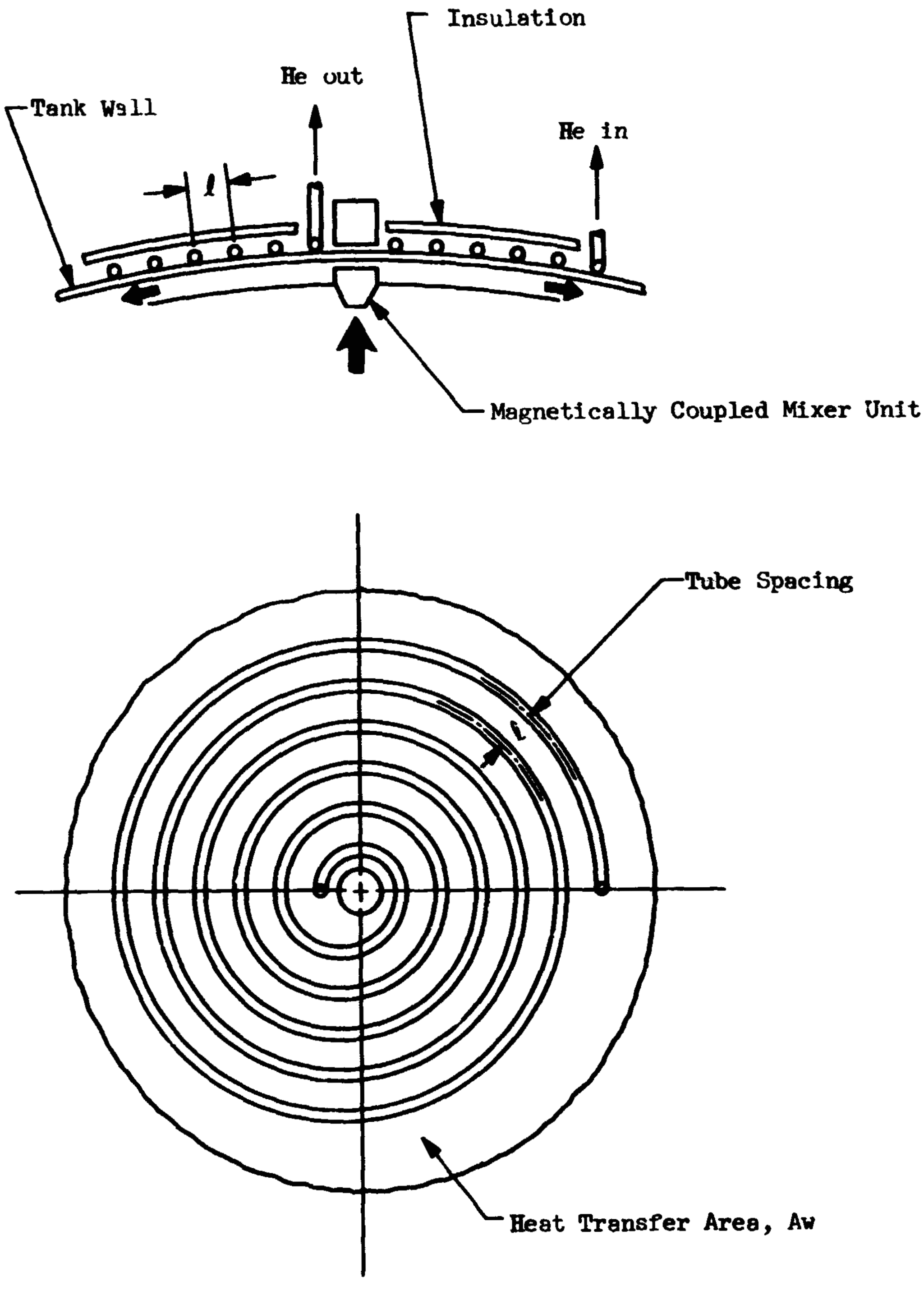

Figure 8-1. Tank Wall Heat Exchanger

stepwise fashion below. It is assumed that the liquid storage temperature, the tank dimensions, the heat absorption rate q, and the helium gas temperature rise through the exchanger ΔT_{He} are all given.

Table 8-1
HELIUM GAS PROPERTIES AT HIGH PRESSURE
(25 Atmospheres)

	T = 20K (36R)	T = 90K (162R)
Density, lbm/ft^3	3.81	0.847
Specific Heat, Btu/lbm R	1.40	1.25
Thermal Conductivity, Btu/Hr ft R	0.016	0.040
Viscosity, lbm/hr ft	0.0087	0.0227
Prandtl Number	0.76	0.71

1. Look up values of helium gas properties from Table 8-1 or Reference 8-3.
2. Compute helium flow rate from the known capacity rate.

$$\dot{W}_{He} = \frac{q}{\Delta T_{He}}$$

3. Select a tubing material and values for tubing dimensions, R, Ro (Fig. 8-3). Look up the thermal conductivity K_T of the tubing material.
4. Use Figure 7-3 to compute the helium gas heat transfer coefficient h_g.
5. Setting ℓ = 2 Ro compute the overall resistance 1/U from

$$\frac{1}{U} = \frac{t_w\left(1 + \dfrac{\ell^2}{12\, t_W^2}\right)}{K_W} + \frac{\ell}{2\left[\sqrt{h_g K_T t_T}\cdot\tanh\sqrt{\dfrac{h_g}{K_T t_T}}\, R\theta + h_g\,(\pi - \theta)R\right]}$$

or, if $\theta < 15^o$,

$$\frac{1}{U} = \frac{t_w}{K_w}\left(1 + \frac{\ell^2}{12\, t_w^2}\right) + \frac{\ell}{2\,\pi R\, h_g}$$

6. Compute the required wall area A_W of the heat exchanger:

$$A_W = \frac{(\dot{w}\, Cp)_{He}}{U}$$

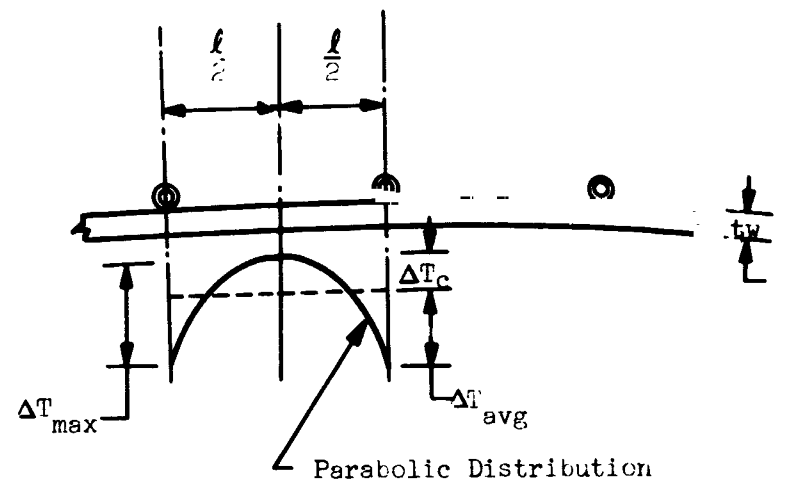

FIGURE 8-2 Wall Temperature Distribution

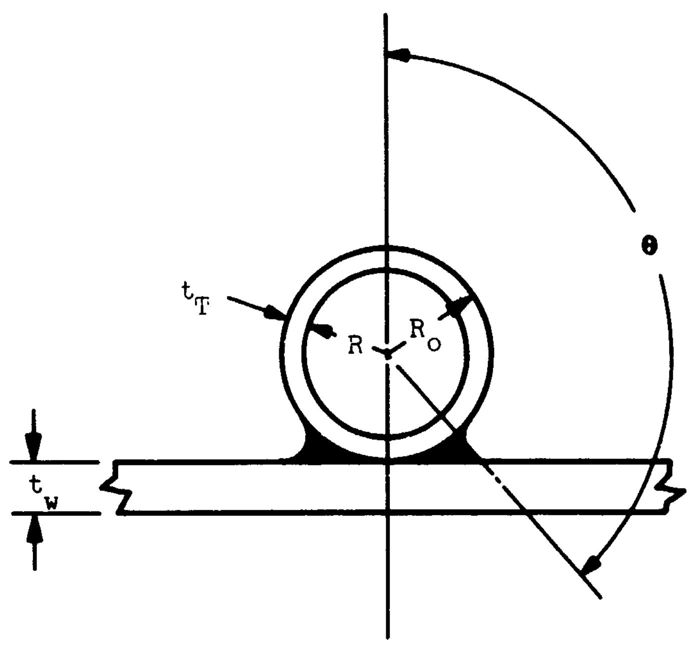

Figure 8-3 Tube-Wall Attachment Geometry

7. Compute the required number of tube turns N from

$$N = \frac{1}{\ell} \sqrt{\frac{A_w}{\pi}}$$

8. Compute the total tubing length L from

$$L = 2\pi\ell \left[\frac{N}{2} + \sum_{n=1}^{N} (n-1)\right]$$

9. Compute the weight of tubing plus helium from

$$W_{TUBE} = \pi \rho_T (R_o^2 - R^2) L + \pi \rho_{He} R^2 L$$

10. The total weight of the tank wall heat exchanger system is then

$$W_{HEX} = W_{TUBE} + W_{FILLET} + W_{MIXER} + W_{BAFFLE}$$

where W_{FILLET} refers to the weld fillet shown in Figure 8-3.

8.2.2 Sample Calculations

The procedure outlined in Section 8.2.1 has been carried out for a range of heat absorption rates and helium temperature rises. These calculations were performed for two cryogen storage temperatures, 20°K (liquid hydrogen) and 90°K (liquid oxygen) and for an assumed tubing diameter of 0.375 inches. It was also assumed that circumferential temperature gradients around the tubing walls were small.

The results of these computations are shown in Figures 8-4 and 8-5. The tank wall surface area required for the exchanger is plotted in Figure 8-4, and the tubing weight, plus the weight of helium contained in the tubing is plotted in Figure 8-5. It can be seen from these results that both the area and weight penalties associated with such an exchanger are fairly small, even for the highest rates of heat transfer.

8.3 FLUID CIRCULATION PUMPS

If a separate cooling loop is used to transfer the heat from the cryogen tank to the refrigerator, a small pump or compressor is required. No attempt has been made to design such a unit; however, in order to be able to estimate a complete system weight approximate weight and power data (Figures 8-6 and 8-7) has been

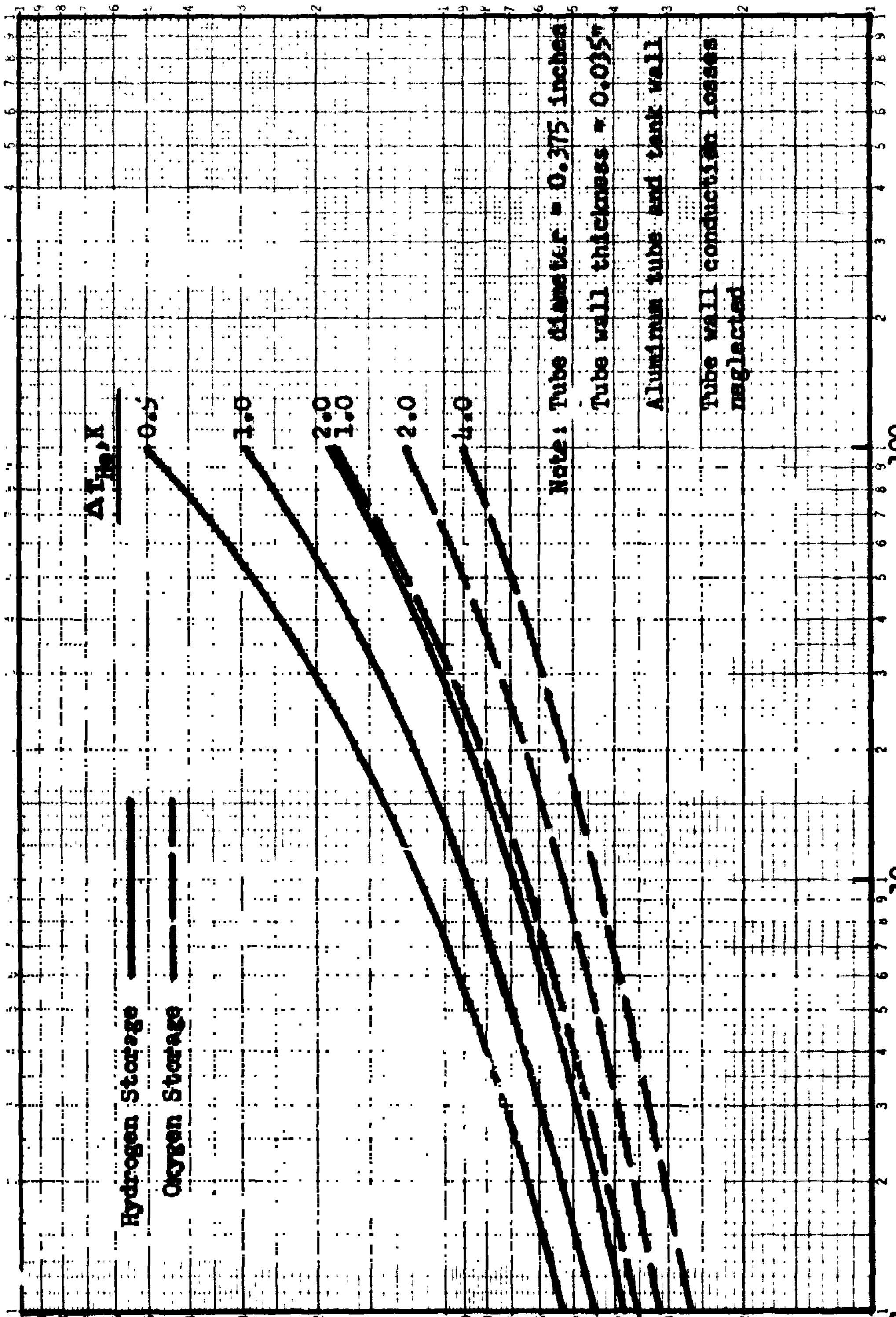

Figure 8-4 Heat Exchanger Surface Area Requirements

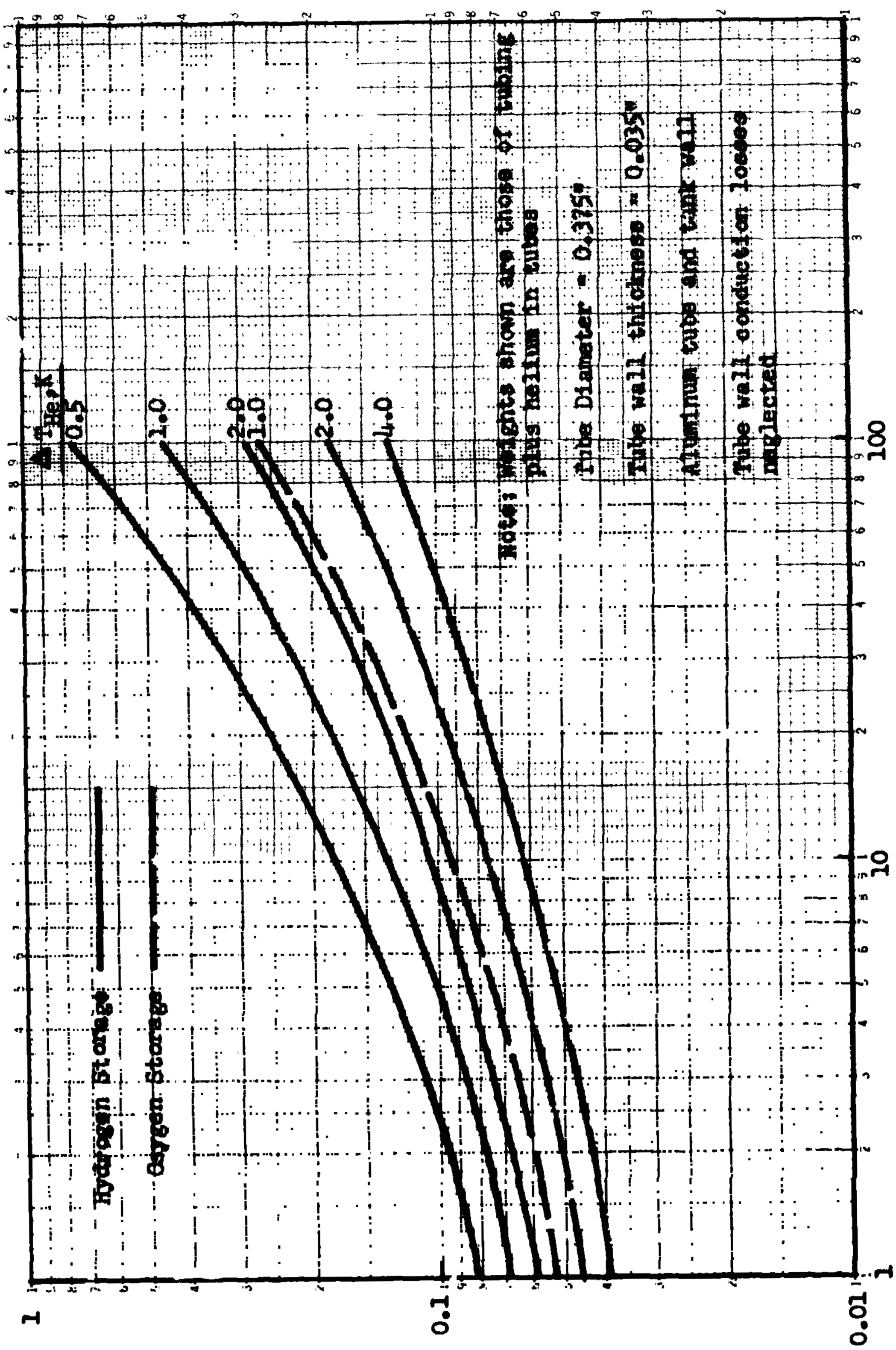

Figure 8-5 Tank Wall Heat Exchanger Weight

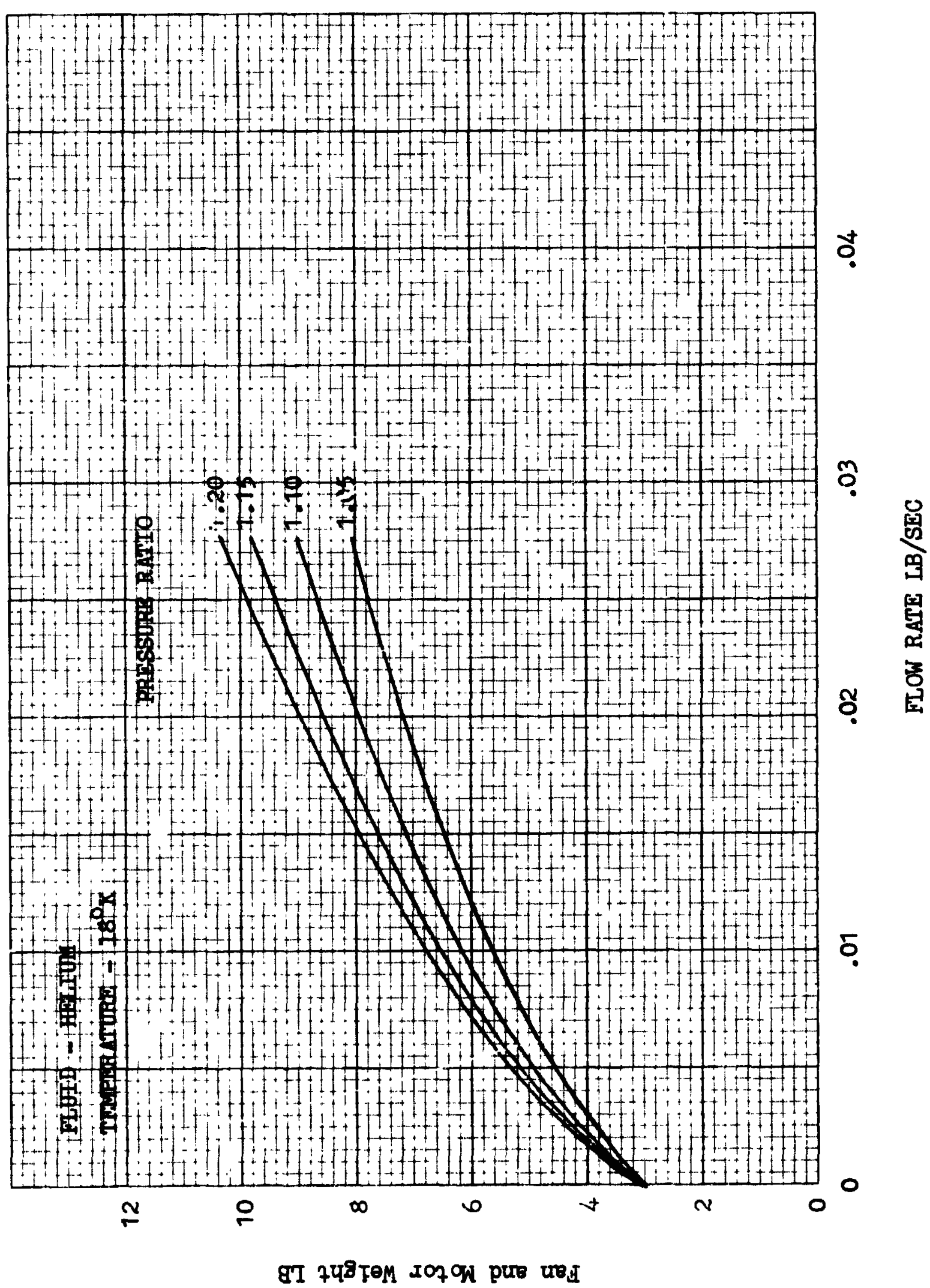

Figure 8-6 Helium Circulation Fan and Motor Weight

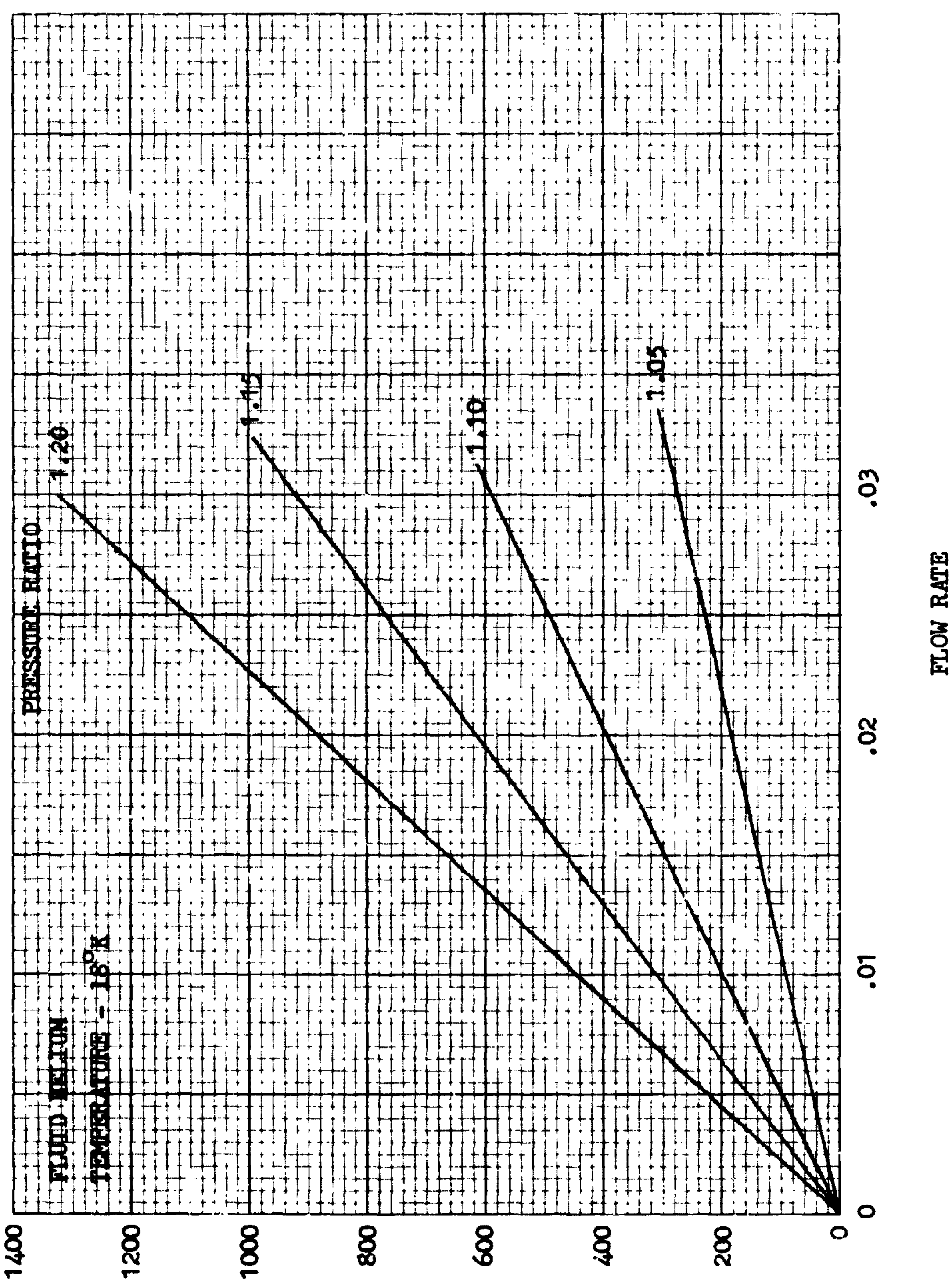

Figure 8-7 Helium Circulation Power

supplied for a circulation unit. These data are based on the same reference as in Section 7. The power was computed assuming an adiabatic compression and compressor and motor efficiencies of 0.80 and 0.85 respectively. Since the units are rather small, a positive displacement type of compressor was envisioned; however, no attempt was made to do a design analysis. The weights are based on a minimum case and hardware weight of 3.0 lb.

8.4 CRYOGENIC HEAT PIPES

The design of cryogenic heat pipes follows essentially the same procedures as that for moderate and high temperature heat pipes. Due to the high internal pressures in cryogenic heat pipes while inoperative at ambient temperatures, the pipe wall thickness, and thus the total weight, is somewhat higher than that of moderate temperature heat pipes. Internal pressures can range from 1 to 3000 psia.

The design equations presented in Section 7 may also be used for the design of cryogenic heat pipes. However, the unique properties of cryogenic fluids require special consideration.

8.4.1 Fluid Selection

The factors described in Section 7 related to the wicking limit, boilout limit and the gas choking limit also apply to cryogenic fluid selection. The optimization parameters G_1, G_2 and G_3 are shown for three fluids, nitrogen, oxygen and fluorine in Figure 8-8 and in Figure 8-9 for hydrogen. The normal boiling point to critical point temperature range is shown in Figure 8-10 for several additional fluids.

8.4.2 Evaporator and Condenser Temperature Drops

A major cause of poor cryogenic heat pipe performance can be attributed to boiling in the evaporator. Brentari and Smith (Reference 8-4) have compiled data for nucleate boiling of LH_2, LN_2 and LO_2 at one atmosphere. Values of nucleate boiling heat flux from this reference have been plotted in Figure 8-11 for these fluids. These data show that nucleation may begin at $2^{o}K$ of superheat and a heat flux of approximately 0.2 W/ft^2 for LN_2 or LO_2. These small superheat values emphasize the need to minimize the temperature drop across the evaporator

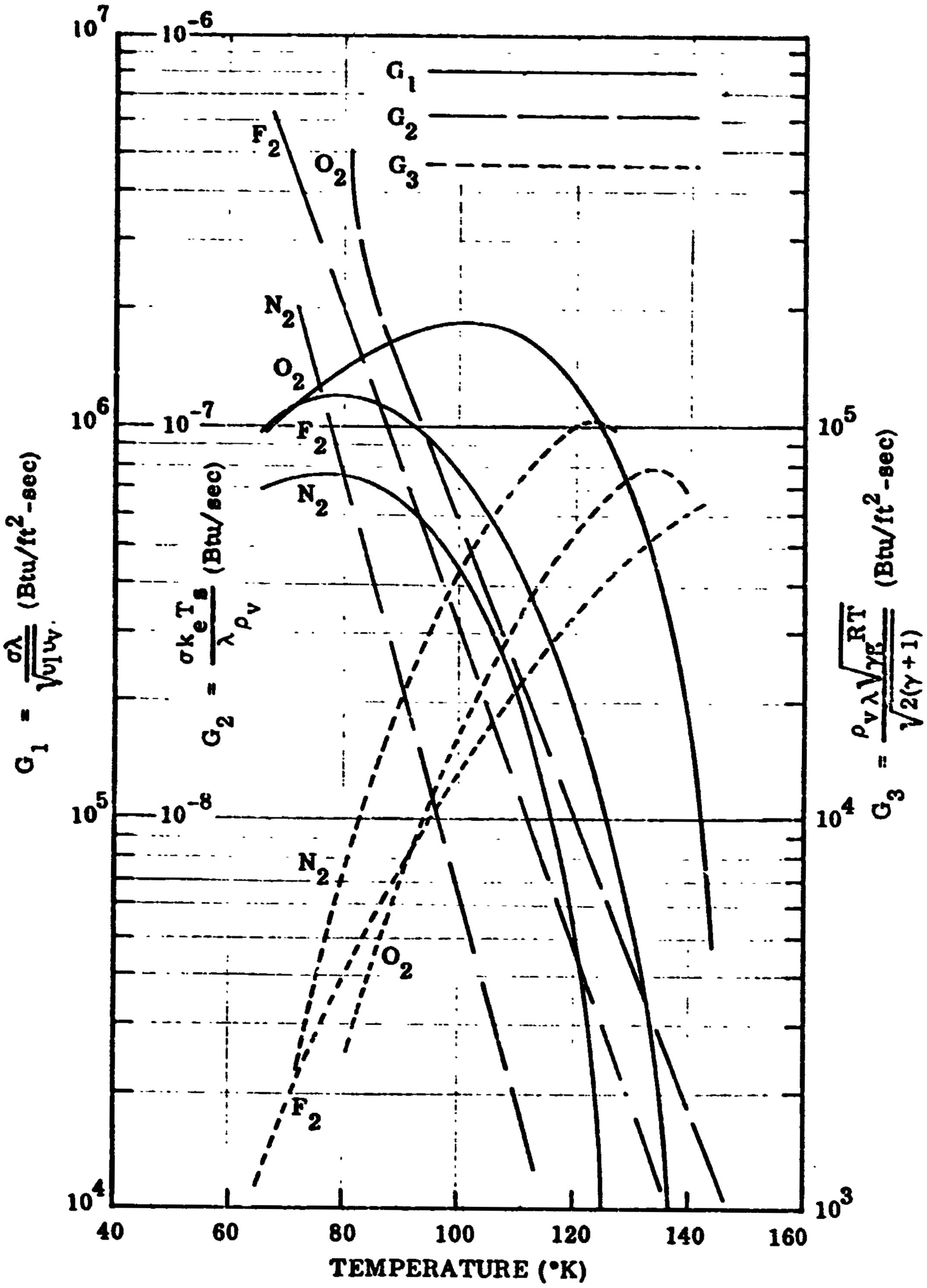

Figure 8-8 Fluid Property Groups at Low Temperatures

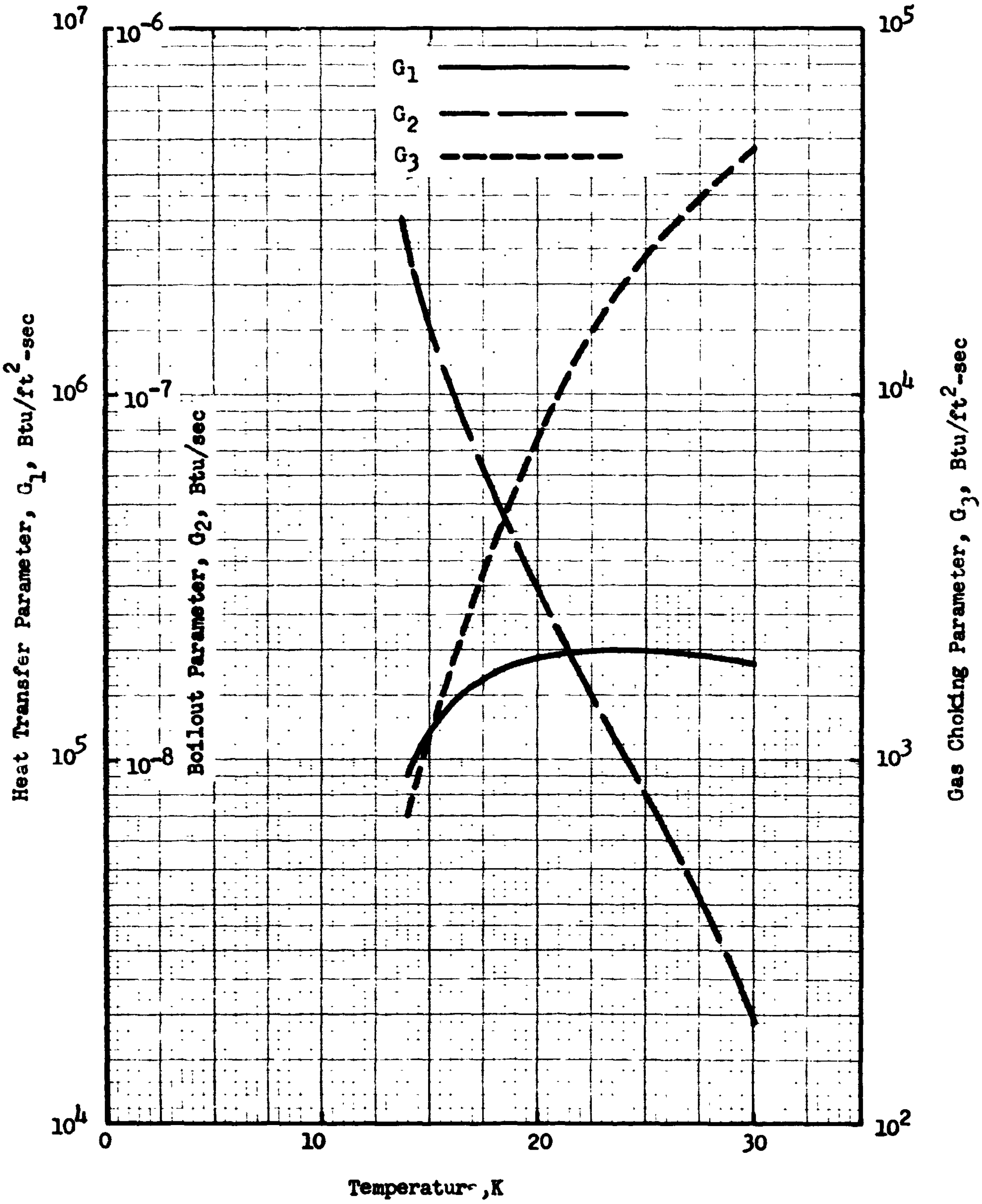

Figure 8-9 Fluid Property Groups at Low Temperatures (Hydrogen)

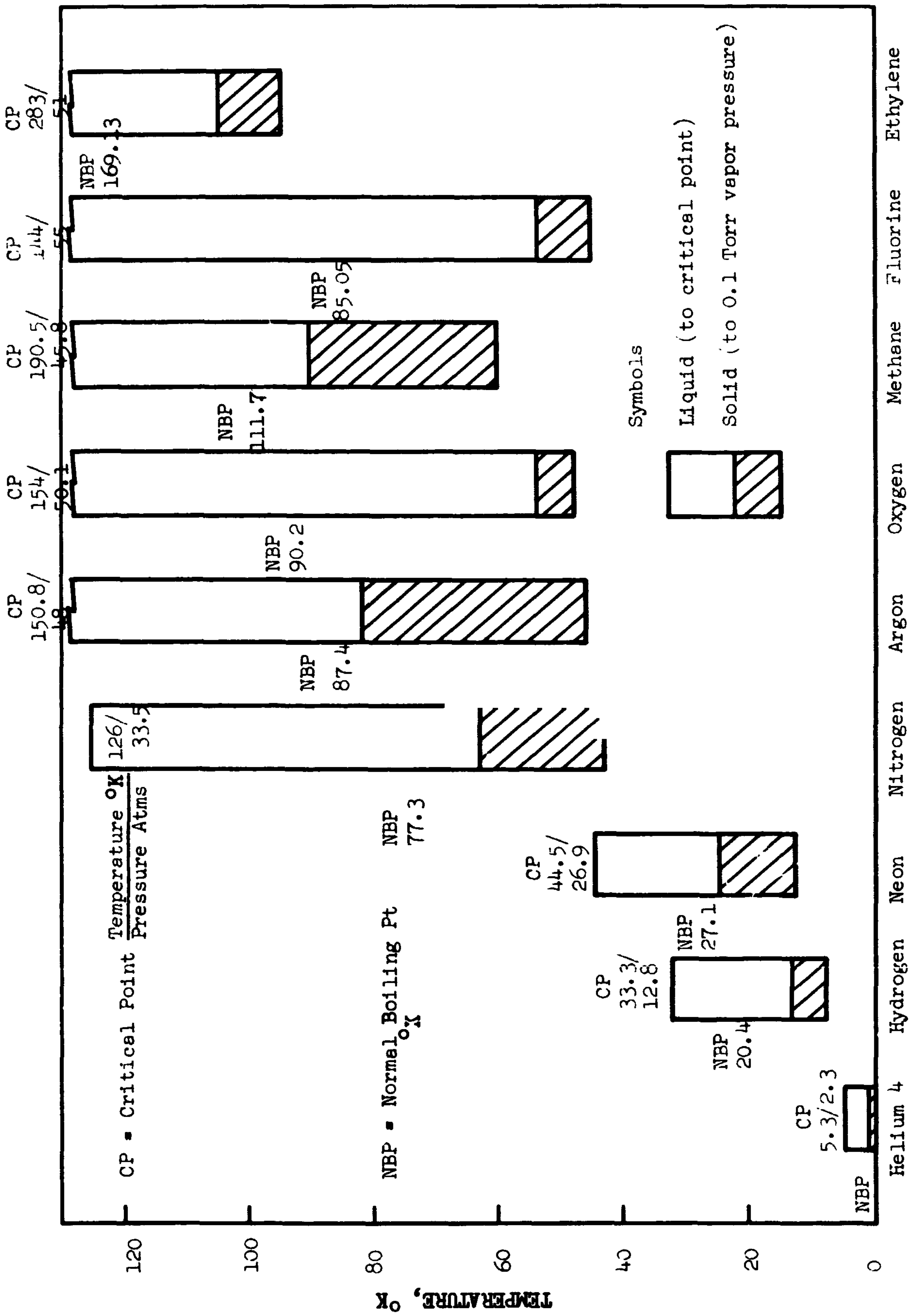

Figure 8-10 Cryogenic Heat Pipe Fluids

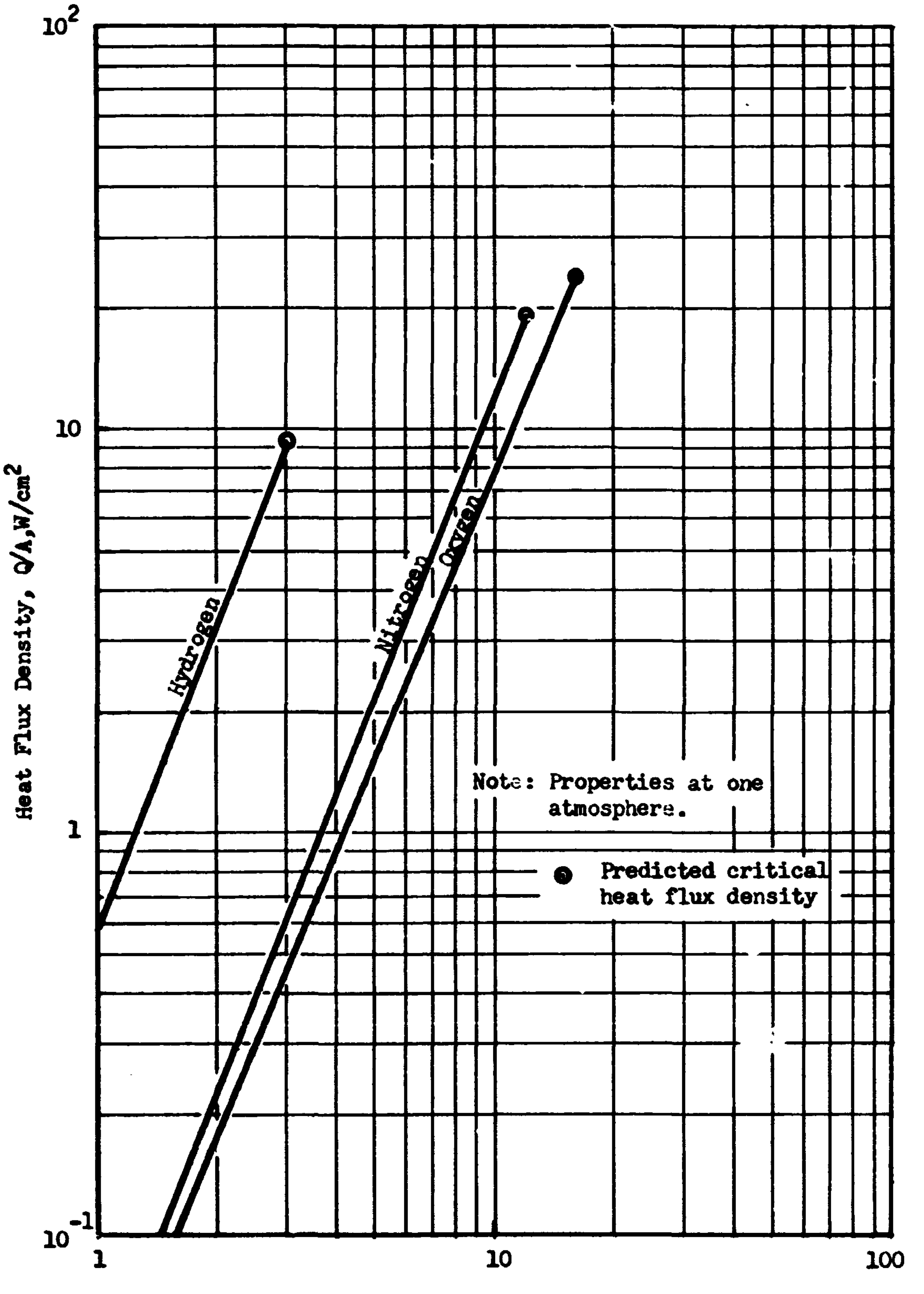

Figure 8-11 Nucleate Boiling Heat Fluxes for Cryogenic Fluids

wick. This can be accomplished in three ways: (1) the evaporator area can be increased to reduce the radial heat flux density; (2) the wick-liquid matrix can be reduced in thickness; or (3) the thermal conductivity of the wick can be increased. The most appealing of these alternatives is generally that of reducing the wick thickness; however, this alternative may lead to practical difficulties. For example, with LN_2 or LO_2 the excess ΔT across the evaporator should be kept below $3^{o}K$ in order to prevent excess superheating in the wick structure. The corresponding value of (Q/A) maximum from Figure 8-11 is about 0.5 W/cm^2. Rewriting the equation in Section 7 for the wick thickness, we get

$$t = \frac{\Delta T}{Q/A_e} K_m = 6\ K_m, \text{ cm}$$

If the thermal conductivity of the wick matrix is assumed to that of the liquid alone, then the wick thickness for LO_2 would be 8×10^{-3} cm. This is an extremely thin wick which would be difficult to manufacture and would have very low capacity for axial flow.

On the other hand, the use of a sintered metal wick can provide conductivities close to those obtained assuming parallel conduction paths. Using such a wick, the matrix conductivity can be increased sufficiently to provide a maximum wick thickness on the order of 0.1 cm. It is for this reason that the use of thin sintered metal wicks in the evaporator section is desirable.

8.4.3 Wick Design

Figures 8-12 and 8-13 show a comparison of optimized homogeneous and channel wicks using equations developed in the final report. Values of the wick characteristic parameters used were $\epsilon = 0.8$, $b = 20$, and $K = 1.5$. These results show that channel wicks give better zero-g performance than homogeneous wicks, but degrade rapidly at higher acceleration.

8.4.4 Size and Weight

The size and weight of a cryogenic heat pipe are dependent upon a combination of design factors. These include the required heat transfer capacity, overall length and diameter, materials used and maximum internal pressure.

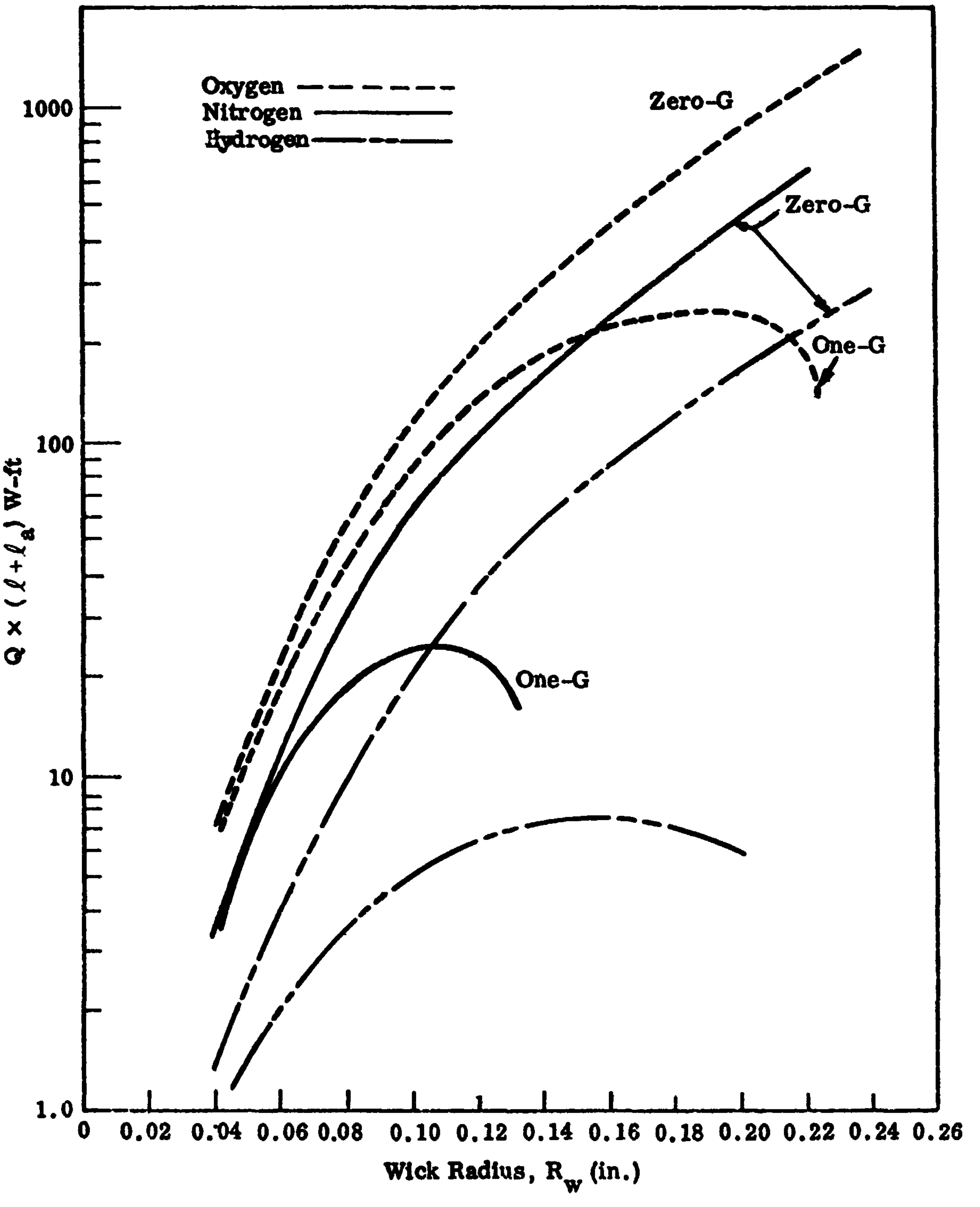

Figure 8-12 Homogeneous Wick Heat Pipe Performance

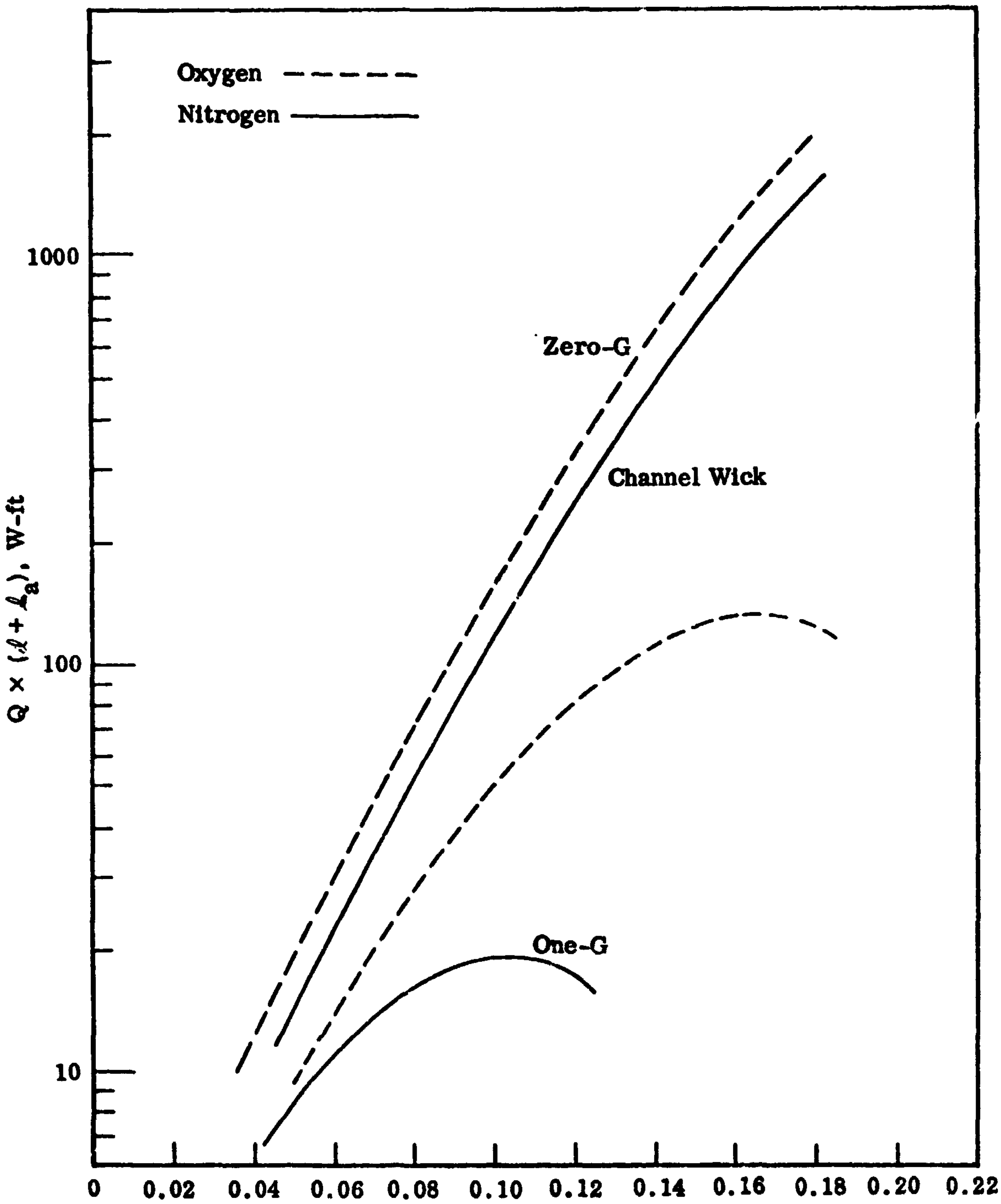

Figure 8-13 Channel Wick Heat Pipe Performance

The internal pressure of a cryogenic heat pipe at ambient temperature ($0^{o}F$ - $120^{o}F$) is given by

$$P = Z \rho_{HP} RT$$

where

$$\rho_{HP} = \rho_{\ell} \frac{V_{\ell}}{V_{tot}}$$

For a particular pipe and wick combination, the values of V and V_{tot} are fixed for a saturated wick. Therefore, the pressure will be only a function of Z, ρ_{ℓ} , R and T. The compressibility factor Z for a real gas is pressure and temperature dependent. In evaluating the factor Z, it is useful to determine the reduced pressure and reduced temperature

$$P_r = \frac{P}{P_c}$$

$$T_r = \frac{T}{T_c}$$

The reduced temperature can be determined since the critical and ambient temperatures are known. However an iteration procedure using the Z versus P_r chart (Figure 8-14) is necessary for determination of the final pressure P. Figure 8-15 is a plot of $\frac{PV_{\ell}}{V_{tot}}$ versus temperature for the three liquids. To apply Figure 8-15, the open volume of the wick and the total open volume of the heat pipe must be known. Since the ratio V_{ℓ}/V_{tot} is constant, Figure 8-15 shows that a nitrogen heat pipe would have the lowest pressure at ambient temperature.

The pressure at a given temperature can be significantly reduced by increasing the specific volume. This can be accomplished by decreasing the open volume of the wick; increasing the vapor volume or using a less dense working fluid.

Figures 8-12 and 8-13 can be used to calculate heat pipe size required for a given power and length. Once the pipe wall thickness has been determined, the system weight can be calculated from the known dimensions and material densities. Figure 8-16 is a plot of the power length product, Q $(\ell + \ell_a)$ as a function of heat pipe weight for two fluids, oxygen and nitrogen.

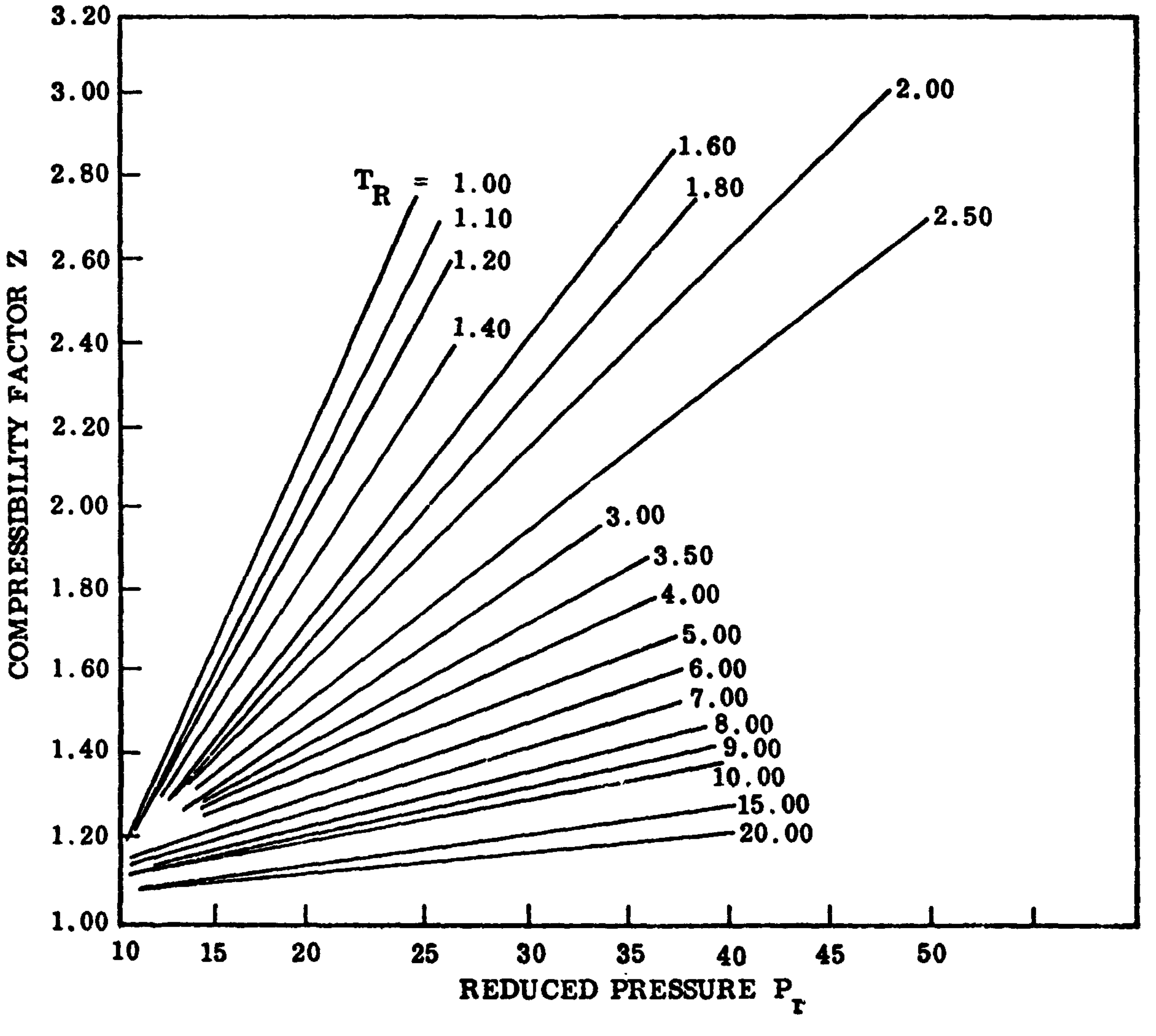

Figure 8-14 Compressibility Factor of Real Gases

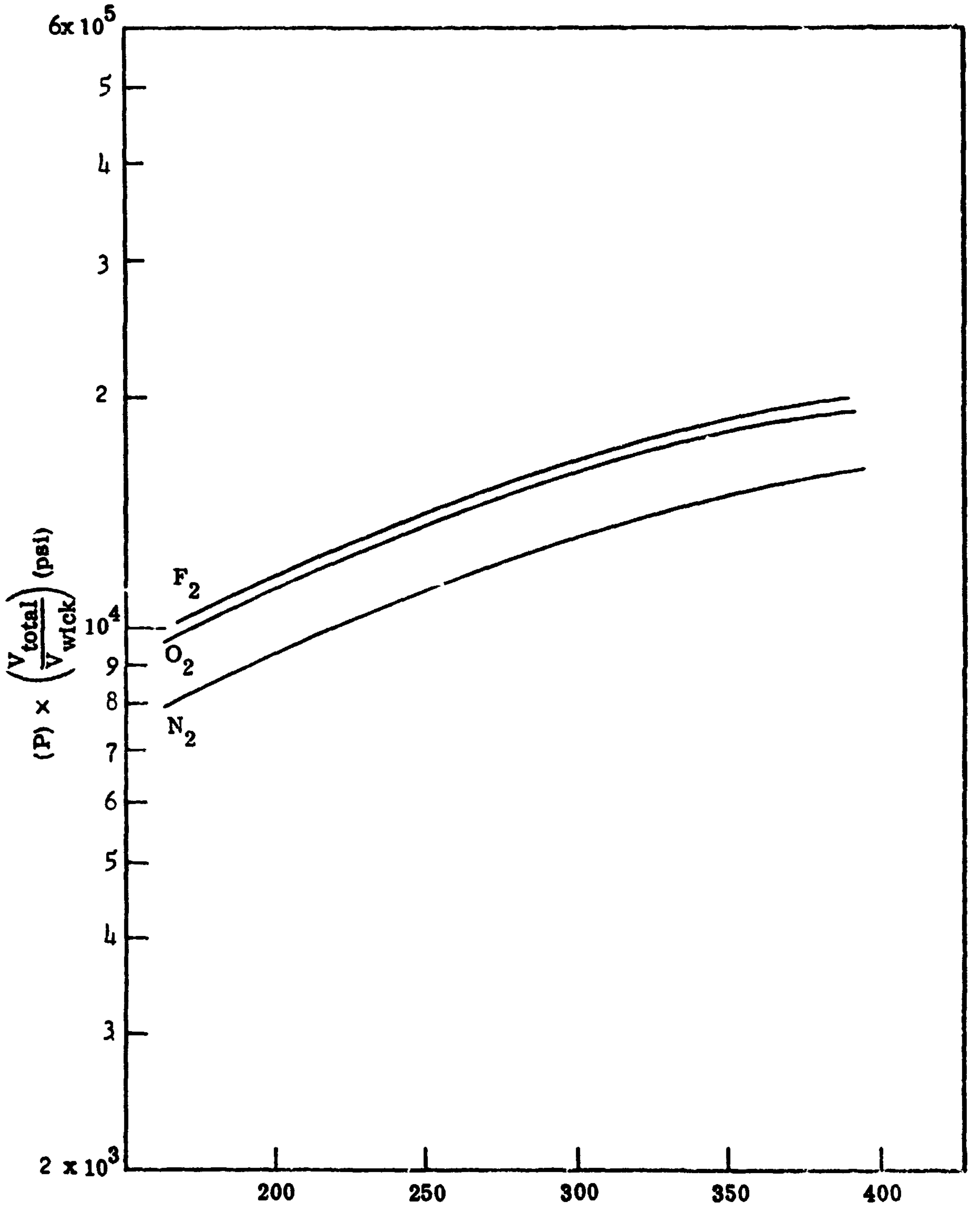

Figure 8-15 Relative Operating Pressures for Nitrogen, Oxygen, and Fluorine Heat Pipes

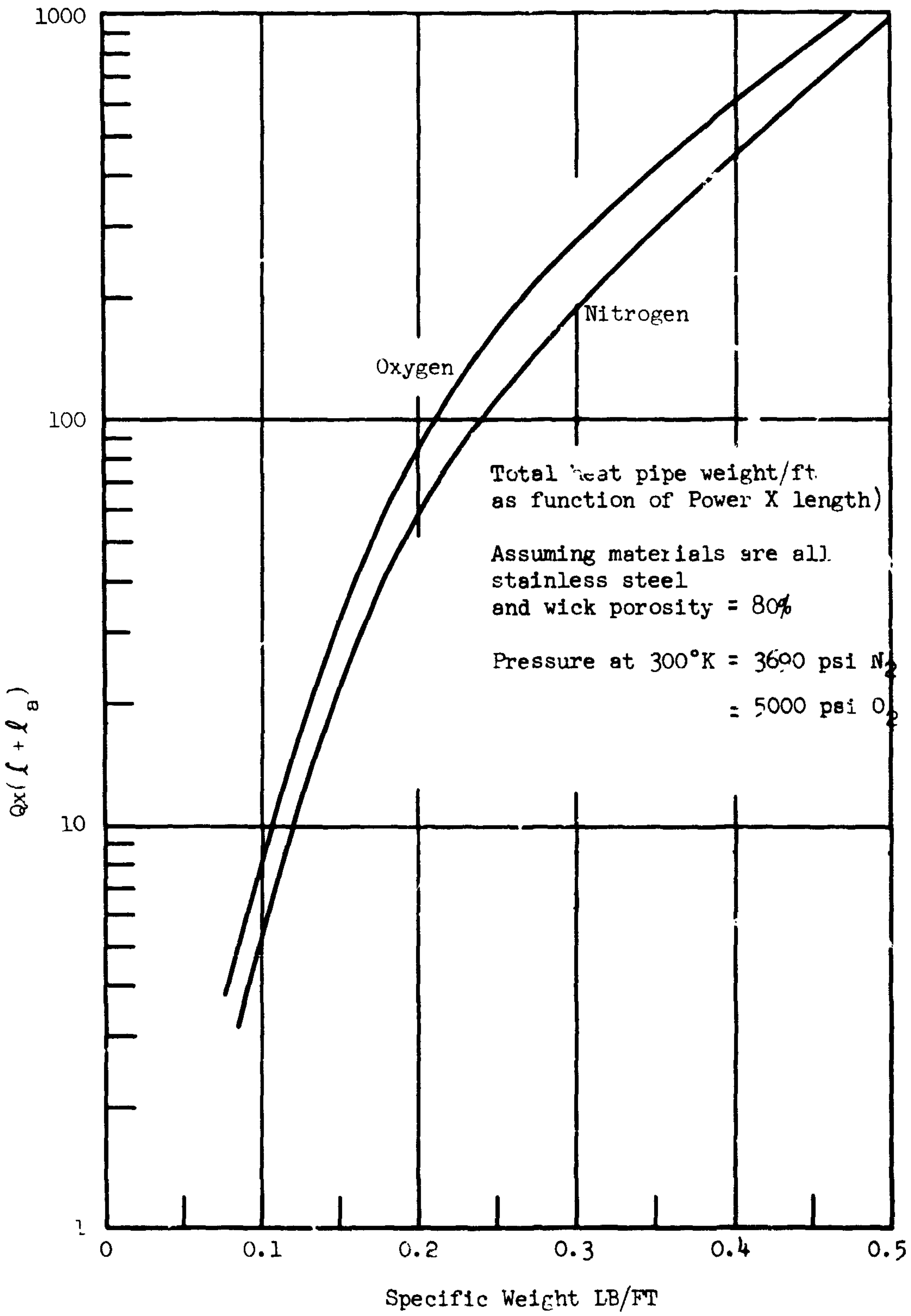

Figure 8-16 Cryogenic Heat Pipe Weight

8.4.5 Heat Pipe Insulation

The possible long length of the heat pipe (up to 5 ft.) and the high surrounding temperatures dictate that some provision be made to reduce the radiation heat load into the adiabatic section. The simplest such provision would be to gold plate the outer surface of the heat pipe. Figure 8-17 shows the radiation heat load into a heat pipe at 80°K from surroundings at 320°K. Emittances of 0.01, 0.03 and 0.1 have been assumed in order to cover the range of possible metal surfaces.

A system using only a gold plated surface ($\epsilon = 0.03$) offers the advantage of simplicity of construction and a low heat capacity which is desirable since the heat capacity directly influences the start up time.

An improvement over a simple surface coating is achieved by using a few wraps of double goldized mylar. The spacer between the wraps would be nylon net to reduce the level of offgassing and flaking experienced with glass cloth spacer materials, and to prevent absorption during storage in a humid environment.

Figure 8-18 shows a plot of the heat leak from 330°K into an insulated pipe at 77°K for a system with $\frac{1}{4}$" of goldized mylar multilayer for various pipe diameters. The advantage gained with the multilayer system over that of a simple low emittance is obvious.

8.5 SOLID CONDUCTION DEVICES

If it is feasible to locate the refrigerator in close proximity to the cryogen storage tank, then the use of solid conduction devices may offer weight and space advantages in comparison to heat exchangers or cryogenic heat pipes. If the conductor is well insulated, the rate of heat conduction in a longitudinal direction is simply

$$q = KA \frac{\Delta T_{COND}}{L}$$

Heat Pipe Exterior Coated with Low Emittance Coating, No Additional Thermal Insulatior

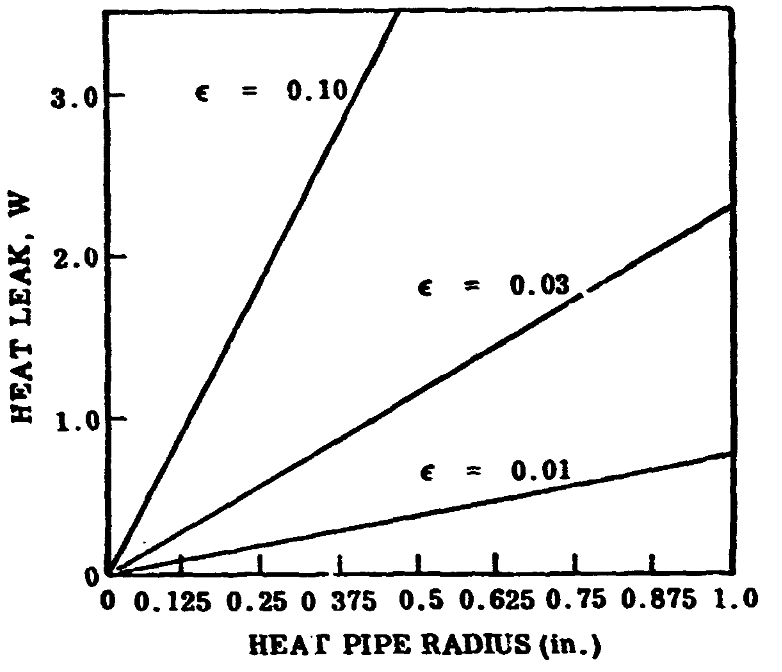

Figure 8-17 Heat Leak as a Function of Heat Pipe Radius for a 5-ft Long Pipe with No Exterior Insulation

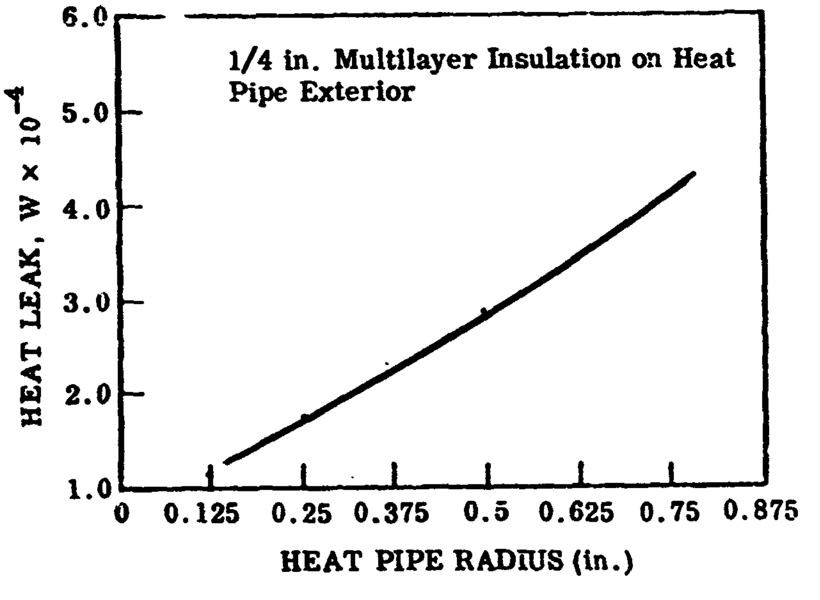

Figure 8-18 Heat Leak as a Function of Heat Pipe Radius for a 5-ft Long Pipe with a Multilayer Insulation

where

K = thermal conductivity

A = conductor cross-sectional area

ΔT = temperature drop between refrigerator cold finger and cryogen tank

L = conductor length

The weight per unit length of a solid conductor is given by

$$\frac{W}{L} = \frac{\rho\, qL}{K\Delta T_{COND}}$$

where ρ is the density of the conductor. Figure 8-19 shows the weight per unit length of a solid aluminum bar as a function of heat flux transmitted from a liquid oxygen container. For purposes of comparison similar data for an oxygen heat pipe are also shown. It can be seen that only for very low power-length products (less than 0.5 watt-feet) does the solid conductor compete in weight with the oxygen heat pipe.

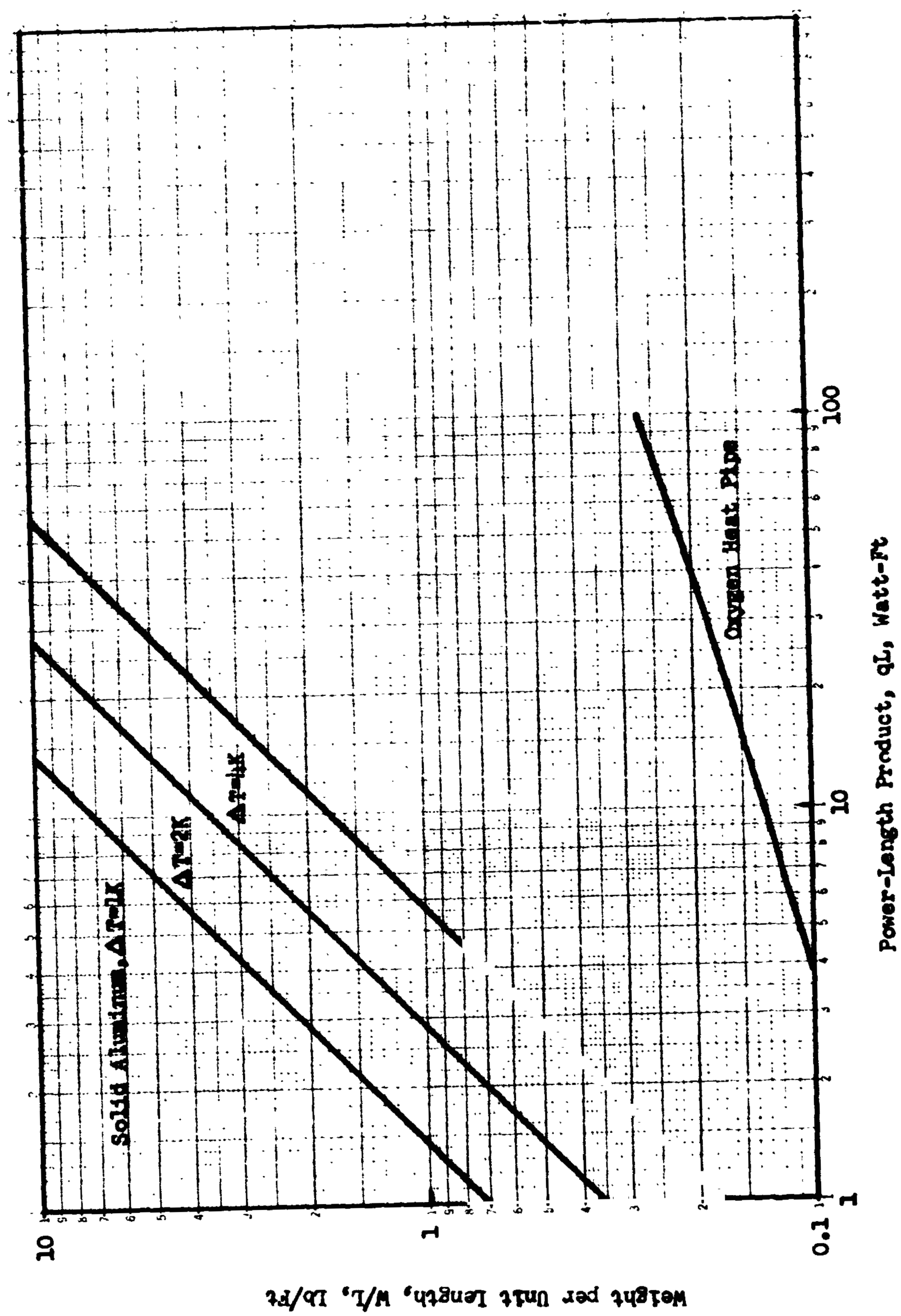

Figure 8-19 Weight of Solid Conductor for Liquid Oxygen Storage

REFERENCES

8-1 Kays, W. H. and A. L. London, "Compact Heat Exchangers," The National Press, Palo Alto, California, 1955.

8-2 Radiator Design for Space Vehicles, Airesearch Division, The Garrett Corporation.

8-3 Johnson, V. J., Ed., "Compendium of the Properties of Materials at Low Temperatures," Phase I, Cryogenic Engineering Laboratory, Boulder, Colorado, December 1959.

8-4 Brentari, E. G., Giarratano, P. J., and Smith, R. V., "Boiling Heat Transfer for Oxygen, Nitrogen, Hydrogen and Helium," NBS-TN-317, National Bureau of Standards, Boulder, Colorado.

Section 9

POWER SUPPLIES

Candidate space electric power systems for external refrigerator systems for long-term cryogenic storage are listed in Table 9-1 by energy source and type of energy conversion device. Also listed are some primary constraints for the systems.

Table 9-2 identifies the characterizations of power and mission that are required to select an electric power system. Table 9-3 presents a listing of design handbook information that ideally is desired for each candidate power system. Table 9-4 gives some selection guidelines for space electric power systems in the 0.1 to 10 kw range examined during this study.

Figure 9-1 graphically shows how the various power systems compare on a specific power basis. It is apparent that solar photovoltaics offer the highest watts/lb over the entire power range. RTG's, Isotope Brayton, and nuclear power systems are logical backup candidates with fuel cells and batteries well down in specific power rating because of energy constraints.

Tables 9-5 to 9-9 and Figures 9-2 to 9-6 present data and schematics for use in defining the system selection information noted in Table 9-3.

Tables 9-10 to 9-12 and Figure 9-7 present data useful in defining radioisotope and solar devices as thermal power sources for a heat-powered refrigerator device.

Table 9-1

CANDIDATE SPACE ELECTRIC POWER SYSTEMS

Energy Source	Conversion Device	Primary Constraints
Chemical	Battery Fuel Cell	Energy
Solar	Photovoltaic Thermionic *	Sun intensity, shade, orientation, extended surface area
Radioisotope	Thermoelectric Brayton-cycle	Isotope availability, nuclear safety, heat rejection area
Nuclear reactor	Thermoelectric Rankine-cycle Brayton-cycle Thermionic *	Nuclear safety, heat rejection area, reactor coolant temperature

* Probably not available before late 1980's

Table 9-2

POWER AND MISSION CHARACTERIZATION REQUIRED

- Power Level, Peak and Average
- Power Duty Cycle
- Power Characteristics
- Energy
- Mission Life
- Mission Orbit Parameters
- Mission Payload Constraints

Table 9-3

INFORMATION DESIRED FOR EACH CANDIDATE

SPACE ELECTRIC POWER SYSTEM

o Weight	o Reliability
o Volume	o Availability
o Area	o Safety
o Cost	o Operating Restrictions

<u>This should include</u>:

- Auxiliary power source requirements
- Power conditioning requirements
- System penalty for added drag from extended surfaces
- System penalty for nuclear shielding and isotope intact reentry

Table 9-4

<u>GUIDELINES</u>

- Use solar photovoltaic power systems unless mission constraints preclude their use
- Use RTG's in 0. - 1.0 kilowatt range if solar photovoltaics cannot be used
- Use radioisotope Brayton cycle in 1.0 - 10.0 kilowatt range if solar photovoltaics cannot be used
- Nuclear reactor power systems would normally not be selected unless large amounts of power $>$ 10 kw were required, or unless they were to be the primary spacecraft power source and much of the shield and system weight were already charged to the spacecraft

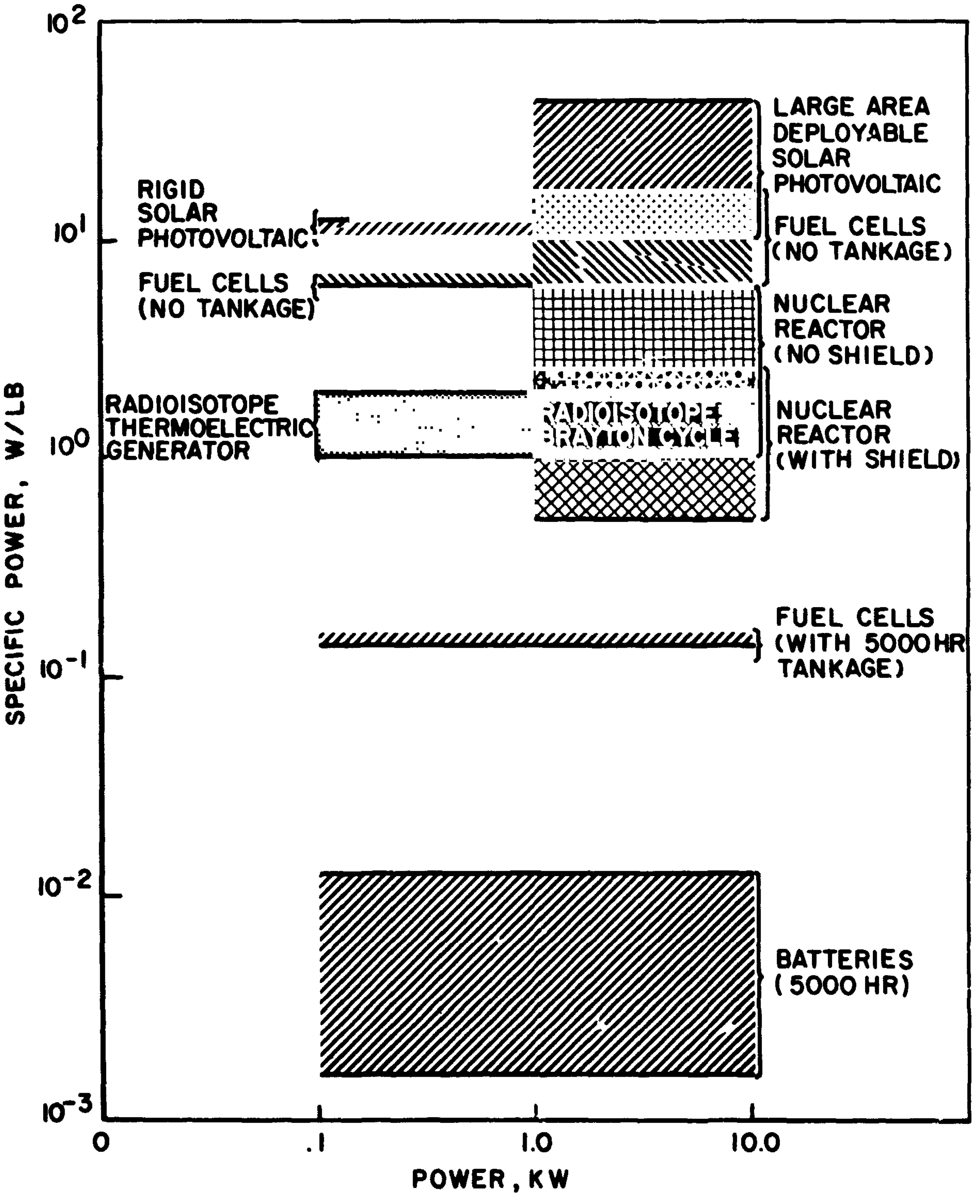

FIGURE 9-1 SUMMARY OF POWER SUPPLY REGIMES OF APPLICABILITY

TABLE 9-5

BATTERY POWER SYSTEM CHARACTERISTICS

Type	Ni-Cd	Ag_2O-Zn	Ag_2O-Cd
Oper Voltage	23.29 - 29.50	25	14.5
Oper Temp, °F	0 - 125	30 - 90	0 - 100
Dimensions	18.80"x7.750"x 6.50"	15.84"x 11.31"x 8.03"	~ 1 ft^3
Weight, Lb	62 (max)	116 (max)	~ 150
Rated Cap.	0 - 40°F, 17 ah 40 - 80 20 ah 80 -125 17 ah	300 ah	150 ah
Internal Impedance	0.05 Ω (max) (70°F, 5 amp, 5 ah depth)	0.05 Ω	not avail.
Chg Rate	5 amp (max)	12 amp	6 amp
Wet Stand Life, 30°F	2.5 yr (disch)	0.5 yr	1 - 2 yr
Watt-Hr/Lb	8	65	~ 20
Number of cells	20	16	13
Typical Cycle Life *	4,000 cycles	100 cycles	1,500 cycles

* 50% depth of discharge; continuous 55-min charge and 35-min discharge cycling

TABLE 9-6

SOLAR PHOTOVOLTAIC POWER SYSTEM CHARACTERISTICS*

Type	Specific Power	Specific Area	Specific Volume
Rigid Panel	8 - 10 w/lb	0.1 ft^2/w	-
Large Area Erectable Panel	10 - 40 w/lb **	0.1 ft^2/w	0.6 - 2 ft^3/kw

* Typically:

Silicon n/p solar cells

2 x 2 cm x 0.01 in thick

with 0.03 - 0.04 in cover

Cell degradation with time is dependent on orbit parameters.

** Ranging from 10 - 12 w/lb for LMSC fold-up flexible array and Hughes large retractable array to designs of self-rigidized folded panels which offer up to 40 w/lb.

TABLE 9-7

HYDROGEN-OXYGEN FUEL CELLS

	Gemini	Apollo	General Electric	Pratt Whitney	Allis Chalmers
Gross Pwr	1.05 kw	1.42 kw	5 kw	5 kw	2 kw
Type	Ion Exchange	Alkaline	Ion Exchange	Alkaline	Alkaline
Life	340 hr	400 hr	5,000 hr	5,000 hr	3,000 hr
Oper Temp	75°F	375 - 500°F	68 - 158°F	330 - 430°F	190 - 220°F
Weight	~ 175 lb	~ 220#	< 300#	< 300#	~ 170#
Effic'y	~ 50%	~ 70%	50 - 60%	65 - 70%	50 - 60%
Specific Power	~ 6 w/#	~ 6 w/#	> 16.7 w/#	> 16.7 w/#	~ 12.5 w/#
Specific Volume	~ 2 ft^3/kw	~ 7 ft^3/kw	~ 2 ft^3/kw	~ 4.5 ft^3/kw	~ 2.7 ft^3/kw
Reactant Consumt'n	0.9 - 0.92#/kwh	1.166#/kwh at 1.42 kw	~ 0.9#/kwh	~ 0.8#/kwh	~ 0.85#/kwh
Parasitic Power	~ 5%	~ 5%	~ 4 - 5%	~ 4%	~ 5%
Tankage Wt	~ 100#	~ 1,600# *	--	--	--

* Includes Life Support O_2

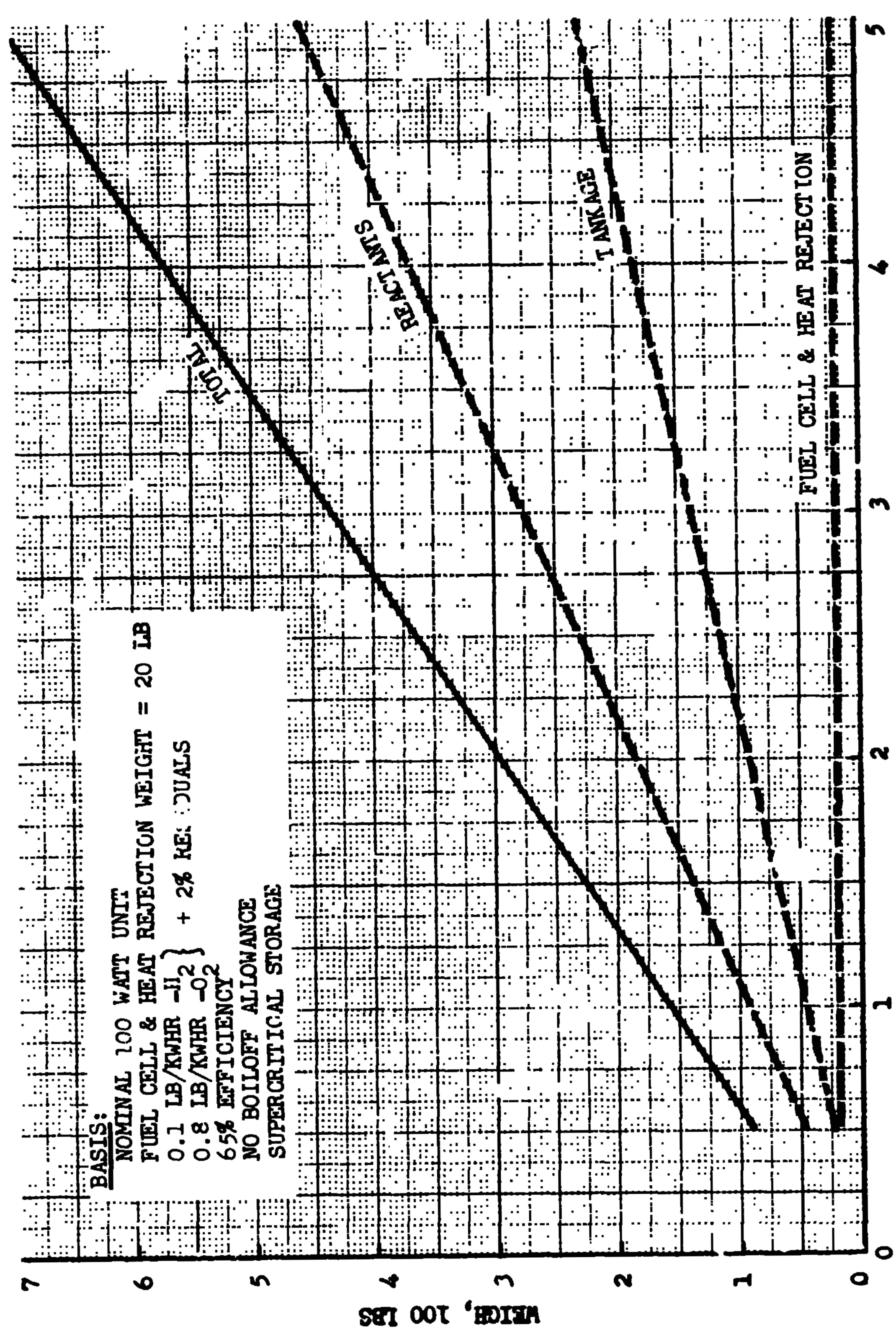

FIGURE 9-2 FUEL CELL POWER SYSTEM WEIGHT, 100 WATT

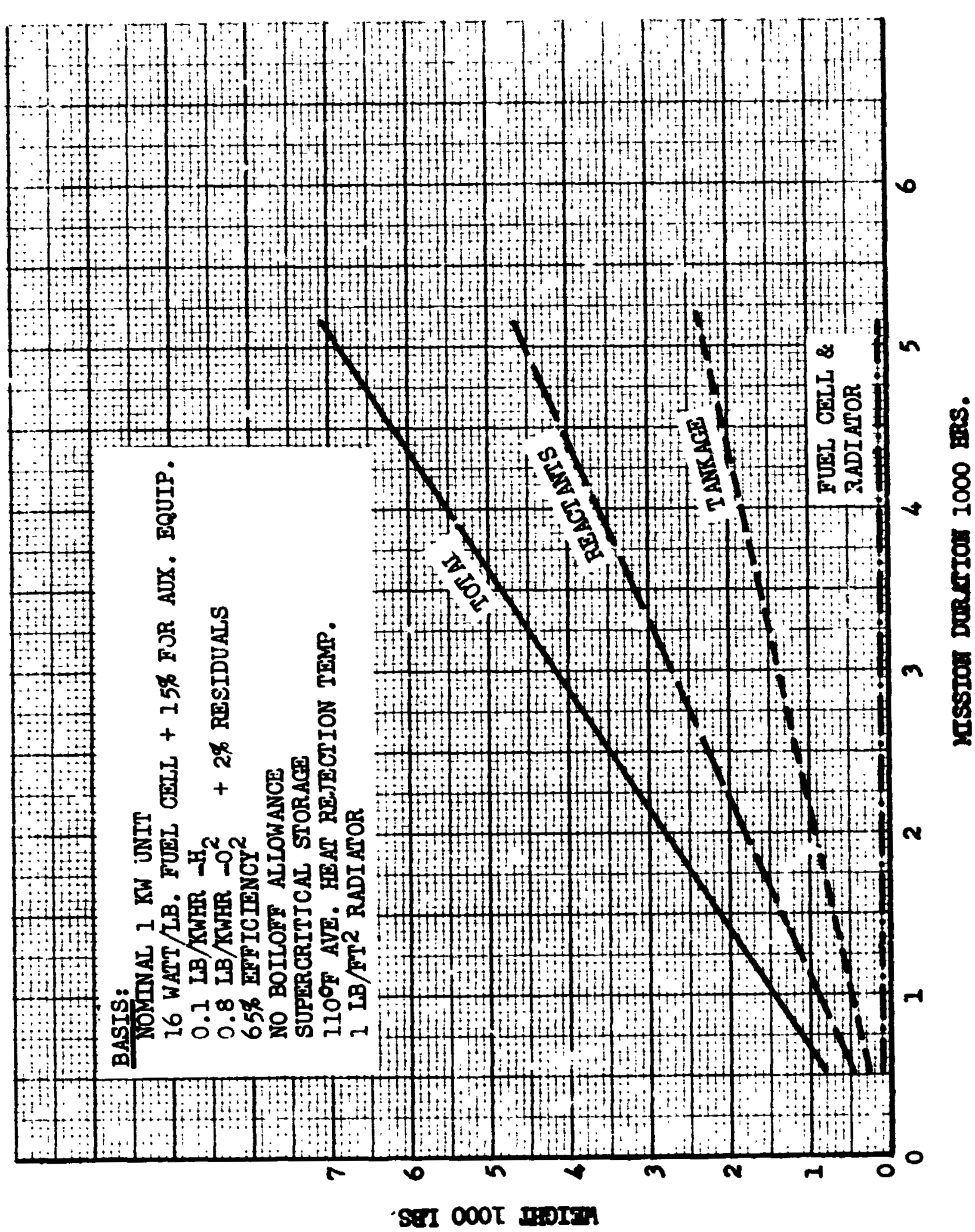

FIGURE 9-3 FUEL CELL POWER SYSTEM WEIGHT, 1000 WATT

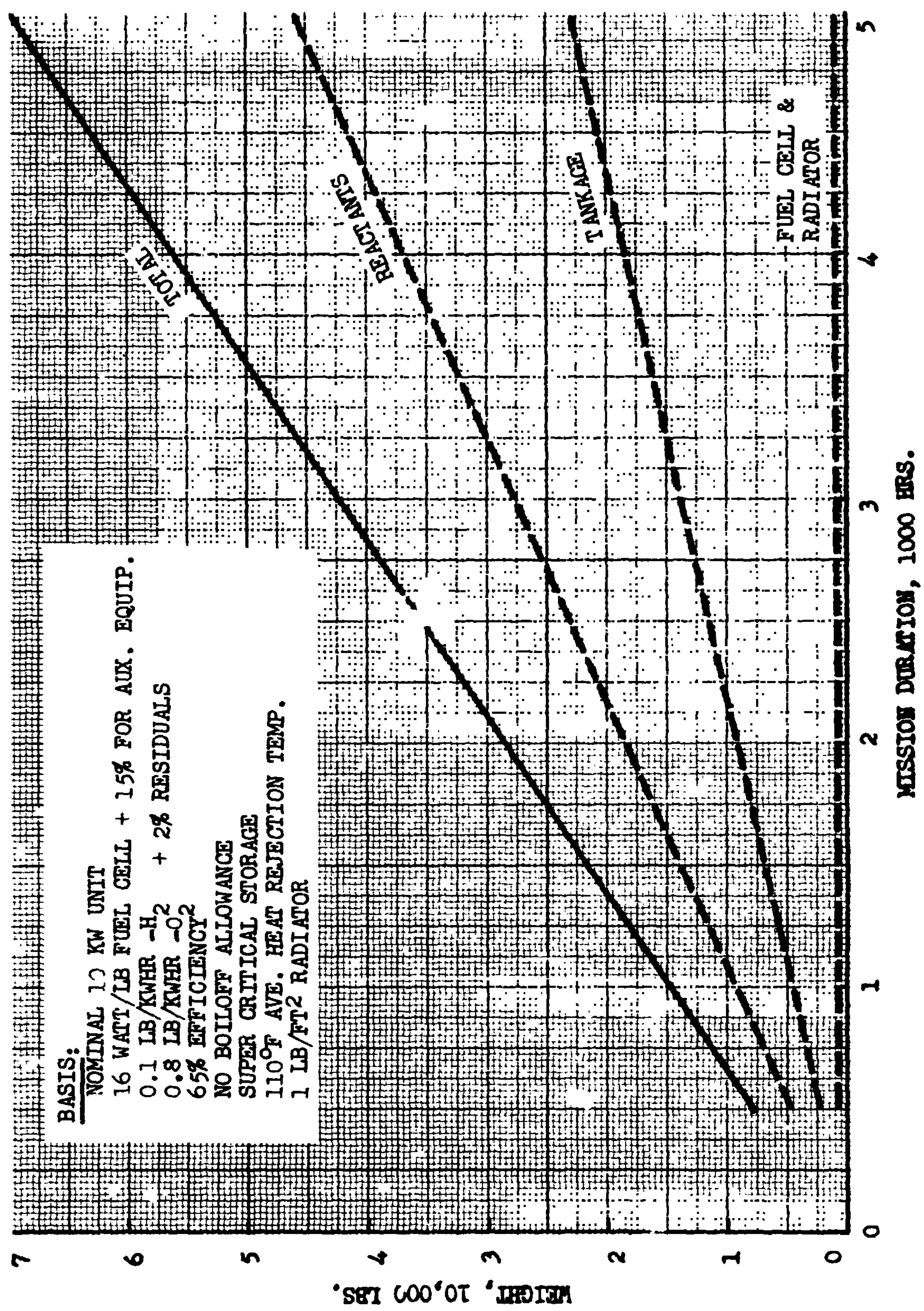

FIGURE 9-4 FUEL CELL POWER SYSTEM WEIGHT, 10,000 WATT

TABLE 9-8

RTG CHARACTERISTICS

	SNAP-19	SNAP-19 Modified	SNAP-27	ISOTEC	ISOTEC Cascaded	Multihundred
Power						
BOL *	~28 w	~40 w	~73 w	~37 w	~100 w	To be defined
EOL **	~24 w	~35 w	~62 w	~30 w	~85 w	100-200 w (5 yr)
Weight	~30 #	~30 #	~44 #	~28 #	+ ~48 #	50 - 100 #
Voltage	~3 vdc	~4 vdc	~14 vdc	~6 vdc	~6 vdc	6 v (min)
Des Life	3 yr	3 yr	1 yr	5 yr	5 yr	3 - 12 yr
Input Pwr	~630 w(th)	~635 w(th)	~1,450 w(th)	~790 w(th)	~980 w(th)	To be defined
Size	Cyl w/fins ~22"dia x 11"	Cyl w/fins ~22"dia x 11"	Cyl w/fins ~16"dia x 18"	12-sided prism ~23"dia x 15"	Similar to Isotec	To be defined
Heat Rej. Temp	350°F	350°F	520°F	290°F	290°F	
Contractor	Isotopes of Teledyne	Isotopes of Teledyne	General Electric	Gulf Gen Atomics & TRW	Gulf Gen Atomics	General Electric
Status	Used in NIMBUS	Scheduled for Pioneer F&G & Viking Lander	Used in Apollo	Scheduled for NavSat	Under Developmt	Ref Des by end of FY '71 Grand Tour is ref mission

* BOL Beginning of Life
**EOL End of Life

\+ Based on 2.1 w/# est.

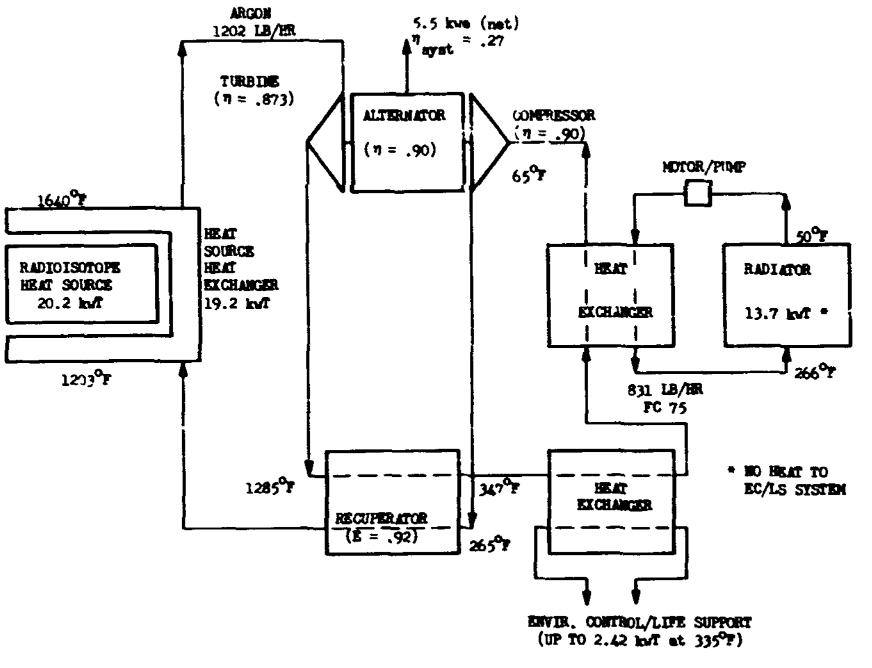

SCHEMATIC OF TYPICAL SYSTEM

Nominal NASA/LaRC 7 kw (E) system covers range from 2 - 10 kw (E)

At 7 kw (E) rating (no redundancy)

- o 1.3 watt/lb w/o shield
- o 550 ft^2 heat rejection area
- o 154°F average heat rejection temperature
- o Required space of about 350 ft^3
- o 500 lb shield with 10 ft separation distance
- o Includes isotope reentry vehicle

Fig. 9-5 RADIOISOTOPE BRAYTON-CYCLE POWER SYSTEM

TABLE 9-9

REACTOR POWER SYSTEM CHARACTERISTICS (TYPICAL)

	Nuc Reactor Brayton-Cycle	SNAP-8	Compact Conv't'r Thermoelec	Direct Rad Thermoelec
ed Power, Unconditioned, KW(e)	24 (net)	40 (net)	25.9 (net)	12 (EOL)
eactor Power, KW(t)	152	414	622	422
System Efficiency	13.2	9.7	4.2	2.8
Design Life	10,000 hr	10,000 hr	5 yr	5 yr
Reactor Coolant Inlet Temp, °F	1,150	1,140	1,100	1,100
Reactor Coolant Outlet Temp, °F	1,300	1,330	1,300	1,300
Reactor Coolant Flow Rate, lb/hr	17,000	34,530	51,120	34,990
Heat Rejection Avg Temp, °F	298	575	550	550
Heat Rejection Area, ft^2	1,150	827	1,891	1,068
Heat Rejection Loop Flow Rate, lb/hr	7,200	32,110	46,570	-
Pwr Conversion Loop Flow Rate, lb/hr	11,070	9,410	49,285	28,800
Lube/Coolant Loop Flow Rate, lb/hr	-	4,970	-	-
Lube/Coolant Radiator Avg Temp, °F	-	227	-	-
Lube/Coolant Radiator Area, ft^2	-	238	-	-
Turbine Inlet Temp, °F	1,250	1,290	-	-
Thermoelectric Hot Side Avg Temp, °F	-	-	1,150	1,150

WEIGHTS, LB

	Nuc Reactor Brayton-Cycle	SNAP-8	Compact Conv't'r Thermoelec	Direct Rad Thermoelec
Reactor & Primary Loop	912	1,329	1,258	1,025
Power Conversion Unit	1,513	1,506	5,229 *	2,270 **
Heat Rejection Loop & Pumps	578	313	1,763	-
Lube/Coolant Loop & Pumps	-	197	-	-
Heat Rejection Radiator	1,064	949	2,106	-
Lube/Coolant Radiator	-	286	-	-
Rad/Converter Support	553	790	870	2,256 **
Miscellaneous Elect Equipment	308	324	510	390
Thermal Shroud	844	698	1,484	1,095
	5,772	6,392	13,220	7,036
Specific Pwr, watt/lb (no shield or reactor disposal system)	4.2	6.3	2.0	1.4

* Includes 6 active & 1 standby heat exchanger; 12 active & 2 standby compact converters

** Includes 5 active & 1 standby Power Conversion Loops and Units

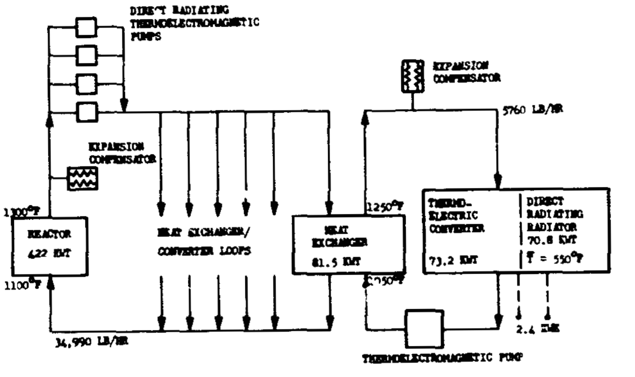

SCHEMATIC OF TYPICAL DIRECT RADIATING T/E SYSTEM

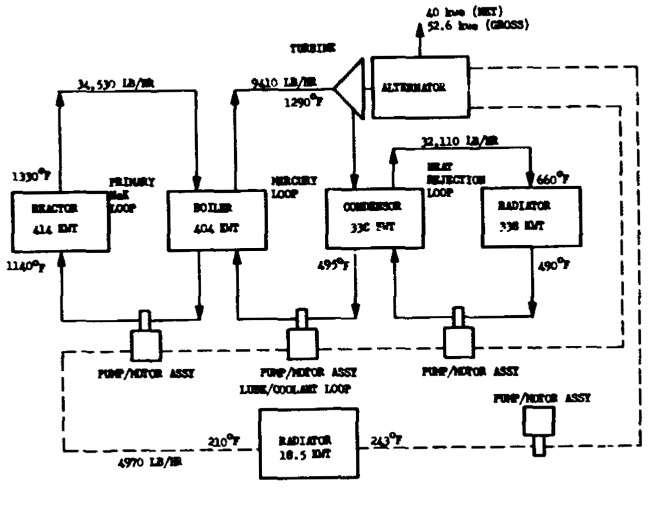

SCHEMATIC OF SNAP 8

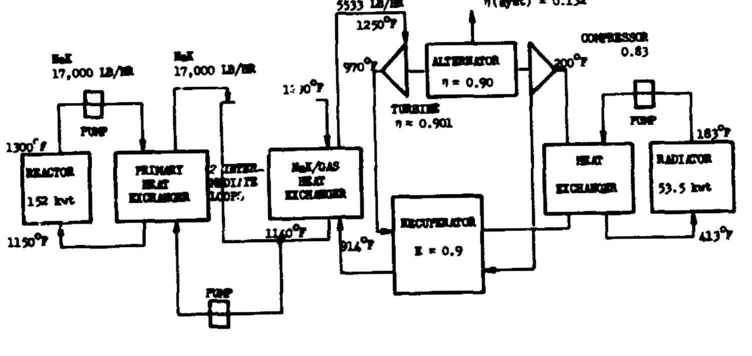

SCHEMATIC OF SNAP-8 REACTOR WITH BRAYTON-CYCLE

FIGURE 9-6 NUCLEAR REACTOR POWER SYSTEMS

TABLE 9-10

TYPICAL RADIOISOTOPE HEAT SOURCE CHARACTERISTICS

Thermal Power	Re-entry Protection	Capsule Dimensions	Capsule Wt (lb)	Heat Source Dimensions	Heat Source Wt (lb)	Unshielded Rad Level, 100 cm mrem/hr
0.1 kw	Graphite on indiv. capsule	~1.8" dia sphere	$\sim 1^1/_2$	2.8" cube **	~ 2	~ 7
1.0 kw	Graphite on indiv. capsule	~2.8" dia x 6.3" cylinder, spherical ends	$\sim 10^1/_2$	~ 3.8" dia x 7.3" cylinder spherical ends **	~15	~65
10.0 kw	Capsuled Arrayed in ablative re-entry vehicle *	~1.3" dia x 4.8" cylinder, spherical ends	$\sim 2^3/_4$	64 - 157 watt capsules in 25" dia array	~500 ***	~660

* Isotope re-entry vehicle is 44" dia blunted cone weighing ~335#

** 1/2" graphite protection

*** Includes capsule support structure, retention system heat sink & plate, truss support, and thermal insulation

Table 9-11

TYPICAL* CHARACTERISTICS OF SOLAR COLLECTOR/ABSORBER HEAT SOURCES

Useful heat absorbed, kw	0.10	1.00	10.0
Collector diameter, ft	1.25	3.95	12.5
Collector weight, lb	0.61	6.10	61.0
Focal length, ft	0.67	2.12	6.7
Aperture diameter, ft	0.037	0.12	0.37
Cavity absorber inner diameter, ft	0.15	0.47	1.5
Cavity absorber weight, lb	0.17	1.70	17.0
System weight, lb	0.94	9.36	93.6

* Basis:

Collector overall efficiency = 0.7

Absorber overall efficiency = 0.9

Rim angle = 50°

Aperture diameter = six times solar image at focal plane

Heat flux limit into heat storage material = 2.93 kw/ft^2

Collector specific weight = 0.5 lb/ft^2

Absorber specific weight = 5.0 lb/ft^2

Near earth orbit

System weight includes 20% for structure support and contingency but no allowance for heat storage material weight

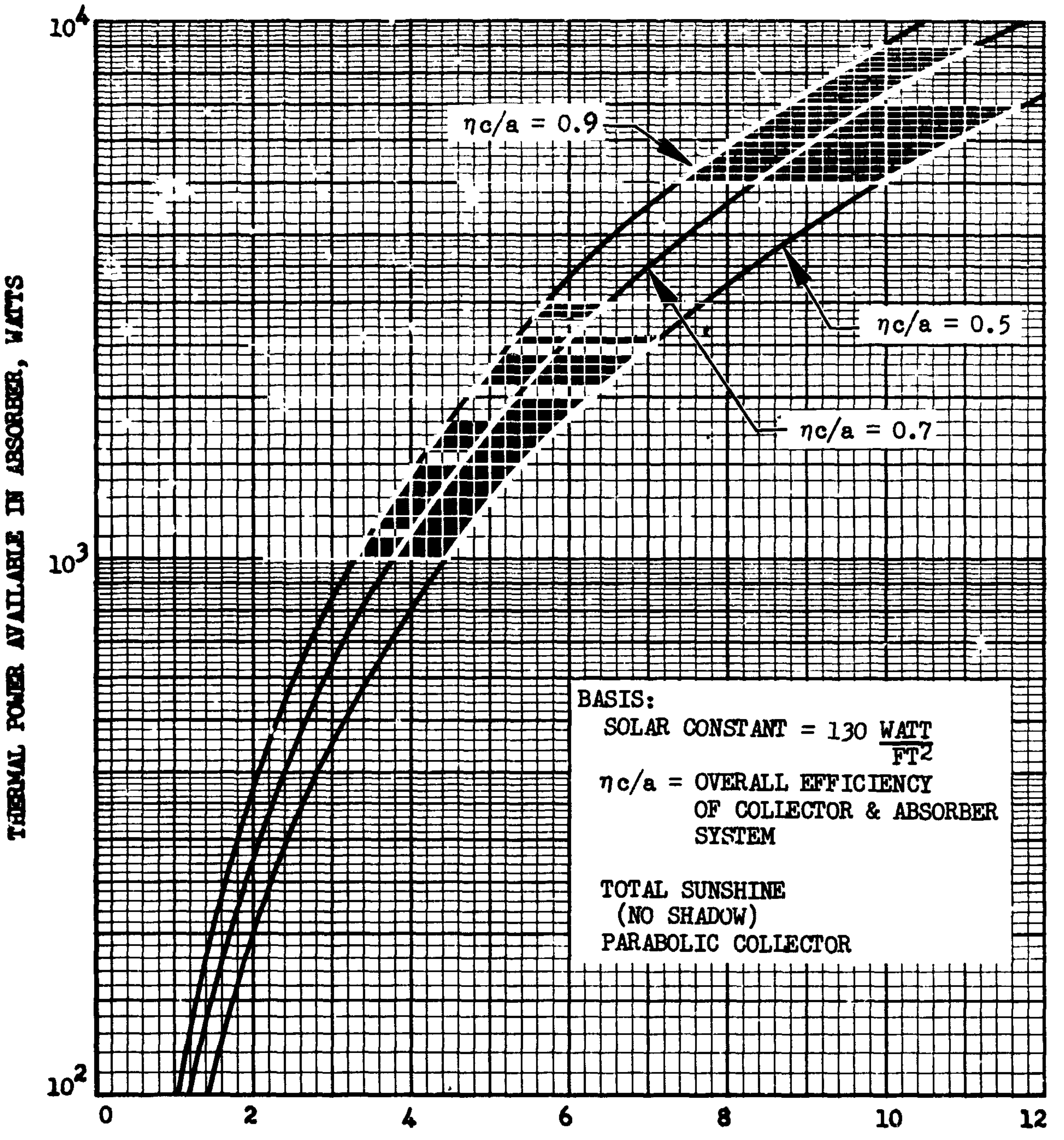

FIGURE 9-7 SOLAR COLLECTOR POWER VERSUS DIAMETER

Table 9-12

CHARACTERISTICS OF A SOLAR HEAT SOURCE
DESIGNED BY MINNEAPOLIS-HONEYWELL

Heat Intercepted by Collector	8.3 kw
Useful Heat for Refrig. (Ave. at 1250°F)	2.5 kw
Collector Diameter	9 ft
Rim Angle	105°
Collector Weight	75 lb
Receiver Diameter (Spherical)	9.7 in
Receiver Coating $\alpha_s = 0.8, \quad \epsilon = 0.12$	
Overall Efficiency	0.5
Potassium Heat Pipe Diameter	1 in
Percent Shadow Time	40%
Concentration Ratio	50
Heat Storage (Lithium Hydride in Cyl Pellows)	5.2 lb
Collector Pointing - 2 axes gimbal with 1° sun sensor and roll axis inertial wheel	

Section 10
CRYOGENS PROPERTIES

A limited amount of cryogen property data have been included in this report so that the user will have a handy source of some of the more often used data that is pertinent to cryogenic refrigeration. No attempt has been made to provide a comprehensive set of data because most of this information is available in NBS technical notes. If detailed property data is required it is suggested that other sources be utilized.

The data included here is the liquid density, saturated pressure, and heat of vaporization versus temperature for each of the cryogens; hydrogen, oxygen, fluorine and nitrogen. A plot of pressure versus internal energy for each of these cryogens has also been prepared and is included. It has been found that these plots greatly facilitate heat-pressure balance calculations in liquid cryogenic tanks.

A summary of the figures are given below.

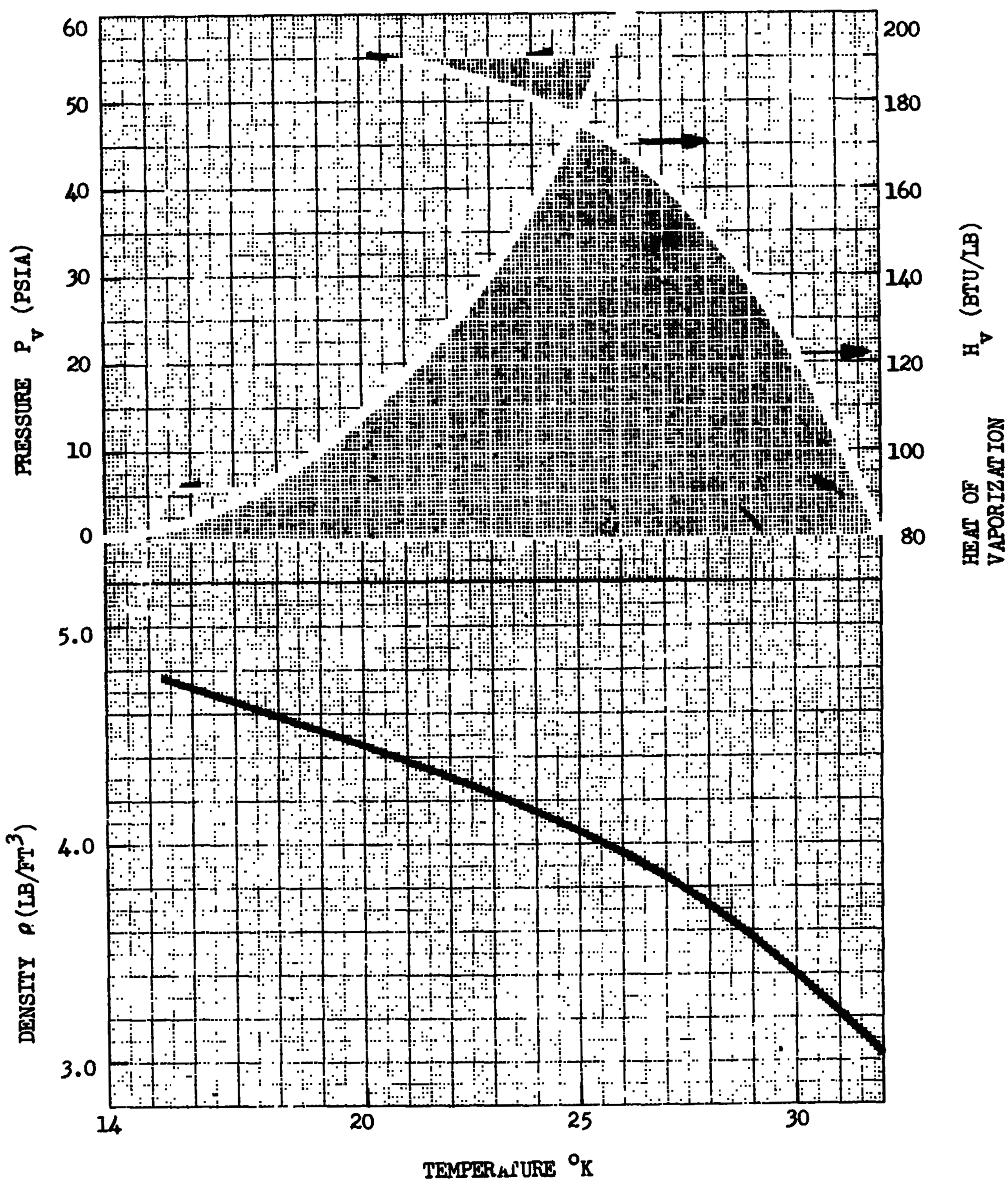

Figure 10-1 Properties of Liquid Hydrogen

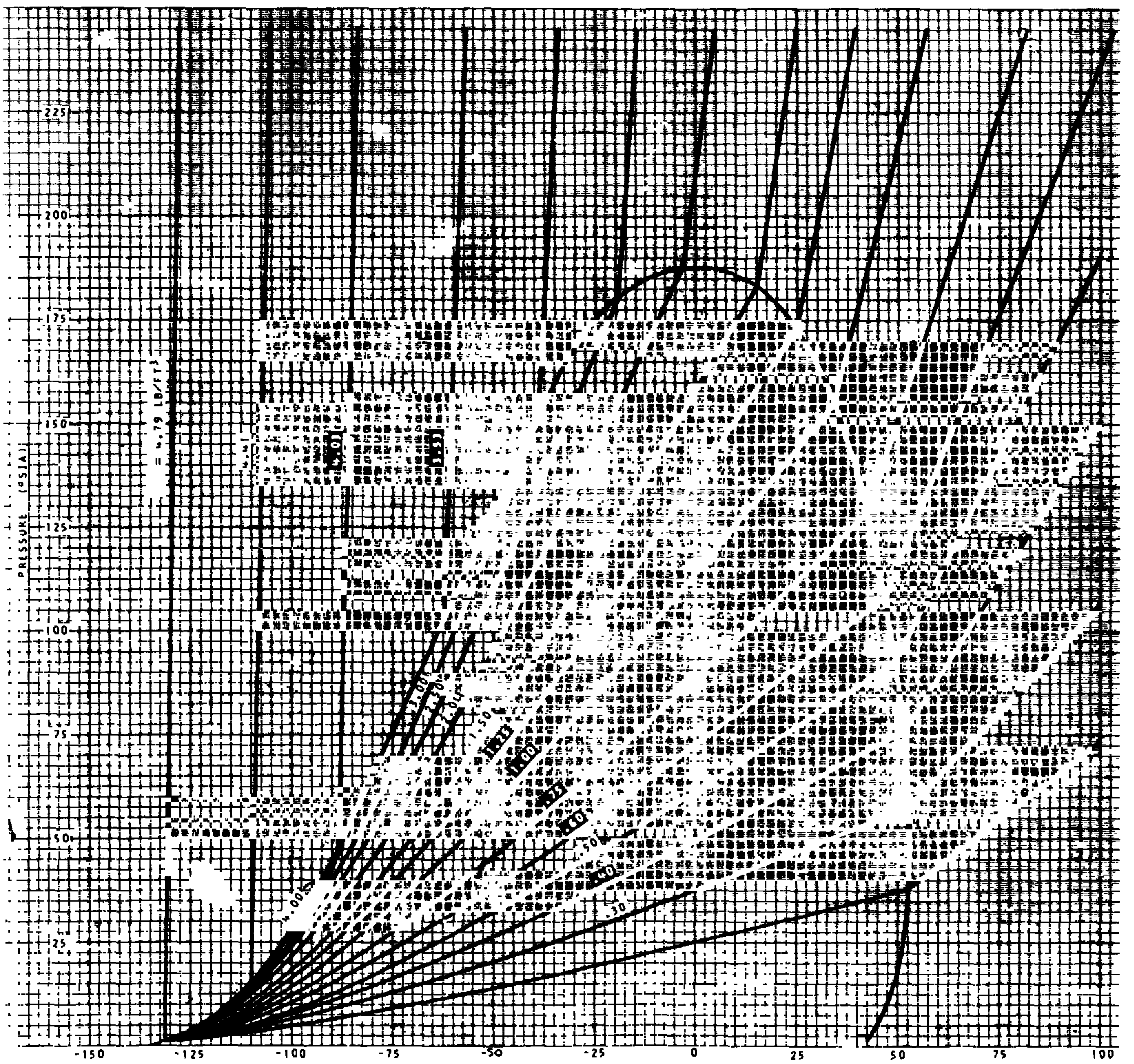

Figure 10-2 Pressure-Internal Energy of Hydrogen

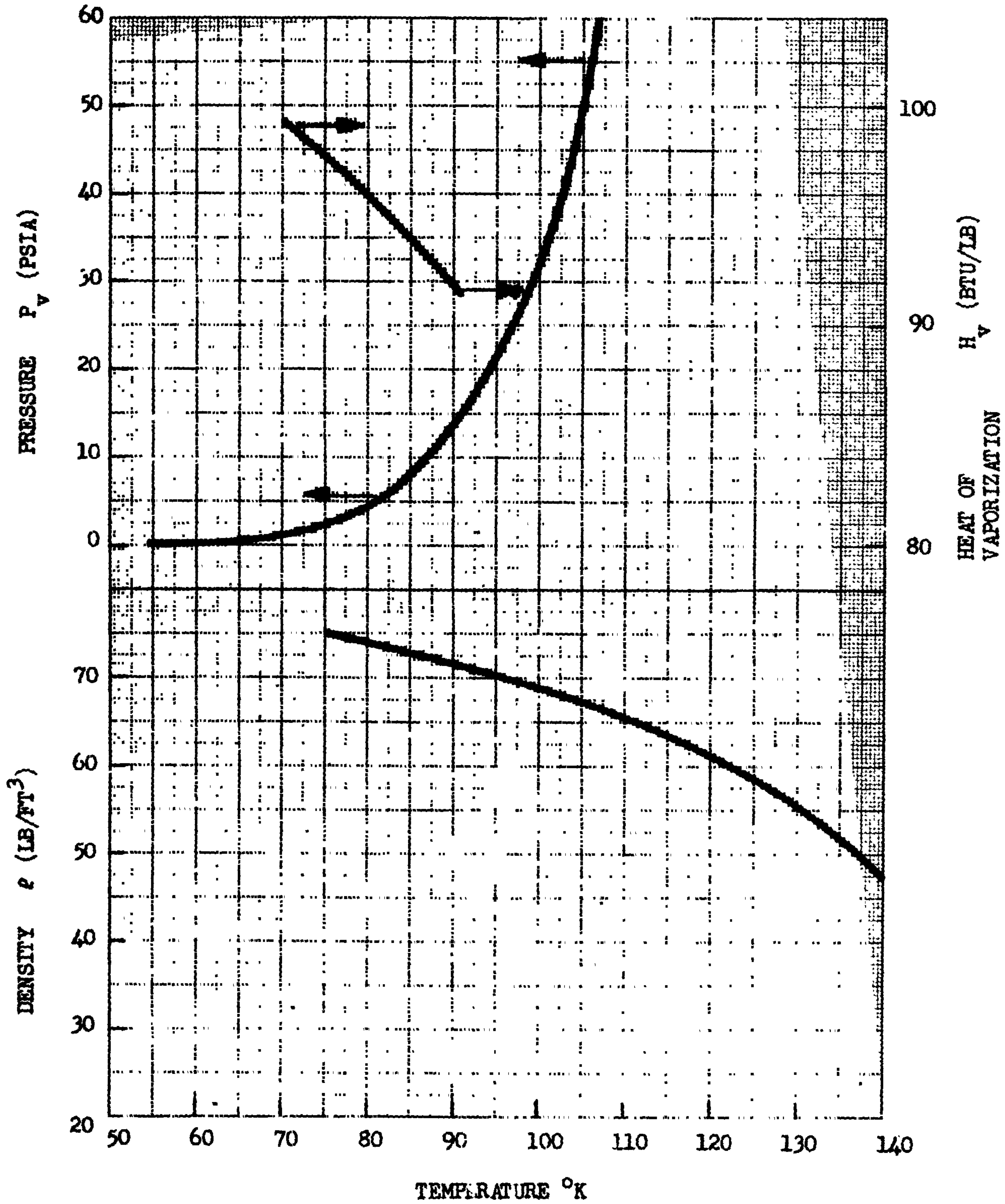

Figure 10-3 Properties of Liquid Oxygen

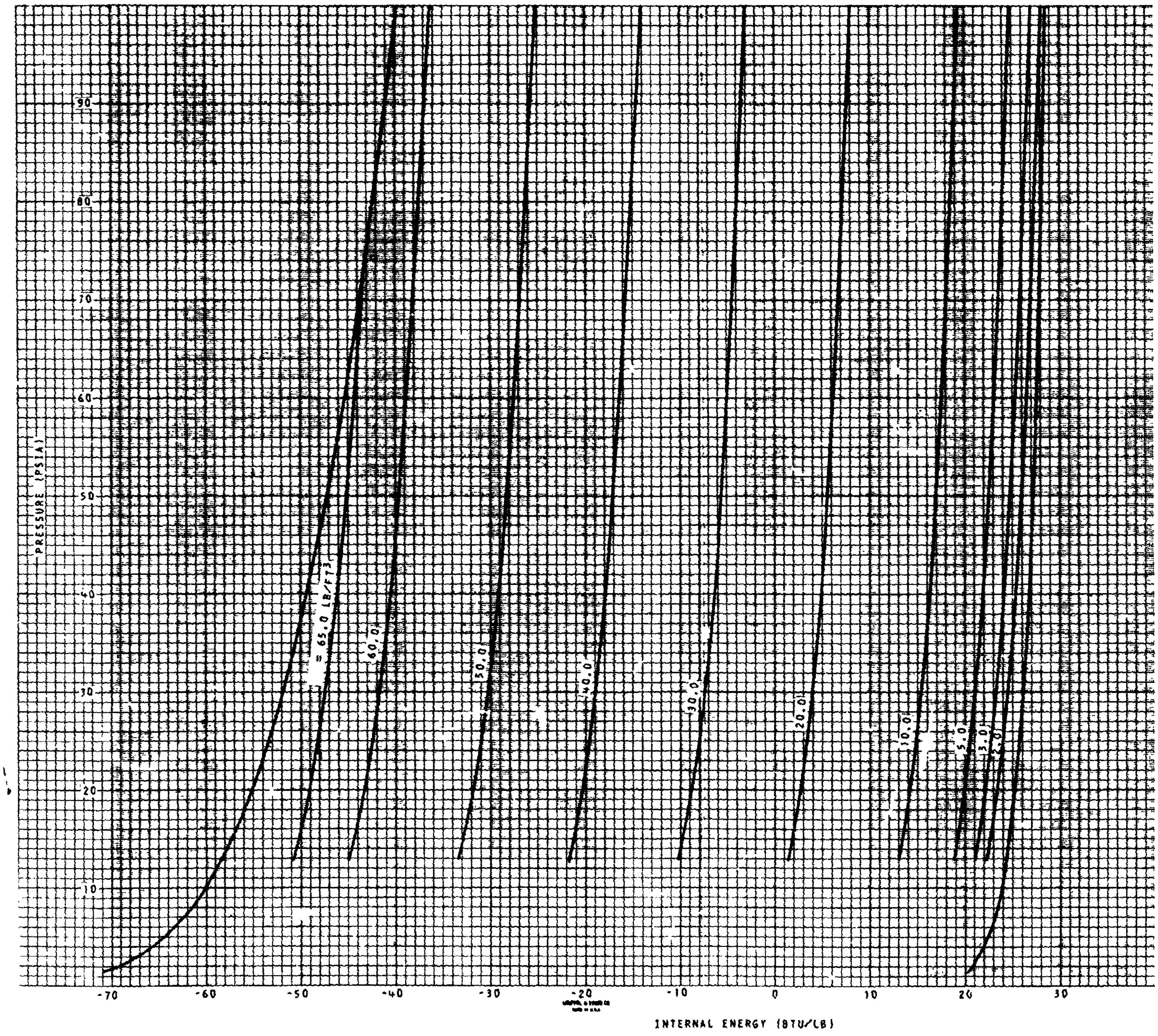

Figure 10-4 Pressure-Internal Energy of Oxygen

PRECEDING PAGE BLANK NOT FILMED

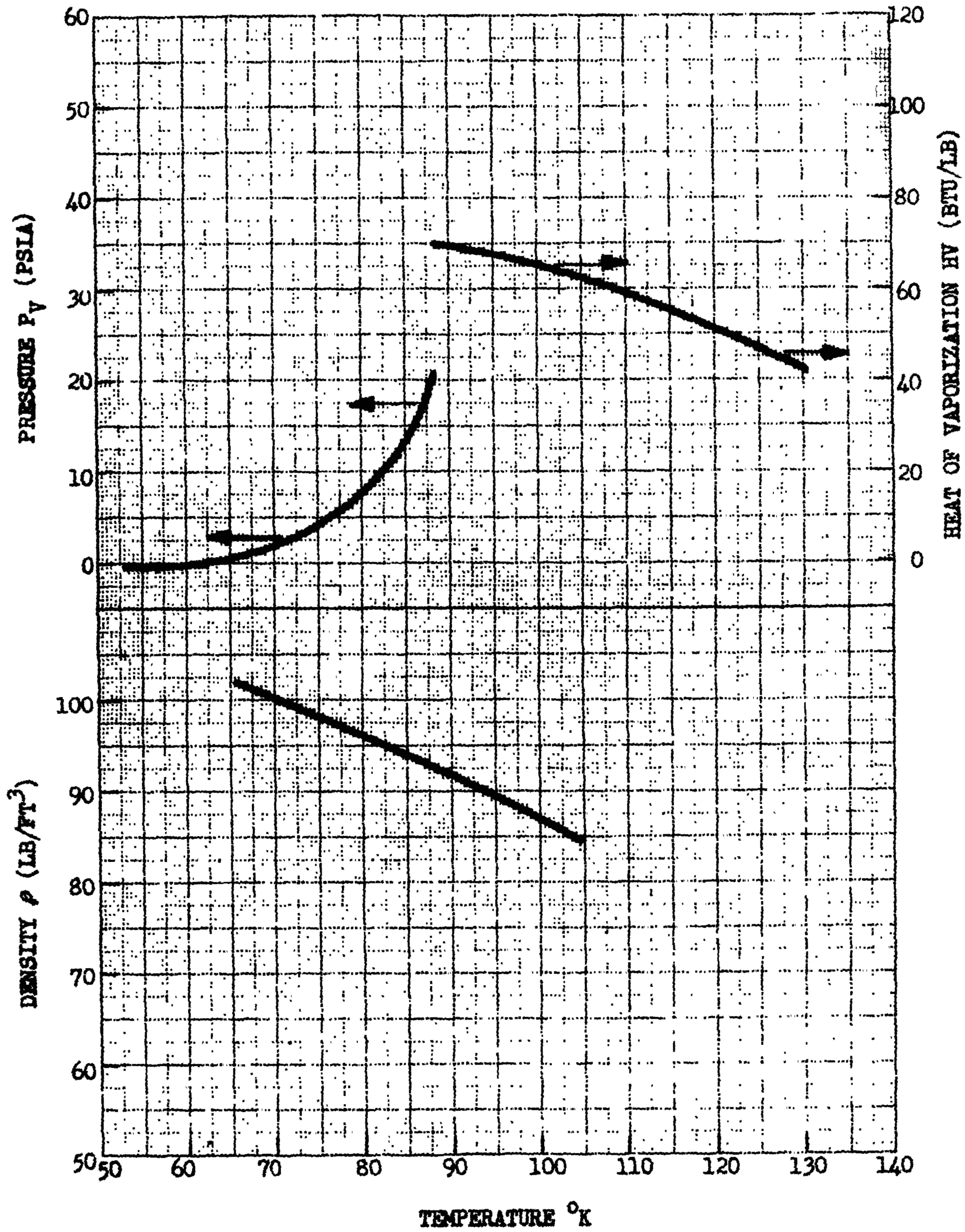

Figure 10-5 Properties of Liquid Fluorine

PRECEDING PAGE BLANK NOT FILMED

FOLDOUT FRAME 1

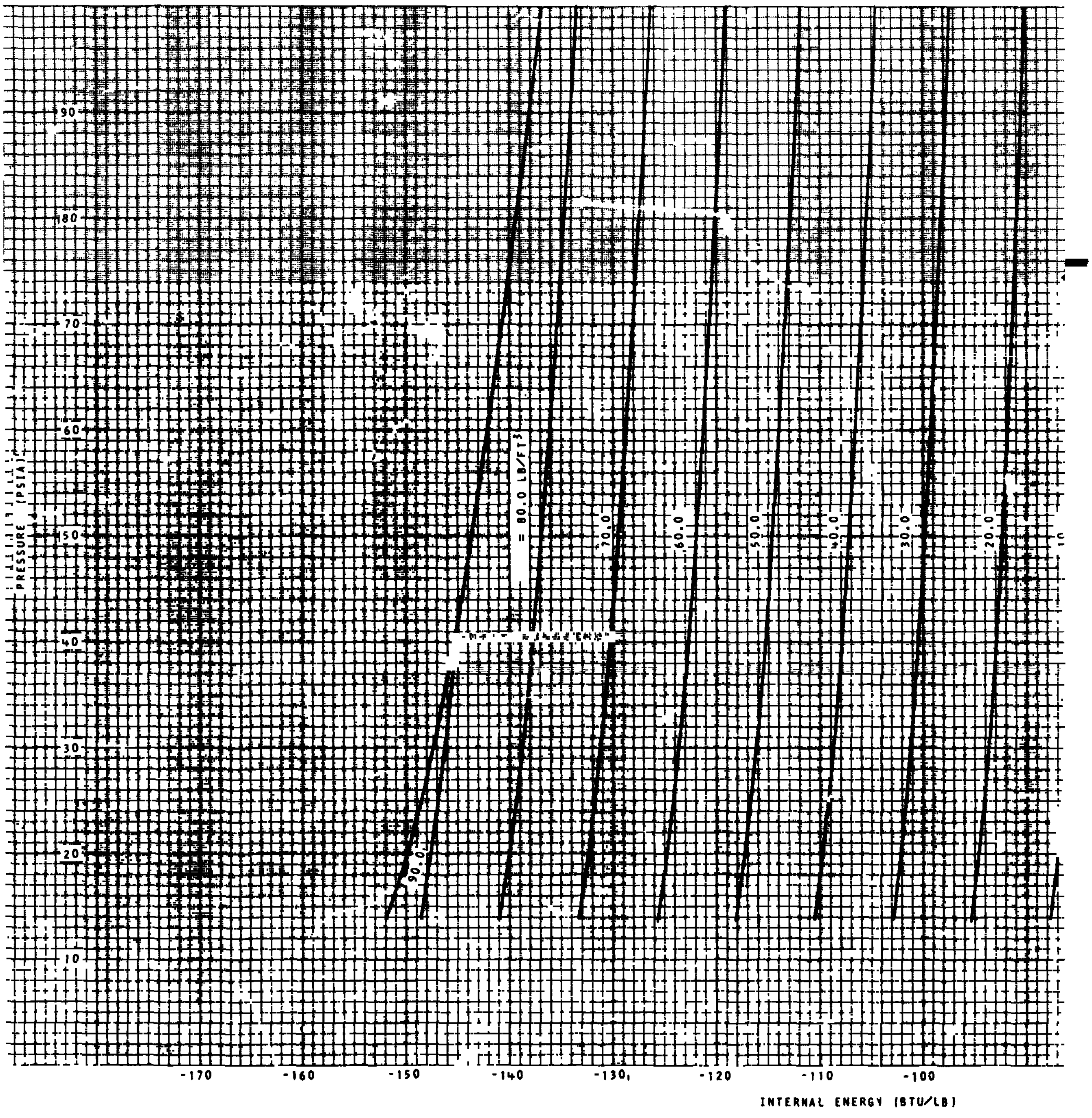

Figure 10-6 Pressure-Internal Energy

FOLDOUT FRAME 2

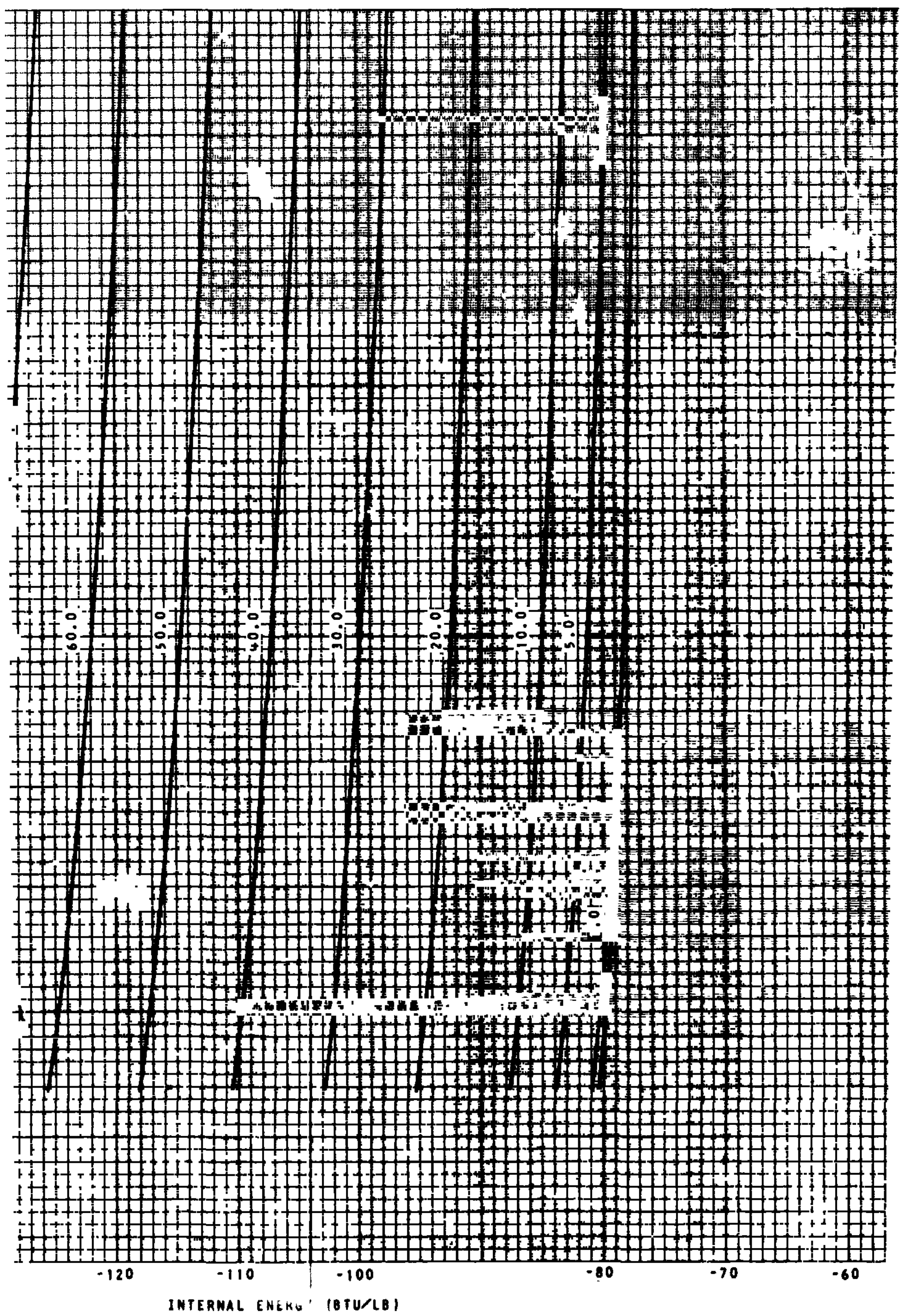

ure 10-6 Pressure-Internal Energy of Fluorine

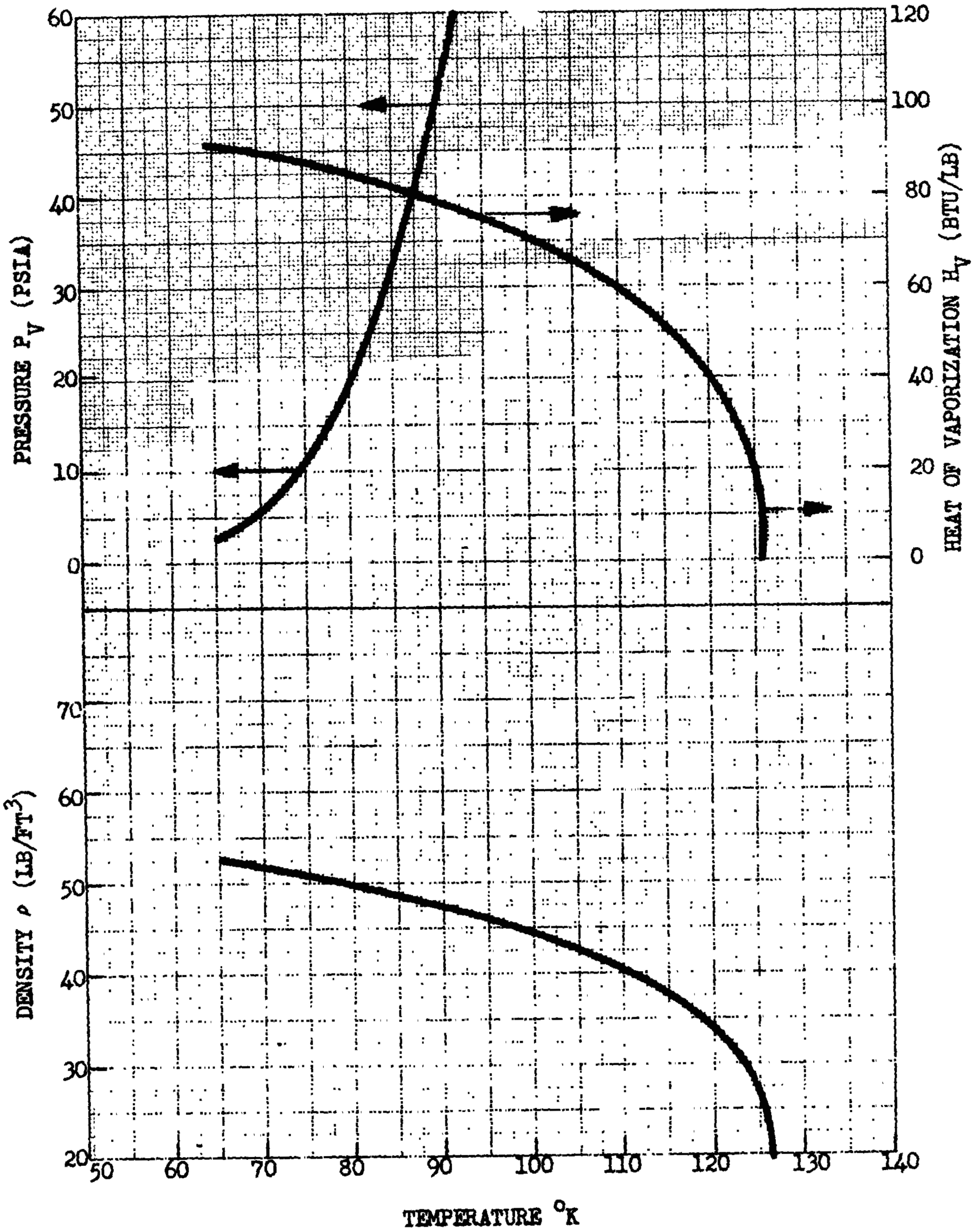

Figure 10-7 Properties of Liquid Nitrogen

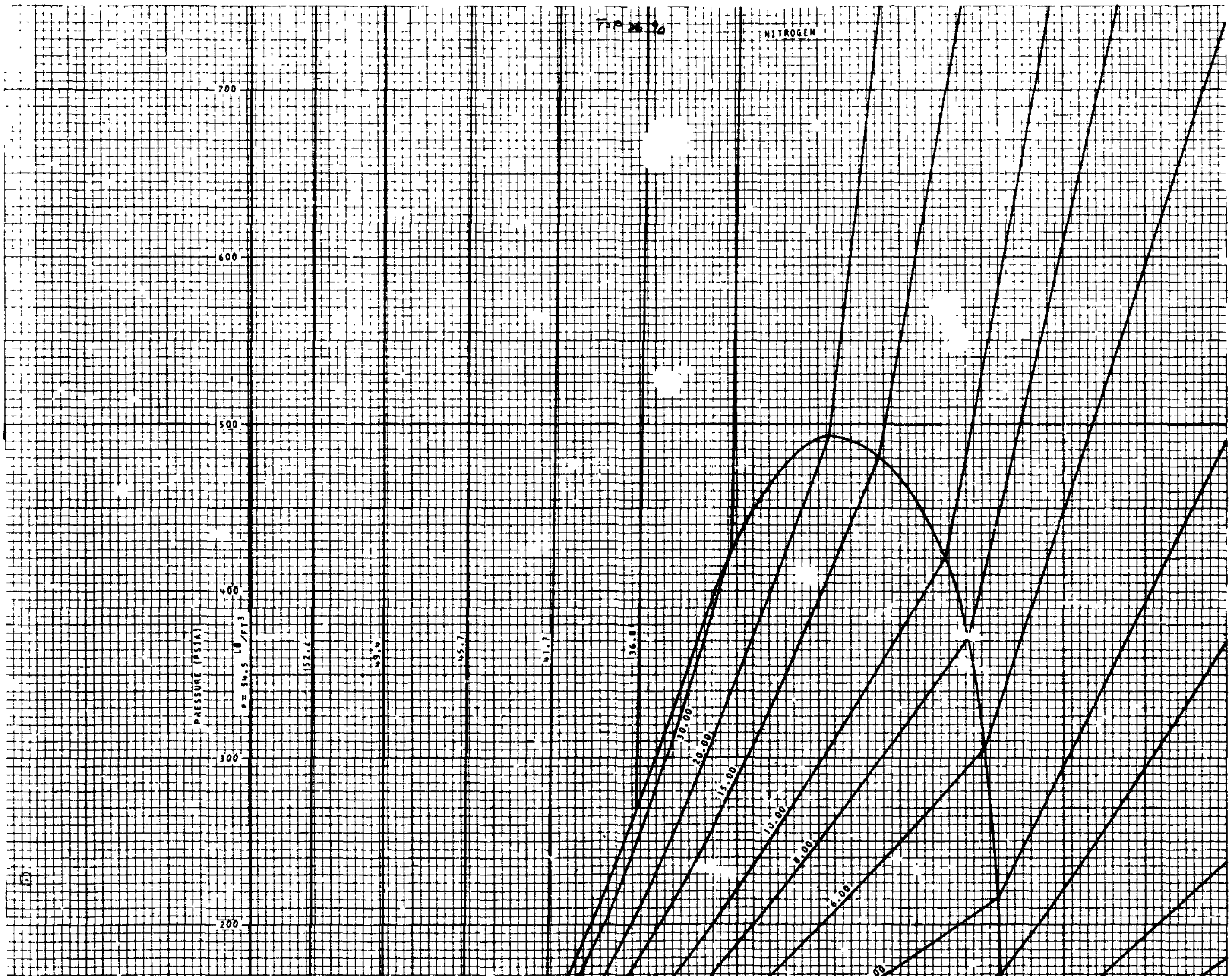

Figure 10-8 Pressure-Internal Energy of Nitrogen

Section 11
CONVERSION UNITS

11.1 INTRODUCTION

It has long been recognized that the use of varied and inconsistent systems of units in the various engineering and scientific disciplines has been a major source of inefficiency, errors and duplication of effort. Also, the lack of a common system of units has handicapped communication between engineers working in different fields of application of the same fundamental discipline.

To alleviate such communications problems on a world-wide basis, the International Committee on Weights and Measures has adopted a system referred to as the International System of Units (Reference 1). This system, abbreviated SI, is based on six fundamental units of measure as follows:

Length	meter	m
Mass	Kilogram	kg
Time	second	s
Electric Current	ampere	A
Thermodynamic Temperature . .	degrees Kelvin	^{o}K
Light Intensity	candle	cd

The purpose of this section is to provide the user of this referation material a convenient set of conversion units. There is presented in this section the definitions of the SI units, a list of thermodynamic constants giving their values in SI units, and a set of conversion tables. Since it is likely that continued emphasis will be placed on using the SI unit st attention has been directed toward them.

11.2 THE INTERNATIONAL SYSTEM OF UNITS

The system based on the six basic units mentioned above is referred to as the International System of Units; the international abbreviation of the name of this system is SI. The defined values of the basic units of measure are given in Table I and a partial list of the set of values of the physical constants recommended by NAS-NRC is given in Table III.

The term "mass" denotes the quantity of matter contained in material objects, and "weight" denotes a force acting on an object. The preferred unit of force is the newton (N); the pound force (lbf) is equivalent to 4.4482216 newton and the pound mass (lbm) is equivalent to .45358 kilogram. Thus a man of 70.0 kg (154 lbm) mass, standing on the surface of the moon where the gravitational acceleration is 1.62 m/s^2, weighs 113 newton (25.4 lbf). On the surface of the earth where the gravitational acceleration is 9.807 m/s^2 he would weigh 686 newton (154 lbf).

The preferred unit of energy (mechanical, electrical, thermal) is the joule (J). The mean British thermal unit (Btu) is equivalent to 1054.8 joules; thus a heat flow rate of 1 Btu per second (Btu/s) is equivalent to 1055 joules per second (J/s) or 1055 watts (W).

The preferred unit of pressure is the newton/meter^2 (N/m^2) or newton/centimeter^2 (N/cm^2). Thus 10.1 N/cm^2 is equivalent to 14.7 psi or 760 Torr.

11.3 SUMMARY OF CONVERSION DATA

The various basic and derived units are listed in the following tables. Also listed are the values of often used constants. An index to the various tables are given here.

These tables have been checked carefully; however, some errors may have escaped detection and the writer would appreciate having them brought to his attention so that corrections may be communicated to other users of these tables.

REF: (1) Translation of "Systeme International d'Unites. Resolution 12.", NASA TTF-8365, February 1963

Table 1

DEFINED VALUES OF BASIC UNITS AND EQUIVALENTS

Meter (m)	1 650 763.73 wavelengths in vacuo of the unperturbed transition $2p_{10}$-$5d_5$ in ^{86}Kr
Kilogram (kg)	Mass of the international kilogram at Sevres, France
Second (s)	1/31 556 925.974 7 of the tropical year at 12^h ET, 0 January 1900
Degrees Kelvin (^oK)	Defined in the thermodynamic scale by assigning 273.16^oK to the triple point of water (freezing point, $273.15^oK = 0^oC$)
Ampere (A)	Current required to produce a force of $2x10^{-7}$ newton per meter of length in two straight parallel conductors of infinite length placed 1 meter apart in a vacuum
Candle (cd)	1/60 of the intensity of 1 square centimeter of a black-body radiator operated at the freezing temperature of platinum
Unified atomic mass unit (u)	1/12 of the mass of an atom of the ^{12}C nuclide
Mole (mol)	Amount of substance containing the same number of atoms as 12g of pure ^{12}C
Standard acceleration of free fall (gn)	9.806 65 ms^{-2}, 980.665 cm s^{-2}
Normal atmospheric pressure (atm)	101 325 N m^{-2}

Table 2

SECONDARY UNITS IN THE INTERNATIONAL SYSTEM

Physical Quantity	Unit	
Area	square meter	m^2
Volume	cubic meter	m^3
Frequency	hertz	Hz, 1/s
Density	kilograms per cubic meter	kg/m^3
Velocity	meter per sec.	m/s
Angular velocity	radians per sec.	rad/s
Acceleration	meters per sec. squared	m/s^2
Angular acceleration	radians per sec. squared	rad/s^2
Force	newton per sq. meter	N, $kg.m/s^2$
Kinematic viscosity	sq. meter per second	m^2/s
Dynamic viscosity	newton-second per sq. meter	$N.s/m^2$
Work, energy, quantity of heat	joule	j, n.m
Power	watt	W, J/s
Electric charge	coulomb	C, A.s
Voltage, potential difference	volt	V, W/A
Electric field intensity	volt per meter	V/M
Electric resistance	ohm	Ω, V/A
Electric capacitance	farad	F, A.s/V
Magnetic flux	weber	Wb, V.s
Inductance	henry	H, V.s/A
Magnetic field	tesla	T, Wb/m^2
Magnetic field intensity	amperes per meter	A/M

Table 2 (Cont.)

Physical Quantity	Unit	
Magnetomotive force	ampere	A
Flux of light	lumen	lm, cd.sr
Luminance	candle per sq. meter	cd/m^2
Illumination	lux	lx, lm/m^2
Plane angle	radian	rad
Solid angle	steradian	sr
Pressure	newtons per sq. meter	N/m^2

Table 3

VALUES OF PHYSICAL CONSTANTS IN SI UNITS

Constant	Symbol	Value
Speed of light in vacuum	c	2.997925×10^{8} ms^{-1}
Elemenetary charge	e	1.60210×10^{-19} C
Avogadro constant	N_A	6.02252×10^{23} mol^{-1}
Electron rest mass	m_e	9.1091×10^{-31} kg 5.48597×10^{-4} u
Planck constant	h	6.6256×10^{-34} Js
Gas constant	R	8.3143 J $^{o}K^{-1}mol^{-1}$
Normal volume perfect gas	Vo	2.24136×10^{-2} $m^{3}mol^{-1}$
Boltzmann constant	k	1.38054×10^{-23} J $^{o}K^{-1}$
First radiation constant	c_1	3.7405×10^{-16} Wm^{2}
Second radiation constant	c_2	1.43879×10^{-2} $m^{o}K$
Wein displacement constant	b	2.8978×10^{-3} m ^{o}K
Stefan-Boltzmann constant	σ	5.6697×10^{-8} Wm^{-2} $^{o}K^{-4}$
Gravitational constant	G	6.670×10^{-11} $Nm^{2}kg^{-2}$
Mean solar constant	S	1.40×10^{3} Wm^{-2}

Table 4

LENGTH

MULTIPLY NUMBER OF → BY → TO OBTAIN ↓	CENTIMETERS*	FEET	INCHES	KILOMETERS	NAUTICAL MILES	METERS*	MILES	MILLIMETERS*
CENTIMETERS*	1	30.48	2.540	10^5	1.853×10^5	100	1.609×10^5	0.1
FEET	3.281×10^{-2}	1	8.333×10^{-2}	3281	6030.27	3.281	5280	3.281×10^{-3}
INCHES	0.3937	12	1	3.937×10^4	7.296×10^4	39.37	6.336×10^4	3.937×10^{-2}
KILOMETERS*	10^{-5}	3.048×10^{-4}	2.540×10^{-5}	1	1.853	0.001	1.609	10^{-6}
NAUTICAL MILES	5.396×10^{-6}	1.645×10^{-4}	1.371×10^{-5}	0.5396	1	5.396×10^{-4}	0.8684	5.396×10^{-7}
METERS*	0.01	0.3048	2.540×10^{-2}	1000	1853	1	1609	10^{-3}
MILES	6.214×10^{-6}	1.894×10^{-4}	1.578×10^{-5}	0.6214	1.1516	6.214×10^{-4}	1	6.214×10^{-7}
MILLIMETERS*	10	304.8	25.40	10^6	1.853×10^6	1000	1.609×10^6	1

Table 5

AREA

MULTIPLY NUMBER OF → BY TO OBTAIN ↓	SQUARE* CENTIMETERS	SQUARE FEET	SQUARE INCHES	SQUARE KILOMETERS	SQUARE* METERS	SQUARE MILES	SQUARE MILLIMETERS
SQUARE* CENTIMETERS	1	929.0	6.452	10^{10}	10^{4}	2.590×10^{10}	0.01
SQUARE FEET	1.076×10^{-3}	1	6.944×10^{-3}	1.076×10^{7}	10.764	2.788×10^{7}	1.076×10^{-5}
SQUARE INCHES	0.1550	144	1	1.550×10^{9}	1550	4.015×10^{9}	1.550×10^{-3}
SQUARE KILOMETERS	10^{-10}	9.290×10^{-8}	6.452×10^{-10}	1	10^{-6}	2.590	10^{-12}
SQUARE* METERS	0.0001	9.290×10^{-2}	$6\ 452 \times 10^{-4}$	10^{6}	1	2.590×10^{6}	10^{-6}
SQUARE MILES	3.861×10^{-11}	3.567×10^{-8}	2.4907×10^{-10}	0.3861	3.861×10^{-7}	1	3.861×10^{-13}
SQUARE MILLIMETERS	100	9.290×10^{4}	645.2	10^{12}	10^{6}	2.590×10^{12}	1

Table 6

VOLUME

MULTIPLY NUMBER OF BY TO OBTAIN	CUBIC* CENTIMETERS	CUBIC FEET	CUBIC INCHES	CUBIC* METERS	GALLONS (LIQUID)	LITERS
CUBIC* CENTIMETER	1	2.832×10^4	16.39	10^6	3785	1000
CUBIC FEET	3.531×10^{-5}	1	5.787×10^{-4}	35.314	0.1337	3.531×10^{-2}
CUBIC INCHES	6.102×10^{-2}	1728	1	6.102×10^4	231	61.02
CUBIC* METERS	10^{-6}	2.832×10^{-2}	1.639×10^{-5}	1	3.785×10^{-3}	0.001
GALLONS (LIQUID)	2.642×10^{-4}	7.481	4.329×10^{-3}	264.2	1	0.2642
LITERS	0.001	28.32	1.639×10^{-2}	1000	3.785	1

Table 7

LINEAR VELOCITY

MULTIPLY NUMBER OF → BY TO OBTAIN ↓	CENTIMETERS PER SECOND	FEET PER MINUTE	FEET PER SECOND	KILOMETERS PER HOUR	KILOMETERS PER MINUTE	METERS PER MINUTE	METERS* PER SECOND
CENTIMETERS PER SECOND	1	0.5080	30.48	27.78	1667	1.667	100
FEET PER MINUTE	1.969	1	60	54.68	3281	3.281	196.8
FEET PER SECOND	3.281 x 10^{-2}	1.667 x 10^{-2}	1	0.9113	54.68	5.468 x 10^{-2}	3.281
KILOMETERS PER HOUR	0.036	1.829 x 10^{-2}	1.097	1	60	0.06	3.6
KILOMETERS PER MINUTE	0.0006	3.048 x 10^{-4}	1.829 x 10^{-2}	1.667 x 10^{-2}	1	0.001	0.06
METERS PER MINUTE	0.6	0.3048	18.29	16.67	1000	1	60
METERS* PER SECOND	0.01	5.080 x 10^{-3}	0.3048	0.2778	16.67	1.667 x 10^{-2}	1

Table 8

ANGULAR VELOCITY

MULTIPLY NUMBER OF → BY TO OBTAIN ↓	DEGREES PER SECOND	RADIANS* PER SECOND	REVOLUTIONS PER MINUTE	REVOLUTIONS PER SECOND
DEGREES PER SECOND	1	57.30	6	360
RADIANS* PER SECOND	1.745 x 10^{-2}	1	0.1047	6.283
REVOLUTIONS PER MINUTE	0.1667	9.549	1	60
REVOLUTIONS PER SECOND	2.778 10^{-3}	0.1592	1.667 x 10^{-2}	1

Table 9

LINEAR ACCELERATION

TO OBTAIN ↓ / MULTIPLY NUMBER OF → BY	CENTIMETERS PER SECOND PER SECOND	FEET PER SECOND PER SECOND	KILOMETERS PER HOUR PER SECOND	METERS* PER SECOND PER SECOND	MILES PER HOUR PER SECOND
CENTIMETERS PER SECOND PER SECOND	1	30.48	27.78	100	44.70
FEET PER SECOND PER SECOND	3.281 X 10^{-2}	1	0.9113	5.281	1.467
KILOMETERS PER HOUR PER SECOND	0.036	1.097	1	3.6	1.609
METERS* PER SECOND PER SECOND	0.01	0.3048	0.2778	1	0.4470
MILES PER HOUR PER SECOND	2.237 X 10^{-2}	0.6818	0.6214	2.237	1

Table 10

ANGULAR ACCELERATION

TO OBTAIN ↓ / MULTIPLY NUMBER OF → / BY	RADIANS* PER SECOND PER SECOND	REVOLUTIONS PER MINUTE PER MINUTE	REVOLUTIONS PER MINUTE PER SECOND	REVOLUTIONS PER SECOND PER SECOND
RADIANS* PER SECOND PER SECOND	1	1.745 x 10^{-3}	0.1047	6.283
REVOLUTIONS PER MINUTE PER MINUTE	573.0	1	60	3600
REVOLUTIONS PER MINUTE PER SECOND	9.549	1.667 x 10^{-2}	1	60
REVOLUTIONS PER SECOND PER SECOND	0.1592	2.778 x 10^{-4}	1.667 x 10^{-2}	1

TABLE 11 - MASS AND WEIGHT

TO OBTAIN ↓ / BY / MULTIPLY NUMBER OF →	GRAMS*	KILOGRAMS*	MILLIGRAMS	OUNCES	POUNDS
GRAMS*	1	1000	0.001	28.35	453.6
KILOGRAMS*	0.001	1	10^{-6}	2.835×10^{-2}	0.4536
MILLIGRAMS	1000	10^{6}	1	2.835×10^{4}	4.536×10^{5}
OUNCES	3.527×10^{-2}	35.27	3.527×10^{-5}	1	16
POUNDS	2.205×10^{-3}	2.205	2.205×10^{-6}	6.250×10^{-2}	1

Table 12

DENSITY

TO OBTAIN ↓ / BY / MULTIPLY NUMBER OF →	GRAMS PER CUBIC CENTIMETER	KILOGRAMS* PER CUBIC METER	POUNDS PER CUBIC FOOT	POUNDS PER CUBIC INCH
GRAMS PER CUBIC CENTIMETER	1	0.001	1.602×10^{-2}	27.63
KILOGRAMS* PER CUBIC METER	1000	1	16.02	2.768×10^{4}
POUNDS PER CUBIC FOOT	62.43	6.243×10^{-2}	1	1728
POUNDS PER CUBIC INCH	3.613×10^{-2}	3.613×10^{-5}	5.787×10^{-4}	1

Table 13

FORCE

MULTIPLY NUMBER OF → BY TO OBTAIN ↓	DYNES	GRAMS	JOULES PER CM	NEWTONS* OR JOULES PER METER	KILOGRAMS	POUNDS	POUNDALS
DYNES	1	980.7	10^{7}	10^{5}	9.807×10^{5}	4.448×10^{5}	1.383×10^{4}
GRAMS	1.028×10^{-3}	1	1.020×10^{4}	102.0	1000	453.6	14.10
JOULES PER CM	10^{-7}	9.807×10^{-5}	1	0.01	9.807×10^{-2}	4.448×10^{-2}	1.383×10^{-3}
NEWTONS* OR JOULES PER METER	10^{-5}	9.807×10^{-3}	100	1	9.807	4.448	0.1383
KILOGRAMS	1.020×10^{-6}	0.001	10.20	0.1020	1	0 4536	1.410×10^{-2}
POUNDS	2.248×10^{-6}	2.205×10^{-3}	22.48	0.2248	2.205	1	3.108×10^{-2}
POUNDALS	7.233×10^{-5}	7.093×10^{-2}	725.3	7.233	70.93	32.17	1

Table 14

PRESSURE OR FORCE PER UNIT PER AREA

TO OBTAIN ↓ / MULTIPLY NUMBER OF → BY	ATMOSPHERES	DYNES PER SQUARE CENTIMETER	MILLIMETERS OF MERCURY AT $0^{o}C$	INCHES OF MERCURY AT $0^{o}C$	KILOGRAMS PER SQUARE METER	POUNDS PER SQUARE FOOT	POUNDS PER SQUARE INCH	NEWTONS* PER SQUARE METER
ATMOSPHERES	1	9.869×10^{-7}	1.316×10^{-3}	3.342×10^{-2}	9.678×10^{-5}	4.725×10^{-4}	6.804×10^{-2}	9.869×10^{-6}
DYNES PER SQUARE CENTIMETER	1.013×10^{-6}	1	1.333×10^{3}	3.386×10^{4}	98.07	478.8	6.895×10^{4}	10
MILLIMETERS OF MERCURY AT $0^{o}C$	760.0	7.501×10^{-4}	1	25.40	7.356×10^{-2}	0.3591	51.71	7.50×10^{-3}
INCHES OF MERCURY AT $0^{o}C$	29.92	2.953×10^{-5}	3.937×10^{-2}	1	2.896×10^{-3}	1.414×10^{-2}	2.036	1.953×10^{-4}
KILOGRAMS PER SQUARE METER	1.033×10^{4}	1.020×10^{-2}	13.60	345.3	1	4.882	703.1	0.1020
POUNDS PER SQUARE FOOT	2117	2.089×10^{-3}	2.7845	70.73	0.2048	1	144	2.089×10^{-2}
POUNDS PER SQUARE INCH	14.70	1.450×10^{-5}	1.9337×10^{-2}	0.4912	1.422×10^{-3}	6.944×10^{-3}	1	1.450×10^{-4}
NEWTONS* PER SQUARE METER	1.013×10^{5}	0.10	133.3	3.386×10^{3}	9.807	47.88	6.395×10^{3}	1

Table 15

TORQUE

BY MULTIPLY NUMBER OF → / TO OBTAIN ↓	DYNE-CENTIMETERS	GRAM-CENTIMETERS	KILOGRAM-METERS	POUND-FEET	NEWTON*-METER
DYNE-CENTIMETERS	1	980.7	9.807×10^{7}	1.356×10^{7}	10^{7}
GRAM CENTIMETERS	1.020×10^{-3}	1	10^{5}	1.383×10^{4}	1.020×10^{4}
KILOGRAM METERS	1.020×10^{-3}	10^{-5}	1	0.1383	0.1020
POUND-FEET	7.376×10^{-3}	7.233×10^{-5}	7.233	1	0.7376
NEWTON-* METER	10^{-7}	9.807×10^{-4}	9.807	1.305	1

Table 16

MOMENT OF INERTIA

MULTIPLY NUMBER OF → BY TO OBTAIN ↓	GRAM-CENTIMETERS SQUARED	KILOGRAM-* METERS SQUARED	POUND-INCHES SQUARED	POUND-FEET SQUARED
GRAM-CENTIMETERS SQUARED	1	10^7	2.9266×10^3	4.21434×10^5
KILOGRAM-* METERS SQUARED	10^{-7}	1	2.9266×10^{-4}	4.21434×10^{-2}
POUND-INCHES SQUARED	3.4169×10^{-4}	3.4169×10^3	1	144
POUND-FEET SQUARED	2.37285×10^{-6}	23.7285	6.944×10^{-3}	1

Table 17

ENERGY, WORK, AND HEAT

MULTIPLY NUMBER OF → BY → TO OBTAIN ↓	BRITISH THERMAL UNITS	CENTIMETER-GRAMS	ERGS OR CENTIMETER-DYNES	FOOT-POUNDS	HORSEPOWER HOURS	JOULES, WATT-SECONDS OR NEWTON - METERS	KILOGRAM-CALORIES	WATT-HOURS
BRITISH THERMAL UNITS	1	9.297×10^{-8}	9.480×10^{-11}	1.285×10^{-3}	2545	9.4709×10^{-4}	3.969	3.413
CENTIMETER-GRAMS	1.076×10^{7}	1	1.020×10^{-3}	1.383×10^{4}	2.737×10^{10}	1.020×10^{4}	4.269×10^{7}	3.671×10^{7}
ERGS OR CENTIMETER-DYNES	1.055×10^{10}	980.7	1	1.356×10^{7}	2.684×10^{13}	10^{7}	4.186×10^{10}	3.60×10^{10}
FOOT-POUNDS	778.3	7.233×10^{-5}	7.367×10^{-8}	1	1.98×10^{6}	0.7376	3087	2655
HORSEPOWER-HOURS	3.929×10^{-4}	3.654×10^{-11}	3.722×10^{-14}	5.050×10^{-7}	1	3.722×10^{-7}	1.559×10^{-3}	1.341×10^{-3}
JOULES, WATT-SECONDS OR NEWTON - METERS	1055.87	9.507×10^{-5}	10^{-7}	1.356	2.684×10^{6}	1	4186	3600
KILOGRAM-CALORIES	0.2520	2.343×10^{-8}	2.389×10^{-11}	3.239×10^{-4}	641.3	2.389×10^{-4}	1	0.8600
WATT-HOURS	0.2930	2.724×10^{-8}	2.778×10^{-11}	3.766×10^{-4}	745.7	2.778×10^{-4}	1.163	1

Table 18

POWER, HEAT FLUX, RADIANT FLUX

TO OBTAIN ↓ / BY / MULTIPLY NUMBER OF →	BRITISH THERMAL UNITS PER SECOND	BRITISH THERMAL UNITS PER HOUR	ERGS PER SECOND	FOOT-POUNDS PER SECOND	HORSEPOWER	KILOGRAM-CALORIES PER MINUTE	WATTS*	KILOWATTS
BRITISH THERMAL UNITS PER SECOND	1	2.777×10^{-4}	9.480×10^{-11}	1.285×10^{-3}	0.707	6.614×10^{-2}	9.480×10^{-4}	0.9480
BRITISH THERMAL UNITS PER HOUR	3600	1	3.413×10^{-7}	4.6275	2.545×10^{3}	233.1	3.413	3.413×10^{3}
ERGS PER SECOND	1.0548×10^{10}	2.930×10^{6}	1	1.356×10^{7}	7.457×10^{9}	6.977×10^{8}	10^{7}	10^{10}
FOOT-POUNDS PER SECOND	778	0.2161	7.376×10^{-8}	1	550	51.44	0.7376	737.6
HORSEPOWER	1.414	$3\ 929 \times 10^{-4}$	1.341×10^{-10}	1.818×10^{-3}	1	9.355×10^{-2}	1.341×10^{-3}	1.341
KILOGRAM-CALORIES PER MINUTE	15.12	4.20×10^{-3}	1.433×10^{-9}	1.943×10^{-2}	10.69	1	1.433×10^{-2}	14.33
WATTS*	1054.8	0.2930	10^{-7}	1.356	745.7	69.77	1	1000
KILOWATTS	1.0548	2.930×10^{-4}	10^{-7}	1.356×10^{-3}	0.7457	6.977×10^{-2}	10^{-3}	1

Table 19

POWER DENSITY, HEAT FLUX DENSITY

MULTIPLY NUMBER OF → / BY / TO OBTAIN ↓	BTU PER SECOND PER SQUARE FOOT	BTU PER HOUR PER SQUARE FOOT	ERGS PER SECOND PER SQUARE CENTIMETER	FOOT-POUNDS PER SECOND PER SQUARE FOOT	WATTS PER SQUARE CENTIMETER	WATTS PER SQUARE METER	WATTS PER SQUARE FOOT
BTU PER SECOND PER SQUARE FOOT	1	2.777×10^{-4}	8.807×10^{-8}	1.285×10^{-3}	0.8807	8.807×10^{-5}	9.480×10^{-4}
BTU PER HOUR PER SQUARE FOOT	3600	1	3.171×10^{-4}	4.626	3171	0.3171	3.413
ERGS PER SECOND PER SQUARE CENTIMETER	1.1354×10^{7}	3153	1	1.459×10^{4}	10^{7}	1000	1.076×10^{4}
FOOT-POUNDS PER SECOND PER SQUARE FOOT	778	0.2161	6.852×10^{-5}	1	685.2	6.852×10^{-2}	0.7375
WATTS PER SQUARE CENTIMETER	1.1354	3.153×10^{-4}	10^{-7}	1.459×10^{-3}	1	10^{4}	1.076×10^{-3}
WATTS PER SQUARE METER	1.1354×10^{4}	3.153	10^{-3}	14.59	10^{4}	1	10.76
WATTS PER SQUARE FOOT	1054.8	0.2929	9.290×10^{-5}	1.355	929	9.290×10^{-2}	1

Table 20

TEMPERATURE

$X^{o}K$ =	. . . . .	$(T^{o}C) + 273.16$	$0.556(T^{o}F-32)+273.16$	$0.556\ (T^{o}R)$
$X^{o}C$ =	$(T^{o}K) - 273.16$	. . . . .	$0.556\ (T^{o}F - 32)$	$0.556\ (T^{o}R - 491.6)$
$X^{o}F$ =	$1.8(T^{o}K - 273.16)+32$	$1.8\ (T^{o}C) + 32$	. . . . .	$(T^{o}K) - 459.6$
$X^{o}R$ =	$1.8\ (T^{o}K)$	$1.8\ (T^{o}C) + 491.6$	$(T^{o}F + 459.6$	. . . . .

Note: ^{o}K = Degrees Kelvin
^{o}C = Degrees Centigrade or Celsius
^{o}F = Degrees Fahrenheit
^{o}R = Degrees Rankine

Table 21

THERMAL CONDUCTIVITY

MULTIPLY NUMBER OF → BY, TO OBTAIN ↓	WATTS PER* CM-°K	WATTS PER INCH-°R	CALORIES PER SEC-CM-°K	BTU-IN PER HR-FT²-°R	BTU PER HR-FT-°R	BTU PER SEC-IN-°R	BTU PER HR-IN-°R	K CAL PER HR-M-°K
WATTS* PER CENTIMETER-°K	1	0.7087	4.184	1.4423 x 10^{-3}	1.731 x 10^{-2}	747.7	0.2077	1.1622 x 10^{-2}
WATTS PER INCH-°R	1.4111	1	5.904	2.035 x 10^{-3}	2.442 x 10^{-2}	1.0550	0.2931	1.6400 x 10^{-2}
CALORIES PER SECOND-CENTIMETER-°K	0.2390	0.1694	1	3.447 x 10^{-4}	4.136 x 10^{-3}	178.70	4.964 x 10^{-2}	2.778 x 10^{-3}
BTU-IN PER HR-FT²-°R	693.4	491.4	2901	1	12	5.1840 x 10^{5}	144	8.058
BTU PER HR-FT-°R	57.78	40.946	241.8	8.333 x 10^{-2}	1	4.320 x 10^{4}	12	0.6715
BTU PER SEC-IN-°R	1.337 x 10^{-3}	9.478 x 10^{-4}	5.596	1.9290 x 10^{-6}	2.3148 x 10^{-5}	1	2.778 x 10^{-4}	1.5545 x 10^{-5}
BTU PER HR-IN-°R	4.815	3.413	20.15	6.944 x 10^{-3}	8.333 x 10^{-2}	3600		5.596 x 10^{-2}
K CAL PER HR-M-°K	86.04	60.97	360	0.12409	1.4891	6.433 x 10^{4}	17.87	1

Table 22

THERMAL RESISTANCE

BY ↘ MULTIPLY NUMBER OF → / TO OBTAIN ↓	°R PER WATT	°K PER WATT*	SECOND-°K PER CALORIE	HOUR-FEET-°R PER BTU-INCH	HOUR-°R PER BTU	SECOND-°R PER BTU	HOUR-°K PER KILOCALORIE
°R PER WATT	1	1.80	0.430	40.956	3.413	9.480 x 10^{-4}	1.548
°K PER WATT*	0.5556	1	0.2389	22.76	1.896	5.267 x 10^{-4}	0.860
SECOND-°K PER CALORIE	2.326	4.187	1	95.26	7.939	2.205 x 10^{-3}	3.60
HOUR-FEET-°R PER BTU-INCH	2.442 x 10^{-2}	4.396 x 10^{-2}	1.050 x 10^{-2}	1	8.335 x 10^{-2}	2.315 x 10^{-5}	3.780 x 10^{-2}
HOUR-°R PER BTU	0.2930	0.527	0.126	12	1	2.778 x 10^{-4}	0.4536
SECOND-°R PER BTU	1054.8	1898.6	453.6	4.32 x 10^{4}	3600	1	1632.8
HOUR-°K PER KILOCALORIE	0.646	1.163	0.278	26.458	2.205	6.124 x 10^{-4}	1

Table 23

THERMAL CAPACITANCE

MULTIPLY NUMBER OF → BY TO OBTAIN ↓	BTU PER °R	JOULES* PER °K	CALORIES PER °K	KILOCALORIES PER °K
BTU PER °R	1	5.26 x 10^{-4}	2.2046 x 10^{-4}	0.22046
JOULES PER °K OR WATT-SECONDS PER °K	1899.11	1	4.1868	4186.8
CALORIES PER °K	4536	0.2389	1	1000
KILOCALORIES PER °K	4.536	2.389 x 10^{-3}	0.001	1

Table 24

THERMAL DIFFUSIVITY

TO OBTAIN ↓ / By MULTIPLY NUMBER OF →	SQUARE FEET PER HOUR	SQUARE FEET PER SECOND	SQUARE INCHES PER SECOND	SQUARE CENTIMETERS PER HOUR	SQUARE METERS PER HOUR	SQUARE CENTIMETERS PER SECOND	SQUARE METERS* PER SECOND
SQUARE FEET PER HOUR	1	3600	25	1.0764×10^{-3}	10.764	3.875	3.875×10^{4}
SQUARE FEET PER SECOND	2.778×10^{-4}	1	6.944×10^{-3}	2.990×10^{-7}	2.990×10^{-3}	1.0764×10^{-3}	10.764
SQUARE INCHES PER SECOND	0.040	144	1	4.306×10^{-5}	0.4306	0.1550	1.550×10^{3}
SQUARE CENTIMETERS PER HOUR	929.0	3.3445×10^{6}	2.323×10^{4}	1	10^{4}	3600	3.600×10^{7}
SQUARE METERS PER HOUR	9.290×10^{-2}	334.45	2.323	10^{-4}	1	.3600	3600
SQUARE CENTIMETERS PER SECOND	0.2581	929.0	6 452	2.778×10^{-4}	2.778	1	10^{-4}
SQUARE METERS PER SECOND	2.5806×10^{-5}	9.290×10^{-2}	6.452×10^{-4}	$2\ 778 \times 10^{-8}$	2.778×10^{-4}	10^{-4}	1

Table 25

SPECIFIC HEAT

MULTIPLY NUMBER OF → BY ↘ TO OBTAIN ↓	GRAM-CALORIES PER GRAM °K	JOULES * PER GRAM °K	BTU PER POUND °R	KILOGRAM-CALORIES PER GRAM °K
GRAM-CALORIES PER GRAM °K	1	0.239	1.000	1000
JOULES * PER GRAM °K	4.187	1	4.187	4187
BTU PER POUND °R	1.000	0.23825	1	1000.00
KILOGRAM-CALORIES PER GRAM oK	0.001	2.3901 X 10^{-4}	1.00065 X 10^{-3}	1

Tat'e 26

LATENT HEAT

MULTIPLY NUMBER OF → BY / TO OBTAIN ↓	KILOCALORIES PER GRAM	CALORIES PER GRAM	JOULES * PER GRAM	BTU PER POUND
KILOCALORIES PER GRAM	1	0.001	2.39 X 10^{-4}	5.56 X 10^{-4}
CALORIES PER GRAM	1000	1	0.23901	0.556
JOULES * PER GRAM	4187	4.187	1	2.326
BTU PER POUND	1800.0	1.80	0.4279	1

Table 27

VISCOSITY

MULTIPLY NUMBER OF → / BY / TO OBTAIN ↓	GRAM PER CM SEC (POISES)	KILOGRAM PER METER SECOND	POUND MASS PER FOOT SECOND	POUND FORCE SECOND PER SQUARE FOOT	CENTIPOISES	POUND MASS PER FOOT HOUR
GRAM PER CENTIMETER SECOND (POISES)	1	10	1.488×10^{1}	4.788×10^{2}	10^{-2}	4.134×10^{-3}
KILOGRAM PER METER SECOND	10^{-1}	1	1.488	4.788×10^{1}	10^{-3}	4.134×10^{-4}
POUND MASS PER FOOT SECOND	6.7197×10^{-2}	6.7197×10^{-1}	1	32.174	6.7197×10^{-4}	2.778×10^{-4}
POUND FORCE SECOND PER SQUARE FOOT	2.0886×10^{-3}	2.0886×10^{-2}	3.1081×10^{-2}	1	2.0886×10^{-5}	8.6336×10^{-6}
CENTIPOISES	10^{2}	10^{3}	1.4882×10^{3}	4.788×10^{4}	1	4.1338×10^{-1}
POUND MASS PER FOOT HOUR	2.4191×10^{2}	2.4191×10^{3}	3.6×10^{3}	1.1583×10^{5}	2.4191	1

Table 28

KINEMATIC VISCOSITY

MULTIPLY NUMBER OF → BY → / TO OBTAIN ↓	SQUARE CENTIMETER PER SECOND	SQUARE METER PER SECOND	SQUARE FOOT PER HOUR	CENTISTOKES
SQUARE CENTIMETERS PER SECOND	1	10^4	2.5807×10^{-1}	10^{-2}
SQUARE METER PER SECOND	10^{-4}	1	2.5807×10^{-5}	10^{-6}
SQUARE FOOT PER HOUR	3.8750	3.8750×10^4	1	3.8750×10^{-2}
CENTISTOKES	10^2	10^6	2.5807×10^1	1